Proceedings of the Third PRC-US Workshop on Seismic Analysis and Design of Special Bridges

Edited by

Lichu Fan
State Key Laboratory for Disaster Reduction in Civil Engineering
Tongji University
Shanghai, China

George Lee
Multidisciplinary Center for Earthquake Engineering Research
University at Buffalo, State University of New York
Buffalo, New York

MCEER
MULTIDISCIPLINARY CENTER FOR EARTHQUAKE ENGINEERING RESEARCH
A National Center of Excellence in Advanced Technology Applications

ISSN 1520-295X

Technical Report MCEER-05-0003
April 20, 2005

This workshop was held October 21-22, 2004 and hosted by the State Key Laboratory for Disaster Reduction in Civil Engineering, Tongji University, Shanghai, China. It was supported by the National Science Foundation of China under grant number 50278068 and by the U.S. Federal Highway Administration under contract number DTFH61-98-C-00094.

TONGJI UNIVERSITY 1907

Proceedings of the Third PRC-US Workshop on Seismic Analysis and Design of Special Bridges

Held at
State Key Laboratory for Disaster Reduction in Civil Engineering
Tongji University
October 21-22, 2004

Edited by
Li-Chu Fan[1] and George C. Lee[2]

Publication Date: April 20, 2005

Technical Report MCEER-05-0003

Workshop Steering Committee

Lichu Fan, SLDRCE, Tongji University
Mengling Lou, Tongji University
Weigang Bao, PRC Ministry of Communication
George Lee, MCEER, University at Buffalo
Ian Buckle, University of Nevada, Reno
W. Phillip Yen, Federal Highway Administration

Local Organizing Committee

Lichu Fan, Shide Hu, Yan Xu and Jianzhong Li, all of Tongji University, Shanghai, PRC

National Science Foundation of China Grant Number 50278068
FHWA Contract Number DTFH61-98-00094

1 Professor, State Key Laboratory for Diasaster Reduction in Civil Engineering, Tongji University, Shanghai, PRC
2 Special Tasks Director, Multidisciplinary Center for Earthquake Engineering Research, University at Buffalo, State University of New York

MULTIDISCIPLINARY CENTER FOR EARTHQUAKE ENGINEERING RESEARCH
University at Buffalo, State University of New York
Red Jacket Quadrangle, Buffalo, NY 14261

Participants at the Third PRC-US Workshop on Seismic Analysis and Design of Special Bridges

Preface

This seismic analysis and design of special bridges (SADSB) workshop series is based on a Memorandum of Understanding (MOU) between the Multidisciplinary Center for Earthquake Engineering Research (MCEER), University at Buffalo, State University of New York, Buffalo, New York and the State Key Laboratory for Disaster Reduction in Civil Engineering (SLDRCE), Tongji University, Shanghai China. The MOU was signed by Professor George C. Lee of MCEER and Professor Lichu Fan of SLDRCE on May 26, 2001, and resulted from the PRC-US earthquake engineering and earthquake disaster mitigation collaboration project. Four international workshops will be carried out in China and the U.S. between 2002-2005, alternating locations each year. In the U.S., the workshop series is sponsored by the Federal Highway Administration and in China, it is sponsored by the Chinese National Science Foundation.

The purpose of these workshops is to share technical information and construction experience in the seismic design and performance of "special" highway bridges. For the purpose of these meetings, "special" bridges include major long span bridges as well as those with small to moderate spans with complex geometries or located on particularly hazardous sites. The long-term objective is to develop a knowledge base, from which guidelines for these unique structures can be developed.

The third workshop was held on October 21-22, 2004 in Shanghai, China, at the State Key Laboratory for Disaster Reduction in Civil Engineering, Tongji University. A total of 24 participants, 10 from the U.S. and 14 from China, attended this workshop. These proceedings contain 20 papers covering a wide range of research fields. Of the 20 papers, one was not presented orally at the workshop due to scheduling problems.

The first workshop was held on October 8 - 10, 2002 at Tongji University in Shanghai, and the second was held on December 3-5, 2003 in Buffalo, New York.

Contents

Contents (continued)

Construction Materials and Methods for Building Seismic Resistant Bridges and Structures

M. Myint Lwin [1]

ABSTRACT

Major earthquakes around the world result in increased public awareness of the potential damage and disruption to the transportation systems. The bridge engineering community has learned and relearned many lessons from these earthquakes for developing improved earthquake design criteria, analysis tools, structural details and connections, building materials and construction practices. Extensive research and studies have been done to improve the seismic performance of new and existing bridges and structures. The main objective of this paper is to discuss the importance of selecting the proper materials, such as, high performance concrete, high performance steels and reinforced concrete polymers, and applying good construction practices in building seismic resistant bridges and structures.

[1] M. Myint Lwin, Office of Bridge Technology, Federal Highway Administration, United States Department of Transportation, 400 Seventh. Street, SW Room 3203, Washington, DC 20590, USA

INTRODUCTION

Highway bridges have been and will continue to be an important and integral part of the transportation infrastructure. They form key links in roadways and highways. They are part of the “life-lines” in our transportation systems. The reliable performance of highway bridges in seismic events is crucial to the social, economic and health care services of the communities.

Strong earthquakes in recent memories have caused thousands of lives, billions of dollars of damages and other indirect costs incurred as a result of the damages to buildings, highways and bridges. The public is concerned and the bridge engineering community is intensifying effort to minimize the loss of lives, properties and commerce in small, moderate and severe earthquakes due to structural failures in the future. The bridge engineers can use the lessons learned from past earthquakes and apply the state-of-the-knowledge in science and engineering to design, build and retrofit bridges to perform well in a given level of ground shaking with a small probability of exceedance during the service life of the bridge.

High performance concrete, including self-compacting/consolidating concrete, high performance steels and fiber reinforced polymers are important materials in the design, and construction of new bridges, and retrofit of existing bridges.

LESSONS FROM RECENT EARTHQUAKES

Older highway bridges, especially those designed and constructed before the lessons learned from the 1971 San Fernando Earthquake, have been designed with very little or no attention to seismic resistance and details. Many of these older highway bridges were severely damaged or collapsed due to concrete and/or steel substructure failures in major earthquakes.
Many States are evaluating and retrofitting older highway bridges as seismic retrofit funds become available.

In the 1980s, the Federal Highway Administration (FHWA) published a document under the title, Seismic Design Guidelines for Highway Bridges. This document was subsequently approved by the AASHTO Highway Subcommittee on Bridges and Structures as the Standard Specifications for Seismic Design of Highway Bridges. Bridges designed, analyzed, detailed and constructed in accordance with these Specifications are expected to withstand major earthquakes without collapse or extensive damage while maintaining function of essential bridges. Bridges constructed before the 1980s are more susceptible to earthquake damage, unless seismic retrofit measures are taken.

The October 1989 Loma Prieta earthquake, the January 1994 Northridge earthquake, the January 1995 Kobe earthquake, the August 1999 Turkey earthquake, and the September 1999 Taiwan earthquake confirmed that bridges with in-span hinges, with narrow support widths over the piers and with inadequate confinement reinforcement and shear capacity in the columns are highly susceptible to major damage and collapse. These earthquakes also showed that bridges designed in accordance with the current criteria generally performed well with relatively minor damage, and bridges retrofitted to meet current retrofit philosophy and techniques performed well.

Seismic retrofit has been proved to be very effective in earthquakes in California and Japan, and most recently in Washington State. The relatively light damage to highway bridges during the February 28, 2001 Nisqually earthquake in Washington could be attributed to the work of seismic retrofit. Where structural damage did occur, it was due to foundations on soft soil or older bridges that have not been retrofitted.

Concrete, steel and fiber reinforced polymer are the materials of choice by structural engineers in the design, construction and retrofit of seismic resistant bridges and structures.

ATTRIBUTES OF HIGH PERFORMANCE CONCRETE

High Performance Concrete (HPC) is one of seven key technologies considered by the Strategic Highway Research Program (SHRP) for further development and implementation. In 1991, Congress provided funding to assist states in building HPC bridges and to showcase the beneficial results. HPC has enhanced durability and strength not normally attainable in conventional concrete. HPC is denser, stronger and less permeable. The advantages of HPC are: improved engineering properties, increased durability, longer spans, fewer piers, fewer beams, shallower beams and less overall cost than conventional concrete. With HPC we can design and build bridges and highways to achieve 100-year lives!

In the 1990’s FHWA sponsored HPC showcases and participated in HPC Lead State activities to provide guidance and assistance to the States for implementing HPC. The IBRC program also provided funds to support the states in designing, constructing and monitoring the performance of HPC in bridges. Through these activities, most States are using HPC to take advantage of the durability and strength characteristics in substructures, superstructures and bridge decks. The results are: better long-term performance and reduced life-cycle costs.

In the last 10 years, HPC has made tremendous progress in technological advances and implementation. HPC is now the standard practice for many states. A recently survey indicates that all but six states have used HPC in project specifications in the last 10 years. HPC has been used in different types of concrete structures (Lwin, 1997). Table 1 shows the contractors’ approved mix proportions and the structural design characteristics for a prestressed concrete bridge, the tower of a cable-stayed bridge, the housings of a bascule bridge and a floating concrete bridge.

Table 1 Approved Mix Design (Weight Per Cubic Meter)

Ingredients		LVM	FAS	TFW	CWB
Portland Cement Type/Weight	Type/kg	II/370	II/338	I/371	III/432
Fly Ash	kg	50	71	59	132
Silica Fume	kg	30	36	30	30
Fine Aggregate	kg	770	773	724	528
Coarse Aggregate	kg	1050	1145	997	1109
Water	kg	150	125	153	157
Water Reducer, ASTM C494	ml	965	1764	122	1126
Superplasticizer, ASTM C494	ml	5 065	4851	2419	8316
Air Entrainment		None	None	5%	None
Water/Cementitious Materials Ratio		0.33	0.28	0.33	0.265
Slump	mm	180	178	114	152
56-Day Compressive Strength	MPa	80	96	59	74

Chloride Permeability (56-Day)	Coulombs	790	1250	950	1000
Shrinkage (28-Day)	Microstrain	330	NR	500	400

LVM = The Lacey V. Murrow Floating Bridge
FAS = The First Avenue South Bascule Bridge
TFW = The Theo Foss Waterway Cable-Stayed Bridge
CWB = The Covington Way Precast Prestressed Girder Bridge.
NR = Not Required

Some Lessons Learned from HPC Applications

Concrete Mix

Trial mix designs have proved to be very valuable in developing the project specifications and in assuring the proper mix for construction. There are many factors that affect the properties of the concrete mixes. Trial mixes performed by the ready-mix suppliers help to reflect the conditions of the site and to minimize surprises and delays in production.
Trial mixes save time and dollars in arriving at an approved design mix that has minimal construction problems. For members with complex geometry and congested components, building test sections prior to the start of construction has proved to be very valuable to the contractors and the owners.

Silica Fume

Silica fume in the range of 5 to 8% of cementitious materials has significant benefit in increasing early compressive strengths and reducing permeability. However, it causes increase in heat of hydration and provides little or no bleed water to the surface, requiring special attention in curing to avoid plastic shrinkage cracking.

Permeability

Permeability is a key durability parameter in assuring long term performance of concrete. AASHTO Test Method T277, "Rapid Determination of the Chloride permeability of Concrete," is currently the most widely used method for determining chloride permeability in terms of electric charge in coulombs. It is relatively simple and fast six-hour test method. The results are quite variable, especially when the electric charge drops below 1,000 coulombs. However, this method serves as a quick means to estimate the penetration of chloride into concrete. For all practical purposes, it is quite reasonable.

Consolidation of Concrete

Proper consolidation of concrete is key to achieving dense concrete free of surface defects. Internal vibration supplemented with external vibration is important when placing concrete in deep walls with heavy reinforcing steel and post-tensioning ducts. External vibration needs more expensive formwork. But the resulting quality concrete more than offsets the extra cost for better formwork. The contractor does not need to spend labor and time in repairing, reworking and patching concrete.

Curing of Concrete

Silica fume concrete mixes yield very little bleed water to the surface. It is essential to supply the water or moisture to surfaces of flatwork or other unformed surfaces to avoid shrinkage cracking. This is done by fog-spraying immediately after finishing the concrete surfaces. After initial set, the unformed surfaces of the concrete are kept continuously wet with water for not less than fourteen days. This is done by immediately covering the concrete surfaces completely with wet burlap and 2 layers of 6 mil white plastic sheet and keeping the burlap continuously wet during the 14-day curing period. When this is carried out diligently and successfully, a relatively crack-free and trouble-free concrete is achieved. Otherwise numerous cracks show up on the flatwork, which can be problematic. The plastic sheets should be overlapped and held down adequately against wind. The wet burlap should be checked frequently to make sure it is kept wet continuously. As simple as these instructions may seem, they are not always followed diligently in the field.

Remarks on HPC

High performance concrete is constructable and can be used advantageously in highway bridge construction in cast-in-place and precast applications. It has enhanced durability characteristics and strength parameters not normally attainable by using conventional concrete mixes. The enhanced durability characteristics improve resistance to thermal freeze-thaw cycles and to salts and other chemicals. The enhanced strength parameters include reduced creep and shrinkage, higher modulus of elasticity and higher strength. The bridge engineers can specify high performance concrete to reduce weight and construction cost by using smaller, fewer or longer members; to improve durability in marine or other harsh environments; and to improve seismic performance.

High performance concrete containing fly ash and silica fume is very cohesive and has good workability when properly proportioned. Enhanced with high range water reducers, the concrete can be mixed with a low water cement ratio and placed with a slump as high as 230 mm (9 inches) with no loss in strength or density. The concrete flows laterally with ease in the forms and can be dropped from a height without segregation.

As the HPC Lead State activities were sunset by AASHTO, FHWA forms the HPC Technology Delivery HPCTD Team with a vision to provide leadership in advancing HPC technology. The HPCTD Team consists of members from FHWA, State DOT's, Industry and Academia, and maintains a website dedicated to the exchange of knowledge and information throughout the HPC community. The website address is: http://knowledge.fhwa.dot.gov/cops/hpcx.nsf/home.

ATTRIBUTES OF SELF-COMPACTING/CONSOLIDATING CONCRETE

Self-compacting/consolidating concrete (SCC) offers many advantages for the precast, prestressed concrete industry and for cast-in-place construction, e.g. low noise-level in the plants and construction sites, eliminated problems associated with vibration, less labor involved, faster construction, improved quality and durability, higher strength, and lower cost.

Eliminating vibration cuts down on the labor needed and speeds up construction, resulting in cost savings and less traffic disruption. It also reduces the noise level in the concrete plants and at the construction sites. The overall quality of the concrete is better and the weights of the structures are reduced for improved seismic performance.

Japan has developed and used SCC since the early 1990's. In the last few years, a number of SCC bridges, walls and tunnel linings have been constructed in Europe. In the U.S., SCC is rapidly gaining interest and use, especially by the precast concrete industry (Ouchi, Nakamura, Osterberg, Hallberg, and Lwin, 2003. Some precast plants have retooled and invested in SCC mixing plants to cost-effectively produce precast elements of all shapes and sizes, and level of intricacy. Ready-mixed SCC is being used in columns, walls, piers, crossbeams and drilled shafts of congested reinforcement. Properly engineered SCC flows into and completely fill intricate and complex forms under its own weight, passes through and bonds to congested reinforcement under its own weight, and is highly resistant to aggregate segregation.

Developing SCC Mixes

SCC mixes must meet three key properties: (1) Ability to flow into and completely fill intricate and complex forms under its own weight, (2) Ability to pass through and bond to congested reinforcement under its own weight, and (3) High resistance to aggregate segregation.

The SCC mixes are designed and tested to meet the demands of the projects. For example, the mix for mass concrete is designed for pumping and depositing at a fairly high rate. SCC was used in the construction of the anchorages of the Akashi-Kaikyo Suspension Bridge. The SCC was mixed at a batch plant at the job site and pumped through a piping system to the location of the anchorages 200 m away. The SCC was dropped from a height of as much as 5 m without aggregate segregation. For mass concrete, the maximum size of coarse aggregates may be as large as 50 mm. The SCC construction reduced the construction time for the anchorages from 2.5 years to 2 years. Similarly, SCC mixes can be designed and placed successfully for concrete members with normal and congested reinforcement. The coarse aggregate size for reinforced concrete generally varies from 10 mm to 20 mm.

Examples Of SCC Mixes

When designing an SCC mix, a suitable mix is selected among "Powder- type" by increasing the powder content, "VMA-type" using viscosity modifying admixture and "Combined- type" by increasing powder content and using viscosity agent in consideration of structural conditions, constructional conditions, available material, restrictions in concrete production plant, etc. Examples of SCC mixes are given in the following tables to provide a feel for how SCC mixes differ from normal concrete mixes and from each other based on the specific needs of a project. In comparison to the conventional concrete, all three types work with an increased amount of superplasticizer.

Table 2 shows typical SCC mixes in Japan. Mix J1(Powder-type) is an example of SCC used in a LNG tank, Mix J2(VMA-type) is an example of SCC used for a massive caisson foundation of a bridge, and Mix J3(Combined- type) is an example of SCC used in usual reinforced concrete structures.

Table 2 Examples of SCC Mixes in Japan

Ingredients	Mix J1 (Powder-type)	Mix J2 (VMA-type)	Mix J3 (Combined- type)
Water, kg	175	165	175
Portland Cement Type, kg	530***	220	298
Fly Ash, kg	70	0	206
Ground Granulated Blast Furnace Slag, kg	0	220	0
Silica Fume, kg	0	0	0
Fine Aggregate, kg	751	870	702
Coarse Aggregate, kg	789	825	871
*HRWR, kg	9.0	4.4	10.6
**VMA, kg	0	4.1	0.0875
Slump Flow Test – Diam. of Spread, mm	625	600	660

Notes: * HRWR = High-range water reducing admixture.
** VMA = Viscosity-modifying admixture
*** Mix J1 uses low-heat type Portland cement.

Table 3 Examples of SCC Mixes in the U.S.

Ingredients	Mix U1	Mix U2	Mix U3
Water, kg	174	180	154
Portland Cement Type, kg	408	357	416
Fly Ash, kg	45	0	0
Ground Granulated Blast Furnace Slag, kg	0	119	0
Silica Fume, kg	0	0	0
Fine Aggregate, kg	1052	936	1015
Coarse Aggregate, kg	616	684	892
*HRWR, ml	1602	2500	2616
**VMA, ml	0	0	542
Slump Flow Test – Diam. of Spread, mm	710	660	610

Notes: *HRWR = High-range water reducing add mixture.
**VMA = Viscosity-modifying admixture

Structural Properties

The basic ingredients used in SCC mixes are practically the same as those used in the conventional HPC vibrated concrete, except they are mixed in different proportions and the addition of special admixtures to meet the project specifications for SCC. The hardened properties are expected to be similar to those obtainable with HPC concrete. Laboratory and field tests have demonstrated that the SCC hardened properties are indeed similar to those of HPC. Table 4 shows some of the structural properties of SCC.

Table 4 Structural Properties of SCC

Items	SCC
Water-binder ratio (%)	25 to 40
Air content (%)	4.5-6.0
Compressive strength (age: 28 days) (MPa)	40 to 80
Compressive strength (age: 91 days) (MPa)	55 to 100
Splitting tensile strength (age:28 days) (Mpa)	2.4 to 4.8
Elastic modulus (GPa)	30 to 36
Shrinkage strain (x 10^{-6})	600 to 800

Remarks on SCC

SCC has high potential for greater acceptance and wider applications in highway bridge design and construction. A U.S. National Cooperative Highway Research Program (NCHRP) project titled "Self-Consolidating Concrete for Precast, Prestressed Concrete Bridge Elements" has started in August 2004. The objective of this research is to develop guidelines for the use of SCC, including design mixes, test methods, and design and construction specifications.

The South Carolina State Department of Transportation (SCDOT) has received an Innovative Bridge Research and Construction (IBRC) grant to study the use of SCC in drilled shafts. This study consists of constructing 4 test shafts, 2 with SCC and 2 with normal SCDOT concrete mixes. These tests will help SCDOT determine the use of SCC in production drilled shafts. The Kansas State Department of Transportation (KSDOT) has received an IBRC grant to study the fresh and hardened properties SCC for use in Kansas prestressed concrete bridge girders. KSDOT will build a 3-span bridge, using SCC in all the prestressed concrete girders in one of the spans and the remaining prestressed girders will be constructed of Kansas standard concrete mixes. The bridge will be instrumented and monitored for five years to determine the performance of the bridge.

The U.S, Precast/Prestressed Concrete Institute (PCI) reports that a significant number of fabricators in the U.S. are already retooling to use SCC. Cast-in-place concrete construction in tight space and congested reinforcement, such as, drilled shafts, columns and earth retaining systems, can be accelerated by using SCC.

FHWA has co-sponsored, in collaboration with state DOT's, industry and academia, SCC workshops in Texas and Hawaii to disseminate SCC information on bridge and highway construction. FHWA will continue to organize workshops and conduct training to meet the needs of the states that are interested in incorporating SCC in their projects.

ATTRIBUTES OF HIGH PERFORMANCE STEEL

Structural steels have high strengths enabling engineers to design and build skyscrapers and long span bridges. However, extra care must be taken in welding, corrosion protection and crack prevention. To overcome these weaknesses in structural steels, a cooperative research program between the Federal Highway Administration (FHWA), the U.S. Navy and the American Iron and Steel Institute (AISI) was launched in 1994 to develop HPS for bridges and structures. In three years' time, the research program resulted in high performance steel (HPS) with improved weldability, excellent corrosion resistance, high toughness, high crack tolerance, and high strengths. The combination of these improved properties of HPS leads to cost effective applications in bridge design and construction (Lwin, 2003). Three grades of HPS are now available: HPS 50W, HPS 70W and HPS 100W. Many states are already taking advantage of these properties in new bridge designs to improve long-term performance, lower first cost and reduce life-cycle cost.

The following four documents cover the design, fabrication and construction of steel bridges using high performance steels:

1. AASHTO LRFD Bridge Design Specifications, 3rd. Edition, 2004.
2. AASHTO Standard Specifications for Highway Bridges, 17th. Edition, 2002.
3. AASHTO Guide Specifications for Highway Bridge Fabrication with HPS 70W Steel. (An addendum to the Bridge Welding code).
4. AASHTO/AWS D1.5-2002 Bridge Welding Code.

These documents reflect the findings and experiences on the applications of HPS by researchers, fabricators, manufacturers, owners and engineers working with high performance steels, and are the best references, as they are modified over time. The designers must make sure that all or parts of these documents are made a part of the contract document and add any supplemental requirements in the project special provisions.

HPS 70W

The Grade HPS 70W was the first one developed and commercialized in the HPS program. This grade is now also present in ASTM A709-01a and AASHTO M270-02. The chemistry is shown in Table 5 compared to the Grade 70W that it replaced.

Table 5 Chemistries for conventional and high-performance steels

		C	Mn	P	S	Si	Cu	Ni	Cr	Mo	V
Old 70W	Min.	-	.80	-	-	.25	.20	-	.40	-	.02
	Max.	.19	1.35	.035	.04	.65	.40	.50	.70	-	.10
HPS 70W and HPS 50W	Min.	-	1.10	-	-	.30	.25	.25	.45	.02	.04
	Max.	.11	1.35	.020	.006	.50	.40	.40	.70	.08	.08
Traditional 100W	Min.	.10	.60	-	-	.15	.15	.70	.40	.40	.03
	Max.	.20	1.00	.035	.035	.35	.50	1.00	.65	.60	.08
HPS 100W, Cu-Ni	Min.	-	.95	-	-	.15	.90	.65	.40	.40	.04
	Max.	.08	1.50	.015	.006	.35	1.20	.90	.65	.65	.08

HPS 70W is produced by quenching and tempering (Q&T) or Thermo-Mechanical-Controlled Processing (TMCP). Grade HPS 70W is available from a number of steel producers. Figure 1 presents the distribution of Charpy-V-Notch (CVN) results for over 700 plates, showing the excellent performance of this grade, well above specification minimums. Because Q&T processing limits plate lengths to 15.2 m (50 ft.) in the U.S., TMCP practices have been developed on the identical HPS 70W chemistry to produce longer plates to 50 mm (2”) thick. Currently, HPS 70W plates produced by TMCP are available to 38 m (1500”) long depending on weight. Q&T plate girders over 15.2 m (50 ft.) can be specified, but will require additional welded shop splices.

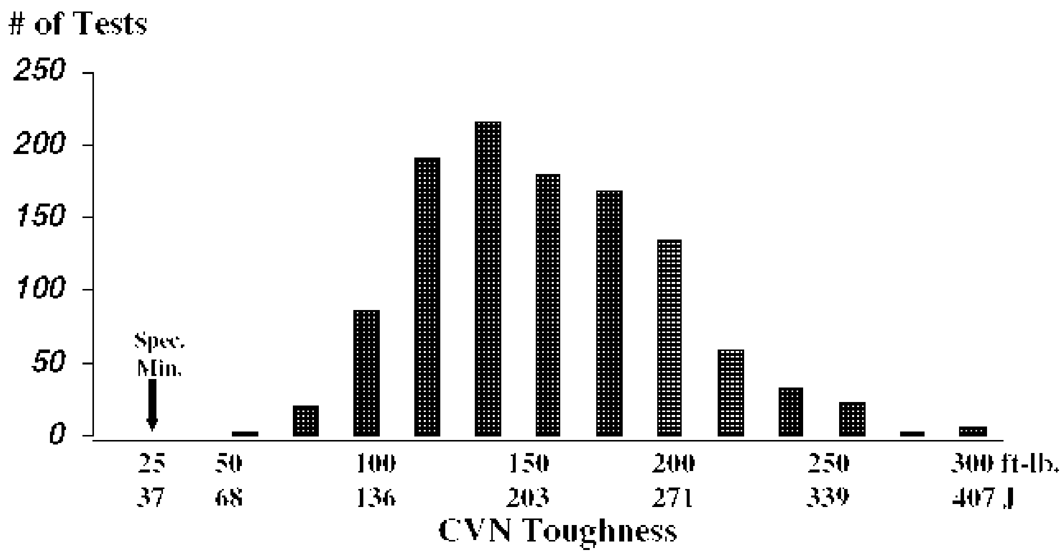

Figure 1 Charpy V-Not ch Toughness Tests

The improved weldability of HPS 70W has been demonstrated to allow welding with limited preheat requirements to 64 mm (2-1/2 in.) thick, whereas the former grade 70W required preheat at thickness over 19 mm (0.75 in.). To take advantage of this improved weldability, new welding consumables were developed for submerged arc welding with low hydrogen conditions.

Fatigue and Fracture Properties

The fatigue resistance of high performance steels is controlled by the welded details of the connections and the stress range, as is the case for conventional steels. The fatigue resistance is not affected by the type and strength of steels. Tests on high performance steel conclude that the fatigue categories given in the AASHTO LRFD, Section 6.6.1 Fatigue also apply to high performance steel welded details. The fracture toughness of high performance steels is much higher than the conventional bridge steels. This is evident from Figure 2, which shows the Charpy-V-Notch (CVN) transition curves for HPS 70W(485W) and conventional AASHTO M270 Grade 50W steel. The brittle-ductile transition of HPS occurs at a much lower temperature than conventional Grade 50W steel. This means that HPS 70W(485W) remains fully ductile at lower temperatures where conventional Grade 50W steel begins to show brittle behavior.

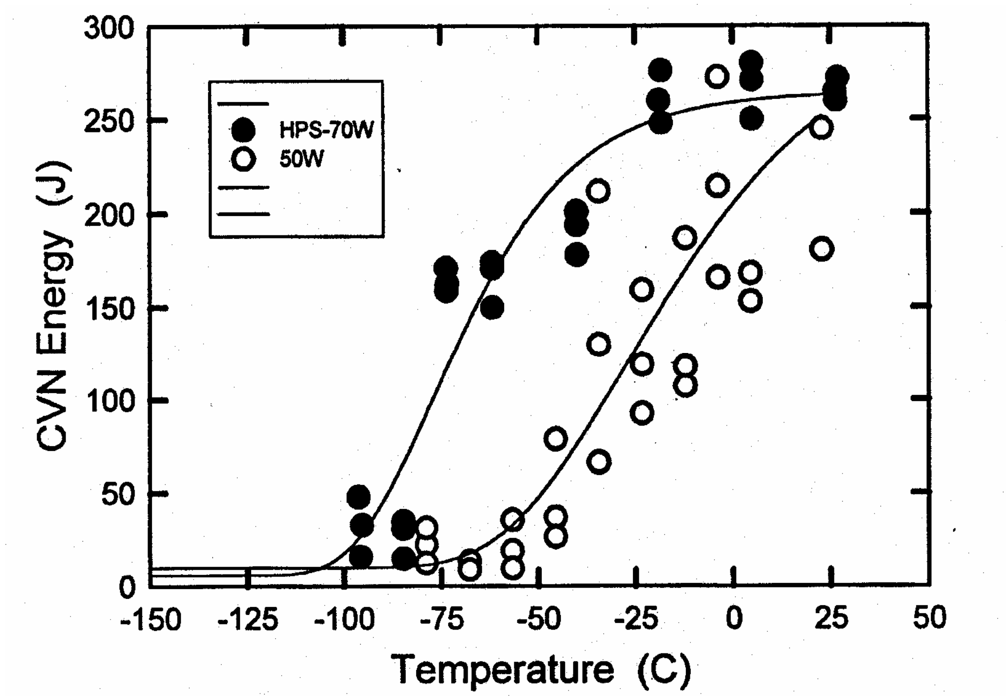

1 ft.-lb. = 0.729 J
1° F = 1.8° C + 32

Figure 2 CVN Transition Curves

The current AASHTO CVN toughness requirements are specified to avoid brittle failure in steel bridges above the lowest anticipated service temperature. The service temperatures are divided into three zones as shown in Table 3.

Table 6 Temperature Zones for CVN Requirements

Minimum Service Temperature	Temperature Zone
0°F (-18°C) and above	1
-1° to –30°F (-18 to -34°C)	2
-31° to –60°F (-35 to -51°C)	3

The AASHTO CVN requirements for these zones are shown in Table 6.6.2-2 Fracture Toughness Requirements in the AASHTO LRFD. The HPS 70W(485W) steels tested so far show ductile behavior at the extreme service temperature of -60°F (-51°C) for Zone 3. It is a major accomplishment of the HPS research and an important advantage of HPS in controlling brittle fracture.

With higher fracture toughness, high performance steels have much higher crack tolerance than conventional grade steels. Full-scale fatigue and fracture tests of I-girders fabricated of HPS 70W (485W) in the laboratory showed that the girders were able to resist the full design overload with fracture even when the crack was large enough to cause 50% of loss in net section of the tension flange [8]. Large crack tolerance increases the time for detecting and repairing fatigue cracks before the bridge becomes unsafe.

Remarks on HPS

The development of HPS is a very successful story of putting research into practice in a very short span of time. It exemplifies the vision and leadership of a strong collaborative partnership between governmental agencies, industry and academia. HPS is justifiably claimed to be “The Bridge Construction Material for the New Century.”

The high strength of HPS allows the designers to use fewer and lighter elements in a bridge system. Higher strengths also increase the span lengths of bridges to reduce the number of piers on land or obstructions in the streams. Lighter structures and few piers contribute to better structural performance in seismic and other extreme events.

Improved weldability of HPS eliminates hydrogen induced cracking, reduces the cost of fabrication by lower preheat requirement, and improves the quality of weldment.

Significantly higher fracture toughness of HPS minimizes brittle and sudden failures of steel bridges in extreme low service temperatures. Higher fracture toughness also means higher cracking tolerance, allowing more time for detecting and repairing cracks before the bridge becomes unsafe.

Presently over 40 states in the U.S.are using HPS in over 200 projects. Many of these projects are in service, while the others are in various stages of design and construction.

ATTRIBUTES OF FIBER REINFORCED POLYMER

Fiber reinforced polymers (FRP) has unique properties, such as high strength, light weight, corrosion resistance, high toughness, etc., which make it very attractive for strengthening, repair and seismic retrofit of bridges and structures (Alliance, 2000 and Corporation, 2000). However, it has a high first cost and the long-term performance is not well established. FRP is adversely affected by environmental factors, such as ultraviolet light, alkalines, etc. FRP behaves quite differently than the conventional structural materials, such as concrete and steel. New design codes have to be developed for FRP.

FRP has great potential for providing engineering solutions to rebuilding our aging infrastructure. It has attracted the interest and attention of the research community, government and private industry to find ways to successfully integrate FRP in structural applications. The collective effort has resulted in many new developments and field applications of FRP composites. In recent years, FRP composites have been used as rebars and prestressing tendons in concrete structures, sheets and laminates for strengthening concrete and steel members, wraps and shells for seismic retrofit of concrete columns, structural shapes for bridges and pultrusions for bridge decks.

The Innovative Bridge Research and Construction (IBRC) Program, established and funded by U.S. Congress, provides opportunities to the States to experiment, demonstrate and document the applications of FRP composites in the construction of bridges and other structures. Currently, over 60 FRP demonstration projects are funded by the IBRC Program.

We expect to see FRP gaining wider acceptance and greater applications in the years ahead.

CONCLUDING REMARKS

The major causes of highway bridge failures in past major earthquakes were:

(1) Pull off and collapse of concrete or steel spans from the supports due to inadequate seat widths and inadequate restraints at joints and connections.
(2) Failure of non-ductile single-column piers constructed of steel and concrete.
(3) Concrete columns failed due to insufficient confinement of reinforcing steel, and steel columns failed due to local or global buckling.
(4) Failures of foundations in soft soils, in reclaimed lands and in artificial fills due to liquefaction, lateral spread and subsidence.

Proper selection of construction materials and methods in earthquake design, construction and retrofit is essential to assure quality and performance of highway bridges. High performance concrete, self-compacting/consolidating concrete, high performance steels and fiber reinforced polymers will no doubt play important roles in reducing the seismic risk of the transportation infrastructure.

REFERENCES

AASHTO, 2004, *LRFD Bridge Design Specifications*, Third Edition, Washington, D.C.

AASHTO, 1998, *LRFD Bridge Construction Specifications*, First Edition, Washington, D.C.

Lwin, M.M., 1997, "Use of High Performance Concrete in Highway Bridges in Washington State," Proceedings of *PCI/FHWA International Symposium on High Performance Concrete*, New Orleans, Louisiana, October 1997.

Lwin, M .M., 2003, *High Performance Steel Designers' Guide*, FHWA Western Resource Center, San Francisco, CA, April 2003.

Market Development Alliance, 2000, *Product Selection Guide: FRP Composite Products for Bridge Applications*, Market Development Alliance of the FRP Composites Industry, Harrison, NY.

Ouchi, M, Nakamura, S., Osterberg, T, Hallberg, S. and Lwin, M.M., 2003 "Applications of SCC in Japan, Europe, and the U.S.," *Third International Symposium on Highway Performance Concrete and PCI National Bridge Conference*, Orlando, FL, October 19-22, 2003.

The Aerospace Corporation, 2000, *Composite Materials for Seismic Retrofit*, the Aerospace Corporation, El Segundo, CA.

Inelastic Response and Damage Analysis of High-rise Bridge Pier under Pulse-type Near-fault Ground Motions

Xi Zhu[1] and Jian-wen Huang[2]

ABSTRACT

According to the engineering example of 8# bridge pier of Huatupo bridge, the inelastic response demands and seismic damage performance evaluation of reinforced concrete high-rise bridge pier under pulse-type near-fault ground motions and responding equivalent pulses were studied by using nonlinear dynamic time-history analysis method, and the rationality of equivalent velocity pulse model was checked.

[1]Xi Zhu, School of Civil Engineering and Architecture, Beijing Jiaotong University, Beijing 100044, PRC
[2]Jian-wen Huang, School of Civil Engineering and Architecture, Beijing Jiaotong University, Beijing 100044, PRC

INTRODUCTION

Near-fault ground motions characterized by long-period pulse with high peak ground velocity have caused much damage in the vicinity of seismic sources during recent earthquakes. This pulse-type motion is particular to the forward direction, where the fault rupture propagates towards the site at a velocity close to the shear wave velocity. The radiation pattern of the shear dislocation of the fault causes the pulse to be mostly oriented perpendicular to the fault so that the fault-normal component of the motion is more severe than the fault-parallel component[1]. The special response characteristics of near-fault ground motions deserve much scrutiny.

It is recognized that near-fault problem is very complex, and that pulse-type near-fault ground motions come in large varieties. This variety very much complicates the evaluation or prediction of structural response unless near-fault ground motions can be represented by a small number of simplified pulse motions that can reasonably replicate important near-fault response characteristics. There are clear similarities between the response of inelastic systems to near-fault ground motions and the response to pulse-type excitations. Up to now, many scholars such as C.Menum[2], B.Alavi[3] and N.Makris[4-6] have proposed equivalent pulse models to represent the pulse-type near-fault ground motions with forward directivity. It is important to note that the use of equivalent pulses to describe near-fault ground motions is an approximation to a very complex problem. If this approximation proves to be reasonably effective, it can significantly simplify the process of predicting inelastic response demands of structures located in the near-fault region of a seismic source.

As well known, impulsive near-fault ground motions generally impose high demands on structures compared to ordinary ground motions. In this study, the inelastic response demands and seismic damage performance evaluation of reinforced concrete high-rise bridge pier subjected to pulse-type near-fault ground motions and responding equivalent pulses would be investigated by using nonlinear dynamic time-history analysis method. The goal of this study was intended to identify salient inelastic response and damage characteristics of high-rise bridge pier under near-fault ground motions, and to check whether pulse-type near-fault ground motions could be reasonably represented by simple equivalent pulses.

EQUIVALENT PULSE MODEL

N.Makris and Chang(1997,1998) classified velocity pulses in near-fault ground motions into three types of pulses, namely, type A pulse, type B pulse and type C_n pulse represented by a unique set of closed-form tri-geometric functions. In this study, the equivalent velocity pulse model proposed by N.Makris et al.(1997,1998) would be used to simplify the pulse-type near-fault ground motions. The amplitude of the velocity pulse v_p was determined by applying the recommended method shown in reference [9], and the pulse period T_p for a pulse-type near-fault record was identified from the location of a global and clear peak in the velocity response spectrum. The values of characteristic parameters of three near-fault pulse-type records and the equivalent pulse parameters such as pulse period, effective peak velocity were summarized in Table.1 for the fault-normal component of the recorded near-fault ground motions with forward directivity. Figure 1(a), (b) and (c) illustrated plots of acceleration, velocity and displacement time history traces respectively of the fault-normal components of two typical near-fault records ErzicanNSacc and NorthridgeNewhall#046 by a dashed curve, of responding equivalent pulses by a solid curve. A comparison of solid and dashed curves in Figure 1(a)-(c) clearly showed that the patterns of acceleration, velocity and displacement histories of equivalent pulses matched those of the near-fault ground motions very well, so it appeared to be reasonable to represent near-fault ground motions by the equivalent pulse used in this study. In the following process, the near-fault records and their equivalent pulses would be applied into the inelastic time-history response demands and damage analysis for reinforced concrete high-rise bridge pier.

Table.1 Pulse-type near-fault records and their characteristic parameters

Name of near-fault records	M_w	R (m)	Field condition	PGA (g)	PGV (cm/s)	PGD (cm)	PGV/PGA	T_P (s)	v_P (m/s)	T_{g1} (s)	T_{g2} (s)
ErzincanNSacc	6.9	2.0	soil	0.515	83.9	27.3	0.166	1.80	0.70	1.57	1.04
NorthridgeNewhall#046	6.7	7.1	soil	0.455	92.8	56.6	0.208	1.92	0.93	1.72	1.31
NorthridgeParkinglot360	6.7	2.0	soil	0.843	128.9	32.5	0.156	0.84	1.25	0.92	0.98

Note: T_{g1}, T_{g2}-characteristic period of ground motions, T_{g1}=6.28*S_v/S_a, T_{g2}=6.28*PGV/PGA[10]; S_v, S_a-the peak value of velocity and acceleration response spectrum; PGV, PGA-the peak value of velocity and acceleration time history.

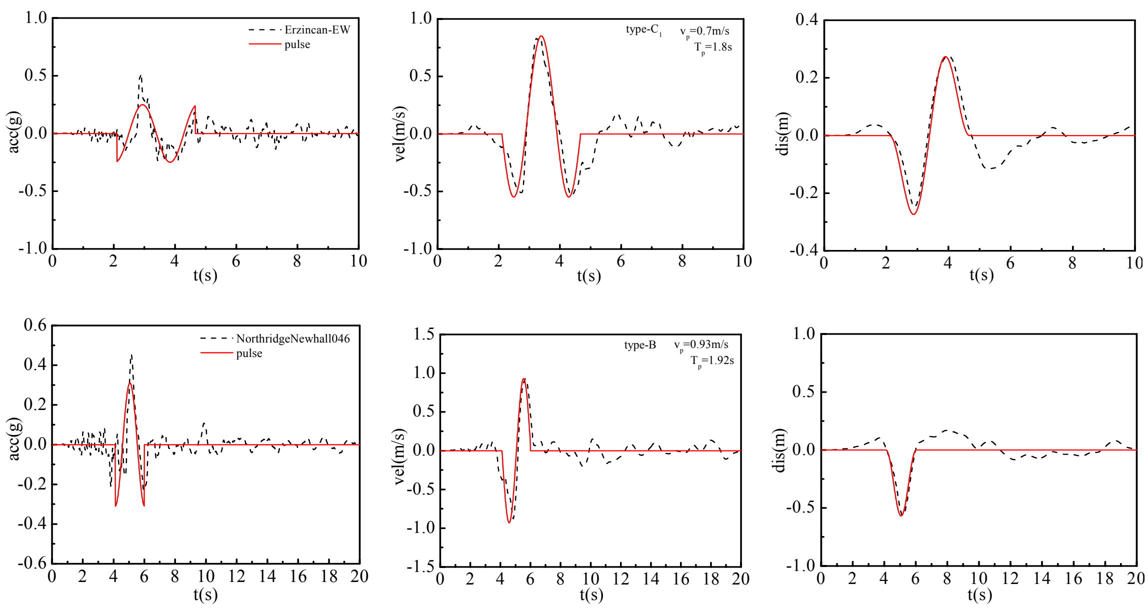

（a）acc(g)　（b）vel(m/s)　（c）dis(m)

Fig.1 Comparison of acceleration, velocity and displacement time histories of record ErzicanNSacc, NorthridgeNewhall#046 and their equivalent pulses

CALCULATING MODEL

A long-span continuous girder railway bridge with high piers was taken as the example. The longitudinal profile of Hutupo bridge was shown in Figure 2. The pier No.8, with height of 110m, was the highest reinforced concrete pier with hollow circle-nosed sections. Figure 3 showed the section information of pier 8. The fixed bearing of the continuous girder was set on this pier, and the slipped bearings were set on other piers. So 8# high-rise bridge pier almost took the whole horizontal seismic force along the bridge subjected to ground motions.

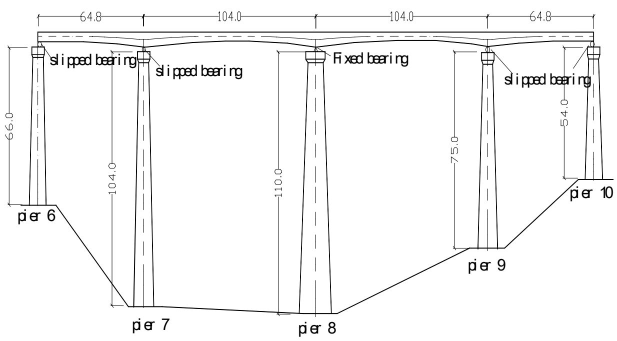

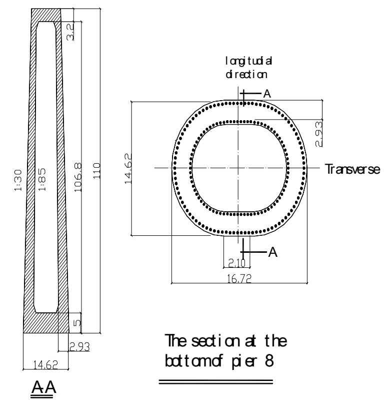

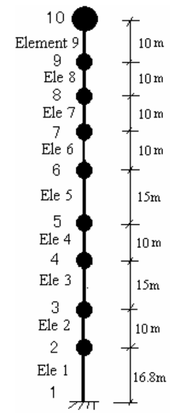

Fig.2 Huatupo bridge Fig.3 Section of 8# pier Fig.4 Calculating model

The longitudinal inelastic response and damage performance analysis of 8# high-rise bridge pier under pulse-type near-fault ground motions would be the research focus in this study. The nonlinear time history analysis was performed to estimate the seismic response and the elasto-plastic seismic behaviors of the variable-cross-section bridge pier. Figure 4 showed the dynamic calculating model for nonlinear time history analysis. The whole pier was divided into 9 beam elements and the pier mass was lumped to 9 nodes. The Takeda degrading tri-linear hysteretic model was adapted as the skeleton model of each element. In references [7,8], bending moment-curvature relationships of the hollow circle-nosed sections of 8# high-rise bridge pier at different height levels were obtained, and figure 5(a) showed the longitudinal bending moment-curvature curves of different sections over the height of 8# pier.

According to the values, determined by moment-curvature analysis, of cracking bending moment M_c, cracking curvature Φ_C, yielding moment M_q, yielding curvature Φ_q, ultimate moment M_u and ultimate curvature Φ_u of predetermined sections at different height levels of 8# high-rise bridge pier, the responding skeleton curves of Takeda degrading tri-linear hysteretic model could be generated[11] which were shown in Fig. 5(b), and the initial stiffness K_e, cracking stiffness K_f and yielding stiffness K_q could be expressed as

$$K_e = M_c / \Phi_c \qquad (1)$$

$$K_f = \left(M_q - M_c\right) / \left(\Phi_q - \Phi_c\right) \qquad (2)$$

$$K_q = \left(M_u - M_q\right) / \left(\Phi_u - \Phi_q\right) \qquad (3)$$

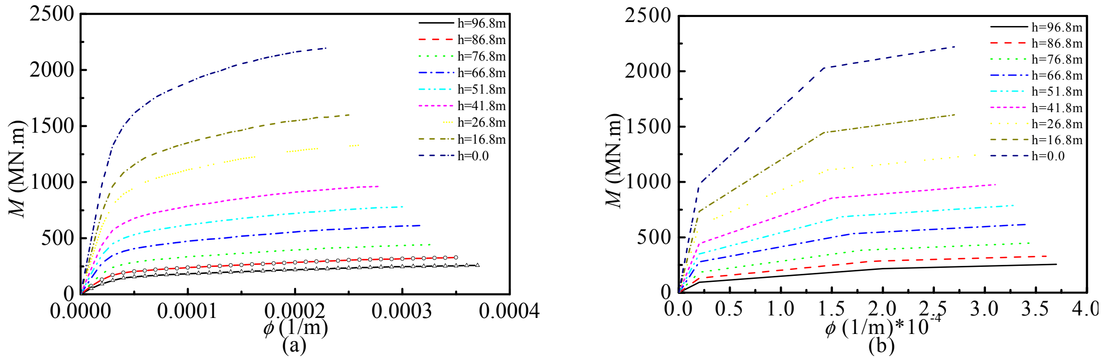

Fig.5 (a) Moment-curvature curves (b) Skeleton curves of 8# bridge pier at different altitude *h*

DAMAGE MODEL

According to Park-Ang dual-parameter damage model[12,13], the damage index DI of each beam element of dynamic calculating model for reinforced concrete high-rise bridge pier shown in Figure 3 can be defined as

$$DI = \frac{\Theta}{\Theta_u} + \beta \frac{E_h}{M_y \Theta_u} \tag{4}$$

where Θ and Θ_u are respectively the actual and ultimate rotations; E_h represents the dissipated hysteretic energy; M_y is the yielding bending moment; β is an empirical constant which depends on structural characteristics, and it is taken as 0.15 in this study.

Under the static load, the static hysteretic energy in the elasto-plastic SDOF system can be expressed as

$$E_{hs} = M_y(\Theta - \Theta_y) = F_y(D - D_y) \tag{5}$$

where F_y, D and D_y is respectively the yielding force, displacement and yielding displacement of equivalent SDOF system, and then the hysteretic energy in the equivalent SDOF system subjected to ground motion can be expressed as[14]

$$E_h = F_y D_y \gamma^2 \mu^2 \tag{6}$$

where μ represents displacement ductility; γ is a non-dimensional parameter, which represents the ductile decrease caused by low-cycle fatigue, and it was taken as 0.8 in this study.

After combining expression (4), (5) and expression (6), the damage index DI of each structural member can be expressed as

$$DI = \frac{\Theta}{\Theta_u}\left(1 + \beta \frac{E_h}{E_{hs}} \frac{\Theta - \Theta_y}{\Theta}\right) \tag{7}$$

Where the ratio E_h / E_{hs} is assumed to be constant for all structural members, and it can be expressed as a function of the parameters of the equivalent system[14]

$$\frac{E_h}{E_{hs}} = \frac{F_y D_y \gamma^2 \mu^2}{F_y(D - D_y)} = \gamma^2 \frac{\mu^2}{\mu - 1} \tag{8}$$

After combining expression (7) with expression (8), the damage index DI of each structural member can be expressed as

$$DI = \frac{\Theta}{\Theta_u}\left(1 + \beta\gamma^2 \frac{\mu^2}{\mu - 1}\frac{\Theta - \Theta_y}{\Theta}\right) \tag{9}$$

The global damage index can be obtained by weighting average damage indices of individual structural member, and the weights are the local damage indices.

$$DI = \sum_i \frac{M_{yi}\left(\Theta_i - \Theta_{yi}\right)}{\sum_i M_{yi}\left(\Theta_i - \Theta_{yi}\right)} DI_i \tag{10}$$

RESULTS ANALYSIS

To put the severity of three pulse-type near-fault ground motions listed in Table 1 in perspective when analyzing inelastic response demands and damage characteristics of 8# high-rise bridge pier, a reference far-fault record El-centro(S00E) was utilized for comparison purposes, and the value of peak ground acceleration(PGA) $a_{g,max}$ of those four records was uniformly adjusted to 0.1g, 0.2g, 0.3g and 0.4g so that inelastic time-history analysis results for high-rise bridge pier under different ground motions could be compared with each other. In the following process, the inelastic time-history response demands and damage analysis results of 8# bridge pier subjected to pulse-type record ErzincanNSacc, record NorthridgeNewhall#046 and responding equivalent pulses were compared in order to check the reasonability of equivalent velocity pulse model used in this study.

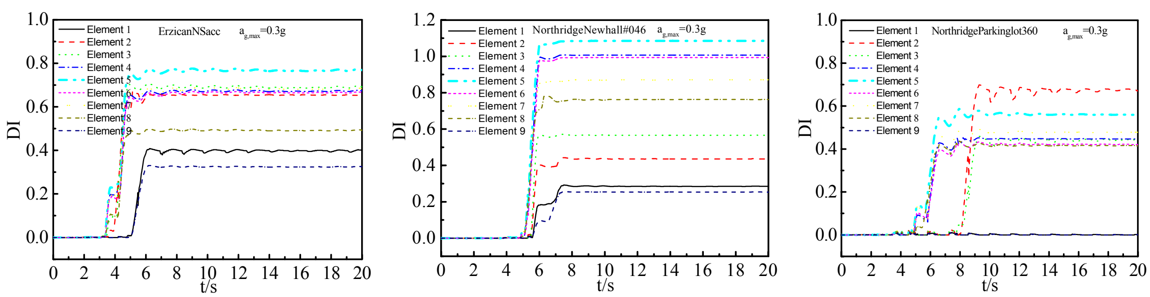

Fig.6 Comparison of damage time-history response of each element under three different near-fault ground motions ($a_{g,max}$=0.3g)

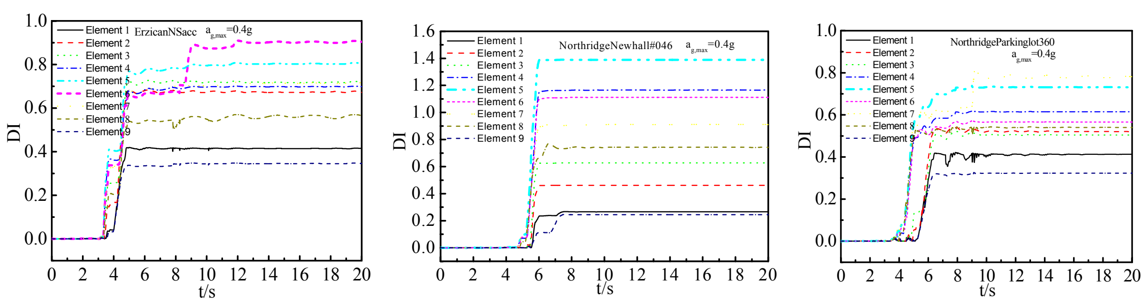

Fig.7 Comparison of time-history damage response of each element under three different near-fault ground motions ($a_{g,max}$=0.4g)

Figure 6 and Figure 7 showed respectively the comparison of time-history damage response results of each element under the pulse-type near-fault records named ErzincanNSacc, NorthridgeNewhall#046 and NorthridgeParkinglot360 when $a_{g,max}$ was adjusted to 0.3g and 0.4g. It was shown from above two figures that time-history damage response value of the 5th element located at the height of 51.8m to 66.8m of 8# high-rise bridge pier was generally larger than that of other elements under three pulse-type near-fault ground motions. The time-history damage analysis results of 8# pier subjected to three near-fault excitations indicated that yielding would start at the height of 60m located in medium portion of pier, not at the lower portion or bottom of pier, and the location of plastic hinges determined by inelastic dynamic time history analysis agreed well with that by capacity spectrum method performed in reference [7,8].

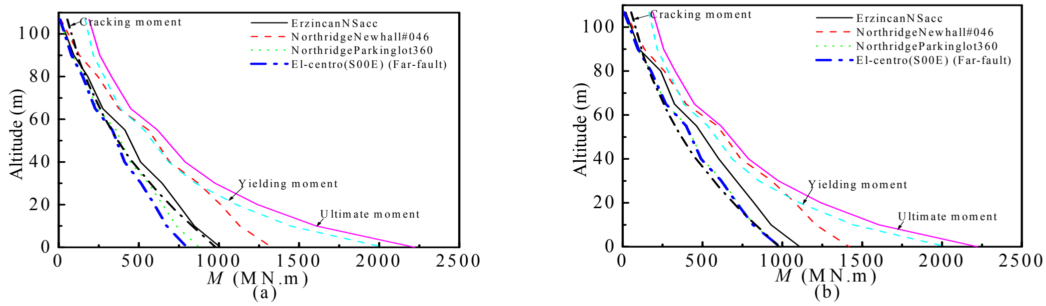

Fig.8 Comparison of maximum bending moment of each section over the height of bridge pier under different ground motions (a)$a_{g,max}$=0.3g (b)$a_{g,max}$=0.4g

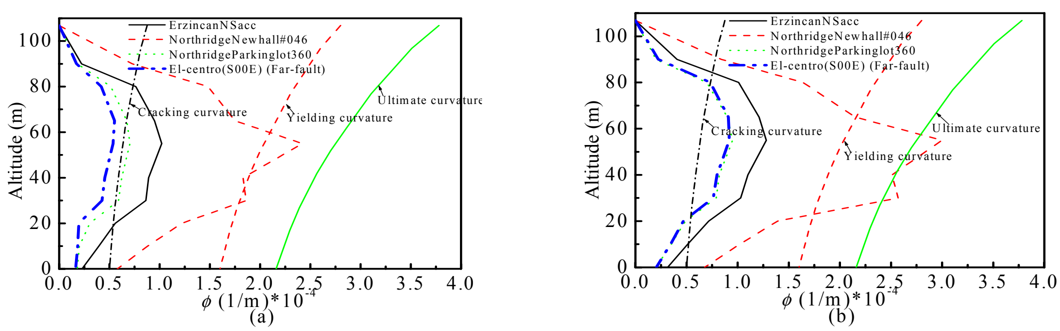

Fig.9 Comparison of maximum curvature of each section over the height of bridge pier under different ground motions (a)$a_{g,max}$=0.3g (b)$a_{g,max}$=0.4g

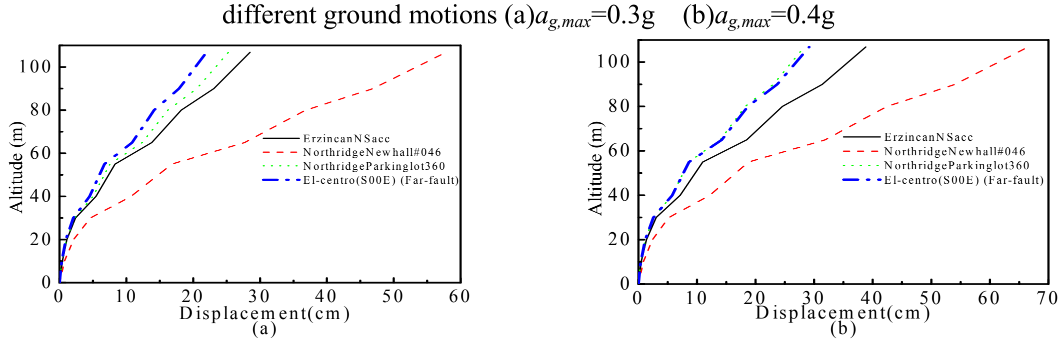

Fig.10 Comparison of maximum joint displacement over the height of bridge pier under different ground motions (a)$a_{g,max}$=0.3g (b)$a_{g,max}$=0.4g

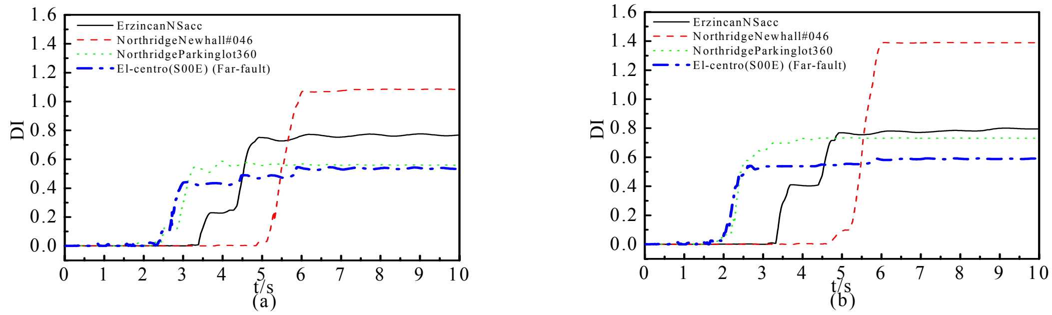

Fig.11 Comparison of time-history damage response of the 5th element under different ground motions

(a)$a_{g,max}$=0.3g (b)$a_{g,max}$=0.4g

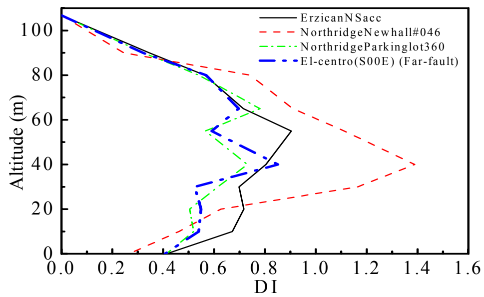

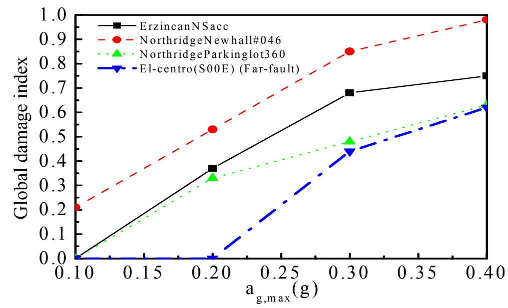

Fig.12 Comparison of local damage index of each section over the height of pier under different ground motions ($a_{g,max}$=0.4g)

Fig.13 Variation of global damage index with the values of $a_{g,max}$ under different ground motions

Table.2 Comparison of roof displacement, bottom bending moment and global damage index at different levels of peak acceleration $a_{g,max}$ under different ground motions

Name of records	Roof displacement（cm）				Bottom bending moment（MN.m）				Global damage index			
	0.1(g)	0.2	0.3	0.4	0.1	0.2	0.3	0.4	0.1	0.2	0.3	0.4
ErzincanNSacc	12.1	23.5	28.5	38.7	451	858	1006	1111	0.00	0.37	0.68	0.75
NorthridgeNewhall#046	18.2	37.5	57.8	66.5	666	1063	1326	1419	0.21	0.53	0.85	0.98
NorthridgeParkinglot360	9.05	18.1	25.2	28.3	333	666	877	981	0.00	0.33	0.48	0.63
El-centro(S00E)（Far-fault）	7.31	14.6	21.9	29.2	275	549	800	985	0.00	0.00	0.44	0.62

Figure 8 to Figure 10 showed respectively comparison of maximum bending moment of each section, maximum curvature of each section and maximum joint displacement over the height of 8# pier subjected to three pulse-type near-fault ground motions and a far-fault ground motion when $a_{g,max}$ was adjusted to 0.3g and 0.4g. It was shown from above figures that the values of maximum bending moment and curvature of each section, and maximum joint displacement over the height of pier under three near-fault records were larger than those under the far-fault ground motion.

Figure 11 showed the comparison of time-history damage response of the 5th element located at the height of 51.8m to 66.8m of 8# bridge pier subjected to three pulse-type near-fault ground motions and a far-fault ground motion when $a_{g,max}$ was adjusted to 0.3g and 0.4g. Figure 12 showed the comparison of local damage index of each section over the height of pier subjected to different ground motions when $a_{g,max}$ was adjusted to 0.4g. As shown in Fig.12, the maximum local damage index was obtained at the height of 60m located in medium portion of 8# pier, and the values of local damage index at the medium to upper portion of pier under near-fault pulse-type ground motions were generally larger than those under intensive far-fault ground motion.

Figure 13 and Table 2 showed the comparison of global damage index of pier subjected to different ground motions when $a_{g,max}$ was adjusted from 0.1g to 0.4g. As shown in Fig.13 and Table 2, the global damage index increased with the increasing value of $a_{g,max}$, and the values of global damage index of pier subjected to near-fault pulse-type ground motions were larger than those obtained under far-fault ground motion.

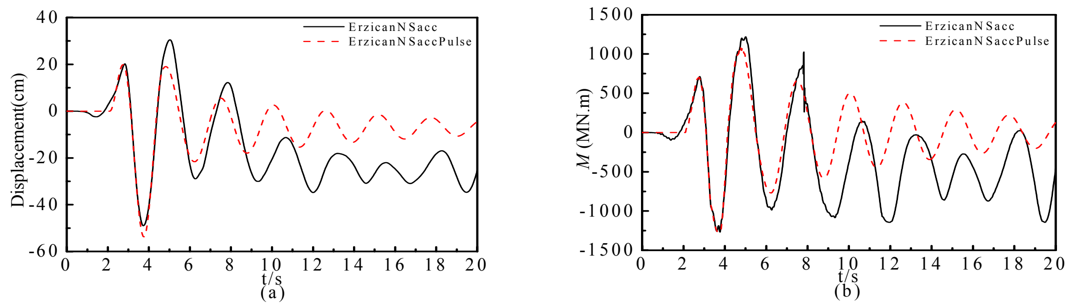

Fig.14 (a)Comparison of roof displacement time-history response (b)Comparison of bottom bending moment time-history response under record ErzicanNSacc and its equivalent pulse

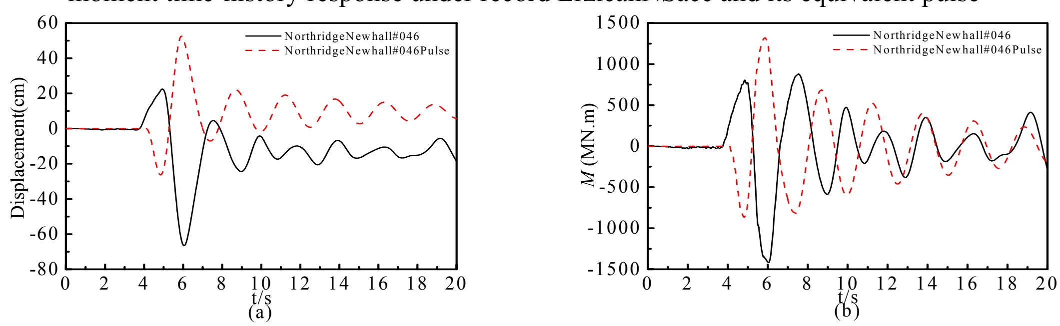

Fig.15 (a)Comparison of roof displacement time-history response (b)Comparison of bottom bending moment time-history response under record NorthridgeNewhall#046 and its equivalent pulse

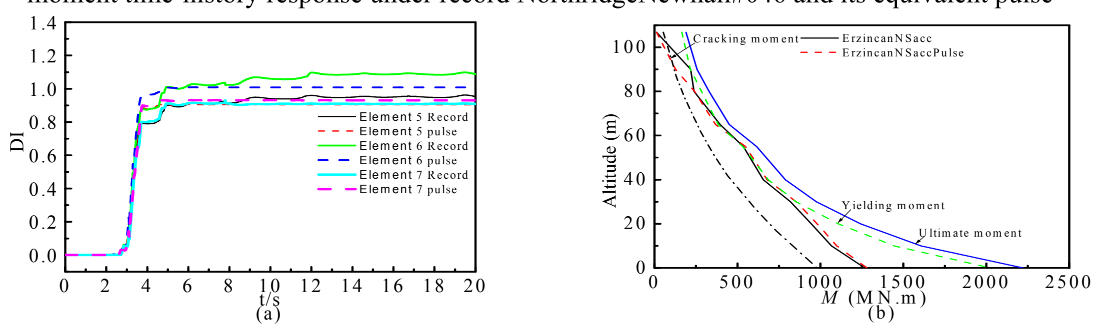

Fig.16 (a)Comparison of damage time-history response of partial elements (b)Comparison of bending moment of each section over the height of pier under record ErzicanNSacc and its equivalent pulse

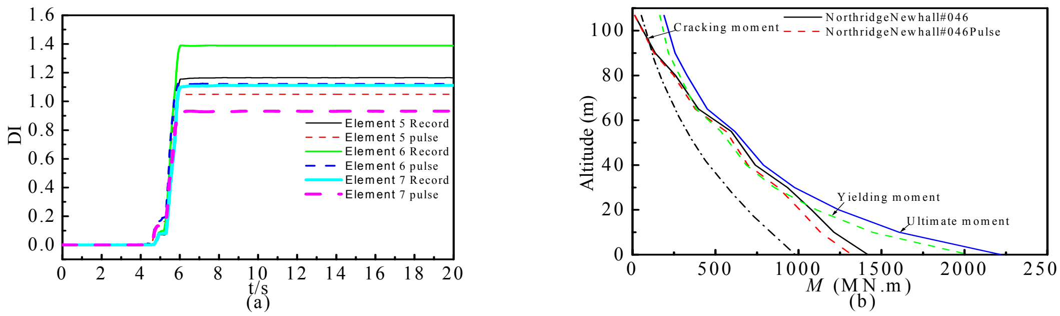

Fig.17 (a)Comparison of damage time-history response of partial elements (b)Comparison of bending moment of each section over the height of pier under record NorthridgeNewhall#046 and its equivalent pulse

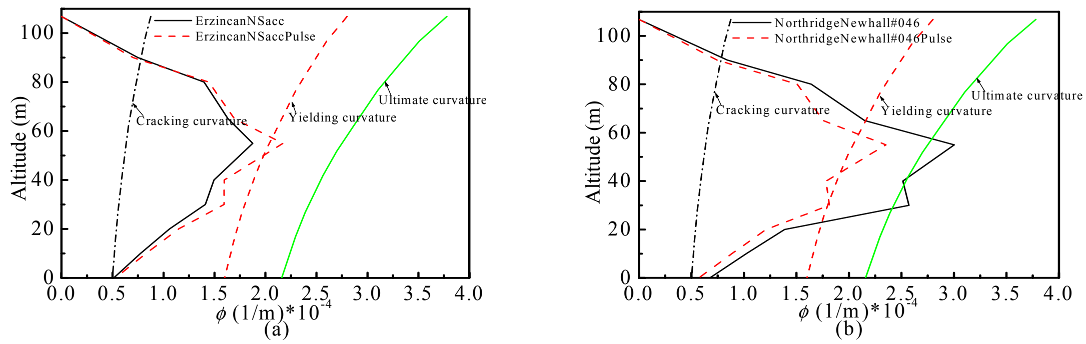

Fig.18 Comparison of maximum curvature of each section over the height of pier (a)under record ErzincanNSacc and its equivalent pulse (b)under record NorthridgeNewhall#046 and its equivalent pulse

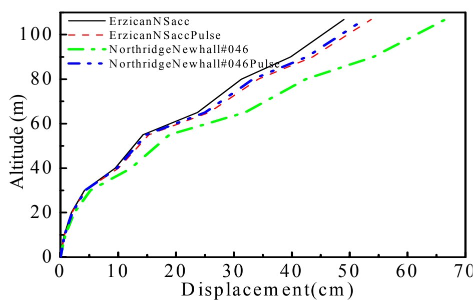

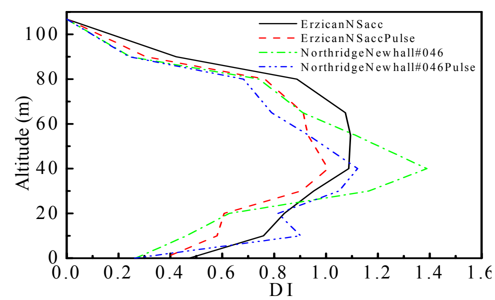

Fig.19 Comparison of maximum joint displacement over the height of pier under near-fault ground motions and their equivalent pulses

Fig.20 Comparison of local damage of each section over the height of pier under near-fault ground motions and their equivalent pulses

Figure 14 and Figure 15 showed respectively the comparison of roof displacement and bottom bending moment of 8# high-rise bridge pier under the record ErzincanNSacc and its equivalent pulse, the record NorthridgeNewhall#046 and its equivalent pulse. Figure 16, 17, 18, 19 and Figure 20 showed respectively the comparison of damage time-history response of partial elements, comparison of maximum bending moment of each section over the height of bridge pier, comparison of maximum curvature of each section over the height of pier, comparison of maximum joint displacement over the height of pier, comparison of local damage value of each section over the height of pier under the record ErzincanNSacc and its equivalent pulse, the record NorthridgeNewhall#046 and its equivalent pulse. It was shown from those figures that inelastic response and damage analysis results of 8# pier subjected to the pulse-type near-fault records and their equivalent pulses agreed well with each other.

CONCLUDING REMARKS

On the basis of results for inelastic response and damage analysis of high-rise bridge pier subjected to pulse-type near-fault ground motions and their equivalent pulses, the summary conclusion was drawn as following:

(1) The equivalent velocity pulse model proposed by N.Makris could represent the near-fault pulse-type ground motions with sufficient accuracy.
(2) By comparing the inelastic time-history response and damage analysis results of 8# pier under three near-fault records and an intensive far-fault record, near-fault ground motions tend to impose larger inelastic response demands such as roof displacement, bottom bending moment, etc., than far-fault ground motions on high-rise bridge pier.
(3) The time-history damage analysis results of 8# pier subjected to near-fault excitations demonstrated that yielding would start at the height of 60m located in medium portion of 8# pier, maximum local damage index was obtained at that location, and the formation of plastic hinges determined by inelastic dynamic time history analysis agreed well with that by capacity spectrum method.
(4) It is recognized that much work remains to be done in order to investigate higher-mode effects, P-delta effects, the traveling wave effect on high-rise bridge pier excited by pulse-type near-fault ground motions.

ACKNOWLEDGMENTS

This study is sponsored by National Nature Science Foundations of China Grant No.50278002. This support is gratefully acknowledged.

REFERENCES

[1] P.Somerville, 1998, "Development of an improved ground motion representation for near fault ground motions," Report, SMIP98 Seminar on Utilization of Strong-motion Data, Oakland, CA

[2] C Menun and Fu Qiang, 2002, "An analytical model for near-fault ground motions and the response of SDOF systems," presented at *7th National Conference of Earthquake Engineering*, Boston, Reference No. 00011

[3] B Alavi, 2000, "Effects of near-fault ground motions on frame structures," Ph.D Dissertation, Department of Civil and Environmental Engineering, Stanford University

[4] N Makris, 1997, "Rigidity-plasticity-viscosity: can electrorheological dampers protect base-isolated structures from near-source ground motions?" *Earthquake Engineering and Structural Dynamics,* 26: 571-591

[5] N Makris and S.P Chang, 2000, "Effect of viscous, viscoplastic and friction damping on the response of seismic isolated structures," *Earthquake Engineering and Structural Dynamics,* 29: 85-107

[6] N Makris and C Black, 2003, “Dimensional analysis of inelastic structures subjected to near fault ground motions,” Report, College of Engineering, University of California, Berkeley, CA

[7] Seismic-resisting research institute, 2001, “Ductility performance and seismic response analysis of high-rise bridge structures,” Report, School of Civil Engineering and Architecture, Beijing Jiaotong University, PRC

[8] Dongwu Zhai, 2001, “Nonlinear seismic behavior of high-rise bridge structures and displacement-based seismic design method,” PH. D. Dissertation, Beijing Jiaotong University, PRC

[9] Xinle Li, Xi Zhu, 2004, “Velocity pulse for near-fault ground motions and its effect on seismic response of pier,” *Journal of Northern Jiaotong University,* 28(1): 11-16

[10] Jingbei Jiang, et al, 2002, “Determination method of characteristic period of ground motions,” presented at *6th National Conference of Earthquake Engineering*, PR.China, 86-90

[11] Dongwu Zhai, Xi Zhu, 1999, “Elasto-plastic seismic behavior of reinforced concrete gravity bridge pier,” *Journal of Northern Jiaotong University,* 23(4): 29-33

[12] Y.J Park, A H-S Ang, 1985, “A mechanistic seismic damage model for reinforced concrete,” *Journal of Structural Engineering,* ASCE

[13] Y.J. Park, A.H-S. Ang, 1985, “Seismic damage analysis of reinforced concrete buildings,” *Journal of Structural Engineering,* 112(2): 102-109

[14] P Fajfar et al, 1996, “The N2 method for the seismic damage analysis for RC buildings,” *Earthquake Engineering and Structural Dynamics,* 25: 63-67

Recent Studies on Fragility Information on Highway Bridges

M. Shinozuka, Y. Zhou and S. Banerjee

Department of Civil Engineering, University of California, Irvine
Irvine, CA, USA

INTRODUCTION

Resent studies on fragility information on highway bridges are presented, highlighting statistical procedures for empirical curve development. Maximum likelihood method is used for estimation of fragility parameters and statistical confidence of these parameters by means of analytical simulation. The confidence interval is quantitatively demonstrated to become narrower as the sample size of bridges at each damage level of interest increases. Dependence of the fragility curves on different bridge characteristics such as skew angle, number of spans, and soil conditions are demonstrated using empirical fragility curves. The empirical fragility curves are used to calibrate the parameters in the analytical fragility models such as the effect of retrofit and threshold values of ductility factors that define the state of damage.

PARAMETER ESTIMATION

Fragility Function

The most commonly used fragility curve takes the functional form of lognormal distribution with two parameters. For a well-defined limit state, it can be expressed as

$$F(a) = \Phi[\frac{\ln(a/c)}{\zeta}] \tag{1}$$

in which a represents ground motion demand PGA (could be any other measure of ground motion intensity) and $\Phi[.]$ is standard normal distribution with parameters (referred to as fragility parameters) consisting of median fragility c and log-standard deviation ζ. In this fragility model, it is assumed that ζ describes the inherent randomness of the capacity of the structure to the earthquake ground motion, and the uncertainty due to modeling and imperfect information affects only the estimated median c. This uncertainty is taken into account by assuming c is a random variable satisfying a probability distribution.

This assumption reflects the fact that this risk assessment result is more sensitive to the variation in c than in ζ .

Maximum Likelihood Method

A set of parameters of lognormal distributions representing fragility curves associated with all levels of damage state involved in the sample of bridges under consideration can be estimated simultaneously. A common log-standard deviation is estimated along with the medians of the lognormal distributions with the aid of the maximum likelihood method. The common log-standard deviation forces the fragility curves not to intersect. The following likelihood formulation is developed for the purpose (Shinozuka and etc., 2003).

Although this method can be used for any number of damage states, it is assumed here for the ease of demonstration of analytical procedure that there are four states of damage including the state of no damage. A family of three (3) fragility curves exist in this case as schematically shown in Figure 1 where events E_1, E_2, E_3 and E_4 respectively indicate the state of no, at least minor, at least moderate and major damage. $P_{ik} = P(a_i, E_k)$ in turn indicates the probability that a bridge i selected randomly from the sample will be in the damage state E_k when subjected to ground motion intensity expressed by PGA = a_i. All fragility curves are represented by two-parameter lognormal distribution functions

$$F_j(a_i; c_j, \varsigma_j) = \Phi\left[\frac{\ln(a_i / c_j)}{\zeta_j}\right] \tag{2}$$

where c_j and ζ_j are the median and log-standard deviation of the fragility curves for the damage state of "at least minor", "at least moderate" and "major" identified by j = 1, 2 and 3 respectively. From this definition of fragility curves, and under the assumption that the log-standard deviation is equal to ζ common to all the fragility curves, one obtains:

$$P_{i1} = P(a_i, E_1) = 1 - F_1(a_i; c_1, \zeta) \tag{3}$$

$$P_{i2} = P(a_i, E_2) = F_1(a_i; c_1, \zeta) - F_2(a_i; c_2, \zeta) \tag{4}$$

$$P_{i3} = P(a_i, E_3) = F_2(a_i; c_2, \zeta) - F_2(a_i; c_3, \zeta) \tag{5}$$

$$P_{i4} = P(a_i, E_4) = F_3(a_i; c_3, \zeta) \tag{6}$$

The likelihood function can then be introduced as

$$L(c_1, c_2, c_3, \zeta) = \prod_{i=1}^{n} \prod_{k=1}^{4} P_k(a_i; E_k)^{x_{ik}} \tag{7}$$

where

$$x_{ik} = 1 \tag{8}$$

if the damage state E_k occurs for the i-th bridge subjected to $a = a_i$, and

$$x_{ik} = 0 \tag{9}$$

otherwise. The maximum likelihood estimates c_{0j} for c_j and ζ_0 for ζ are obtained by solving the following equations,

$$\frac{\partial \ln L(c_1, c_2, c_3, \zeta)}{\partial c_j} = \frac{\partial \ln L(c_1, c_2, c_3, \zeta)}{\partial \zeta} = 0 \qquad (j = 1,2,3) \tag{10}$$

by again implementing a straightforward optimization algorithm.

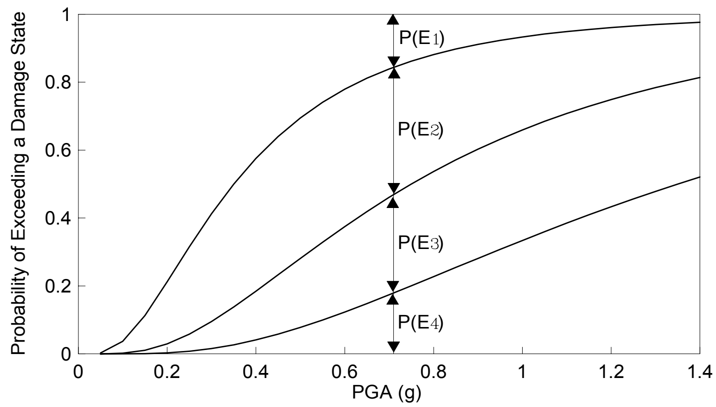

Figure 1 Schematics of Fragility Curves

Four fragility curves for Caltrans' bridges associated with the four states of damages are plotted in figure 2 upon estimating the parameters involved by the above described method. These fragility curves are constructed on the damage data of Caltrans' bridges associated with the 1994 Northridge earthquake.

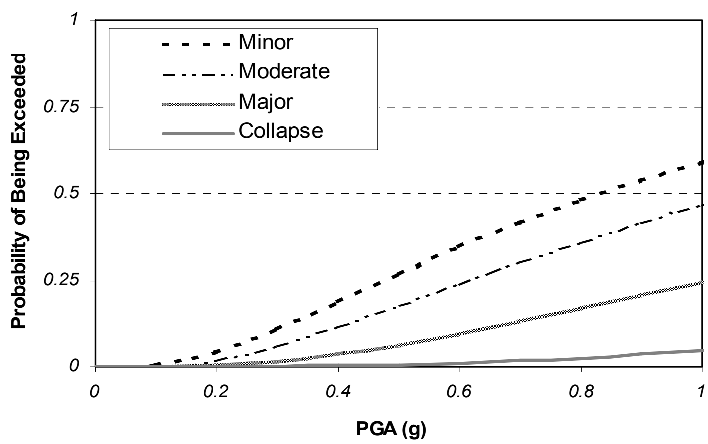

Figure 2 Empirical fragility curve for composite (first level)

STATISTICAL UNCERTAINTY

The magnitude of the statistical uncertainty of estimated parameters, however, cannot be expressed in explicit form. In the proposed Monte Carlo simulation method, a number of samples of damage data of different sizes are simulated based on the fragility curve with parameters c_0 and ζ_0 estimated on the initial damage data acquired either analytically, experimentally or from actual earthquake damage record. Then, for each sample of this size, a set of realizations of the parameter pair is obtained by utilizing the same maximum likelihood method. Finally, the confidence interval of the original estimated parameters of this sample size is estimated, based on the assumption that the variation of these sets of realizations approximately represents the statistical uncertainty of the fragility parameter (Zhou and Shinozuka, 2004). Use of the maximum likelihood method dictates that the distribution of these parameters is asymptotically Gaussian (Shinozuka and etc., 2000) . The simulation results quantitatively demonstrate dependence of the statistical uncertainty of the parameters on sample size. The quantified uncertainty of the fragility parameter can be used to give more reliable risk estimate for both structural components and systems subjected to seismic disturbance.

Figure 3 shows 500 sets of simulated realizations of $\hat{c}_j$ $(j = 1,2,3,4)$ and $\hat{\zeta}$ in two cases: sample size $N = 128$ and $N = 512$, based on the same set of original estimates of fragility parameters, $c_{01} = 0.64g$, $c_{02} = 0.80g$, $c_{03} = 1.25g$, $c_{04} = 2.55g$ and $\zeta_0 = 0.70$. Figure 3 demonstrates the realizations of the medians and log standard deviation in the case of $N = 512$ are far more concentrated than those in the case of $N = 128$. In figure 4a-d, the marginal distributions of the realizations of $\hat{c}_j$ $(j = 1,2,3,4)$ are separately plotted on lognormal probability papers for the case of $N = 128$, each of which indicates the log-normality of the marginal distribution of the realizations of $\hat{c}_j$.

Assuming that the marginal distributions of $\hat{c}_j$ are lognormal, their corresponding medians $\hat{c}_{jm}$ log-standard deviation $\sigma_{\ln \hat{c}_j}$ $(j = 1,2,3,4)$ and therefore $\hat{c}_j = c_p$ associated with any exceedance probability of $p\%$ of $\hat{c}_j$ could be obtained. Again, the $\zeta = \hat{\zeta}$ associated with $c = \hat{c}_{jm}$ is used for every $\hat{c}_j = c_p$. For each of $\hat{c}_j$, three fragility curves thus obtained, corresponding to c_p with confidence level of 5%, 50% and 95%, are plotted in figure 5 a-d, based on the simulation results shown in figure 4a-d.

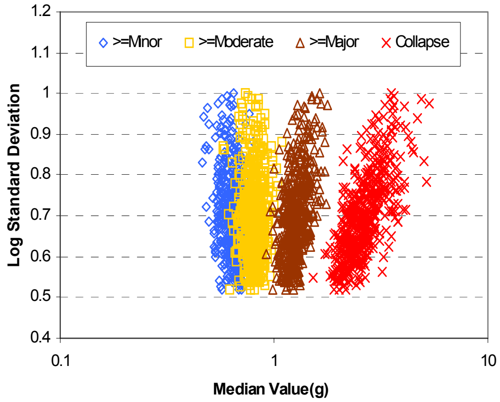

(a)N=128

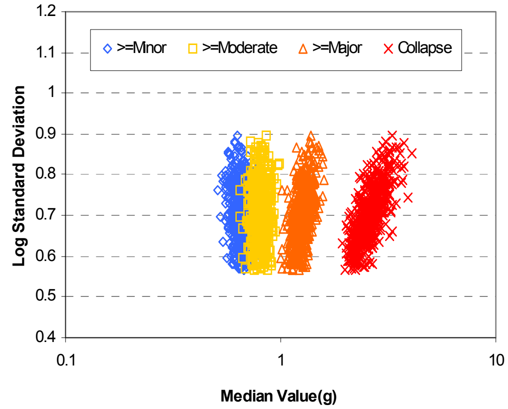

(b)N=512

Figure 3 Simulated distribution of $\hat{c}_j$ $(j = 1,2,3,4)$ and $\hat{\zeta}$

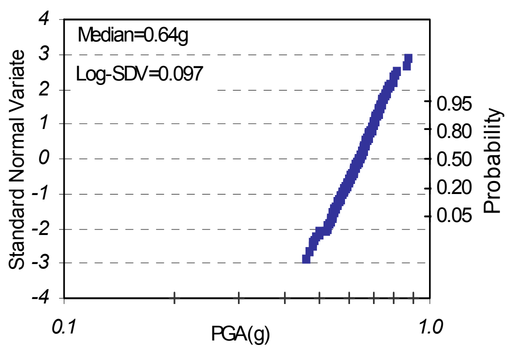

(a) $\hat{c}_1$

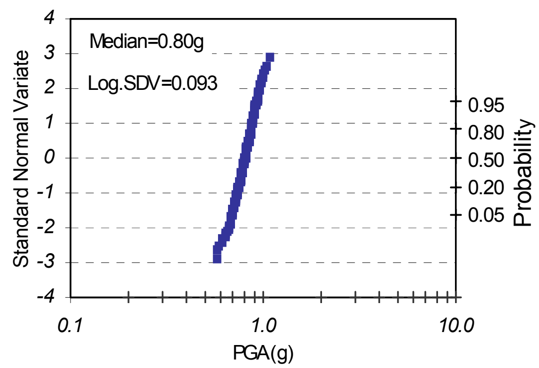

(b) $\hat{c}_2$

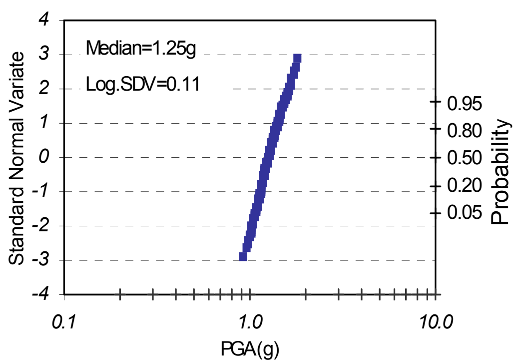

(c) $\hat{c}_3$

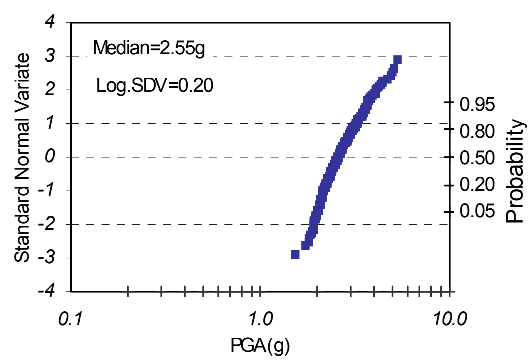

(d) $\hat{c}_4$

Figure 4. Lognormal Plot of Realizations of $\hat{c}_1$, $\hat{c}_2$, $\hat{c}_3$ and $\hat{c}_4$

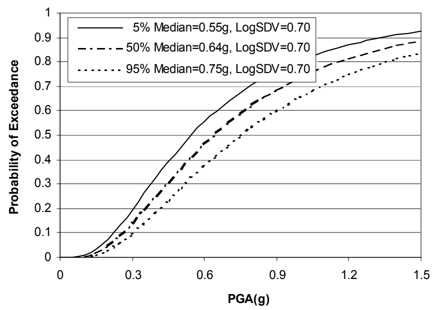

(a) at least minor damage

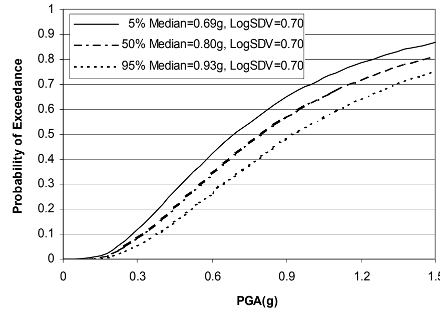

(b) at least moderate damage

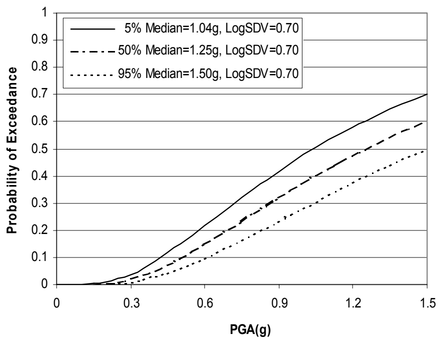

(c) at least major damage

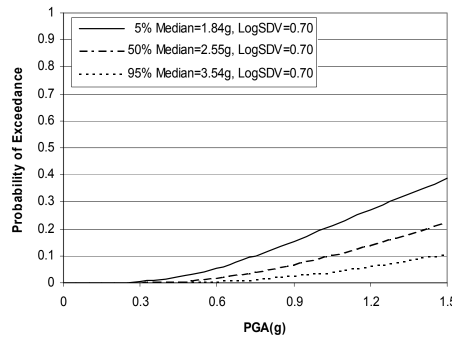

(d) collapse

Figure 6 Confidence Band

FRAGILITY CURVES ACCORDING TO BRIDGE ATTRIBUTES

It is reasonable to sub-divide the sample of the Caltrans' bridges into a number of sub-sets in accordance with the pertinent bridge attributes and their combinations. The sample can then be sub-divided into a number of sub-sets according to the bridge attributes, soil condition and their combinations. Figure 7 shows the empirical fragility curves considering skew angle of bridges. Seismic performance of bridges can be enhanced by retrofit measures (Shinozuka and etc., 2002). Figure 8 depicts the enhancement in each damage states of bridge after retrofitting.

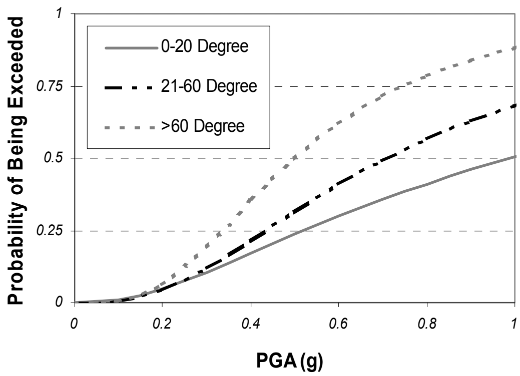

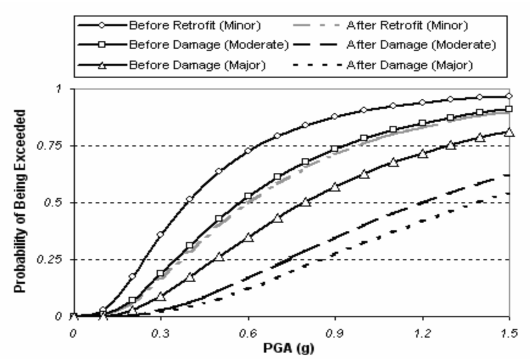

Figure 7 Effect of skew

Figure 8 The effect of retrofit

SIMULATION OF FRAGILITY CURVES

From seismic response of bridges, analytical fragility curves are developed following the statistical analysis procedure described in the previous part of the paper. Sixty ground motion time histories (selected for FEMA/SAC project; *http://quiver.eerc.berkeley.edu:8080/studies/system/motions*) of Los Angeles earthquakes are considered for this nonlinear dynamic analysis. To compare these analytically obtained fragility curves with empirical ones, empirical fragility curves for a third level subset (considering 'multiple span' and 'soil type C') have been accounted. Results indicate that the analytical curves are more probable to exceed a damage state than empirical ones (Shinozuka and Banerjee, 2004). In order to explain the discrepancies observed between the analytical and empirical fragility curves it is imperative to revisit the issue of defining the damage states of bridges. It was also understood that the new definition of the damage states are required to minimize the difference between the analytical and empirical results.

Bridge Models

Three different Caltrans' reinforced concrete bridge models with various geometric configurations are considered to compare the analytical and empirical fragility curves. Details of these example bridges are given in Table 1. The geometric configurations of the example bridges are shown in Figure 9.

TABLE 1
DESCRIPTION OF THREE (3) SAMPLE BRIDGES

Bridge	Overall Length	Number of Spans	Number of Hinges	Column Height
1	242 m	5	1	21.0 m
2	500 m	12	1	12.8 m
3	483 m	10	4	9.5 ~ 34.4 m

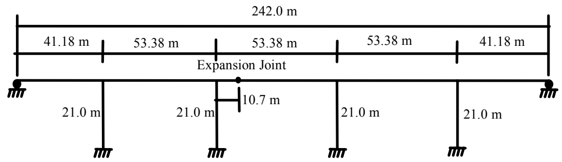

(a) Bridge 1

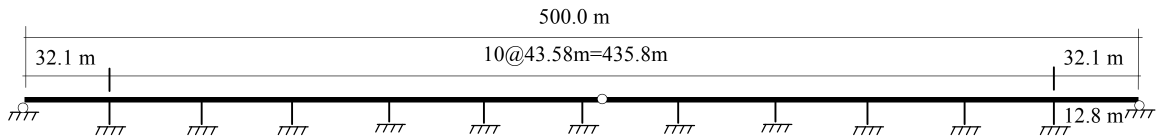

(b) Bridge 2

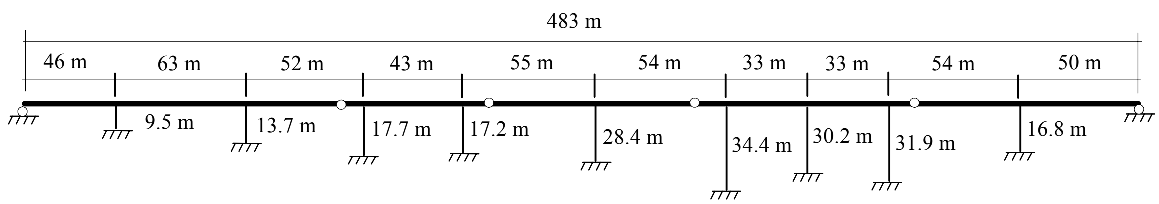

(c) Bridge 3

Figure 9 Elevation of sample bridges

Estimation of Ductility Capacities at Various Damage States

This study aims to define the damage states of bridges in terms of ductility capacity, which will produce fragility curves similar to empirical curves. Seismic response of bridges from nonlinear time history analysis for sixty ground motions is used as input in this part of analysis. While comparing with empirical fragility curves, numerical analysis is done to get best-fit distribution, for minor, moderate and extensive damage states and their corresponding ductility capacities. As stated earlier, it is assumed that fragility curves can be expressed in the form of two-parameter lognormal distribution functions. The parameters (median, c_0 and log-standard deviation, ζ_0) of each fragility curve are independently estimated by means of the maximum likelihood procedure as described in Eq. 2.

Alone with the optimization algorithms prescribed in Eq. 10, another optimization is done to minimize the difference between parameters of empirical fragility curves (median, c_{emp} and log-standard deviation, ζ_{emp}) and those obtained in the described analytical procedure (i.e. c_0 and ζ_0). In order to arrest the proper value of ductility capacity at each damage state, which will produce the analytical fragility corves similar to empirical curves, the above two optimization procedures have been performed simultaneously. Figure 10 shows the empirical fragility curves and simulated fragility curves for three already stated damage states of Bridge 1. Obtained ductility capacities at each damage states for the three example bridges are tabulated in Table 2.

TABLE 2
SIMULATED DUCTILITY CAPACITIES OF SAMPLE BRIDGES

Bridge No	Ductility capacities at various damage states		
	Minor	Moderate	Extensive
1	4.5	6.5	16.8
2	4.5	8.4	12.8
3	6.9	7.31	14.5

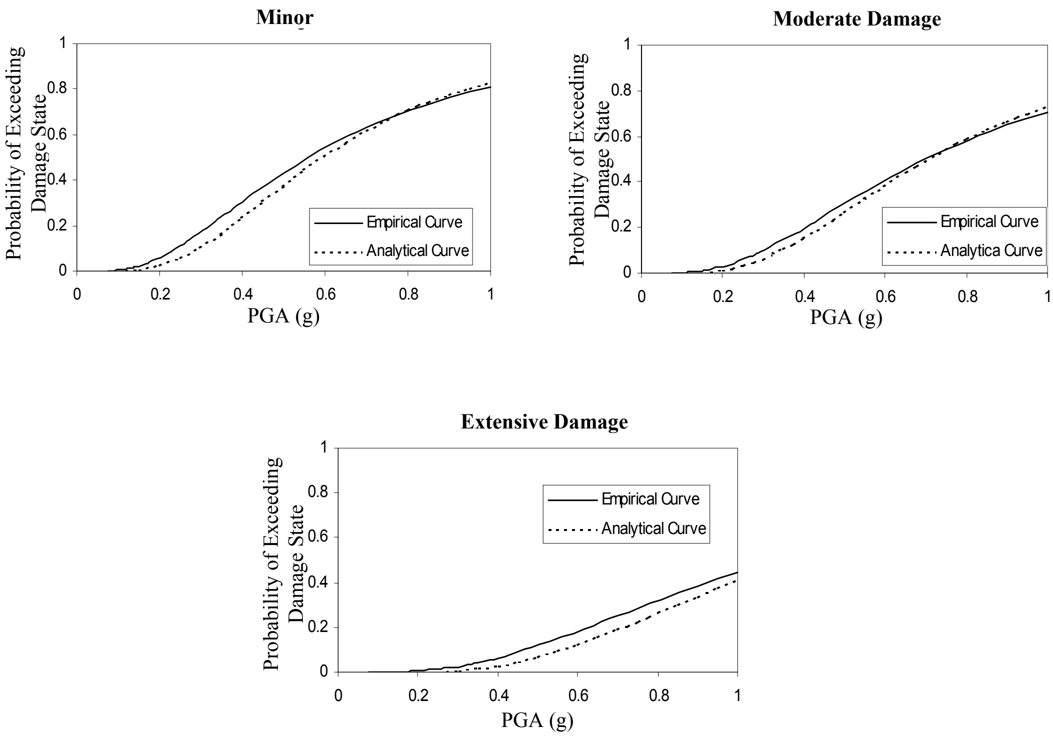

Figure 10 Empirical fragility curves and simulated fragility curves for three damage states of Bridge 1

Figure 11 shows the simulated ductility capacities for various damage states represented by damage state indices. In the figures, the damage states have been indicated by damage state indices 1, 2, and 3. 'Damage State Index 1' stands for 'Minor Damage', while 2 and 3 indicate 'Moderate' and 'Extensive' damage respectively.

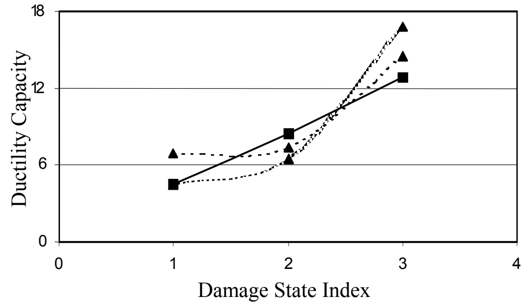

Figure 11 Ductility Capacities of Various Damage States

CONCLUSION

The relationship between empirical and analytical fragility curves is highlighted for the purpose of further improvement of the method of analytical fragility curve development. In this respect, this paper demonstrated the importance of calibration of the analytically developed fragility curves to model the effect of seismic retrofit and to define the threshold of ductility capacity of the bridge columns between different damage states.

Acknowledgments

This study was partially supported by California Department of Transportation and partially by the Multidisciplinary Center for Earthquake Engineering Research under the auspices of National Science Foundation.

References

Shinozuka, M., Feng, M.Q., Kim, H.-K., Uzawa, T., and Ueda, T. (2003). Statistical Analysis of Fragility Curves. *Technical Report at Multidisciplinary Center for Earthquake Engineering Research*, MCEER-03-0002, 2003.

Shinozuka, M., Feng, M.Q., Lee, J., and Naganuma, T. (2000). Statistical Analysis of Fragility Curves. *ASCE Journal of Engineering Mechanics*, 126:12, 1224-1231.

Shinozuka, M., and Banerjee, S. (2004). Dynamic Progressive Damage model for Bridges under Seismic Excitation. *Proceeding of International Conference in Commemoration of 5th Anniversary of the 1999 Chi-Chi Earthquake*, Taiwan, Sep. 8-9, 2004

Shinozuka, M., Kim, S-H., Yi, J-H., and Kushiyama, S. (2002). Fragility curves of concrete bridges retrofitted by column jacketing. *Earthquake Engineering and Engineering Vibration*, 1:2, December, 2002

Zhou Youwei and Shinozuka Masanobu, Model-based Uncertainty Analysis of Bridge Fragility Curves. *ASCE 17th Engineering Mechanics Conference*, Univ. of Delaware, Newark, DE, June 13-16, 2004.

Investigation of Displacement Ductility Capacity for Tall Piers

Jian-zhong Li, Li-chu Fan, Xiao-dong Song

Abstract

In this paper, the incremental dynamic analysis (IDA) is used to investigate the effect of higher vibration modes on the displacement ductility capacity of a tall pier. The results show that if the conventional method is used to evaluate the displacement ductility capacity of tall piers, there will be large error. The contribution of higher vibration modes to response has a significant effect on the yield, ultimate displacement and displacement ductility capacity for a tall pier.

Jian-zhong li, Department of Bridge Engineering, Tongji University. Shanghai 200092, PRC
Li-chu Fan, Department of Bridge Engineering, Tongji University. Shanghai 200092, PRC
Xiao-dong Song, Department of Bridge Engineering, Tongji University. Shanghai 200092, PRC

1 INTRODUCTION

The west mountainous areas of China are the high seismic zones. At these areas, a lot of multi-span continuous deck highway bridges have been built crossing mountain valley. Because of the rugged topography, height of many bridge piers in these areas have been excesses to 40m, some of them have reached about 90m.

During the past three decades, considerable experimental and theoretical research on the ductility capacity of the piers has been carried out [1,2]. In these studies, the ductility capacity for a pier is represented by displacement ductility capacity, which is determined by the yield and ultimate displacements. Through the use of moment-curvature analysis of bridge columns, the yield and ultimate curvature are calculated depend on the column axial load ratio. The yield and ultimate curvatures are used to determine the yield and ultimate displacements by the conventional method (the static method). In this method, the curvature is assumed with a linear distribution along the pier height before yield of reinforcements and plastic curvature is assumed to be constant over the equivalent plastic hinge length, and the effect of higher vibration modes of pier itself can not be considered [3]. For the piers with a lower height and a small mass, this conventional method is suitable, since the piers respond predominantly in its first mode of vibration. However, for the pier with a tall height, a large mass and a long period, neglect of higher mode effects of pier itself will result a large error.

Incremental dynamic analysis (IDA) [4] is a parametric analysis method that has recently emerged in several different forms to estimate more thoroughly structural performance under seismic loads. It involves subjecting a structural model to one (or more) ground motion record (s), each scaled to multiple levels of intensity, thus producing one (or more) curve (s) of response parameterized versus intensity level. By analogy with passing from a single static analysis to the incremental the non-linear static pushover, one arrives at the extension of a single time-history analysis into an incremental one, where the seismic ‘loading’ is scaled.

In this paper, in order to consideration of higher mode effects of tall piers, IDA is used to estimates of the displacement ductility capacity of the tall piers. For simplicity, only single pier model is considered in this paper.

2 THE LIMITATION OF CONVENTIONAL METHOD

Conventionally, displacement ductility capacity for a pier can be estimated as:

$$\mu_m = \frac{u_m}{u_y} \qquad (1)$$

where, u_y is the yield displacement of the pier corresponding to equivalent yield curvature, and u_m is ultimate displacement corresponding to the ultimate curvature, as shown in Fig 1.

It can be seen from Eq.(1) that displacement ductility capacity is determined by the yield and ultimate displacements. Conventional method for calculating the yield and ultimate displacements are as following:

The curvature is assumed with a linear distribution along the pier height before yield of reinforcements, as shown in Fig.1. Then, the yield displacements can be estimated as:

$$u_y = \frac{1}{3}\phi_y H^2 \tag{2}$$

The plastic curvature is assumed to be constant over the equivalent plastic hinge length, so the ultimate displacement can be determined by

$$u_m = L_p(\phi_u - \phi_y)(H - \frac{L_p}{2}) + u_y \tag{3}$$

where, ϕ_y is equivalent yield curvature; ϕ_m is ultimate curvature; L_p is the equivalent plastic hinge length.

For a pier with a tall height, a large mass and a long period, the contributions of higher modes to response are significant. When the effect of high modes and inertia force of pier itself are considered, the curvature distribution along the height of the pier will be very complicated and the assumption of linear curvature distribution along the pier height at structural yield is invalid. At ultimate state, multiple plastic hinges may be formed because of the contributions of higher modes to response and a redistribution of inertia forces. The assumption that plastic curvature is constant over the equivalent plastic hinge length will result a large error. Therefore, for the tall piers, Eq.(2) and Eq.(3) are not suitable to used to estimate yield and ultimate displacement when the contributions of higher modes of pier itself to response are considered.

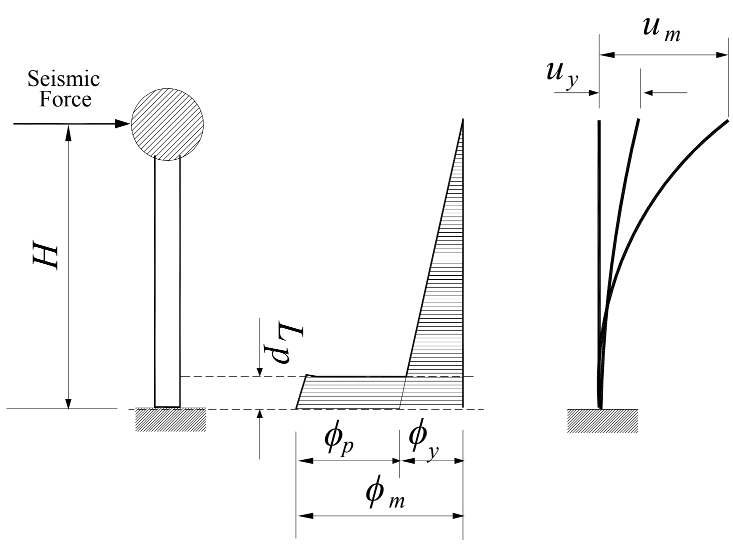

Fig.1 Idealized curvature distributions corresponding to yield and ultimate flexural failure

3 INCREMENTAL DYNAMIC ANALYSIS

Incremental dynamic analysis (IDA) is a parametric analysis method that has recently emerged in several different forms to estimate more thoroughly structural performance under seismic loads. It involves subjecting a structural model to one (or more) ground motion record(s), each scaled to multiple levels of intensity, thus producing one (or more) curve(s) of response parameterized versus intensity level. Methods like the non-linear static pushover (SPO) or the capacity spectrum method [5] offer, by suitable scaling of the static force pattern, a 'continuous' picture as the complete range of structural behaviour is investigated, from elasticityto yielding and finally collapse, thus greatly facilitating our understanding. By analogy with passing from a single static analysis to the incremental SPO, one arrives at theextension of a single time-history analysis into an incremental one, where the seismic 'loading' is scaled.

IDA involves a series of dynamic non-linear runs performed under scaled images of an accelerogram, whose scale factor are, ideally, selected to cover the whole range from elastic to non-linear and finally to collapse of the structure. IDA addresses both demand and capacity of structures. It can be applied to multimode structural response and considered higher mode effects. In this paper, IDA is used to determine yield and ultimate displacements of a tall pier. The main procedure for determination of yield displacement, ultimate displacements and ductility is described as following:

(1) For the acceleration time-history, selected from a ground motion database, which will be referred to as the base $\boldsymbol{a_1(t)}$, a vector with elements $a_1(t_i)$, t_i=0, t_1, ……, t_{n-1}, a simple transformation is introduced by uniformly scaling up or down the amplitudes by a scalar $\lambda \in [0,+\infty]$: $\boldsymbol{a}_\lambda = \lambda \boldsymbol{a}_1$. Here, λ is defined as scale factor (SF). Note how the SF constitutes a one-to-one mapping from the original accelerogram to all its scaled images. A value of λ=1 signifies the natural accelerogram, λ< 1 is a scaled-down accelerogram, while λ>1 corresponds to a scaled-up one.

(2) A series of dynamic non-linear runs performed under scaled images of an accelerogram, whose SF are, ideally, selected to cover the whole range from elastic to non-linear and finally to collapse of the structure. The purpose is to record damage measure (DM) of the structural model at each level of the scaled ground motion.

(3)A curvature IDA curve is a plot of a maximum curvature at the bottom section of a pier recorded in an IDA study versus scale factor that characterize the applied scaled accelerogram as shown in Fig.2a.

(4) A displacement IDA curve is a plot of a maximum horizontal at the top of a pier recorded in an IDA study versus scale factor that characterize the applied scaled accelerogram as shown in Fig.2b.

(5)Find the yield and ultimate curvature from the curvature IDA curve and determine the scale factors corresponding to yield and ultimate curvature (as shown in Fig.2a). Find the yield and ultimate displacement from displacement IDA curve (as shown in Fig.2.b).

(6) The ductility capacity μ_m is estimated by Eq.(3)

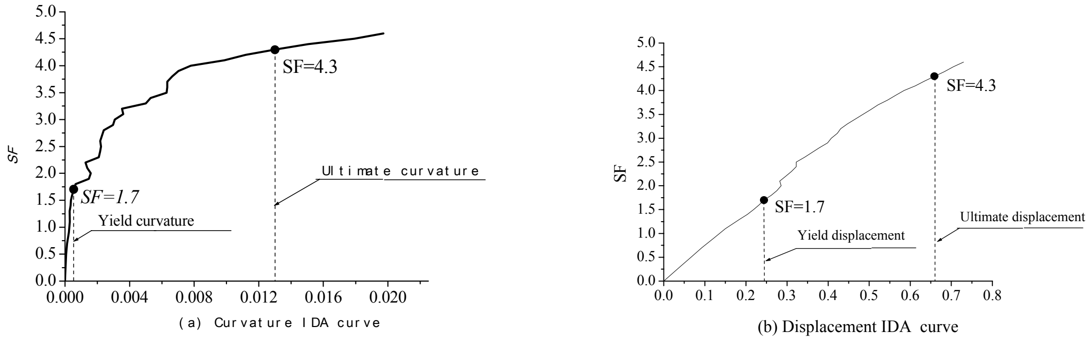

Fig 2 IDA Curve for a pier

4 THE DUCTILITY CAPACITY OF THE TALL PIER

4.1 The computer model and method

In order to investigate higher mode effects on the ductility of tall piers, incremental dynamic analysis and non-linear static pushover analysis are used to estimate ductility capacity for the piers with height 30m and 60m, respectively. The 30m pier represents a pier with moderate height, and 60m pier represents a tall pier.

The section size, mass and longitudinal reinforcement ratios are shown in Tab.1 and Fig.3, respectively. The strength of concrete is 30Mpa and strength of reinforcement is 340Mpa. The equivalent mass of girder to the top of pier is 700t.

In order to investigate the effects of higher modes, a single pier is equivalent to a single mass model and multi-mass model based on that fundament period of both of models is equal, as shown in Fig.4. The mass of girder is equivalent to the top of the piers. Five different ground motions as shown in Tab.2 is chosen for IDA. The lateral forces distribution over the pier height for non-linear static pushover is adopted as [5]

$$\boldsymbol{s}_1 = \boldsymbol{m}\boldsymbol{\phi}_1 \quad [4]$$

where, $\boldsymbol{\phi}_1$ is the fundamental vibration mode and $\boldsymbol{m}$ is the mass.

The computer program DRAIN-3DX [6] was used to perform the non-linear static pushover and incremental dynamic analysis of structure. The inelastic three-dimensional beam-column element with a fiber element of the cross section was used to model each column of the piers. Each fiber has a specified stress-strain relationship, which can be specified to represent unconfined concrete, confined concrete, and longitudinal steel reinforcement. The distribution of inelastic deformation and forces is simply by specifying cross section slices along the length of the element. In this study, Mander's model for confined concrete and unconfined concrete (7) were used to represent the stress-strain behavior of concrete. Five ground motion records as shown in Tab.2 are used when incremental dynamic analysis is carried out.

Tab.1 Properties of the piers

Height (m)	d (m)	Mass of pier m(t)	Equivalent mass of girder M(t)	M/m	Axial load ratio	Reinforcement ratio (%)
30	3.2	336	700	0.48	0.0825	1.27
60	3.8	816	700	1.17	0.100	1.27

Note：Mass of pier is total of each mass m_1， m_2 … m_n

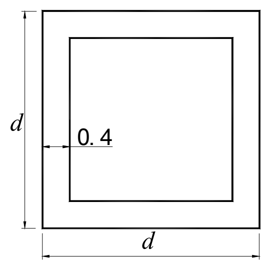

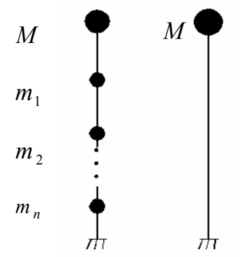

Fig.3 The cross section of the pier   Fig. 4 Multi-degrees and single degree mode for the pier

Tab.2 Free-Field Ground Motions

Earthquake record	Location
El centro	1940, El Centro North South Component
Loma-p1	OCTOBER 17, 1989, LOMA PRIETA EARTHQUAKE
Nridge1	JANUARY 17, 1994, NORTHRIDGE EARTHQUAKE
Oakwh1	OCTOBER 17, 1989, LOMA PRIETA
Sanfern1	FEBRUARY 9, 1971, SAN FERNANDO EARTHQUAKE

5.2 Numerical result

A curvature IDA curve and displacement IDA curve for 30m and 60m piers under the El-centro ground record are shown in Fig.5 and Fig.6, respectively. Two curves are shown on each plot of Fig. 5 and Fig.6. The first curve (the dashed line) is result of single degree model and the second curve (real line) is the result of multi-degree model. The yield and ultimate displacements estimated by the non-linear static pushover and incremental dynamic analysis are presented at Tab.3。

From Fig.5 and Fig.6, it can be seen that when the SF (scale factor) is small, the result from single degree and multi-degree model are close. However, as the SF is increased, the two curves deviate gradually. For the 30m pier, the deviation is relative small, but for the 60m pier, the deviation is very large. When the SF reaches 5, the difference between the result from multi-degree and single degree model is about three times due to contribution of higher modes to structural response. From Tab.3, it can be seen that yield displacement, ultimate displacement and displacement ductility capaciy estimated by the multi-degree model for the 60 m pier is less than those estimated by the single model.. These results show that the contributions of higher modes have a significant effect on the yield displacement, ultimate displacement and displacement ductility capacity of the tall pier, and the neglect of effects of higher modes will result large error. However, for 30m pier, the results estimated by incremental dynamic analysis using multi-degree mode, single degree model and non-linear pushover analysis are close to each other and the contribution of higher modes can be ignored. The conventional method is suitable to estimate yield displacement, ultimate displacement and ductility factor for a pier with moderate height.

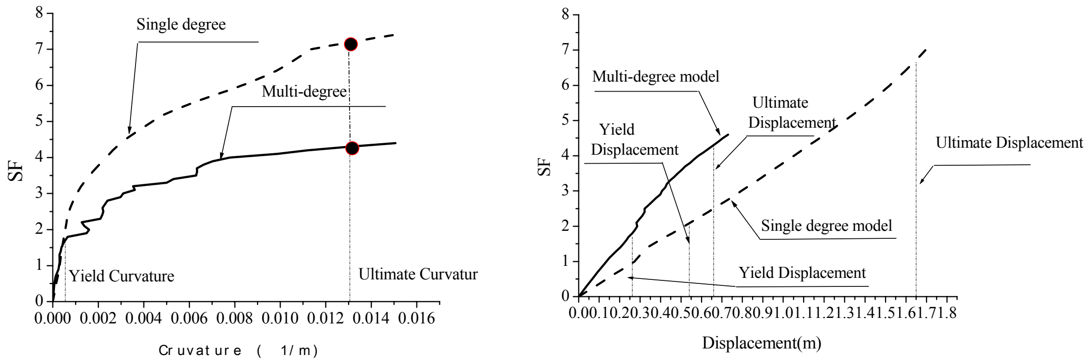

a) Curvature IDA curve b)Displacement IDAcurve

Fig.5 IDA curve for the 60m pier

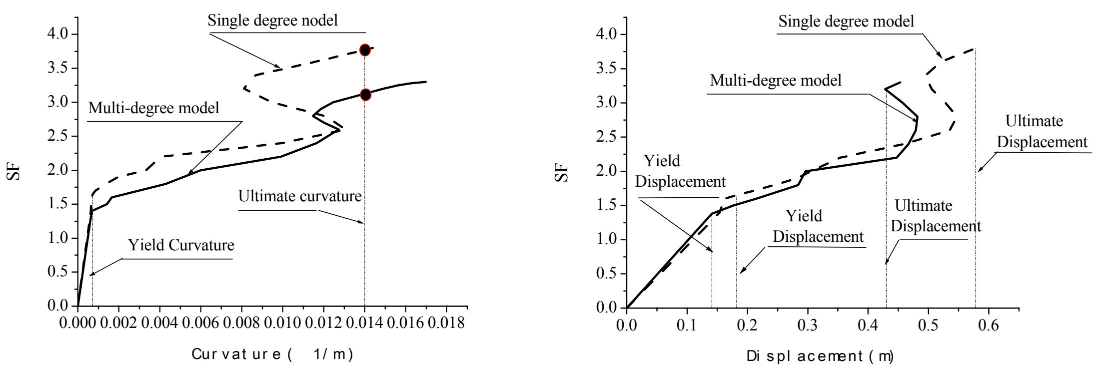

a) Curvature IDA curve b)Displacement IDAcurve

Fig 6 IDA curve for the 30m pier 30m

Tab.3 Results from IDA and non-linear pushover

Height of pier (m)	IDA						SPO		
	Multi-degree model			Single model					
	Yield Displacement u_y(m)	Ultimate Displacement u_m(m)	Ductility factor μ_m	Yield Displacement u_y(m)	Ultimate Displacement u_m(m)	Ductility Capacity ${}_m\mu_m$	Yield Displacement u_y(m)	Ductility factor u_m(m)	Ductility factor μ_m
30	0.141	0.43	3.05	0.182	0.578	3.18	0.176	0.526	2.99
60	0.2618	0.6595	2.52	0.54	1.65	3.05	0.50	0.158	3.16

The curvature and horizontal displacement distribution over height of the 60 m pier estimated by multi-degree model at the moment when the curvature of bottom section reaches maximum value (t=2.91s) and the horizontal displacement at the top of the pier reaches maximum value (t=4.86) are shown in Fig.7a and Fig.7b, respectively. In this case, The SF equals 1.7. For comparison, the curvature and horizontal displacement distribution get by single degree model is also drawn at Fig. 7. For the result obtained by single degree model, the curvature or horizontal displacement distribution over height of the pier will be same at the moment when curvature of bottom section reaches maximum value and the horizontal displacement on the top of the pier reaches maximum value. From Fig.7, it can be seen clearly that the maximum displacement at the top of the pier do not correspond to the maximum curvature at bottom section of the pier when the contributions of higher modes are considered. Similar as Fig.7, Fig.8 represents the curvature distribution over the 30m pier when SF equals 1.38 and 3.2 respectively. From Fig.8, it can be seen that curves of curvature distribution from multi-degree model and single degree model are closely approached.

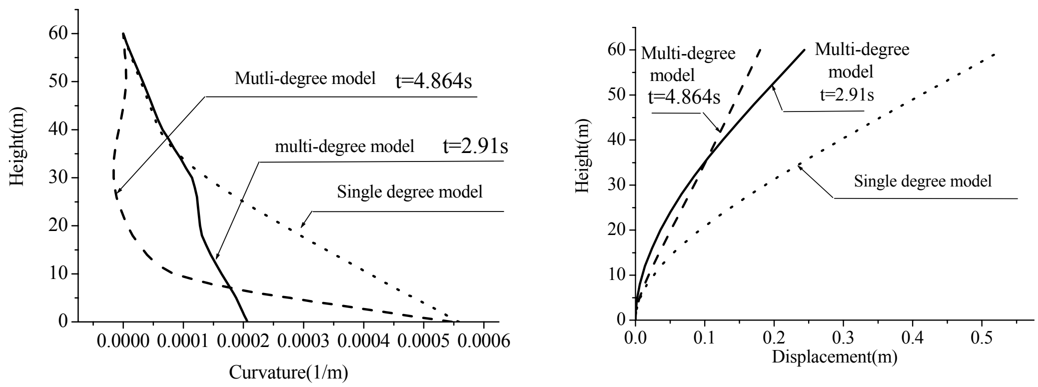

（a） Curvature distribution for SF=1.7 （b） Displacement distribution for SF=1.7

Fig.7 Curvature and displacement distribution for the 60m pier

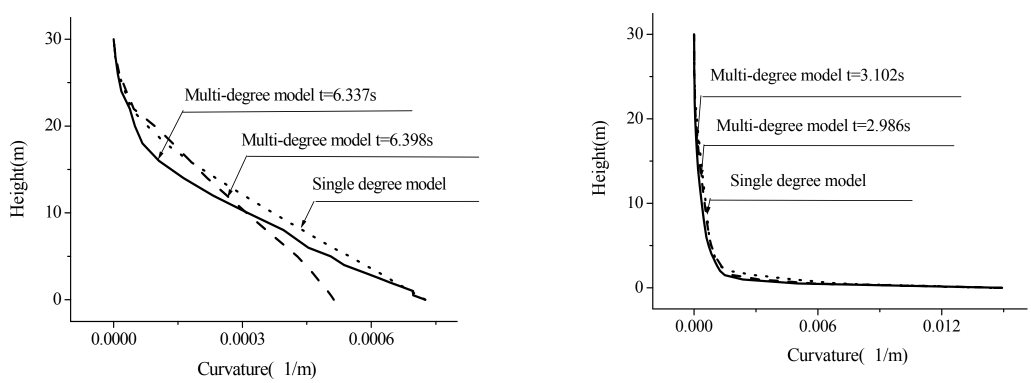

(a) Curvature distribution for SF=1.38 (b) Curvature distribution for SF=3.2

Fig. 8 Curvature distribution for the 30m pier

The yield displacement, ultimate displacement and displacement ductility capacity estimated by incremental dynamic analysis using multi-degree model for the 60m pier under different earthquake records is shown in Tab.4. For a tall pier, when the contribution of higher models is considered, input of different ground motions have some effects on the yield displacement, ultimate displacement and ductility factor.

Tab.4 Ductility factor of 60m pier under different earthquake records

	elcentro	Loma-p1	Nridge1	Oakwh1	Sanfern1
Yield displacement（m）	2.6168e-1	3.5126e-1	2.6483e-1	3.3561e-1	4.0676e-1
Ultimate displacement（m）	6.5948e-1	6.7501e-1	5.4087e-1	6.755e-1	7.2308e-1
Ductility factor	2.52	1.92	2.04	2.01	1.77

5 CONCLUSION

In this paper, incremental dynamic analysis is used to investigate yield displacement, ultimate displacement and ductility of tall piers. The results show that:：

1) For the pier with tall height, large mass and long period, the effects of higher modes of pier itself is significant. The current conventional method may result a large error when it is applied to estimated ductility of tall pier.
2) The maximum displacement at the top of the pier do not correspond to the maximum curvature at bottom section of the pier for tall pier.
3) For tall piers, when the contribution of higher models is considered, input of different ground motions have some effects on the yield displacement, ultimate displacement and displacement ductility capacity.
4) Incremental dynamic analysis IDA is a very effect method to estimate yield, ultimate displacement and displacement ductility capacity for a tall pier.

Reference

M.J.Kowalsky.Deformation limit states for circular reinforced concrete bridge column[J].Journal of Structural Engineering ASCE,2000,126(8):869-878.

Priestley, M. J. N., Seible, F. and Calvi, G. M. Seismic Design and Retrofit of Bridges. New York: John Wiley & Sons, 1996

Seismic design criteria[s], version1.2, California department of transportation, 2001

Dimitrios Vamvatsikos, C.Allin Cornell. Incremental dynamic analysis， Earthquake Engineering And Structural Dynamics, 2002; 31:491-514

Anil k. Chopra, Rakesh k. Goel, a modal pushover analysis procedure for estimating seismic demands for buildings[J]. Earthquake Engineering And Structural Dynamics,2002; 31:561-582.

Prakash,V.;Powell,G.; and Campbell, S., DRAIN-3D Base Program Description and User Guide; Version 1.10, Report No.UCB/SEMM-93/17, Department of Civil Engineering, University of California, Berkeley, Calif., 1993.

Mander,J.B., Priestly, M.J.N and Park, R. Theoretical Stress-Strain Model for Confined Concrete. Journal of Structural Engineer, ASCE, 1988, Vol. 114(8).

Proof-of-Concept Testing of a Laterally Stable Eccentrically Braced Frame for Steel Bridge Piers

Jeffrey W. Berman and Michel Bruneau

ABSTRACT

Eccentrically braced frames have been shown to exhibit excellent seismic performance. However, eccentrically braced frames have had limited use in the steel piers of bridges due to the difficulty to provide the lateral bracing required to prevent possibility of lateral torsional buckling of the link. An eccentrically braced frame system in which lateral bracing of the link can be avoided, would make it desirable in the context of bridge seismic design and retrofit.

This paper describes the design and testing of a proof-of-concept eccentrically braced frame specimen that utilizes a hybrid rectangular shear link that is not laterally braced. Equations used for design, including plastic shear force, plastic moment, stiffener spacing, and limiting flange compactness ratio, are given and references for their derivations are provided. The quasi-static cyclic proof-of-concept testing is described and results are reported. Stable and full hysteretic loops were obtained and no signs of flange, web, or lateral torsional buckling were observed. The link was subjected to 0.15 radians of rotation in the final cycle, which is almost twice the maximum rotation allowed in building codes for links with I-shaped cross-sections. Although the final failure mode was fracture of the bottom link flange, the large rotations achieved were well above what would be required in a seismic event, indicating that hybrid rectangular links without lateral bracing of the link can indeed be a viable alternative for applications in steel bridge piers in seismic regions.

Jeffrey W. Berman, Department of Civil, Structural, and Environmental Engineering, University at Buffalo, Ketter Hall, Buffalo, NY, 14260, USA, jwberman@eng.buffalo.edu

Michel Bruneau, Department of Civil, Structural, and Environmental Engineering, University at Buffalo, Ketter Hall, Buffalo, NY, 14260, USA and Multidisciplinary Center for Earthquake Engineering Research, University at Buffalo, Red Jacket Quad, Buffalo, NY, 14261, USA, bruneau@mceermail.buffalo.edu

INTRODUCTION

Eccentrically braced frames have been shown to exhibit excellent seismic performance. However, eccentrically braced frames have had limited use in the steel piers of bridges due to the difficulty to provide the lateral bracing required to prevent possibility of lateral torsional buckling of the link. An eccentrically braced frame system in which lateral bracing of the link can be avoided, would make it desirable in the context of bridge seismic design and retrofit especially since eccentrically braced frames have been shown to exhibit excellent seismic performance (Roeder and Popov (1977), Hjelmstad and Popov (1983), Kasai and Popov (1986a), Kasai and Popov (1986b), Engelhardt and Popov (1989), among others).

From this motivation the concept of an EBF utilizing a rectangular hybrid cross-section for the link is explored (hybrid in this case meaning the yield stresses of the webs and flanges may be different). Rectangular cross-sections inherently have more torsional stability than I-shaped cross-sections and may not require lateral bracing.

This paper describes the design and testing of a proof-of-concept EBF having a link with a hybrid rectangular cross-section. First, equations used for design, including plastic shear force, plastic moment, stiffener spacing, and the limiting flange compactness ratio are given and references for their derivations are provided. Then, the specimen design and test setup are described. Finally, the experimental results are discussed and conclusions are drawn.

DESIGN EQUATIONS

A link with a hybrid rectangular cross-section is shown in Figure 1. Assuming the moment on the section is less than the reduced plastic moment (described below), the plastic shear force, V_p, for the cross-section is (Berman and Bruneau, 2004):

$$V_p = \frac{2}{\sqrt{3}} F_{yw} t_w \left(d - 2t_f\right) \tag{1}$$

where F_{yw} is the yield stress of the webs, t_w is the web thickness, d is the depth of the section, and t_f is the flange thickness. The plastic moment, M_p, for the cross-section shown in figure is:

$$M_p = F_{yf} t_f \left(b - 2t_w\right)\left(d - t_f\right) + F_{yw} \frac{t_w d^2}{2} \tag{2}$$

where F_{yf} is the yield stress of the flanges, b is the section width, and other terms are as previously defined. This plastic moment may also be reduced the presence of the plastic shear force, as a simple way of accounting for shear-moment interaction in the presence of the full plastic shear. The reduced plastic moment, M_{pr}, can be written as:

$$M_{pr} = F_{yf} t_f \left(b - 2t_w\right)\left(d - t_f\right) + 2F_{yw} t_f t_w \left(d - t_f\right) \tag{3}$$

As with links having I-shaped cross-sections, hybrid links with rectangular cross-sections fall into one of three categories, shear links, intermediate links, and flexural links. Classification of links can be done using the normalized link length, ρ, defined as $e/(M_p/V_p)$, where e is the link length. Links having $\rho \leq 1.6$ are shear links and the inelastic behavior is dominated by shear yielding of the webs. Links having $1.6 < \rho \leq 2.6$ are intermediate links, for which inelastic behavior is a mix of shear and flexural behavior, and links having $2.6 < \rho$ are flexural links where inelastic behavior is dominated by flexural yielding. These ranges are the same as those for I-shaped links, since there is no expected difference in the factors used to determine them, namely, overstrength and strain hardening (Berman and Bruneau, 2004). For I-shaped links, the AISC Seismic Provisions (AISC, 2002) limit the inelastic link rotation for shear links and flexural links to 0.08 rads and 0.02 rads, respectively, with linear interpolation based on normalized link length to be used for intermediate links. At this point there is no data indicating these limits should be different for hybrid rectangular links.

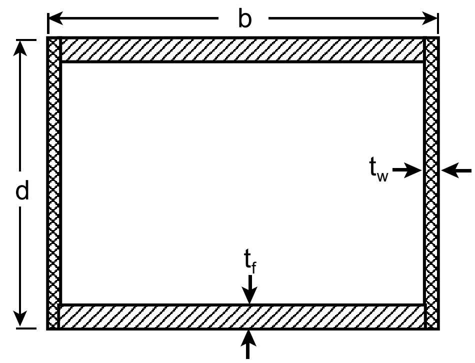

Figure 1. Hybrid Rectangular Link Cross-Section

Stiffener spacing limits for links with hybrid rectangular cross-sections have been proposed in Berman and Bruneau (2004). Their form is similar to that given in the AISC seismic provisions for I-shaped links which were derived by Kasai and Popov (1986a). It is proposed that stiffeners for shear links (maximum inelastic rotation of 0.08 rads) satisfy:

$$\frac{a}{t_w} + \frac{1}{8}\frac{d}{t_w} = 20 \tag{4}$$

where a is the stiffener spacing and all other terms are as previously defined. For intermediate links with a maximum link rotation of 0.02 rads, the stiffeners should satisfy:

$$\frac{a}{t_w} + \frac{1}{8}\frac{d}{t_w} = 37 \tag{5}$$

and linear interpolation can be used to find the maximum stiffener spacing for intermediate links with rotations between 0.08 and 0.02 rads. For flexural links, stiffeners are proposed at 1.5b from each end of the link as they are for I-shaped cross-sections.

Limiting web and flange compactness ratios are given for hollow structural sections (HSS) in the AISC seismic provisions as:

$$0.64\sqrt{E_s / F_y} \tag{6}$$

where E_s is Young's modulus for steel and F_y is the web or flange yield stress as appropriate. In the absence of finite element or experimental data for hybrid rectangular links, it is recommended that those limits be used. However, those limits are based on experimental results for HSS braces subject to repeated compression buckling. Therefore, they may not apply to the webs and flanges of hybrid rectangular links which are subject to large shear forces and bending moments. Berman and Bruneau (2004) derived the following limit for flange compactness based on inelastic plate buckling:

$$1.02\sqrt{E_s / F_y} \tag{7}$$

while for web compactness of shear links, it appears that it may be possible to satisfy either the Eq. (6) or Eq. (4) but not necessarily both. Again, more experimental evidence is necessary to assess the applicability of these limits before they can be codified.

The necessity for using hybrid rectangular cross-sections arises from the short link lengths required for HSS shapes that are listed in the AISC LRFD Manual of Steel Construction (AISC, 1998) to be shear links (i.e. have $\rho \leq 1.6$). The maximum length for a shear link, that also meets the compactness limits of Eq. (6), would be 460 mm and would be obtained with a HSS 250x250x16. Considering a 7.3 m wide by 3.7 m tall frame the drift at a plastic rotation of 0.08 rads is only 0.5% from (Bruneau et al., 1998):

$$\theta = \gamma \frac{e}{L} \tag{8}$$

where θ is the frame drift, γ is the link rotation, L is the frame width, and e is the link length. There may be instances where ductility demand exceeds this drift value. Additionally, a short link has a greater stiffness, which can translate into increased seismic demands on the surrounding framing and foundation. Furthermore, as a minor point, short links can cause congested details and fabrication difficulties. Therefore, hybrid rectangular cross-sections (Figure 1), which offer the ability to change the M_p over V_p ratio by changing the web and flange thicknesses independently, are desirable since they will allow longer link lengths while still having a shear link and the desired shear strength.

SPECIMEN DESIGN AND TEST SETUP

The proof-of-concept EBF with a hybrid rectangular shear link was designed to be as large as possible considering the constraints of the available equipment in the Structural Engineering and Earthquake Simulation Laboratory (SEESL) at the University at Buffalo (UB). Quasi-static cyclic loading was chosen and the maximum force output of the actuator available (1115 kN) was divided by 2.5 to account for the possibility of obtaining material with a higher than specified yield stress as well as strain hardening, making the design base shear 445 kN. The general test setup is shown in Figure 2. Assuming the moments at the middle of the link and clevises are zero, the design link shear can be found to be 327 kN for the dimensions shown. To design the link, the equations described above (i.e, link shear force, Eq. (1), and the AISC web and flange compactness limits Eq. (6)) were used in conjunction with enforcing a minimum link length such that a drift of at least 1% corresponds to a maximum link rotation of 0.08 rads and assuring $\rho<1.6$ (i.e., maintaining a shear link). The following link dimensions were selected: $d = b = 150$ mm, $t_f = 16$ mm, $t_w = 8$ mm, and $e = 460$ mm. A yield stress of 345 MPa was assumed for the steel during the design process and ASTM A572 Gr. 50 steel was specified for fabrication of the link beam which gave an anticipated link shear of 381 kN.

The framing outside the link was designed using capacity principles. Factors to account for the difference between specified and expected (i.e., mean) yield stress of the link material as well as strain hardening were incorporated, resulting in the member sizes shown in Figure 3.

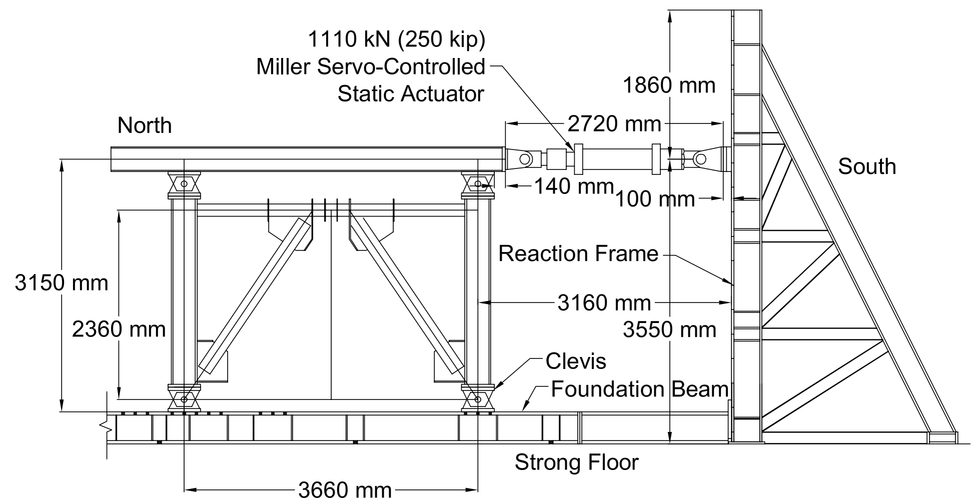

Figure 2. Test Setup

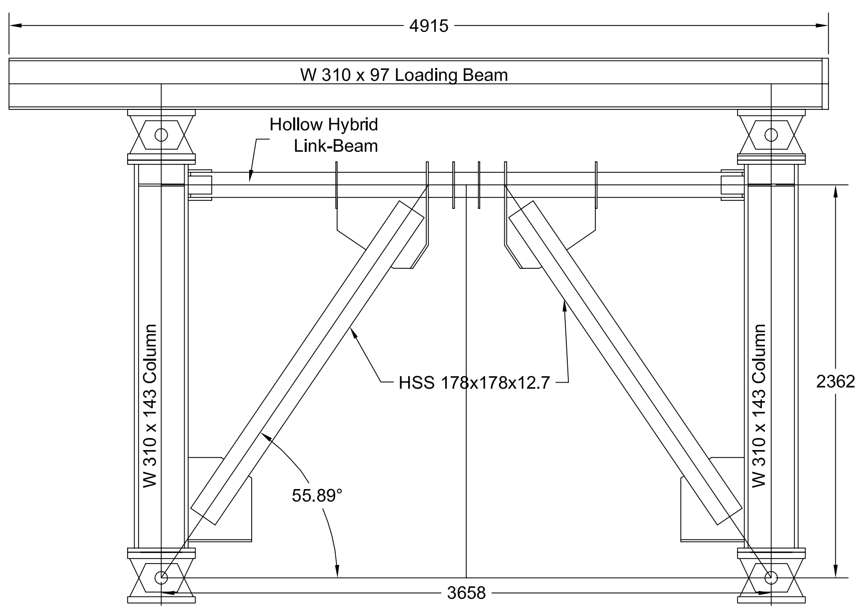

Figure 3. Test Specimen with Dimensions

Link stiffeners were placed at a spacing of 152 mm such that Eq. (5) was satisfied. A full penetration groove weld with the flange beveled at 45° was specified to assemble the link cross-section. The connection of the link to the eccentric braces was designed using standard procedures for the expected link capacity. Link and eccentric brace connection details are shown in Figures 4 and 5.

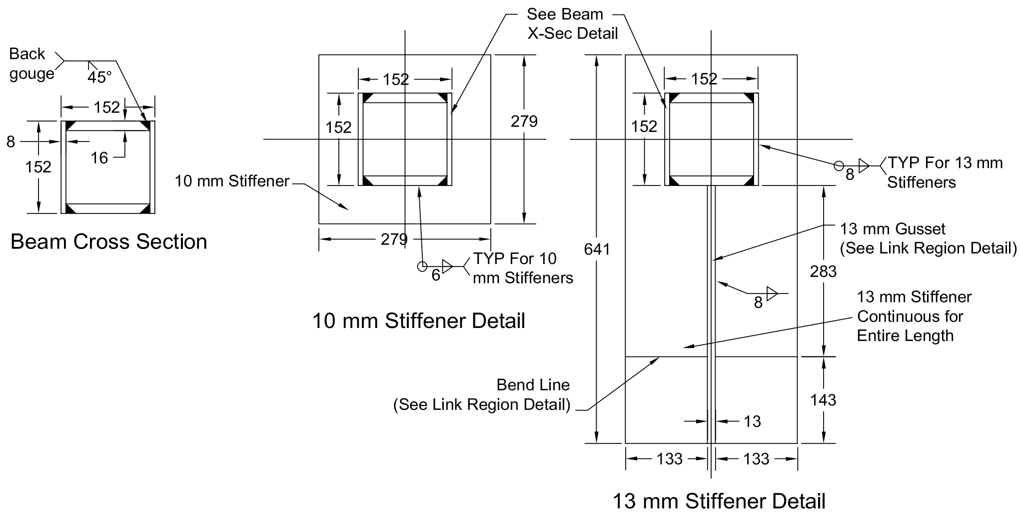

Figure 4. Link Cross-Section Details

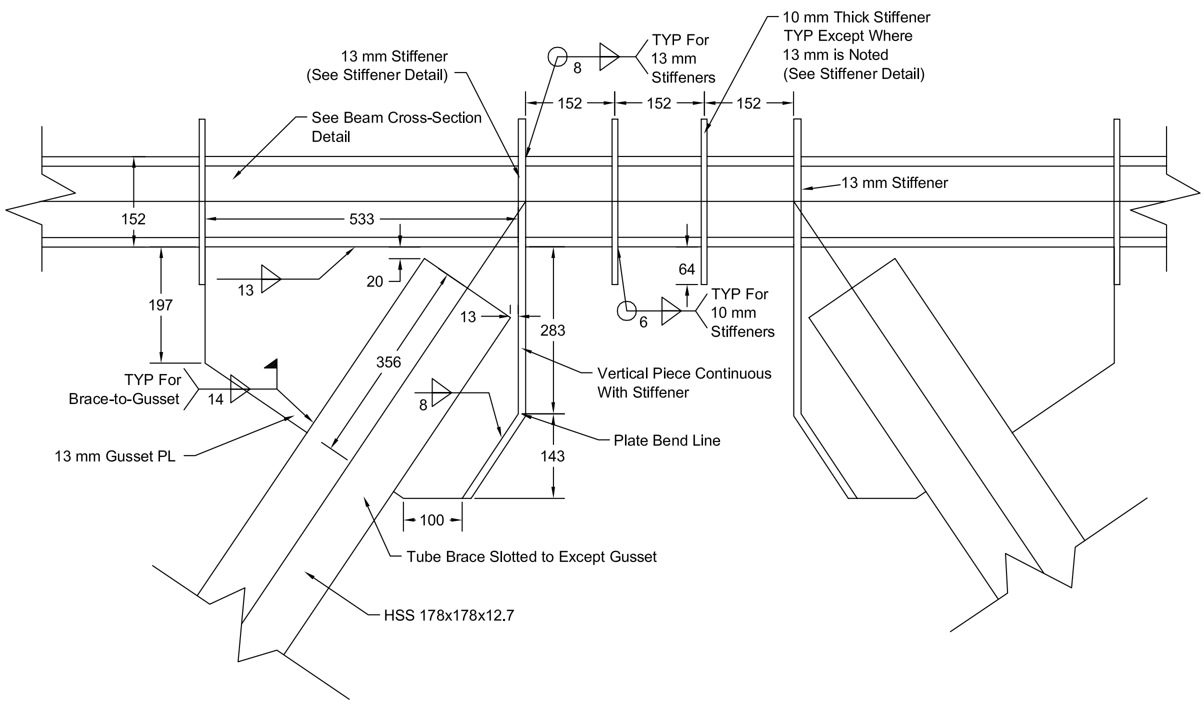

Figure 5. Link and Eccentric Brace Connection Details

Coupon tests of the delivered web and flange material for the link were performed and the results are shown in Figures 6a and 6b. As shown, the web material did not exhibit much of a yield plateau and the yield stress was found to be 448 MPa, which is significantly larger than the 345 MPa specified. The flange material had a defined yield plateau and a yield stress of 393 MPa. Using these yield stresses M_p and V_p were found to be 157.6 kN-m and 495 kN, respectively.

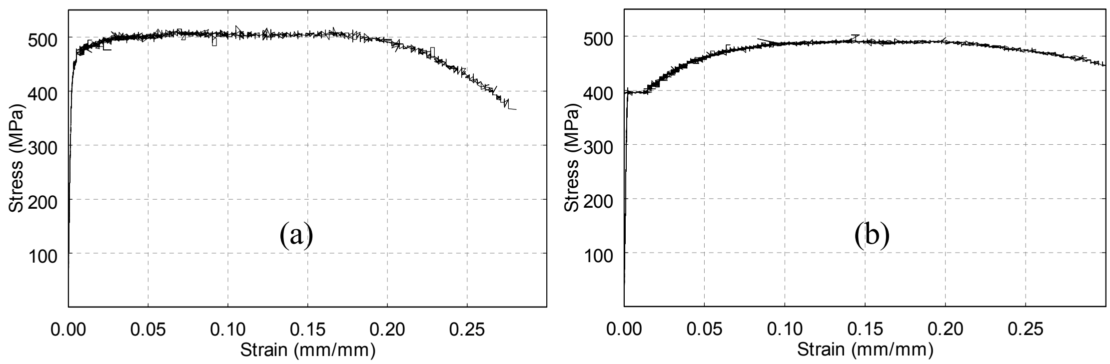

Figure 6. Coupon Test Results for (a) Web Material and (b) Flange Material

The specimen was instrumented with strain gauges and temposonic magnetic strictive transducers (temposonics). Strain gauges were placed such that the forces and moments in the framing members could be obtained as well as on the web and flanges of the link so that specimen yield could be verified. Temposonics were placed so that both link rotation and frame drift could be obtained.

Loading followed the ATC-24 protocol (ATC, 1992) which is illustrated in Figure 7. Force control was used for cycles up to 1δ_y while displacement control was used after that. The frame drift was used as the deformation control parameter.

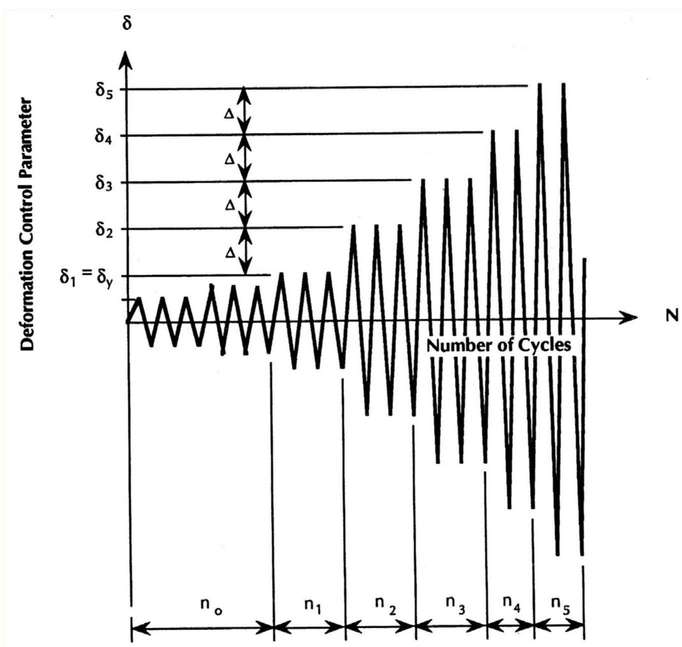

Figure 7. Loading Protocol

It should be noted that no lateral bracing was provided to the link, beam segments outside the link, eccentric braces, or columns. However, for safety, the loading beam shown in Figures 2 and 3 was laterally braced at points above the columns as shown in Figure 8. Figure 9 shows the completed test setup.

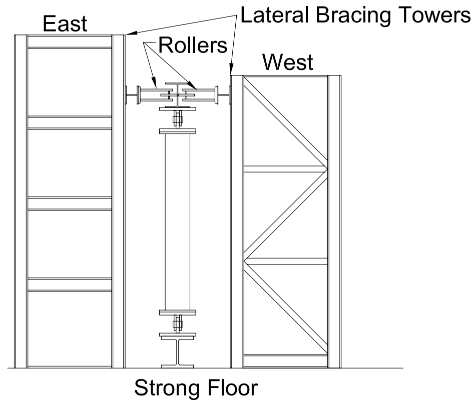

Figure 8. Lateral Bracing of Loading Beam

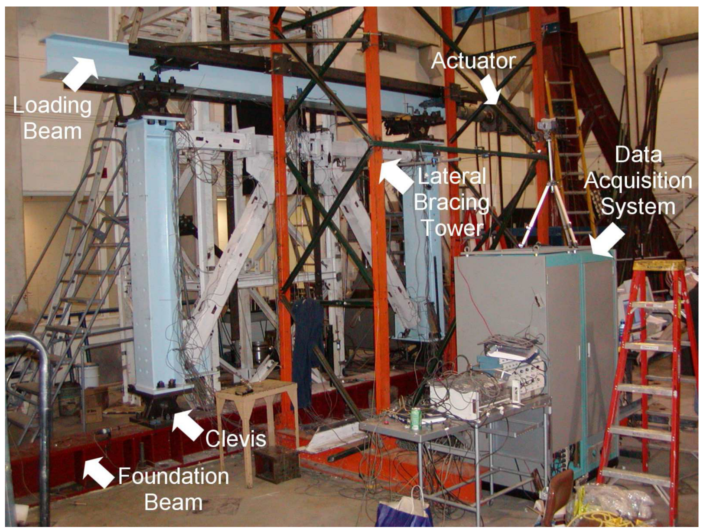

Figure 9. Completed Test Setup

EXPERIMENTAL RESULTS

The experimentally obtained base shear versus frame drift hysteresis is shown in Figure 10 and the link shear force versus link rotation hysteresis is shown in Figure 11. From the elastic cycles of Figure 10, the initial stiffness of the specimen was found to be 80 kN/mm. The yield base shear and frame drift were 668 kN and 0.37% while the maximum base shear and drift were 1009 kN and 2.3%, respectively. Link shear force and rotation at yield were 490 kN and 0.014, while the maximum link shear and rotation achieved were 742 kN and 0.151 rads, respectively. Projecting the elastic and inelastic slopes of Figure 11 leads to an approximation of the plastic link shear force of 520 kN. The link shear force at 0.08 rads of rotation (the current limit for shear links) was 689 kN. Assuming equal link end moments, the end moments at specimen yield, development of V_p, and 0.08 rads of rotation were 112 kN-m, 119 kN-m, and 158 kN-m, respectively, and the maximum link end moment was 170 kN-m.

The link achieved a rotation level 0.151 rads, which is almost twice the current limit for shear links in EBF for buildings (0.08 rads) and the target rotation for the specimen. Furthermore, the EBF reached a frame displacement ductility 6.0 and link rotation ductility of over 10 (the difference in these is due to the flexibility of the surrounding framing). Figure 12 shows the deformed link at 0.123 rads (1.92% drift) during Cycle 19.

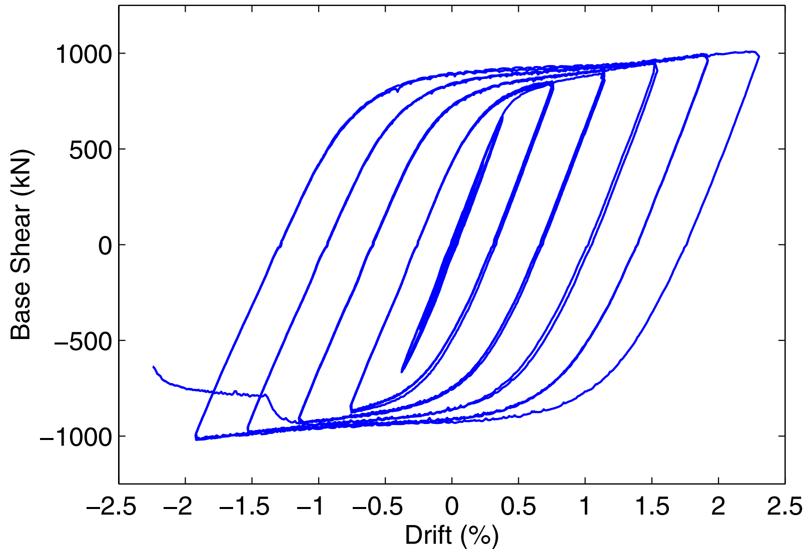

Figure 10. Base Shear vs. Frame Drift

Link failure occurred when the bottom flange at the north end of the link fractured as shown in Figure 13. The fracture occurred in the heat affected zone (HAZ) of the flange adjacent to the fillet weld used to connect the stiffener for the gusset of the brace-to-link connection to the link. Inspection of the failure surface was performed using a magnifying glass and light-microscope with 30x magnification (personal communication, Mark Lukowski, metallurgist, and Dr. Robert C. Wetherhold, mechanical engineer, Department of Mechanical and Aerospace Engineering, University at Buffalo, september 2003). The fracture was assessed as having initiated by cracking in the HAZ of the previously mentioned fillet weld and the propagation of those cracks under load reversals. There was no evidence of crack initiation in the full penetration groove weld used to assemble the webs and flanges of the link.

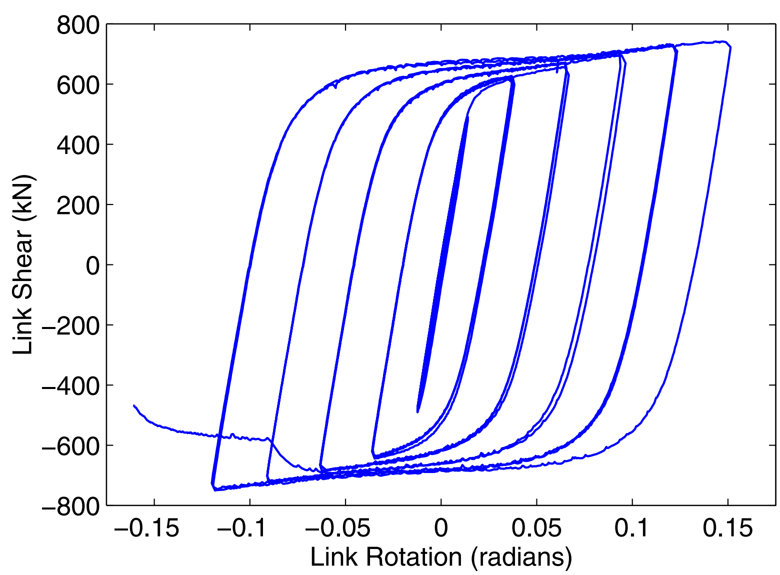

Figure 11. Link Shear vs. Link Rotation

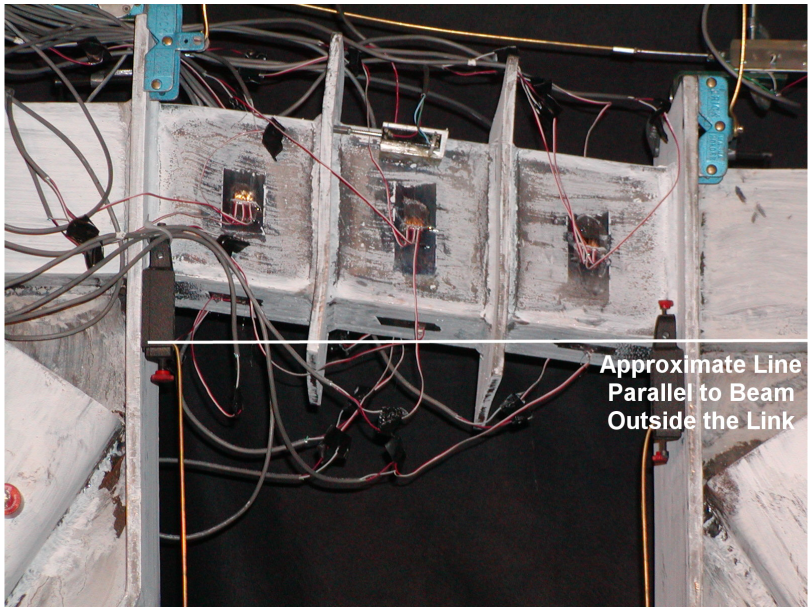

Figure 12. Link Deformed at 0.123 rads of Rotation During Cycle 19

The framing outside the link remained elastic for the duration of testing. Out-of-plane moments in the beam segments outside the link and eccentric braces remained less than 2.5% of those members' yield moments. This small moment can be resisted by the connections to the columns and need not be considered in design. Small out-of-plane moments and the fact that no evidence of lateral torsional buckling was observed, indicates that the goal of developing a link that does not require lateral bracing was achieved. Furthermore, a link rotation of almost double the maximum allowed in design codes for I-shaped links was achieved prior to any strength degradation, indicating that hybrid rectangular shear links are viable alternatives for new and retrofit construction of steel bridge piers. It should also be noted that no evidence of web or flange buckling was observed, indicating that in this case the stiffeners and compactness limits were effective in preventing those buckling modes.

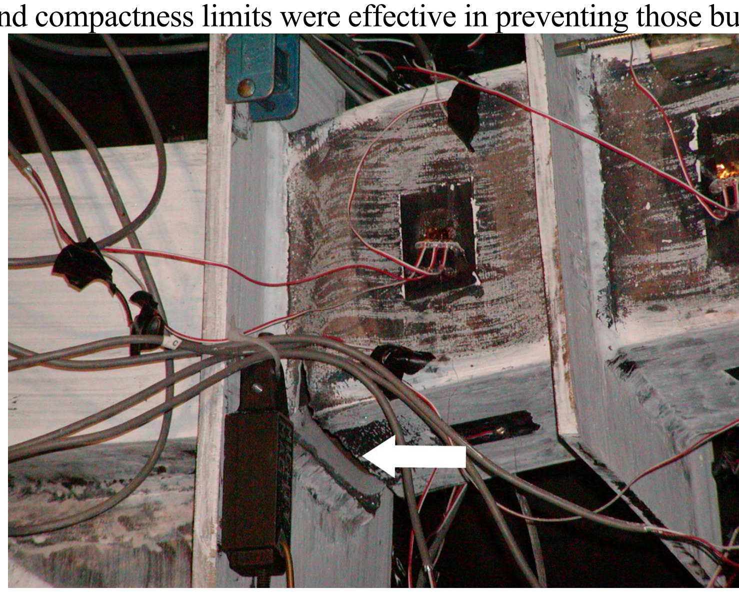
Figure 13. Fractured Bottom Flange at North End of Link

CONCLUSIONS

A laterally stable link for eccentrically braced frames for use in bridge piers where lateral bracing to prevent lateral torsional buckling is difficult to provide, has been developed. Selected design equations to achieve laterally stable hybrid rectangular links have been given and references for their derivations have been provided. The proof-of-concept testing of a single eccentrically braced frame with a hybrid rectangular shear link was successful in that it reached a link rotation of 0.151 rads (almost twice the maximum allowed in building codes for I-shaped links) without strength degradation and showed no signs of lateral torsional buckling. Link failure occurred after reaching a frame displacement ductility of 6 (which corresponded to a link rotation ductility of more than 10) when the bottom flange fractured at the north end of the link. The fracture was found to have started in the heat affected zone of the flange near the fillet weld used to connect the gusset stiffener for the eccentric brace connection to the link and was not affected by the full penetration groove weld used to connect the webs and flanges of the link.

ACKNOWLEDGEMENTS

This research was conducted by the State University of New York at Buffalo and was supported by the Federal Highway Administration under contract number DTFH61-98-C-00094 to the Multidisciplinary Center for Earthquake Engineering Research. However, any opinions, findings, conclusions, and recommendations presented in this paper are those of the authors and do not necessarily reflect the views of the sponsors.

REFERENCES

AISC (1998). *Manual of Steel Construction: Load and Resistance Factor Design,* 3rd Ed. American Institute of Steel Construction, Chicago, IL.

AISC (2002). *Seismic Provisions for Structural Steel Buildings*. American Institute of Steel Construction, Chicago, IL.

ATC (1992). *Guidelines for Seismic Testing of Components of Steel Structures Report-24*, Applied Technology Council, Redwood City, CA.

Berman, J. W., and Bruneau, M., (2004) "Approaches for the Seismic Retrofit of Braced Steel Bridge Piers and Proof-of-Concept Testing of a Laterally Stable Eccentrically Braced Frame" *Technical Report MCEER-03-0001*, Multidisciplinary Center for Earthquake Engineering Research, (submitted for review 9/04).

Bruneau, M., Uang, C.M., and Whittaker, A. (1998) *Ductile Design of Steel Structures*. McGraw-Hill, New York, NY.

Engelhardt, M.D., and Popov, E.P. (1989). "Behavior of Long Links in Eccentrically Braced Frames." *Report No. UCB/EERC-89-01*, Earthquake Engineering Research Center, College of Engineering, University of California Berkeley, Berkeley, CA.

Hjelmstad, K.D., and Popov, E.P. (1983). "Cyclic Behavior and Design of Link Beams." *Journal of Structural Engingeering*, ASCE, 109(10), 2387-2403.

Kasai, K., and Popov, E.P. (1986a). "Study of Seismically Resistant Eccentrically Braced Steel Frame Systes." *Report No. UCB/EERC-86/01*, Earthquake Engineering Research Center, College of Engineering, University of California Berkeley, Berkeley, CA.

Kasai, K., and Popov, E.P. (1986b). "General Behavior of WF Steel Shear Link Beams." *Journal of Structural Engineering*, ASCE, 112(2), 362-382.

Roeder, C.W., and Popov, E.P. (1977) "Inelastic Behavior of Eccentrically Braced Steel Frames Under Cyclic Loadings." *Report No. UCB/EERC-77/18*, Earthquake Engineering Research Center, College of Engineering, University of California Berkeley, Berkeley, CA.

A Comparison of Minimum Confinement in European and American Codes for Circular RC Bridge Columns

Gui-ping Yan[1] and Guan-yuan Zhao[1]

ABSTRACT

The maximum response modification factor (e.g. force reduction factor) in the range of 3 to 4 for ductile bending columns are used in Eurocode 8, AASHTO, ATC-32, and Caltrans *BDS.* Correspondingly, the displacement ductility capacity of structures should be more than 4, and the curvature ductility of structures should be more than 13. Attained curvature ductility levels of columns with the minimum confining reinforcement in the four documents are evaluated taking account of longitudinal reinforcement ratio and axial force ratio. It is shown that, the requirement of ATC-32 can assure expected ductility levels of columns; The minimum confining reinforcement specified in Caltrans *BDS* is not enough; The requirements of Eurocode 8 and AASHTO are relatively conservative for columns with low longitudinal reinforcement ratio and low axial force ratio, but deficient for columns with high longitudinal reinforcement ratio and high axial force ratio.

School of Civil Engineering and Architecture, Beijing Jiaotong University, Beijing 100044, PRC

INTRODUCTION

Performance-based seismic design (PBSD) has been a trend in earthquake engineering. PBSD may be defined as design to reliably achieve target performance objectives. It differs with current design approaches in that multiple seismic events are considered. Most current design approaches only define a level of seismic hazard (e.g. design earthquake) and a level of performance that is generally understood to be life-safety. During recent earthquakes such as 1994 M6.7 Northridge and 1995 M7.2 Kobe earthquakes, although most bridges designed according to current approaches didn't collapse, damage to structures, economic loss due to closure and repair were unexpectedly high.

Ductile seismic design philosophy has been worldwide adopted in current bridge seismic codes due to economical constraints and the inherent uncertainties in predicting seismic demands. In ductile seismic design, plastic hinges are allowed to form in structures. What's most important in ductile seismic design is to assure enough plastic deformation capacity of structures. So the minimum amount of confinement is usually required in most bridge seismic design specifications such as Eurocode 8, AASHTO, ATC-32, and Caltrans *BDS.*

Although the minimum confinement is used to assure enough ductility capacity in above-mentioned specifications, ductility levels are not described explicitly except for Eurocode 8 in which $\mu_\phi \geq 13$ is specified. However, the maximum response modification factor R (e.g. force reduction factor) values in the range of 3 ~ 4 for ductile bending columns are specified in these codes. For structures with relatively long natural period equal displacement rule can be used as approximate relationship between the force reduction factor and displacement ductility demand μ_D. Thus, the maximum displacement ductility demand μ_D should be less than 4 corresponding to the minimum confinement. So the displacement ductility capacity of structure should be more than 4. That is,

$$\mu_\Delta \geq 4 \tag{1}$$

The relationship between the curvature and displacement ductility was previously investigated by Park and Paulay [1]. It should be noted that the $P-\Delta$ effect, rebar slip and shear deformations were neglected in this equation.

$$\mu_\Delta = 1 + 3(\mu_\phi - 1)\frac{L_p}{L}(1 - 0.5\frac{L_p}{L}) \tag{2}$$

Equation (2) indicates that the curvature and displacement ductility have a linear relationship. These relationships are plotted in Figure 2 for various shear span-to-depth ratios (*L*/*h*) and equivalent plastic hinge lengths (L_p) [2]. Figure 2 illustrates that the displacement ductility increases as the shear span-to-depth ratio (*L*/*h*) decreases and the plastic hinge length

(L_p) increases. From Figure 1, curvature ductility should be more than 13 to attain the equation (1) for columns with shear span-to-depth ratio of 6. That is,

$$\mu_\phi \geq 13 \tag{3}$$

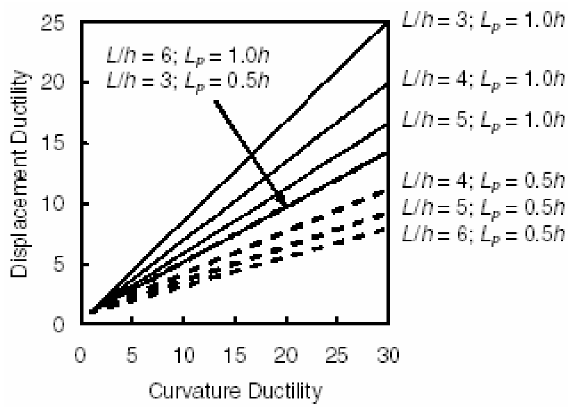

Figure 1. Relationship between curvature and displacement ductility (Park & Pauley, 1975)[2]

By means of section analysis of plastic hinges of columns, the ductility levels attained by the minimum confining reinforcement in codes are evaluated in this paper.

CONFINING REINFORCEMENT PROVISIONS IN CODES

Eurocode 8 [3]

The formula proposed for by Eurocode 8 is a function of curvature ductility and axial load,

$$\omega_{wd} \geq 1.4[1.74\frac{A_g}{A_c}(0.009\mu_\phi + 0.17)\eta_k - 0.07] \geq 1.4\omega_{w,\min} \tag{4}$$

where, A_g is the gross concrete area of the section, A_c is the confined (core) concrete area of the section, μ_ϕ is the required curvature ductility, η_k is axial force ratio. ω_{wd} is mechanical reinforcement ratio:

$$\omega_{wd} = \rho_s \frac{f_{yh}}{f_c^{'}} \tag{5}$$

where, f_{yh} is yield strength of confining reinforcement, $f_c^{'}$ is compressive strength of concrete， ρ_s is volumetric ratio of transverse reinforcement:

$$\rho_s = \frac{4A_b}{sd_c} \tag{6}$$

where, A_b is transverse reinforcement area, s is spacing of spirals, d_c is diameter of concrete core.

For a ductile structure, the minimum curvature ductility and mechanical reinforcement ration are specified in Eurocode 8:

$$\mu_\phi = 13 \quad \text{and} \quad \omega_{w,\min} = 0.12 \tag{7}$$

substituting Equation (5),(6) and (7) into Equation(4),

$$\rho_s \geq 0.7 \frac{f_c^{'}}{f_{yh}} (\frac{A_g}{A_c} \eta_k - 0.07) \geq 0.168 \frac{f_c^{'}}{f_{yh}} \tag{8}$$

AASHTO [4]

$$\rho_s = 0.45(\frac{A_g}{A_c} - 1) \frac{f_c^{'}}{f_{yh}} \tag{9}$$

or,

$$\rho_s = 0.12 \frac{f_c^{'}}{f_{yh}} \tag{10}$$

whichever is greater.

This formula comes from ACI for seismic design of building columns sustaining very high axial forces. Because axial forces in bridge piers commonly are lower those in building columns, the formula may be conservative for bridge piers design.

ATC-32 [5]

$$\rho_s = 0.16 \frac{f_c^{'}}{f_{yh}} (0.5 + 1.25 \frac{P}{f_c^{'} A_g}) + 0.13(\rho_l - 0.01) \tag{11}$$

where, P is axial force on columns, ρ_l is longitudinal reinforcement ratio.

ATC-32 formula considers the effects of axial force ratio and longitudinal reinforcement ratio.

Caltrans *BDS*[6]

Caltrans formula is similar to AASHTO, but axial force is included.

$$\rho_s = 0.45(\frac{A_g}{A_c} - 1) \frac{f_c^{'}}{f_{yh}} (0.5 + 1.25 \frac{P}{f_c^{'} A_g}) \qquad D \leq 900\,\text{mm} \tag{12a}$$

$$\rho_s = 0.12\frac{f_c^{'}}{f_{yh}}(0.5 + 1.25\frac{P}{f_c^{'}A_g}) \qquad D \geq 900\,\text{mm} \tag{12b}$$

The volumetric ratio of confining reinforcement required by Caltrans *BDS* is lower than that required by AASHTO when the axial force ratio is less than 0.4. When the axial force equals zero, the volumetric ratio of confining reinforcement required by Caltrans *BDS* is more than that required by AASHTO by 50%.

DETAILS OF BRIDGE COLUMNS FOR STUDY

Circular columns with a diameter of 1000 mm each are selected as study cases. Three longitudinal reinforcement arrangements considered are 20D24, 28D28 and 40D28, providing longitudinal reinforcement ratios of 1.15%, 2.19% and 3.14% respectively (Figure 2). Axial force ratio is taken as four cases, 5%, 10%, 20% and 30%. Spirals with a diameter of 16 mm are used for confining reinforcement. Spacing of spirals can be determined according to the minimum volumetric confinement ratio in codes.

Strengths and other modulus of materials used are as follows.

Compressive strength of concrete $f_c^{'}$=17.5 MPa

Yield strength of longitudinal reinforcement f_y=380 Mpa

Yield strength of confining reinforcement f_{yh}=210 MPa

Young's modulus of concrete $E_c = 5000\sqrt{f_c^{'}}$ (MPa) (26,458MPa)

Elastic modulus of reinforcing steel E_s= 200,000 MPa

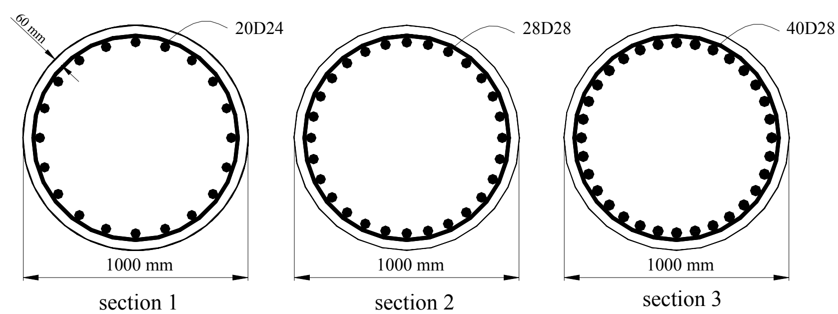

Figure 2. Longitudinal reinforcement arrangement

$$\frac{f_c^{'}}{f_{yh}} = \frac{17.5}{210} = 0.083 \tag{13}$$

Diameter of core concrete is,

$$D^{'} = D - 2c - d_s = 1000 - 2\times 60 - 16 = 864\,\text{mm} \tag{14}$$

$$\frac{A_g}{A_c} = (\frac{D}{D^{'}})^2 = 1.34 \tag{15}$$

Substituting Equation (14) and (15) into Equation (8) ~ (12)，simple equations of the minimum confining reinforcement in codes can be given.

Eurocode 8：

$$\rho_s = 0.078\eta_k - 0.008 \geq 0.014 \tag{16}$$

AASHTO：

$$\rho_s = 0.013 \tag{17}$$

ATC-32：

$$\rho_s = 0.13\rho_l + 0.017\eta_k + 0.006 \geq 0.0002n_b \tag{18}$$

Caltrans *BDS*：

$$\rho_s = 0.012\eta_k + 0.005 \tag{19}$$

Figure 3 compares minimum volumetric confining reinforcement ratio ρ_s specified in the four documents. It is found that ρ_s in Caltrans *BDS* is lowest, ranging from 0.5% to 0.86%.

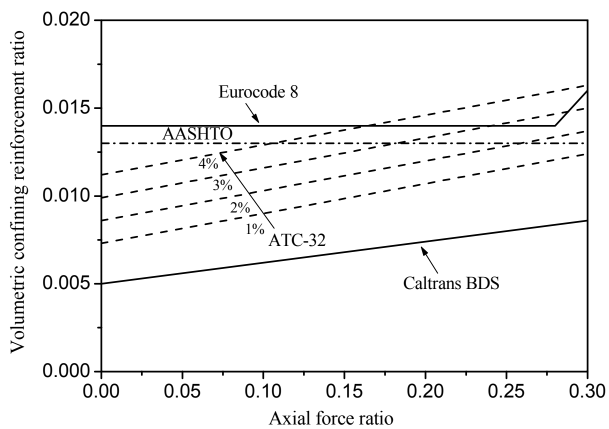

Figure 3. Minimum confinement in different specifications

According to Equation (16) ~ (19), the spacing of spirals are computed (Table 1). For AASHTO, minimum confining reinforcement ratio is constant, and the spacing of spirals is 71mm.

Table 1. Spacing of spirals of columns (mm)

Specifications	Longitudinal reinforcement ratio	Axial force ratio			
		5%	10%	20%	30%
Eurocode 8	--	66	66	66	60
AASHTO	--	71	71	71	71
ATC-32	1.15%	110	101	85	73
	2.19%	96	89	76	65
	3.14%	85	79	69	60
Caltrans *BDS*	--	166	150	125	108

CURVATURE DUCTILITY CAPACITIES ANALYSIS

Curvature ductility capacities of the plastic hinge sections are analyzed using moment-curvature analysis program MCAP developed by the author[7]. In this program, the stress-strain model of confined concrete proposed by Mander[8] is adopted. Figure 4 compares curvature ductility capacities. Figure 5 compares the effect of the longitudinal reinforcement ratio on curvature ductility of columns designed according to different codes.

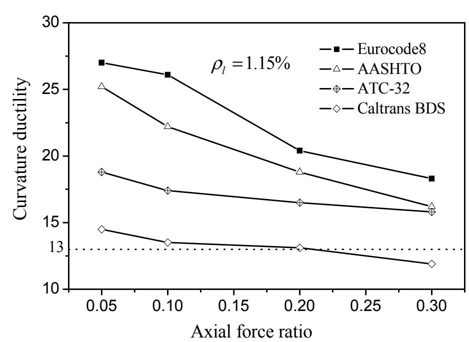

(a)

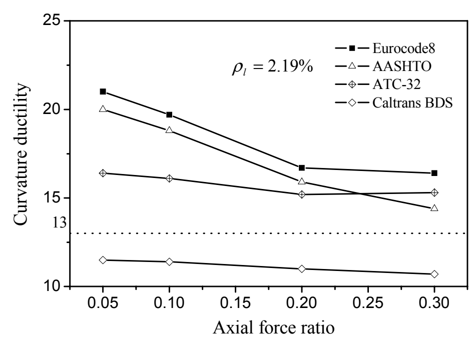

(b)

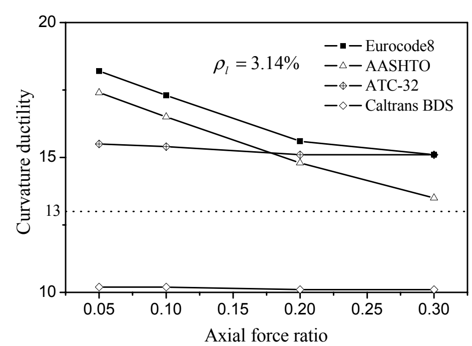

(c)

Figure 4. Curvature ductility of columns designed according different specifications

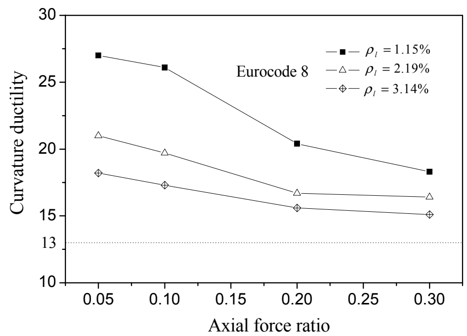

(a)

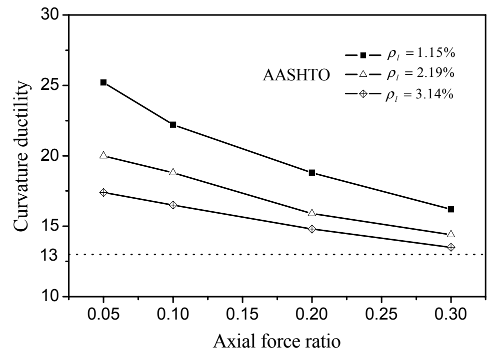

(b)

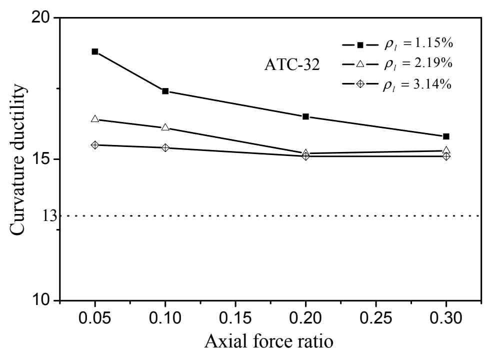

(c)

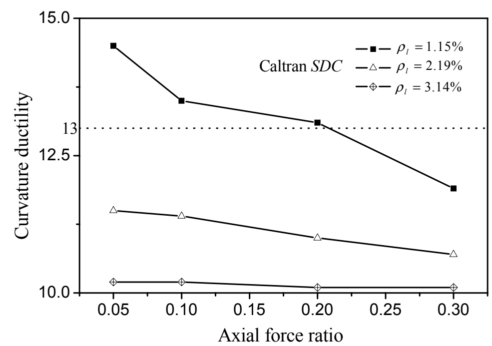

(d)

Figure 5. Effect of the longitudinal reinforcement ratio on curvature ductility of columns

CONCLUSIONS

(1) The minimum confinement for ductile circular column specified in Eurocode 8, AASHTO and ATC-32 is enough to assure curvature ductility of sections in plastic hinges, ranging 15.1-27.0、13.5-25.2、15.1-18.8 respectively. The minimum confinement for ductile circular column specified in Caltrans *BDS* can get target ductility capacity with lower longitudinal reinforcement ratio (below 1%), while fail to supply enough ductility at relatively higher longitudinal reinforcement ratio.

(2) With the increase of axial force ratio from 5% to 30%, curvature ductility of columns designed according to Eurocode 8、AASHTO、ATC-32、Caltrans *BDS* decrease by 17.0%-32.2%、22.4%-35.7%、2.6%-16.0%、1.0%-17.9% respectively. The decrease amplitude of curvature ductility of columns designed according to ATC-32 is lowest, while that according to AASHTO is highest.

(3) With the increase of longitudinal ratio from 1.15% to 3.14%, curvature ductility of columns designed according to Eurocode 8、AASHTO、ATC-32、Caltrans *BDS* decrease by

17.5%-33.7%、16.7%-31.0%、4.4%-17.6%、15.1%-29.7% respectively. The decrease amplitude of curvature ductility of columns designed according to ATC-32 is lowest, while that according to Eurocode 8 is highest.

(4) It is shown that, the confinement design in ATC-32 is comparatively efficient taking account of the effects of axial force and longitudinal reinforcement ratio; The minimum confining reinforcement specified in Caltrans *BDS* is not enough; The requirements of Eurocode 8 and AASHTO are relatively conservative for columns with low longitudinal reinforcement ratio and low axial force ratio, but deficient for columns with high longitudinal reinforcement ratio and high axial force ratio.

REFERENCES

[1] Park, R and Pauley, T. Reinforced Concrete Structures, John Wiley and Sons, New York, 1975.

[2] Bae, S, Bayrak, O and Williamson E. What do we know about the performance-based seismic design of columns? 13th World Conference on Earthquake Engineering, Vancouver, B.C., Canada ,2004. Paper No.997

[3] CEN, Eurocode 8—Design Provisions for Earthquake Resistance of Structures, Part2: Bridges. Brussels: Comite European de Normalization, 1994.

[4] AASHTO. Standard Specification for Highway Bridges, 16th Edition,Division I-A: Seismic Design. Washington: American Association of State Highway and Transportation Officials, Imc., 1996.

[5] ATC-32, Improved Seismic Design Criteria for California Bridges: Provisional Recommendations. California: Applied Technology Council(ATC), 1996.

[6] Bridge Design Specifications. Sacramento, California: California Department of Transportation (CALTRANS), Division of structures, 2004.

[7] Zhao G Y. Comparative study on European and American bridge seismic design specifications. Master's thesis , Beijing Jiaotong University, 2003.

[8] Mander J B, Priestley M J N, Park R. Theoretical stress-strain model for confined concrete. Journal of Structural Engineering , ASCE, 1988, 114(8):1804-1826.

Tappan Zee Bridge Seismic Assessment

Vikas P. Wagh

ABSTRACT

Tappan Zee Bridge is a 4.9 km (3 miles) long, 50-year old bridge that spans the Hudson River between the Towns of Nyack and Tarrytown, north of New York City. The bridge is the "Flag Ship" of the New York State Thruway (NYSTA) system. The bridge carries seven lanes of traffic and is a critical link in the New York City area transportation system.

The subsurface geology of Hudson River at the Tappan Zee Bridge site is unique. A considerable thickness of soil overlies the bedrock. The typical sequence of strata from the top consists of organic silt, silty clay, sand, silty clay, varved clay, glacial till and rock. The bridge foundations are supported on different subsurface conditions.

The 2.4 km (1.5 miles) long western half of the bridge consists of 165 low level trestle spans, each 15.2 m (50 ft) long, supported on 24.4 m (80 ft) long timber piles in the organic clay and silty clay. The top of rock is as deep as 213.4 m (700 ft) below the riverbed in this area.

To the east of the trestle spans, 76.2 m (250 ft) long deck truss spans flank the main navigational crossing. Most of these spans are founded on cofferdam foundations supported on piles supported on rock.

The navigational main span structure is supported on four piers that are supported on partially buoyant pile supported caissons. The caissons support approximately 70% of the dead load of the structure by buoyancy.

Moderate earthquakes have occurred in New York historically and some seismic hazard does exist. According to the United States Geological Survey, on August 10, 1884, an estimated magnitude 5.2 event hit New York City. An earlier magnitude 5.2 earthquake had occurred on December 18, 1737. The unique Hudson River subsurface geology at the Tappan Zee Bridge site made the need for seismic assessment imperative.

In 1994, NYSTA initiated seismic risk assessment of the Tappan Zee Bridge. The intent of the study was to establish seismic characteristics of the existing bridge. Site specific seismicity criteria were developed for this study. As a result of this study, certain initial assessments regarding the seismic vulnerability and the need for seismic retrofit in various segments of the bridge were determined. This study was completed in 1995.

In 2001, the NYSTA initiated the Tappan Zee Bridge/I-287 Corridor Study, which included an independent investigation of seismic risk assessment and retrofit scenarios. New York City Seismic Hazard Guidelines published in 1998 were used for this study. This study was completed in 2004.

The paper presents a qualitative comparison of the two studies and the varying degrees of seismic retrofit recommendations.

Vikas P. Wagh, P.E., Wagh Engineers, P.C., New York, USA

1 INTRODUCTION

The 4.9 km (3 miles) long Tappan Zee Bridge, one of the largest bridges in the United States, carries the New York State Thruway's (NYSTA) mainline across the historic Tappan Zee Section of the Hudson River, about 21 km north of New York City. The bridge was opened on December 15, 1955. The actual construction began in March 1952. The structure and approaches cost approximately $80.8 million. From economic and engineering viewpoints, the bridge is the key structure on the 1,031 km (641 miles) cross-state Thruway system. The bridge connects the Westchester and Rockland counties. Using seven traffic lanes, more than 132,000 vehicles cross the Tappan Zee Bridge everyday with volumes as high as 165,000 vehicles per day.

2 BRIDGE DESCRIPTION

The 4,881 m (16,013 ft) long structure is divided into three types of design. For the west trestle spans which extend about 2,440 m (8,000 ft) from the west, the superstructure consists of a series of 15.2 m (50 ft) composite concrete deck multi-stringer spans. The piers consist of reinforced concrete capbeam and column bents, supported on solid concrete pile caps within the tidal zone, with 24.4 m (80 ft) long timber piles.

The deck truss spans on each side of the main crossing consist of 20 simply supported spans with span lengths between 71.6 m (235 ft) to 76.2 m (250 ft). The piers consist of two hollow reinforced concrete box columns connected by a solid concrete strut at the top. At four of the piers, the columns are founded on buoyant caissons. The remaining piers are supported on solid concrete-filled circular sheet piling cofferdams founded on vertical piles to rock.

The main crossing consists of through truss construction. The two 103.6 m (340 ft) long cantilever truss segments that support the 162.2 m (532 ft) suspended span form the 369.4 m (1,212 ft) long main span. The main span is flanked by two 183.5 m (602 ft) long side anchor spans. The piers are steel trussed towers supported on buoyant reinforced concrete caissons founded on vertical pile to rock. The caissons support 70% of the dead load by buoyancy.

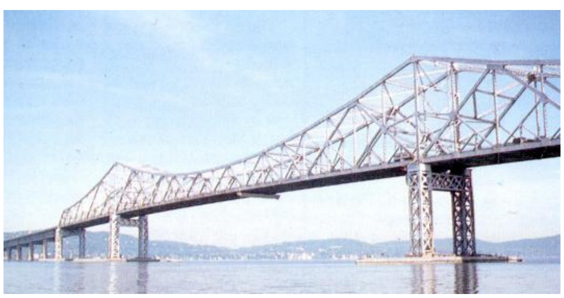

(a) Through Truss Spans

(b) Deck Truss Spans

(c) Trestle Spans

Figure 1. Tappan Zee Bridge

A short segment to the east of the deck truss spans consists of seven 16.8 m (55 ft) spans similar in construction to the west trestle.

3 NEED FOR SEISMIC PERFORMANCE EVALUATION

Moderate earthquakes have occurred in New York historically and some seismic hazard does exist. According to the USGS, on August 10, 1884, an estimated magnitude 5.2 event occurred in New York City. An earlier magnitude 5.2 earthquake had occurred on December 18, 1737. After the 1989 Loma Prieta earthquake in California and its aftermath, a growing sense of urgency to evaluate the seismic risk to the infrastructure in the Northeastern United States developed. The evaluation effort began with the critical structures in the major cities. Site specific seismic vulnerability assessment studies were initiated. In the last 20 years, there has been a considerable amount of earthquake research and seismic design code development.

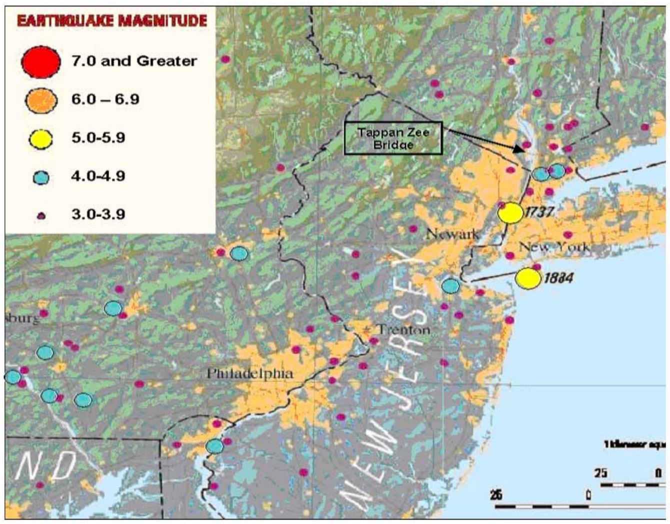

Figure 2. Seismicity Map

In 1994, to establish the seismic characteristics of the Tappan Zee Bridge, NYSTA commissioned Frederic R. Harris, Inc. to perform a seismic evaluation of the bridge. At that time, there were no detailed guidelines available to determine the seismic risk assessment of the critical bridges in the New York State. The generalized response spectra included in AASHTO Specifications were deemed not specific enough for this critical bridge. Therefore, for a site specific seismic risk assessment of the Tappan Zee Bridge, it was necessary to develop analysis criteria relevant to the New York region and the geological conditions at the bridge. The 1995 seismic risk assessment study performed by F.R. Harris was based on developed site-specific response spectra.

Shortly after the 1995 study, the New York City Department of Transportation (NYCDOT) commissioned Weidlinger Associates and a team of researchers to develop comprehensive Seismic Assessment Guidelines. These Guidelines were published in December 1998 and were subsequently adopted by the New York State Department of Transportation (NYSDOT) and NYSTA. In 2002, NYSTA commissioned Ove Arup and Partners Consulting Engineers, P.C. to perform an environmental assessment study. As part of this study, Arup performed an independent seismic risk assessment of the Tappan Zee Bridge.

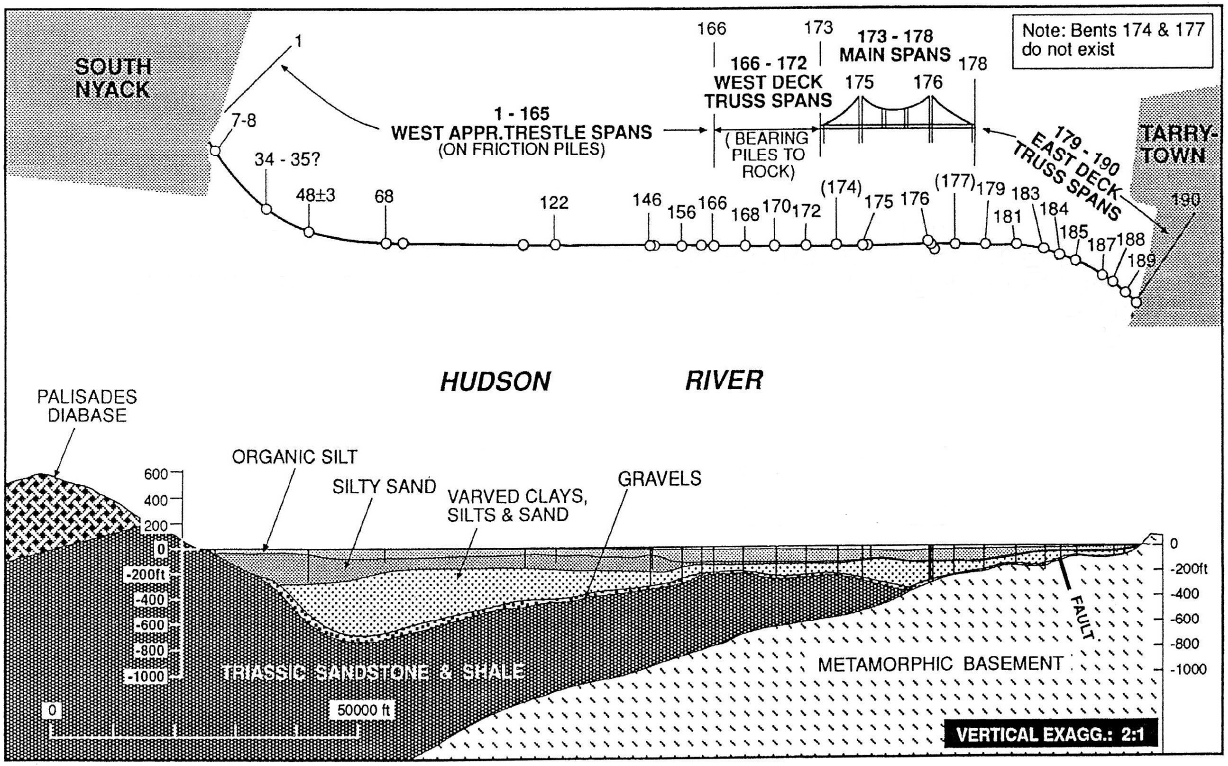

Figure 3. Geological Profile

4 ASSESSMENT CRITERIA DEVELOPMENT

4.1 Design Response Spectra: 1995 Study

In 1994, Lamont Doherty Earth Observatory (LDEO) performed a deterministic seismic hazard assessment of the Tappan Zee Bridge to develop design response spectra. The bridge is located in seismically active geological area known as the Manhattan Prong. Based on the historic seismicity of the area, the regional seismicity was quantified in terms of the frequency of occurrence as a function of magnitude. Three constant (average) recurrence periods (CRP) were chosen to define seismic hazard exposure levels: 500 years, 1000 years and 2500 years. A 500-year return period has a probability of 10% in 50 years, a 1000-year design earthquake has a probability of occurrence of 5% in 50 years and a 2500-year design earthquake has a probability of occurrence of 2% in 50 years. These CRP's were then correlated to certain magnitude-distance event combinations based on the regional seismicity. Three Richter Scale magnitude events, 5, 6 and 7 were selected. The three component ground motion acceleration time series were developed.

As shown in Figure 3, the supporting soil condition varies significantly along the length of the bridge. Due to the variations in soil type and bedrock depth, it was necessary to divide the soil profile into different geologic sections that represent the conditions locally along the length of the bridge. The ground motions were first developed for hard rock and then were modified for nonlinear responses for ten different soil profiles along the bridge.

Smooth response spectra were developed for three categories related to specific soil conditions beneath various portions of the bridge:

- Category I included foundations for through truss spans on caissons and deck truss spans on caissons, with piles bearing on rock,
- Category II included foundations for deck truss spans consisting of cofferdams with piles bearing on rock and

- Category III included foundations of the trestle portion of the bridge supported on timber friction piles.

4.2 Seismic Performance Criteria: 1995 Study

During early phase of seismic investigation, an approach based on two seismic hazard levels was considered:

- Operating Base Earthquake (OBE) - After an OBE, the bridge is expected to be operational within a short period of time. The OBE criteria were as follows:
  - For the through truss spans, which have higher inherent value (i.e. longer expected remaining life) and whose structural safety and stability is critical, use the 1000-year event with 5% probability of occurrence in 50 years.
  - For the deck truss spans and trestle spans, use the 500-year event with 10% probability of occurrence in 50 years.
- Structural Safety Event (SSE) - After an SSE, the bridge may be expected to suffer significant damage but collapse is unlikely; major repairs to the bridge before being operational may be required. An SSE of 2500 year event with 2% probability of occurrence in 50 years was selected.

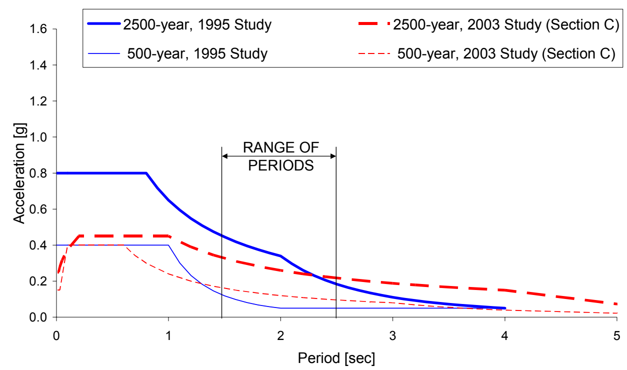

(a) Response Spectra for Trestle Spans

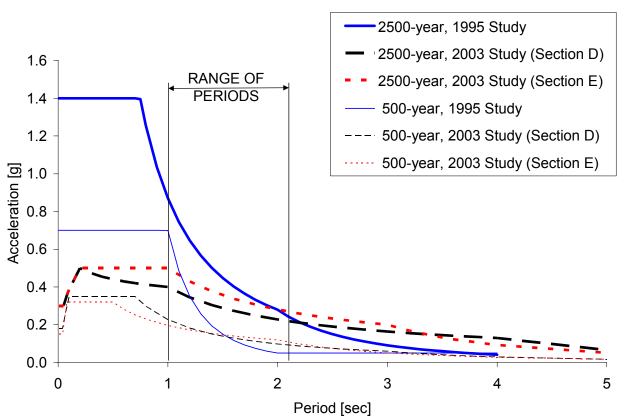

(b) Response Spectra for Deck Truss Spans

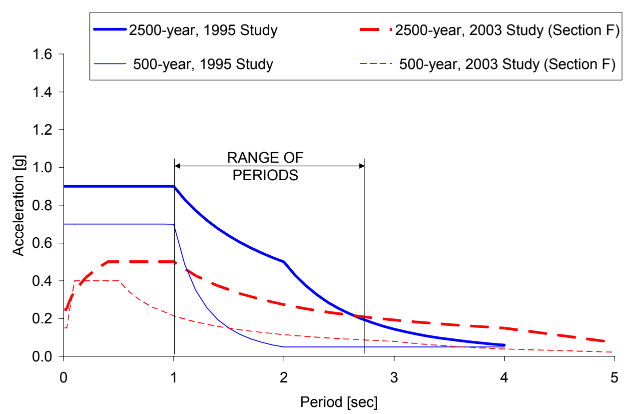

(c) Response Spectra for Through Truss Spans

Figure 4. Response Spectra from 1995 and 2003 Studies

4.3 Design Response Spectra: 2003 Study

In the 2003 Seismic Risk Assessment Study, the newly updated NYSDOT seismic hazard guidelines were used. As per those guidelines, the seismic performance of the bridge shall be analyzed based on earthquakes with a 2500-year and 500-year return period.

The design peak ground accelerations at the bedrock level, or PGA, at the Tappan Zee Bridge are specified by code to be 0.145g and 0.578g (where g is the acceleration of gravity). These accelerations represent the hazard levels associated with 500 and 2500-year return periods, respectively.

In order to develop site-specific surface ground motions, artificial bedrock ground motion time histories were developed in accordance with NYSDOT guidelines. Generally, a 5% critical damping was assumed. Three different spectrum-compatible bedrock acceleration time histories were synthesized for both the upper and lower level events and were used to generate the site specific response spectra.

For the purposes of this investigation, the bridge has been divided into nine representative geologic segments (A to I). For each segment profile, soil stiffness and strength properties were derived.

4.4 Seismic Performance Criteria: 2003 Study

The current NYSDOT specifications recognize that critical bridges must remain functional almost immediately after the design earthquake and continue to function as part of the lifeline/survival network. In accordance with the NYSDOT Specifications, the Tappan Zee Bridge is categorized as a critical bridge and should be capable of achieving the following performance criteria:

- For a lower level seismic event, the bridge must suffer no damage to primary structural members and *Minimal Damage* to other components. The bridge must remain fully operational during and after the 500-year event, allowing a few hours for inspection.
- After an upper level seismic event, the condition of the bridge must allow quick access to emergency vehicles within 48 hours and be repairable within months.

5 PERFORMANCE ASSESSMENT

A multi-mode spectral analysis methodology was adopted for estimating the performance of the bridge under upper and lower level seismic events. This involved four primary activities as listed below and outlined in the following paragraphs:

- Determining the site-specific seismic motion of the ground
- Establishing the stiffness characteristics of the foundations
- Performing the response spectrum analyses of the superstructure with the foundations modeled as “springs” with stiffness in the six degrees of freedom
- Computing the resulting forces and deflections in the structure

Assessment of the performance of the bridge was carried out for three segments of the bridge, namely west trestle spans, deck truss spans and the main through truss spans. For the west trestle and the deck truss spans, different spans were evaluated to account for the variability in geometric and geologic conditions, and forms of construction. The main spans were modeled in their entirety.

The performance was typically assessed on a member-by-member basis using a capacity/demand ratio (C/D ratio) approach. Capacities reported here typically refer to ultimate strengths, and demands are those computed by the response spectrum analysis.

6 ANALYSIS RESULTS

Unless stated otherwise, the results discussed in this section are from the 2003 Study.

6.1 West Trestle Spans

Foundations for piers 2 through 165 consist of 0.30 m (12 inch) diameter 24.4 m (80 ft) long battered untreated timber piles, except at piers near the west shore, which have piles of lesser lengths where the bedrock profile limits the pile length. The maximum depth of water in the trestle portion of the bridge is 4.5 m (15 ft).
Piers 6, 69, and 154 were selected for seismic assessment as representative piers in both the Studies. The individual piles were modeled down to the effective point of fixity, with a vertical spring provided at that level to allow the vertical load distribution amongst the piles. Both Studies generally had similar conclusions about the seismic vulnerability of the trestle spans of the bridge.

6.1.1 Dynamic Behavior

Modal Shape	500-Year			2500-Year		
	Pier 6	Pier 69	Pier 154	Pier 6	Pier 69	Pier 154
1st Longitudinal	1.57	1.47	2.54	1.57	1.78	2.54
1st Transverse	1.28	1.78	2.32	1.58	2.03	2.54
1st Vertical	0.19	0.19	0.19	0.19	0.20	0.19

Table 1. Natural Periods (in seconds) of Trestle Spans Primary Modes of Vibration

6.1.2 Seismic Displacements

At the deck level, a maximum horizontal movement of 38 cm (15 inches) in longitudinal direction is expected.

6.1.3 Foundations

According to AASHTO Division IA, all piles shall be adequately anchored to the pile footing or cap. Timber and steel piles, including unfilled pipe piles shall be provided with anchoring devices to develop all uplift forces adequately. The existing timber piles in the west trestle spans do not satisfy this requirement since they are not positively connected to the pile cap.

6.1.4 Columns

The columns of the concrete piers at the west trestle spans do not satisfy the current AASHTO standards for confinement of longitudinal reinforcement. This reinforcement is not always embedded sufficiently into the cap beam or the footing. Due to this lack of confinement reinforcement, the trestle cannot behave in a ductile manner. The results of the column analysis indicate a number of locations on all three representative piers with C/D ratios of less than 1.

6.1.5 Cap Beams

The cap beam is adequate to resist all seismic loads except for the 2500-year event, primarily from transverse movement. As the cap beams do not have confining reinforcement they cannot behave in a ductile manner and therefore are considered seismically deficient.

6.1.6 Bearings and Anchor Bolts

The west trestle spans of the Tappan Zee Bridge have either individual fixed steel bearings or elastomeric bearings supporting the 15 deck stringers per span. Eleven trestle piers at the eastern end of west trestle spans do not have a sufficient bearing seat width to meet the AASHTO requirements. Both assessment studies assumed that all fixed steel bearings will be replaced by elastomeric bearings and any deficiencies in seat length will be corrected when the deteriorated bearings are replaced.

6.1.7 Retrofit Strategies

Retrofitting the west trestles should consist of the following modifications:

1. Replace the fixed steel bearings with elastomeric bearings.
2. Strengthen the existing foundations by installing new steel shell piles and a pilecap extension. This will require removal of the end battered piles.
3. Strengthen the base of the columns with additional concrete with main and confinement reinforcement.
4. Strengthen the capbeams by installing external post-tensioning rods.
5. As an alternative, install vertical bracing in the plane of the bent to provide an alternative lateral load path and relieve the moments at these connections.

If all of these retrofits were to be implemented, a retrofitted pier would appear similar to what is shown in Figure 5.

Another alternative is to completely replace the west trestle spans with a new structure designed to resist seismic loads.

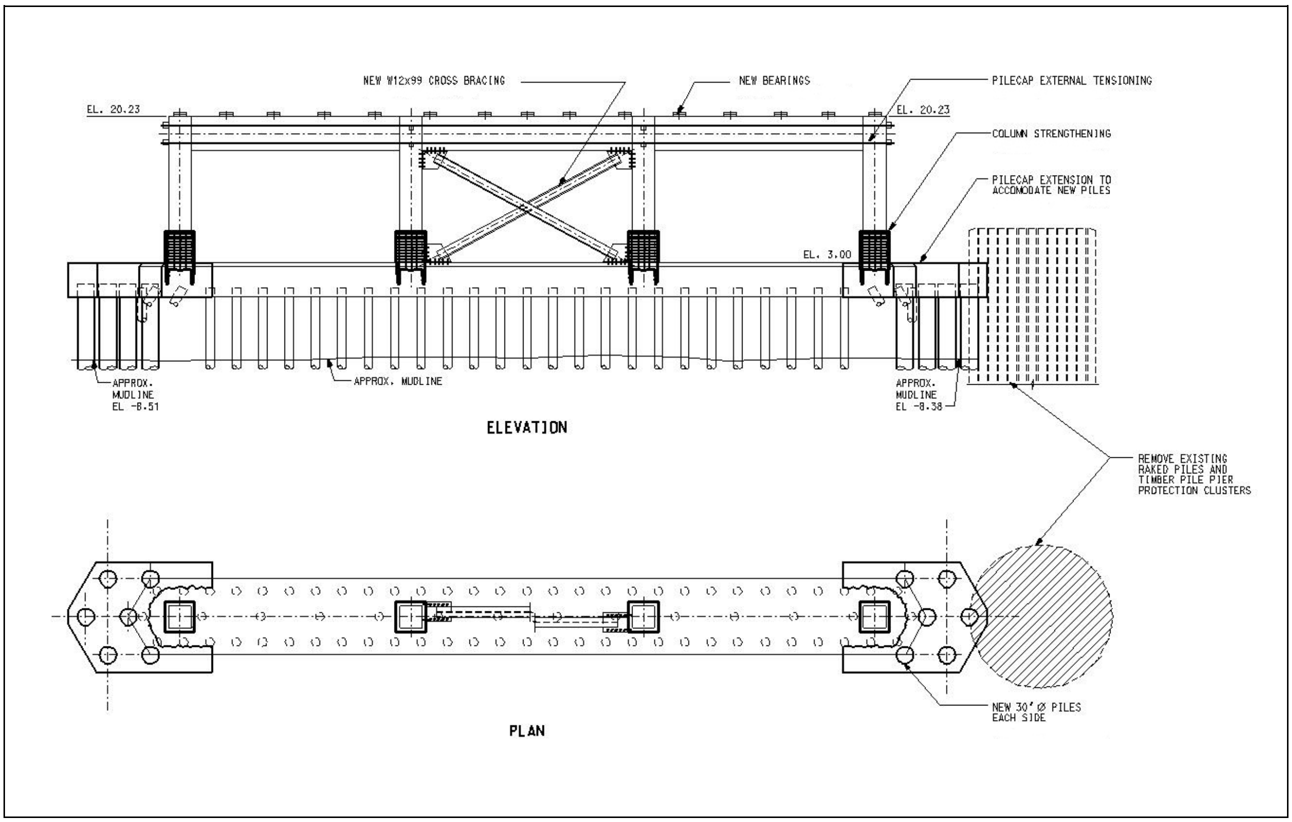

Figure 5. Trestle Spans Pier Retrofit for a 2500-Year Event

6.2 Deck Truss Spans

The superstructure is composed of concrete or exodermic deck, steel stringers, steel floor beam trusses with cantilever brackets, and steel deck trusses. The trusses were originally supported using rocker bearings and roller nests. In 1991, all of the truss roller nests were replaced with sliding pot bearings.

Three dimensional finite element analysis models were developed to perform a multi-modal response spectrum analyses of the deck truss spans. Piers 166, 172, 179 and 181 were selected for seismic assessment as representative piers; two piers supported on cofferdam foundations and two on buoyant caissons. Despite these variations, the seismic analyses indicated that the representative piers had many similarities in their behavior under seismic loading allowing extrapolation of results.

6.2.1 Dynamic Behavior

Modal Shape	500-Year				2500-Year			
	Span 167	Span 173	Span 179	Span 182	Span 167	Span 173	Span 179	Span 182
1st Longitudinal	1.0	2.1	2.0	1.3	1.2	2.1	2.0	1.5
1st Transverse	1.0	1.9	1.9	1.2	1.3	1.9	1.9	1.3
1st Vertical	0.2	0.35	035	0.2	0.22	0.35	0.24	0.22

Table 2. Natural Periods (in seconds) of Deck Truss Spans Primary Modes of Vibration

6.2.2 Seismic Displacements

The displacements resulting from the analysis indicate 22.9 cm or 63.5 cm (9 or 25 inches) movement at the bearing level and 7.6 cm and 22.9 cm (3 and 9 inches) for the base of the caisson under the 500-year and 2500-year events respectively. These displacement results are valid assuming that the behavior of the structure remains elastic throughout the seismic event.

6.2.3 Foundations

Reactions from the multi-modal analysis indicate that the horizontal capacity of the foundation piles, is significantly lower than required. This lack of capacity is particularly severe at the buoyant caissons.

An independent displacement analysis of piles indicated that the existing movement capacity of 6.1 cm to 8.6 cm (2.4 to 3.4 inches) was adequate to accommodate the resulting movements due to a 500-year event. However, under the 2500-year event, the deflection limit of the cofferdams is approximately 8.4 cm (3.3 inches), which is below the displacement demands of between 10.7 cm and 13.2 cm (4.2 and 5.2 inches). This deficiency indicates that to meet the performance criteria for an upper level seismic event, retrofit of the cofferdam foundations will be required.

For the buoyant caisson at pier 172, the maximum estimated deflection for the 500-year event marginally exceeds the available capacity. However, under the 2500-year event, a maximum demand of 20.8 cm (8.2 inches) far exceeds the 8.6 cm (3.4 inches) capacity.

6.2.4 Pier Columns

Similar to the trestle columns, the reinforcement details of the columns do not provide adequate confinement of the column section to allow for plastic hinging to occur and therefore the post-hinging allowable reduction in seismic design loads cannot be applied. For this reason, the capacities of the columns are compared directly to the elastic seismic forces without reduction by using R factor = 1.0 for both upper and lower level seismic events.

All pier columns do not satisfy the demand for both the upper and lower level events. The lowest C/D ratio for representative piers was 0.5 for 500-year event and 0.2 for the 2500-year event.

6.2.5 Cap Beams

The cap beam proves adequate to resist all seismic loads except for the 2500-year primarily transverse event. Under this condition, the cap beam is overstressed.

6.2.6 Truss Bearings

As shown in Figure 6, each deck truss span is simply supported, with a rocker bearing at one end, and sliding pot bearings at the other. It is important to note that the actual behavior of this type of joint system is difficult to predict with confidence. If the deck joints were to behave the same way as in the closed position, then the lateral forces associated with a seismic event would likely damage the deck joint itself. If the deck joints were open, then the longitudinal seismic loads would have to be transferred through the pin of the rocker connections. The shear strength of these pins is, however, insufficient to carry these loads.

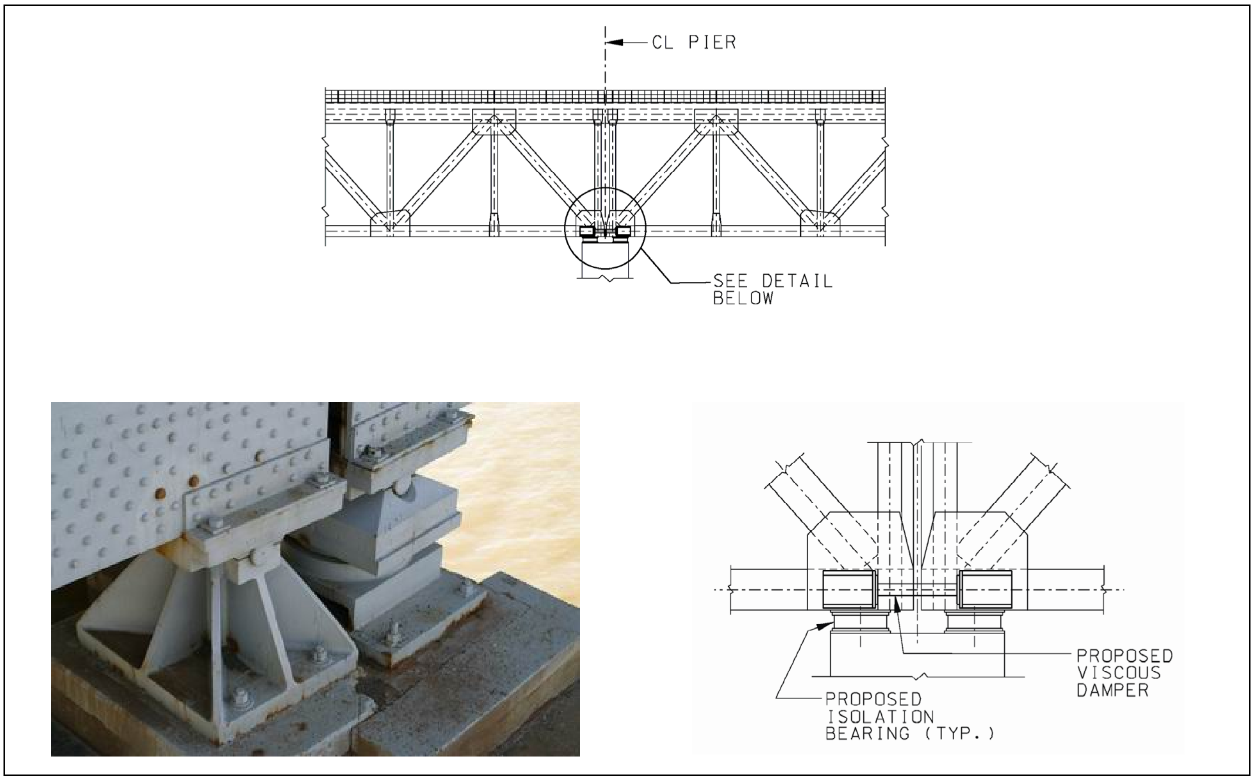

Figure 6. Truss Bearings and Retrofit of Deck Truss Spans

6.2.7 Deck Truss Superstructure

For the 500-year seismic event, the analysis suggests that the majority of the superstructure members will perform satisfactorily but that some members will be overstressed. Under the 2500-year event a significant number of members are likely to be overstressed.

6.2.8 Seismic Response of Existing Structural System

The sequence of potential damage based on the C/D ratios is listed below:

1. Deck finger joints become bent or fail due to contact.
2. Truss fixed bearing anchor bolts fail in shear.
3. Pier columns crack. Concrete cover may spall and reinforcement may buckle due to lack of confinement.
4. Piles supporting the buoyant caisson foundations begin to yield in bending.
5. Isolated primary structural steel begins to yield.

6. Piles supporting concrete cofferdams begin to yield.
7. Top of column to cap beam connection cracks and spalls.

This sequence is not a *prediction* of the behavior of the structure under an earthquake, but identifies areas of the structure that are at risk to the different levels of seismic hazard with respect to their identified performance targets. The sequence and degree of overstress forms the basis for determining what level of retrofit would be required in order to achieve these targets.

6.2.9 Retrofit Strategies

Retrofitting the deck truss spans should consist of the following modifications:

1. Replace the existing fixed and expansion deck truss bearings with seismic isolation bearings. To alleviate the risk of superstructure pounding, provide continuity across the deck joints under seismic loading by installing a viscous lock-up device across the joint, as indicated in Figure 6.
2. Strengthen the base of the columns.
3. Introduce a perimeter frame with additional piles to restrain the buoyant caisson foundations. The concrete cofferdam foundations should be strengthened by driving an additional row of piles around the perimeter of the existing cofferdam.
4. Provide isolated structural steel strengthening to limit localized distortion due to overstress.
5. Strengthen the cap beam by addition of transverse post-tensioning and additional concrete to prevent damage.

It is fully recognized that the process of detailing the design of these retrofits may show that the level of required construction is less than what has been shown here. Therefore, the estimate of construction required is considered to be an upper bound.

6.3 Through Truss Spans

Assessment of the main spans indicates that they do not meet the performance requirements of either the upper or lower level seismic event with the former governing the extent of required retrofit. Primary critical elements include the truss bearings, the pier towers and holding down bolts, and the foundations. The assessment also shows that some primary structural steel members in the superstructure are also at risk of being overstressed under a seismic event.

6.3.1 Dynamic Behavior

Results of both the 1995 Study and the 2003 Study were compared to ambient vibration measurements taken for this segment of the bridge in 1994. See Table 3.

Mode	Modal Shape	Field Measurement in 1994	Calibrated Computer Model
1	1st Transverse	2.70	2.74
2	1st Vertical	1.81	1.93
3	1st Longitudinal	1.74	1.74
4	2nd Transverse	1.53	1.48
5	3rd Transverse	1.43	1.4
6	1st Torsional	0.938	0.99

Table 3. Natural Periods (in seconds) of Through Truss Spans Primary Modes of Vibration

A three dimensional finite element analysis model was developed to perform multi-modal response spectrum analyses for the main spans. The influence of the adjacent deck truss spans was incorporated into the model using lumped masses at the bearing nodes. The partially buoyant caissons were modeled as a series of rigid links with the mass and inertias lumped at the center of gravity and foundation springs located at the bottom of the caisson.

Although the main span straddles soil profiles E, F, and G, only a single spectrum can be used in a given direction in the model for any single analysis. For the purposes of this assessment, geologic section E, which encompasses piers 173 and 175 of the main truss, was selected for providing the input ground spectrum.

It is notable that the forces associated with the wind on the main spans are substantially less than those for the 500-year event.

6.3.2 Seismic Displacements

The maximum displacements range from 5 cm (2 inches) to 17.8 cm (7 inches) at foundation level and up to 155 cm (61 inches) in the transverse direction at the truss top chord level.

6.3.3 Foundations

The main spans are supported on 0.76 m (30 inches) diameter grout filled steel shell piles with 127 mm (0.5 inch) wall thickness and steel H-pile cores.

The 2003 Study and the 1995 Study response spectra analyses of the main spans indicated that piles would be overstressed under a seismic event.

The substantial difference in capacity and demand for both the anchor and main piers indicates post-elastic failure behavior of the pile. The pile to caisson connection is unlikely to be adequate for the post elastic failure behavior. Furthermore, any failure or damage to the pile could not be inspected after an earthquake. As the consequence of failure of the pile to caisson connection failure may cause a breach of the caisson and the loss of its buoyant capability. This may lead to major consequences for the bridge including loss of service, need for major refurbishment and possible partial collapse.

The cost implications associated with retrofitting foundations can be prohibitively high therefore effort was made to reconsider these demands in light of the conservative nature of the approach used initially. To realistically interpret the results of the response spectrum analysis, a dynamic behavior of the foundations based on displacement demands rather than force demands was evaluated.

That evaluation confirmed the earlier results that show significant damage.

6.3.4 Pier Columns

For the 500-year event, the analysis showed that the average anchor bolt C/D ratio for tension was 0.89 at the anchor piers and 0.38 at the main towers. Under the 2500-year event, C/D ratios for the anchor pier and main tower anchor bolts were computed to be 0.47 and 0.14 respectively. Note that a response modification factor of 0.8 was used in the analysis of the column base plate connections for the lower level event and an R factor of 1.0 was used for the upper level event.

The current bearing arrangement results in the majority of the longitudinal forces in the superstructure being resisted solely by the main towers, with little contribution from the anchor piers. A 1.5 R factor was used in the 2500-year event pier analyses.

The anchor piers are likely to perform better than the main piers under a seismic event since the through trusses are supported on expansion bearings at the anchor piers but are pinned to the main piers. The analysis showed that for the 500-year event, the majority of the members in the anchor piers would perform adequately.

6.3.5 Retrofit Strategies

Figure 7 shows the proposed retrofit for the through truss spans.

DEMAND REDUCTION STRATEGY – 2500 YEAR EVENT:

At both Anchor Piers (Bents 173, 178):
1. Replace anchor span roller expansion bearings with free sliding pot bearings.
2. Replace deck truss fixed bearings with free sliding pot bearings.
3. Install viscous dampers, in longitudinal and transverse arrangement, connecting anchor span to anchor pier and deck truss span to anchor tower.

Replace Existing Deck with Lighter Exodermic Deck

Retrofit Dummy Upper Chord Members to function as load carrying members.

Eliminate expansion joint and make truss continuous

At both Main Tower Piers (Bents 174, 177):
1. Replace monolithic connection between truss and tower with free sliding connection using pot bearings.
2. Strengthen truss bottom chord connection to accommodate new bearings. Install transverse strengthening members.
3. Install viscous dampers, in longitudinal and transverse arrangement, connecting main pier to truss.

SUBSTRUCTURE STRENGTHENING – 2500 YEAR EVENT:

At both Anchor Piers (Bents 173, 178):
1. Retrofit column to caisson pedestal connection.

Verticals

Column to Caisson Pedestal Connection

Transverse Diagonals

At both Main Piers (Bents 177, 177):
1. Strengthen selected verticals and column transverse diagonals.
2. Retrofit column to caisson pedestal connection.

Figure 7. Through Truss Spans Retrofit Strategy

7 CONCLUSIONS

In the last ten years, as described in this paper, two independent seismic risk assessments of the Tappan Zee Bridge were performed. The seismic response spectra developed in each study were based on different assumptions and the resulting design response spectra show significant variations. The regions of particular interest of these spectra correspond to the natural periods of the three distinct types of structures of the Tappan Zee Bridge.

With minor variations, the conclusions regarding the performance capabilities of the bridge drawn from both the studies are consistent. As a result, the independent 2003 study seems to confirm and validate the findings of the initial 1995 study.

8 ACKNOWLEDGEMENTS

The author acknowledges efforts of all the individuals and organizations involved in both studies. Particular thanks to Christopher Waites, Jim Mauro, Peter Melewski and Thomas Mahar of NYSTA. Author is grateful to Mark Roche, John Eddy and other engineers from Arup for their cooperation. The following organizations are recognized for their participation in the studies:

- 1995 Study: New York State Thruway Authority – Owner; Frederic R. Harris, Inc, New York, NY – Prime Consultant; Hardesty & Hanover, New York, NY; Lamont Doherty Earth Observatory, Palisades, NY
- 2003 Study: New York State Thruway Authority – Owner; Ove Arup and Partners Consulting Engineers – Prime Consultant, New York, NY; Lichtenstein Consulting Engineers, P.C., New York, NY; Wagh Engineers, P.C., New York, NY; Mueser Rutledge Consulting Engineers, New York, NY

Author acknowledges input and assistance of Ondrej Kalny of Wagh Engineers in preparation of this paper.

9 REFERENCES

Frederic R. Harris, Inc., 1995, “Tappan Zee Bridge, Project D211593, Seismic Analysis: Superstructure, Preliminary Results”

Hardesty and Hanover, LLP, 1995, “Tappan Zee, Bridge Project D211953, Appendix A to Preliminary Seismic Analysis, Preliminary Substructure and Foundation Seismic Analysis”

Jacob, K.; Horton, S.; Barstow, N. and Armbruster, J., 1995, “Tappan Zee Bridge Seismic Study, Final Report Part I, Seismic Hazard Assessment, Design Ground Motions and Comments on Liquefaction Potential”, Lamont Doherty Earth Observatory of Columbia University, Palisades, NY

Mueser Rutledge Consulting Engineers, 2003, “Tappan Zee Bridge, Project D213230: Inspection and Assessment, Appendix C, Geotechnical Report”

New York State Standard Specifications for Highway Bridges, 2002

Ove Arup and Partners Consulting Engineers, P.C., 2003, “Tappan Zee Bridge, Project D213230: Inspection and Assessment, Volume 4, Appendix L1: Seismic Assessment Summary Report”

Wagh, V. P.; Pourhamidi, S.; Drugge, H. E. and Rolwood, C., 1995, “Seismic Investigation of Tappan Zee Bridge”, IBR 95-41, presented and published at the International Bridge Conference in Pittsburgh, PA, USA

A Brief Introduction to the New Code for Seismic Design of Railway Engineering

NI-Yanping

ABSTRACT:

In China, the seismic design of railway bridges is included in the code for seismic design of railway engineering. In recent years, the code for seismic design of railway engineering has been revised to adapt to the new trends for railway engineering. Some problems in the new code were presented and discussed in this paper. Furthermore, some practical examples about seismic design for railway bridges are introduced in this paper.

Yan-ping Ni, The First Survey & Design Institute of China Railway, Lanzhou, 730000, PRC

INTRODUCTION

The code for seismic design of railway engineering has been used for 15 years, and the theories and engineering practice in bridge seismic design have highly developed in the past 15 years. The traditional seismic design method based on strength is being replaced with the ductility design method or performance based seismic design method, and linear/nonlinear dynamic time history response analysis is used in design of bridges with complex structural response.

Under this background, it is necessary to revise the old code fully. The new revised code had been completed by the First Survey & Design Institute of China Railway. The key modification to the old code is about basic criterion for seismic design of railway bridges, and the seismic isolation design of railway bridges is introduced in new revised code.

MAIN CONTENTS OF THE NEW CODE

Response spectral curve

In the new code, the characteristic period for a response spectrum is estimated by the site type and period zone as shown in Table 1. In China, the site type is classified as four types and three period zones according to zoning maps of earthquake intensity and ground motion parameters of China.

Table 1 Characteristic period for the response spectrum T_g (s)

Period zone	Site type			
	I	II	III	Ⅳ
一	0.25	0.35	0.45	0.65
二	0.30	0.40	0.55	0.75
三	0.35	0.45	0.65	0.90

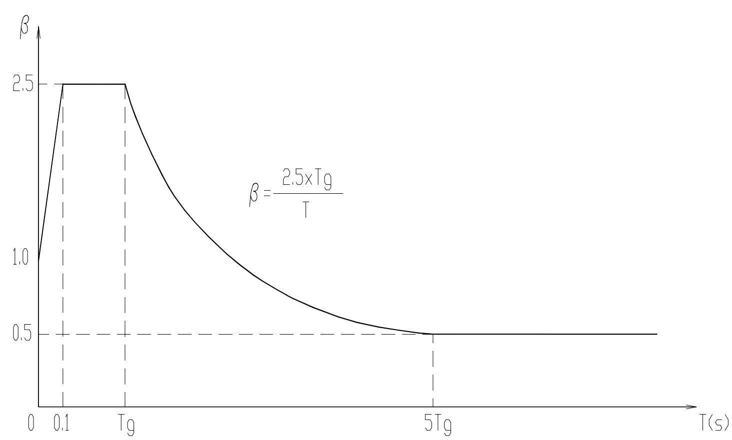

Figure 1 Response spectral curve in the new code

Based on the characteristic period of ground motion, the response spectrum for railway bridges is shown in Figure 1. Different to the old response spectrum, the maximum value of response spectrum is adjusted from 2.25 to 2.5, and the minimum value is changed from 0.45 to 0.5 (Figure 1).

When the damping ratio ξ is not equal to 0.05, the value of response spectrum shall be multiplied by a damping modification factor η , and η can be estimated as

$$\eta = 1 + \frac{0.05 - \xi}{0.06 + 1.7\xi} \tag{1}$$

if η less than 0.55, let η=0.55

Design Criteria and method

In the old code, the traditional seismic coefficient method was adopted. Seismic force effects on each component are obtained from the elastic response and multiplied by synthetical effect coefficient η_c under a design earthquake. The structural components are designed according to the seismic force effects.

Table 2 Seismic fortification criterion of railway engineering

Earthquake level	Minor earthquake	Design earthquake	Severe earthquake
Exceeding probability in 50 years	63.2%	10%	2%
Seismic peak ground acceleration （m/s2）	0.33Ag	Ag	1.6Ag

Note: A_g in the table represents peak acceleration value for a design earthquake

Table 3 Design method and performance levels

	Minor earthquake	Design earthquake	Severe earthquake
Design method	Linear design Common bridge: Use response spectral method Important bridge: Use time-history analysis method	Concept design	Ductility design 1、Common bridge □Pier using cast steel bearing; Carry out ductility analysis of reinforced concrete □Pier using lead-rubber bearing; Carry out equivalent linearization analysis 2、Important bridge: Carry out nonlinear time-history analysis

Structure response and engineering fortification target	Elastic response, little damage, not interrupt the operation.	Nonlinear response, damage occurred in projects in Ⅲ、Ⅳ type site, open to traffic with restricted speed after 1～3 days inspection	Nonlinear response, serious damage occurred in projects in Ⅱ～Ⅳ type site, open to traffic with restricted speed after short time inspection

In the new code, the three-level seismic design approach corresponding to the performance levels was adopted for the seismic design of railway bridges. Three levels of earthquake loads which shown in Table 2, minor, design and severe earthquakes are defined as ground motion with 63%, 10% and 2% probability of exceedance in 50 years, respectively. Corresponding to the three levels of earthquake loads, the design method and performance levels for railway bridges are presented in Table 3.

Strength and Deformation Verification

In order to satisfy above performance levels in new code, the structure components of railway bridges should be designed to insure in elastic range under a minor earthquake, and have enough ductility capacity for ductile member under a severe earthquake. The piers of railway bridges shall meet the displacement ductility requirements under a severe earthquake as follow:

$$\bar{\mu}_u \leq [\mu_u]/K \tag{2}$$

Where, $\bar{\mu}_u$ is the average value of displacement ductility demand for a pier under severe earthquakes, $[\mu_u]$ is displacement ductility capacity of a pier, and K is safety factor.

$\bar{\mu}_u$ can be estimated as

$$\bar{\mu}_u = \lambda_m \times \bar{\mu}_m \tag{3}$$

$$\bar{\mu}_m = \frac{M_{\max}}{M_y}$$

where, M_y is the yield moment at bottom section of a pier, $M_{\max}$ is maximum linear response value of moment at bottom section under a severe earthquake, and λ_m is a factor which can be determined from figure 2.

Seismic isolation design requirement

In recent years, a relative new technology called seismic isolation has emerged as a practical and economical alternative to conventional design. In China, the technology of seismic isolation had been used in some railway bridges as shown in table 4. In these seismic isolation designs, lead-rubber bearings have been mostly used as isolating devices.

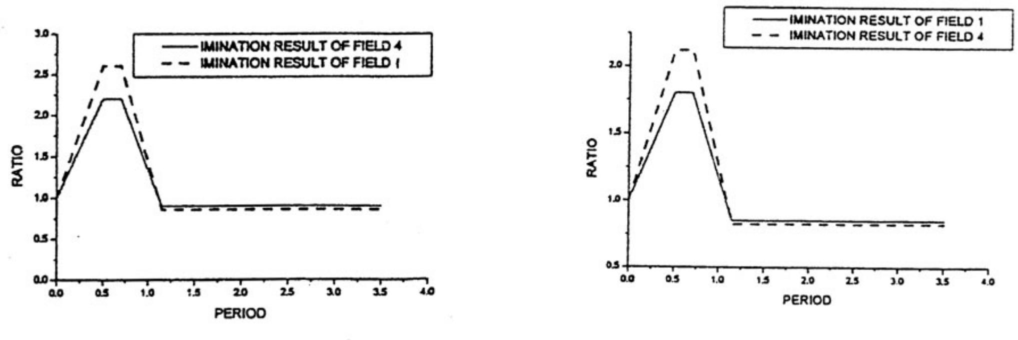

Acceleration≤0.3g Acceleration＞0.3g

Figure 2 λ_m value with period

Basing on the work, seismic isolation design requirement is introduced in the new code. In the new code, the mechanical characteristic and technical requirement of lead-rubber bearing are given. Besides, an approximate method about the calculation of simple-supported beam bridge with the lead rubber bearing is presented.

Table 4 The application of isolation technology

Railway line	Bridge name	Span	Time	Isolation technology
Beijiang railway	Huashanzi bridge	2x4m	1990	Rubber isolation bearing
Beijiang railway	Weizigou bridge	5x4m	1990	Rubber isolation bearing
Baoji-Zhongwei railway	Qianhe bride	18x20m	1993	Plate-type elastomeric bearing
Nanjiang railway	Buguzi bridge	8x32m	1999	Lead-rubber bearing

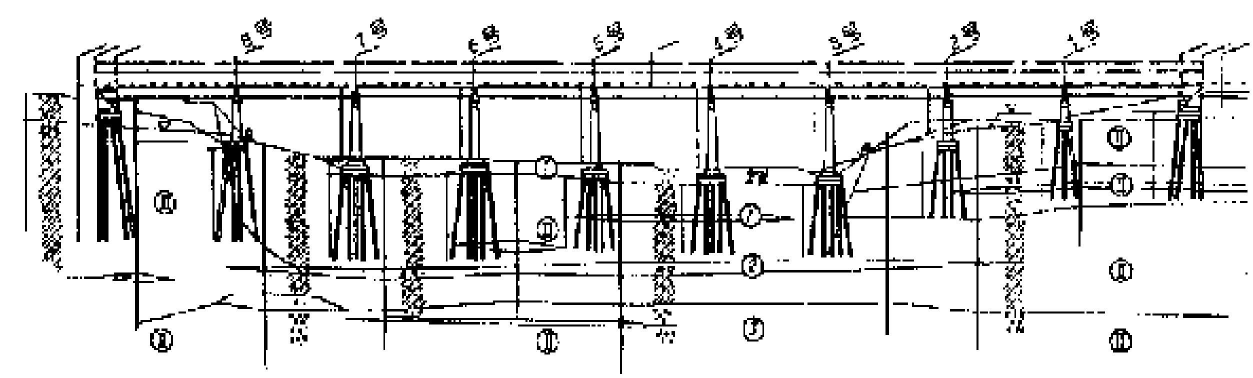

Figure 3 Buguzi bridge in Nanjiang railway

PRACTICAL EXAMPLES

Buguzi bridge is located on the west of Atushi railway station(9x32m post-stressed concrete simple supported beam bridge, total lenth is 290m, height is 23m). The bridge is located in the high frequency earthquake intensity region(9 intensity degree), the bridge site is about only 70kM from the famous earthquake region—Jiashi county, Xinjiang, China(110kM from another famous earthquake region Wuqia County). In order to reduce the dynamic response, lead-rubber bearing was used to substitute the traditional bearings for the bridge. Lead-rubber bearing used in the bridge were designed by the First Survey & Design Institute of China Railway, Guangzhou University, and were produced by Hetai vibration isolating equipment company, Shantou, China.

If we define the isolating ratio *Rt* as
Rt= Moment (with lead rubber bearing)/ Moment (with cast steel bearing)

Isolating ratio for the bridge pier under different earthquake records is present in Table 5.

Table 5 Vibration isolating ratio of the Buguzi bridge

Earthquake record	1#	2#	3#	4#	5#	6#	7#	Average value
Elcentro wave	0.23	0.33	0.33	0.33	0.32	0.31	0.20	0.29
Tianjin wave	0.36	0.29	0.30	0.31	0.35	0.34	0.34	0.33
Adjusted Tianjin wave	0.75	0.65	0.72	0.89	0.94	0.92	0.85	0.82

According to the result, when the pier height is less than 20m, isolating effect is very evident for the bridge with lead-rubber bearings. After construction, the Buguzi bridge had subjected the Wuqia and Jiashi earthquake, especially the Jiashi earthquake. In the year of 2003, there were 4000 earthquakes occurred from Jan. to June. Among them there were 9 earthquakes that Magnitude M⩾5.0 (as shown in Table 6), and the maximum magnitude is 6.8. After suffering these earthquakes, there is no damage on the Buguzi bridge. Isolation with lead-rubber bearing is proven to be a very effect method for reducing seismic response.

Table 6 Earthquakes of M⩾5.0 occurred in Jiashi region, Xinjiang,China since 2002

Date	Time	Latitude(N°)	Longitude(E°)	Magnitude	Place
2002-12-25	20-57-00	39.6	75.4	5.7	XinjiangWuqia,China
2003-01-04	19-07-15.6	39.5	077.0	5.4	Jiashi,Xinjiang,China
2003-02-24	10-03-45.8	39.5	077.2	6.8	Jiashi,Xinjiang,China
2003-02-25	05-18-45.2	39.6	077.2	5.0	Jiashi,Xinjiang,China
2003-02-25	11-52-44.0	39.5	077.3	5.5	Jiashi,Xinjiang,China
2003-03-12	12-47-51.9	39.5	077.4	5.9	Between Bachu and Jiashi

2003-03-16	06-59-25.2	39.5	077.4	5.0	Between Bachu and Jiashi
2003-03-31	07-15-45.0	39.6	077.5	5.2	Between Bachu and Jiashi
2003-05-04	23-44-36.1	39.4	077.3	5.8	Jiashi,Xinjiang,China
2003-06-05	00-28-41.9	39.5	077.6	5.2	Jiashi,Xinjiang,China

REFERENCE

The code for seismic design of railway engineering, 1987

The code for seismic design of railway engineering , The First Survey & Design Institute of China Railway, (2nd Draft for Seeking Comments), 2002.3

Design of lead-rubber bridge bearings [M], Civil Division publication 818/A, New Zealand, 1983

Seismic Ground Motion Parameter Zonation Map of China[s], China Quality and Technical State Bureau of Supervision,2001.8.

Experimental report on shock insulation support, shear key and gird seam buffer, The First Survey & Design Institute of China Railway, 2000.8.

Seismic Analysis of Xiaoxihu Partial Cable-stayed Bridge in Lanzhou, Chen Xingchong etc. Journal of Lanzhou Railway University, 2003.3.

Protective Measures in the Seismic Design and Retrofit of Long-Span Bridges

Tim J. Ingham[1]

ABSTRACT

The use of protective measures in the seismic retrofit and/or design of six major U.S. bridges is described. The protective measures include the use of dampers for energy absorption and control of displacement; the use of isolation bearings for energy absorption and force-reduction; the use of ductile links for the control and localization of damage; and the use of stiffeners to prevent buckling and enhance ductility.

[1] T.Y. Lin International, Two Harrison Street, Suite 500, San Francisco CA, 94105, USA

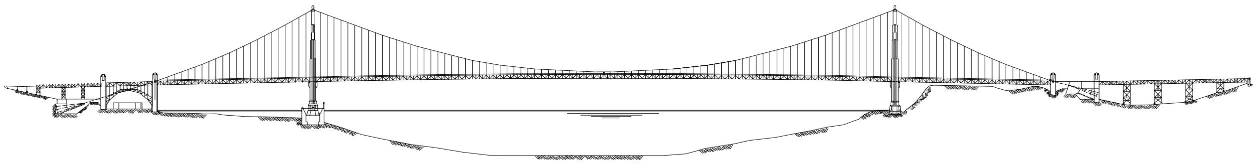

Figure 1. The Golden Gate Bridge.

GOLDEN GATE BRIDGE

Since 1937 the Golden Gate Bridge has served as a vital transportation link connecting San Francisco with the counties to its north. Prompted by the Loma Prieta earthquake of October 1989, the Golden Gate Bridge District engaged consultants to study the seismic vulnerabilities of the bridge and design a seismic retrofit.

The seismic retrofit of the suspension bridge will be its fourth major retrofit since its completion in 1937. The previous retrofits were the addition of a bottom lateral bracing system in the 1950s to improve the flutter stability of the bridge, the replacement of the bridge suspenders in the 1970s, and the replacement of the original reinforced concrete deck with a steel orthotropic deck in the 1980s. These retrofits are a testimony to the diligence of the Bridge District in maintaining the bridge.

The bridge is shown in elevation in Figure 1. The suspension bridge has a center span of 1,280 m and side spans 343 m long, for a total length of 1966 m. It is supported at the ends by reinforced concrete pylons, and flanked by steel viaduct and steel arch approach structures. It carries six lanes of traffic.

Stiffening of critical locations of the steel towers to prevent plate buckling is a part of the bridge retrofit. As shown in Figure 2, the bases of the towers will rock during a (maximum credible) earthquake; the magnitude of the uplift is about 45 mm at the extreme fibers of the base. As shown in the figure, the uplift causes concentrations of stress (and strain) on the opposite side of the tower, both at the base and above the setback in the tower elevation. In a finite element study of the base of the tower, the peak strains were found to be about four times the yield strain.

Compact sections can accommodate strains of this magnitude, but, unfortunately, the tower base is not compact. The tower is of multi-cellular construction; it consists of plates riveted together with cor-

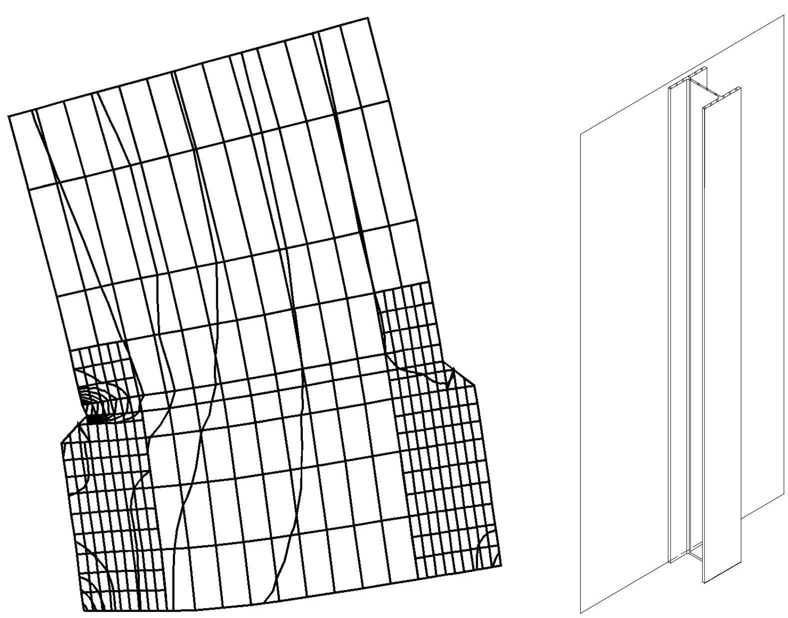

Figure 2. Retrofit of Golden Gate Bridge with Stiffeners.

Figure 3. The Vincent Thomas Bridge.

ner angles. At the base, the cross-section consists of 103 cells, each 1070×1070 mm square (just large enough to work inside). The plates are 22 mm thick, giving a width-to-thickness ratio of 48. Plates of this dimension buckle shortly after yielding, with a significant loss of strength. A finite element analysis of a typical cell showed the corner angles to be only minimally effective in restraining the buckling of the plates, because of the large spacing (180 mm) of the rivets connecting the two elements (Nader, 1995).

A finite element study of the tower base suggested that the buckling might propagate towards the center of the cross-section. This will be prevented by the retrofit shown on the right hand side of Figure 2, where a stiffener is added along the vertical centerline of the plate (between diaphragms). The stiffeners will delay buckling of the tower plates until after a displacement ductility of four is reached. Propagation of the buckling will then be prevented.

VINCENT THOMAS BRIDGE

The Vincent-Thomas Suspension Bridge, shown in Figure 3, was constructed in the early 1960's across the main channel of the Los Angeles Harbor between the community of San Pedro and Terminal Island. The suspended part of the structure consists of a 457 m long center span and two 154 m side spans. The roadway is 16 m wide from curb to curb and accommodates four lanes of traffic. The bridge is one of six major toll bridges retrofitted by the State of California. Like the Golden Gate Bridge, the towers of this bridge were stiffened to prevent plate buckling. In this case, however, the stiffening elements took the form of cover plates (Baker).

The installation of hydraulic, viscous dampers between the suspended structure and the towers is another important part of the bridge retrofit. These were modeled with nonlinear damping elements with a force-velocity relationship of $F = C \cdot V^n$. An optimization study was performed in order to determine the optimum damper characteristics. The study considered the energy dissipation within the dampers and the energy flow through the dampers, i.e., the transfer of energy between the side and main spans and the towers. The study showed that linear dampers, with an exponent of unity, were preferable to dampers with an exponent of one-half. This is in contrast to the damper retrofit for the Golden Gate Bridge, where dampers with an exponent of one-half were shown to be more efficient that linear dampers (Rodriguez).

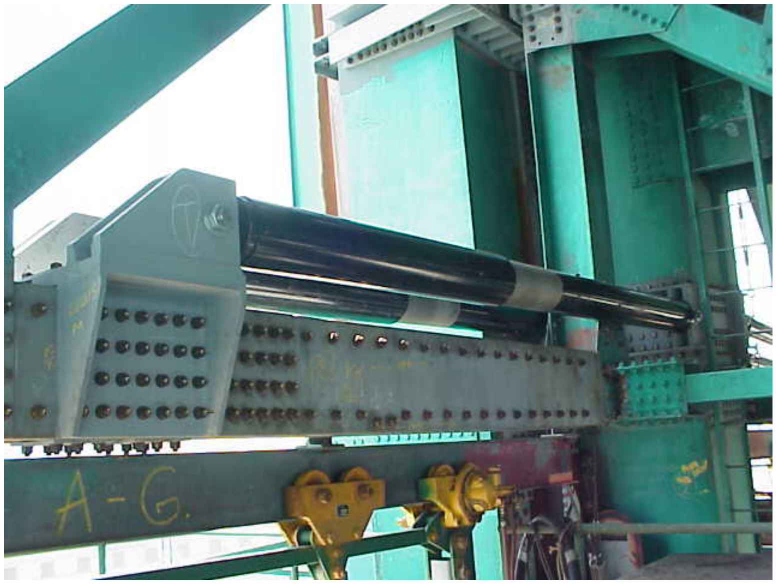

Figure 4. Dampers Installed on the Vincent Thomas Bridge.

The main effect of the dampers is to limit the displacements across the span / tower expansion joints and to eliminate impact between the suspended spans and the towers. The installed dampers are shown in Figure 4.

SAN FRANCISCO-OAKLAND BAY BRIDGE

The San Francisco-Oakland Bay Bridge was constructed in 1936. At that time, it was one of the longest high-level bridges in the world. Today, it carries 280,000 vehicles a day and is the busiest bridge in the world. The 1989 Loma Prieta Earthquake seriously damaged the east span of the bridge when a 15-m portion above Pier E-9 collapsed onto the lower deck. The bridge was closed for repairs for a period of

Figure 5. The East Bay, Self-Anchored Suspension Bridge.

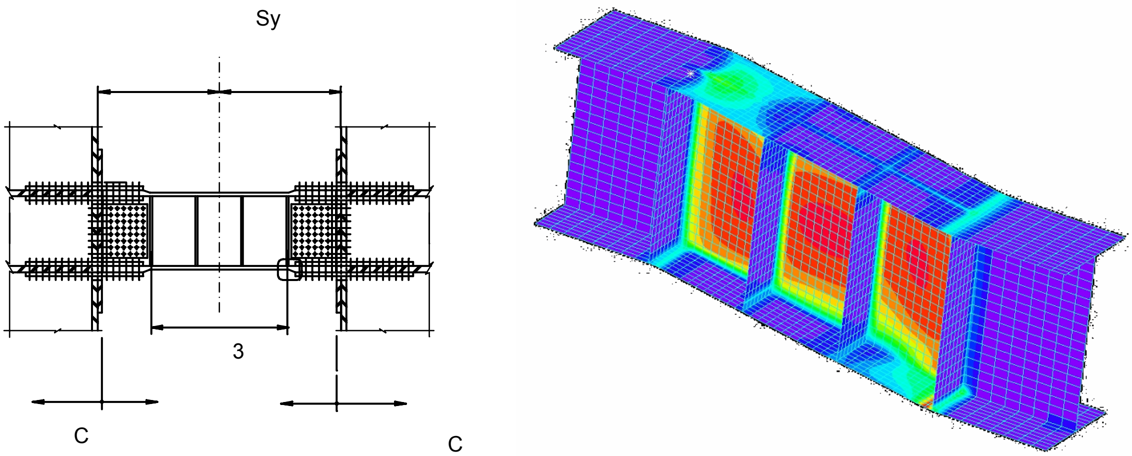

Figure 6. Shear Links. East Bay, Self-Anchored Suspension Bridge.

four weeks. Seismic evaluation of the bridge performed by the California Department of Transportation concluded that replacing the east span would be more cost effective than a seismic upgrade of the 50 year old bridge. T.Y.Lin International and Moffatt & Nichol, a joint venture, were hired in 1998 to design a new bridge consisting of a skyway portion and a self-anchored suspension main span. The self-anchored suspension bridge (see Figure 5) was selected by the Metropolitan Transportation Commission out of four competing designs.

The self-anchored suspension bridge consists of a 385 m main span and a 180 m back span, making it the longest self-anchored suspension bridge in the world when completed. The 0.78 m diameter cable is anchored to the deck at the east bent and is looped around the west bent through deviation saddles. The weight of this cap beam is designed to balance the dead load up-lift at the west bent arising from the asymmetry of the bridge. The suspenders are splayed to the exterior sides of the box girders and are spaced at 10 m. The superstructure consists of dual hollow orthotropic steel box girders. These boxes are in compression (supporting the cable tension forces) and are a part of the gravity load system. The box girders are connected together by 10 m wide × 5.5 m deep crossbeams spaced at 30 m.

The single tower is 160 m tall and is composed of four shafts connected with shear links along its height. The tower shafts are tapered stiffened steel box members with diaphragms spaced at 3 m. The tower is fixed to the 6.5 m deep pile cap (consisting of a steel moment frame encased with concrete) and is supported on 13 - 2.5 m diameter steel pipe piles (filled with concrete), which in turn are embedded and fixed into rock.

The shear links between the tower shafts are shown in Figure 6. These links are expected to yield in shear (as shown on the right-hand side of the figure) during a major (safety evaluation) earthquake, thereby absorbing energy and protecting the tower shafts from damage. The links themselves will be welded together from steel plates, but they will be bolted to the tower shafts. Thus, it will be possible to replace the links if they are permanently deformed or otherwise badly damaged during an earthquake. The calculated rotational demand on the links is 0.05 radians. The ultimate rotational capacity of the links is 0.09 radians according to AISC design rules; and 0.15 radians, judging from both half-scale and full-scale tests (Nader, 2001).

SAN DIEGO-CORONADO BAY BRIDGE

This bridge, shown in Figure 7, connects San Diego and Coronado by carrying State Route 75 across San Diego Bay. The bridge is 2.6 km long; it has a 90-degree, 549 m radius horizontal curve between Piers 4 and 17. The bridge includes 31 spans, ranging in length form 47 m to 201 m. The substruc-

Figure 7. The San Diego-Coronado Bay Bridge.

ture of the bridge consists of 32 reinforced concrete piers supported on prestressed and reinforced concrete piles from Piers 2 to 23, and spread footings at the remaining piers. Pier heights range from 12 m to 67 m at the channel spans.

The seismic retrofit of this bridge includes replacement of the original pin and rocker bearings with lead-rubber seismic isolation bearings, as shown in Figure 8 (Ashley). In this case the effectiveness of the bearings in isolating the bridge from ground motions is minimal. The structure has a fundamental period of 4.1 seconds even with rigid bearings. The value of the isolation bearings is threefold, however. Firstly, they replace the potentially vulnerable pin and rocker bearings. Secondly, they damp the response of the bridge to ground motions and reduce seismic demands throughout the structure. And thirdly, where a minor fault crosses the bridge alignment between two piers, they may help to accommodate the displacement demands on the bridge due to fault rupture.

Near the main channel spans, the piles supporting the bridge have a significant free height between the soffit of the pile cap and the mudline. The free height is 11 m at Pier 17. Because of this free height, the piles are subjected to significant bending during an earthquake. Unfortunately, they are not especially ductile. But retrofit of the bridge foundations—which would have been very expensive if un-

Figure 8. Bearing Replacement, San Diego-Coronado Bay Bridge.

Figure 9. The Aurora Avenue Bridge.

derwater work was needed—was avoided through a combination of several efforts. These included careful analysis of the demands on the piles (Ingham, 1999), wherein each of the 491 piles was modeled directly with inelastic elements. Also a series of tests was conducted at the University of California, San Diego to determine the actual ductility of the piles—which was higher than predicted by the typically used models. And another factor was the reduction in demand due to the use of the aforementioned seismic isolation bearings.

AURORA AVENUE BRIDGE

The Aurora Avenue Bridge across Lake Union in Seattle, Washington is shown in Figure 9. Exclusive of its approaches, this cantilever steel truss bridge is 572 m long and has a main span of 244 m. It was designed and built between 1929 and 1931. Retrofit of this bridge with friction pendulum seismic isolation bearings is now underway. This retrofit will effectively protect the concrete substructure of the bridge, which is very lightly reinforced and vulnerable to large earthquakes. The isolation bearing retrofit avoids retrofit of the concrete substructure itself. This would have been very costly because the piers are embedded in contaminated soil, which would have required remediation of hazardous materials and special disposal. Friction pendulum bearings were chosen for the retrofit because they are able to accommodate the significant weight of the bridge (25.4 MN per main pier bearing) within the footprints available on the tops of the piers.

An interesting feature of the seismic response of the bridge is its large aspect ratio. The bridge is significantly taller (34 m above the bearings) than it is wide (12 m). Thus, lateral loads will result in significant changes in the vertical reactions on the bearings on opposite sides of the bridge. Since the stiffness of a friction pendulum bearing is proportional to the instantaneous vertical force acting on it, it was necessary to consider this effect in analysis and design. To this end, the contact surface model (Ingham, 2001) shown in Figure 10 was developed. In this model, the bearing dish is modeled with a spherical mesh of contact segments that together constitute a contact surface. The bearing slider is modeled with a single contact point that exists on a contact segment (surface) that lies on one face of a solid finite element. This solid element and its mirror image define the body of the slider. The opposing contact surfaces are defined as a contact pair with a coefficient of friction equal to that specified for the bearing. This modeling faithfully reproduces the force-deformation behavior of the bearing, including the dependence

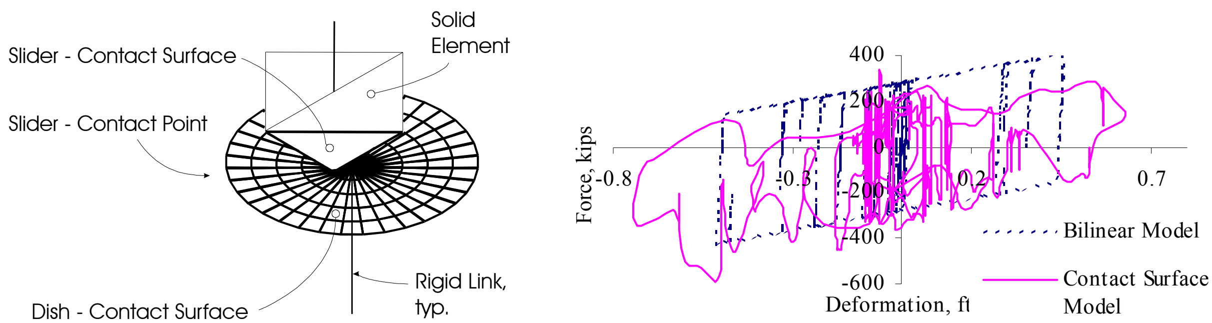

Figure 10. Contact Surface Model of Friction Pendulum Bearing, Aurora Avenue Bridge.

of the restoring force (arising from the curvature of the bearing) and the frictional force on the instantaneous vertical force acting on the bearing. The modeling also captures the bi-directional coupling of the frictional force.

The transverse direction force-deformation hysteresis loops for one of the main span bearings are shown in Figure 10 for both the contact surface model and a conventional bilinear model (where the dependence of behavior on vertical force is ignored). The results for the contact surface model deviate significantly from the idealized hysteresis loops produced by the bilinear model. The contact surface model predicts a peak force of 2630 kN whereas the bilinear model predicts only 1890 kN. The peak *radial* displacement predicted by the contact surface model is 300 mm versus 240 mm predicted by the bilinear model. In part, these differences reflect the large variation in axial force acting on the bearing during an earthquake. This varies between 15.9 MN and 38.3 MN from an initial dead load of 25.4 MN for the design ground motion.

MILLION DOLLAR BRIDGE

The Million Dollar Bridge carries the Copper River Highway across the Copper River, near Cordova, Alaska. The bridge is shown in Figure 11. It consists of four Pratt truss spans measuring 122 m, 91 m, 137 m, and 122 m between centerlines of pins, from south to north of the bridge. The bridge is sup-

Figure 11. The Million Dollar Bridge (Spans 2, 3, & 4 and Piers 2 & 3).

Figure 12. Lifting of Span 4, Million Dollar Bridge.

ported in the river on three massive concrete piers, numbered 1-3 from south to north. Spans 2, 3, & 4 and Piers 2 & 3 are visible in the figure.

The bridge was built in 1909-1910 by the Katalla Corporation to carry the Copper River and Northwestern Railway from Cordova to the Kennecott/Bonanza copper mine. The bridge was first called the Miles Glacier Bridge; it takes its current name from the cost of construction of the bridge, which was actually $1,424,774 (Quinn).

The bridge was badly damaged in the Prince William Sound earthquake (Mw 9.2) on Good Friday March 27, 1964. The southern end of Span 4 fell off of Pier 3 into the Copper River and Span 3 was shifted several feet on top of the pier. Pier 3 was tilted several degrees from the vertical and the top part of the pier was sheared several feet relative to the bottom part. All of the rocker bearings were toppled and all of the bolts at fixed bearings were sheared. Because of the severe damage the bridge was closed to traffic. The volume of traffic using the bridge did not justify repairing it at the time.

The bridge was listed on the National Register of Historic Places on March 31, 2000. This is the nations official list of cultural resources worthy of preservation. The listing has prompted the Alaska Department of Transportation & Public Facilities to rehabilitate the bridge and perform a seismic retrofit so that it won't be destroyed in a future earthquake. The rehabilitation and retrofit must be done in a way that respects the historic nature of the structure, generally in accordance with "The Secretary of the Interior's Standards for Rehabilitation," and the "Guidelines for Rehabilitating Historic Buildings" (Secretary of the Interior).

The most obvious repair to the bridge is the raising of the fallen Span 4 (see Figure 12). As illustrated in the figure, the span was raised using temporary support towers built upstream and downstream of the fallen span and a lifting beam passed underneath the truss. The lifting beam engaged the upstream and downstream faces of the truss at a panel point; at pins connecting the bottom chords, verticals, and diagonals. The lifting beam was raised using a system of jacks and high-strength rods operating from the support towers. Thus, the span was raised to its original position. The truss will be repaired while it's temporarily supported. The bottom chords of the truss were badly bent when the span fell, and many of the bottom lateral braces were smashed. These members will be replaced with new, built-up members similar to the original members.

The other main repair of the bridge will be the replacement of the damaged Pier 3 with a new pier. The main cause of the failure of the bridge in the 1964 earthquake may have been liquefaction of the river sands beneath Pier 3. This would explain the observed 5° tilt of the pier and the inferred tilt (from

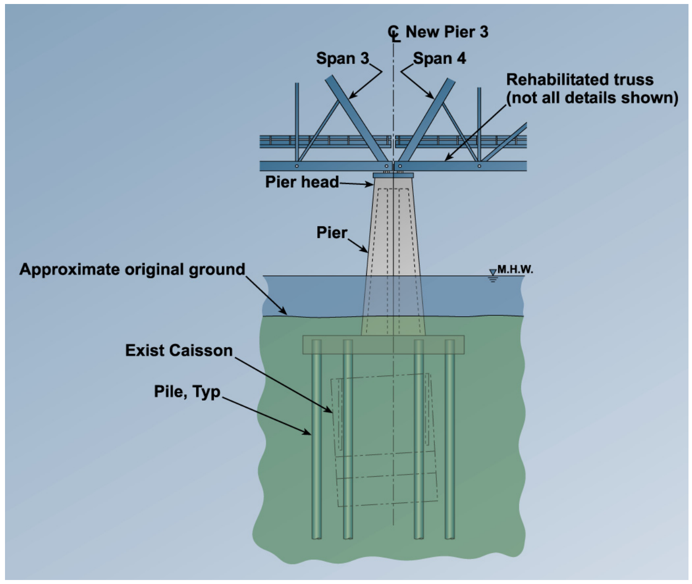

Figure 13. New Pier 3, Million Dollar Bridge.

various evidence) of the caisson supporting it. It's possible that Span 4 fell off of the pier because of the tilt. In any case, the span hit the pier as it fell, breaking it along a construction joint (see Figure 11). The most cost effective and permanent repair is to remove the existing pier and replace it with a new hollow pier supported on a pile foundation, as illustrated in Figure 13. This new foundation will bridge over the old caisson, which will be abandoned. The new piles will be tipped 46 m below the riverbed, below the zone of liquefiable sands.

The main element of the seismic retrofit of the bridge will be the installation of friction pendulum isolation bearings (see Figure 14). All of the existing fixed and rocker bearings were destroyed during the 1964 earthquake and must be replaced. Although friction pendulum bearings are more expensive ($30,000 each) than other bridge bearings they're cost effective in this case because they'll minimize the number of piles required to support the new Pier 3. These 1.83 m diameter pipe piles will cost about

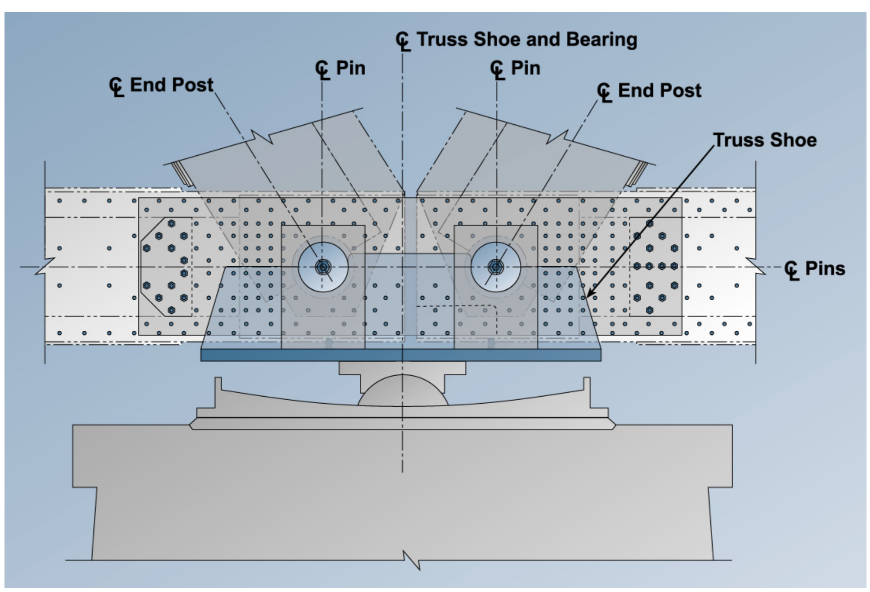

Figure 14. Friction Pendulum Bearing Retrofit, MDB.

$300,000 each because of the difficult site conditions.

SUMMARY

Protective measures in the seismic retrofit and/or design of bridges may take many forms, including the use of dampers for energy absorption and control of displacement; the use of isolation bearings for energy absorption and force-reduction; the use of ductile links for the control and localization of damage; the use of stiffeners to prevent buckling and enhance ductility; and others. The unique circumstances of each bridge and project dictate which measures may be effective and economical.

REFERENCES

Ashley, M., B. Dougherty, R.M. Jones, T. A. Kompfner, and S. Pourvahidi, 2001, "Holding Steady," *Civil Engineering*, Vol. 71, No. 7.

Baker, G., T. Ingham, and D. Heathcote, 1998, "Seismic Retrofit of Vincent Thomas Suspension Bridge," *Transportation Research Record*, No. 1624.

Ingham, T.J., S. Rodriguez, R. Donikian, and J. Chan, 1999, "Seismic Analysis of Bridges with Pile Foundations," *Computers & Structures*, 72:49-62.

Ingham, T.J., 2001, "Modeling of Friction Pendulum Bearings for the Seismic Analysis of Bridges," presented at the *First M.I.T. Conference on Computational Fluid and Solid Mechanics*, Cambridge, MA.

Nader, M. and T.J. Ingham, 1995, "Seismic Retrofit of the Towers of the Golden Gate Bridge," presented at the *National Seismic Conference on Bridges and Highways*, San Diego, CA.

Nader, M., R. Manzanarez, G. Baker, and V. Toan, 2001, "San Francisco-Oakland Bay Bridge Self-Anchored Suspension Span Steel Design Challenges and Solutions," presented at the *National Bridge Steel Alliance Conference*, Chicago, IL.

Secretary of the Interior, *Standards for Rehabilitation & Illustrated Guidelines for Rehabilitating Historic Buildings*, http://www2.cr.nps.gov/tps/tax/rhb/index.htm.

Quinn, A.O., *Iron Rails to Alaska Copper*, NY, D'Aloquin Publishing Co.

Rodriguez, S. and T.J. Ingham, 1995, "Seismic Protective Systems for the Stiffening Trusses of the Golden Gate Bridge," presented at the *National Seismic Conference on Bridges and Highways*, San Diego, CA.

A Structural System for Controlling Longitudinal Movements of a Super Long-Span Cable-stayed Bridge

Aijun Ye [1] Liping Xu [2] Xigang Zhang [3] Lichu Fan [1]

ABSTRACT

The structural behavior of a cable-stayed bridge is highly dependent on its structural system, so it is a key issue in the design of a cable-stayed bridge. For a super long-pan cable-stayed bridge, both floating system and fixed system have serious disadvantages, and the combination of floating system and supplementary longitudinal restraining devices may be a good solution. The investigation of structural system for the Sutong Bridge, which is a cable-stayed bridge with a main span of 1088m, has provided a case study that can supply references to other super long-span cable-stayed bridges.

To limit longitudinal displacements of the Sutong Bridge from service load and earthquake, two supplementary restraining devices were proposed in the technical design stage, namely, elastic links and dampers with ultimate stops. This paper will focus on the investigation of the two devices, including the effect on static and seismic behavior, determination of parameters, and the effectiveness comparison of the two devices, finally, the selection of the final structural system of the bridge was introduced. The final structural system of the Sutong Bridge is the combination of floating system and dampers with ultimate stops allowing 750mm relative movement between girder and pylon, which is a good structural solution that ensures the safety of the bridge in the critical load cases.

[1]State Key Laboratory for Disaster Reduction in Civil Engineering, Tongji University, Shanghai 200092, PRC

[2]Bridge Design Branch, the Architectural Design and Research Institute of Tongji University, Shanghai 200092, PRC

[3]China Highway Planning and Design Institute, Beijing 100010, PRC

1. INTRODUCTION

Quite a lot of long span cable-stayed bridges have been constructed in the world, and their structural systems can be classified under the following four types:1) Free floating system where no bearing is placed between girder and tower, and deck is longitudinally free; 2) Half floating system where longitudinal movable bearings are placed between girder and tower; 3) Fixed system where deck girder is fixed with pylon cross beam; 4) Floating system with supplementary longitudinal restraining device.

The structural behavior of a cable-stayed bridge is highly dependent on its structural system，so it is a key issue in the design of a cable-stayed bridge. In the investigation of structural system, the effect of all loads including service load and seismic load must be taken into account cautiously.

The cable-stayed bridge under investigation is Sutong Highway Bridge over Yangtze River. The Sutong Bridge connects two cities of Jiangsu Province in China, namely, Suzhou and Nantong, and has a main span of 1088m, which will be the longest span of cable-stayed bridge in the world. Because of the super long span, the structural behavior of the bridge is different from general cable-stayed bridge. In order to ensure the safety of the bridge in the critical load cases, the structural system is investigated carefully in the technical design of the bridge.

In the early preliminary design stage of Sutong Bridge, the above-mentioned four types of structural system were compared in view of the static and seismic performance. The comparison of static response indicates that[1]: the floating system will result in large longitudinal displacement at the end of girder and at the top of pylons, also, the bending moment at the bottom of pylons caused by longitudinal static wind and brake force will be very large; adding vertical supports between girder and tower can only change the bending moment of girder near the bearings; the fixed system can greatly reduce longitudinal movements of deck, but will introduce very large axial force of girder and very large bending moment at the bottom of pylons; supplementary longitudinal restraining devices can dramatically improve the static behavior of the bridge. On the other hand, seismic response analysis indicates that: the floating system will result in smaller internal forces of pylon and large longitudinal displacement at the end of girder and at the top of pylons; the fixed system can greatly reduce longitudinal movements of deck, but will increase internal forces of pylons; supplementary longitudinal restraining devices can clearly improve the seismic performance of the bridge. Overall, it is concluded that the combination of floating system and supplementary longitudinal restraining devices is an appropriate system for the Sutong Bridge.

So，the key issue is the choice and design of supplementary restraining devices. In term of operating principle, supplementary restraining devices which have been previously used on long span bridges internationally can be classified under two types, namely, elastic link and damper. The elastic link such as large rubber bearings erected on Tataro Bridge in Japan, steel cables erected on the second Shantou Bay Bridge in China provides elastic stiffness to all loads, but little energy dissipating capability. Supplemental damping devices which provide damping act by dissipating seismic input energy, thereby reducing seismic demands on the structure. Fluid viscous dampers (FVDs) are a type of damping device, which is most popular for long span bridges, and has been erected on lots of large bridges such as the Golden Gate Bridge, Oakland Bay Bridge in USA. Fluid viscous dampers allow for slow movements caused by temperature change, traffic, etc., but reduce stress and deflection caused by earthquake by dissipating energy from the bridge. Moreover, combination of two restraining devices has been used before, for instance, combination of dampers and fuse links is adopted by the Rion-Antirion Bridge in Greece.

To limit longitudinal displacements of the Sutong Bridge from service load and earthquake, two supplementary restraining devices were proposed in the technical design stage, namely, elastic links and dampers with ultimate stops. This paper will focus on the investigation of the two devices, including their effect on structural behavior and determination of parameters, and the selection of the final structural system of the bridge was introduced.

2. BRIDGE DESCRIPTION

The Sutong Bridge has a 1088m center span and two 500m side spans, as shown in Figure 1. Each side span is supported by two auxiliary piers and one transition pier. A counterweight of 37828kN is placed on each side span so as to balance the weight of the center span. The streamlined steel box girder is 40.6m wide and 4.0m deep, as shown in Figure2. The reinforced concrete towers of inverted Y shape are 300.4m high, as shown in Figure3. Towers and piers are all founded on bored piles.
The deck is supported by sliding bearings sitting on top of each auxiliary pier and transition pier, and there is no bearing between girder and crossbeam of each tower.

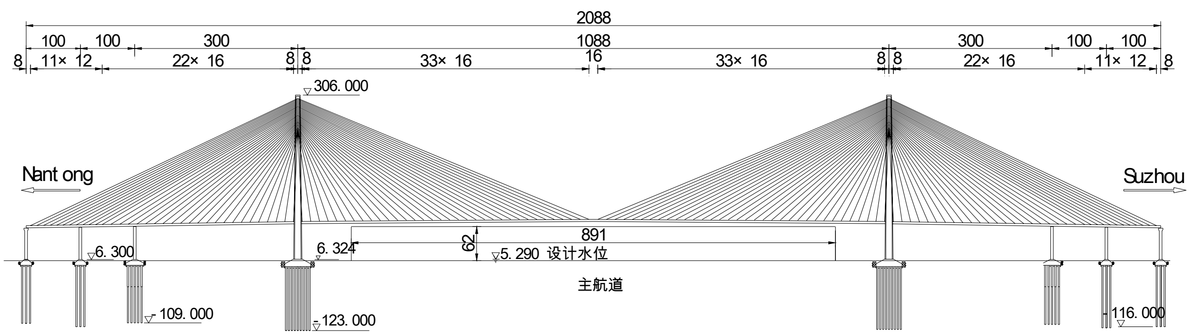

Figure 1 Elevation of the Sutong Bridge

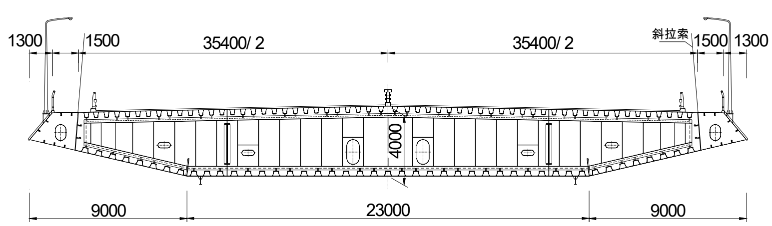

Figure 2 Cross-section of steel box girder

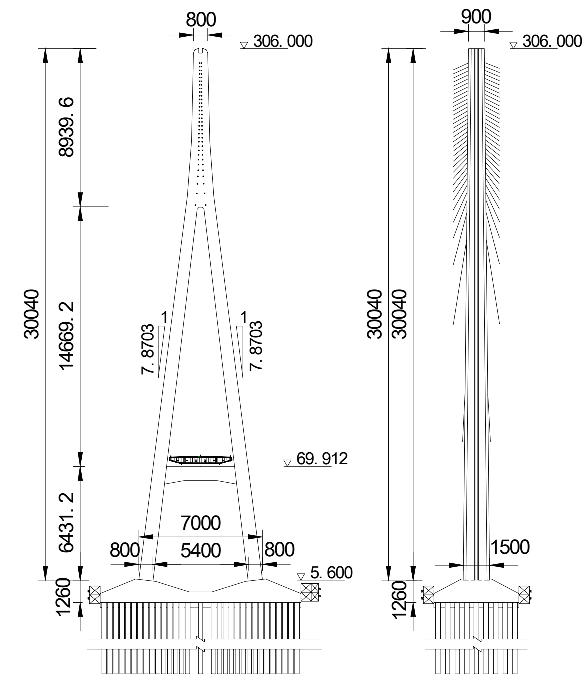

Figure3 Pylon of the Sutong Bridge

3. ANALYSIS MODELS AND LOADS

3.1 Static analysis

The analysis was based on a 2D FEM model, of which the girder, pylons, piers were simulated as 2D beam elements, and flexibility introduced by pile foundations were included. The included loads are vertical traffic, temperature and static wind, which are sensitive to structural system.

3.2 Seismic response analysis

The seismic response was performed using time-history analysis method. The analysis model is a 3D FEM model, as shown in Figure 4. Of the model, the girder, towers, side piers were simulated as beam elements, cables were simulated as truss elements considering the influence of cable's sag, and geometric stiffness caused by dead load was included. Nodes of main girder and cable's anchorage on deck were connected as a master-slave relation.

The constraint condition of the model is as follows: in the longitudinal direction, the girder is connected to pylons with restraining devices, and to all piers with sliding bearings; in the transverse direction, the girder is fixed to all piers and pylons. All piles are fixed at a specific depth below scour elevation, which is determined based on the equivalence of horizontal stiffness for a single pile.

When the deck is free floating, the first order mode shape of the Sutong Bridge will be floating longitudinally, and the corresponding frequency will be 0.0649HZ.

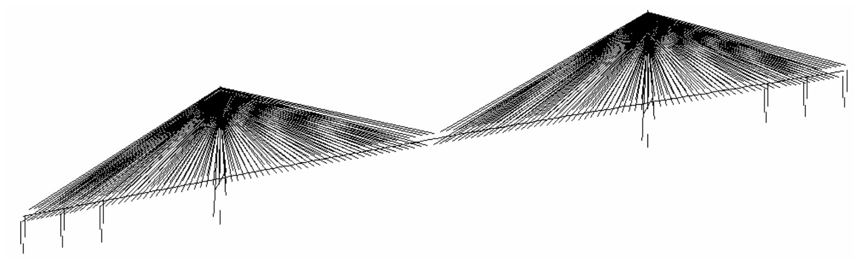

Fig.4 Dynamic analysis model of the Sutong Bridge

A site-specific target response spectrum, which is representative of a 2500-year return period earthquake, was developed by the Earthquake Engineering Research Institute of Jiangsu Province, as shown in Figure 5, in which 5% damping was assumed. Then ten compatible ground motions were developed, Figure 6 shows one of them. The response values of the bridge were obtained as the average results.

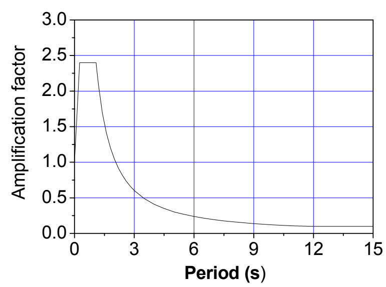

Fig.5 Target response spectrum

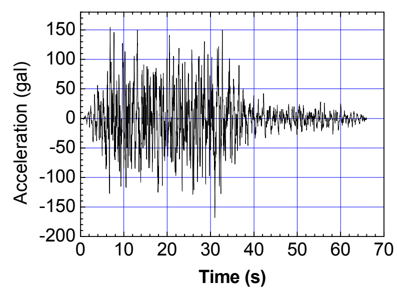

Fig.6 Acceleration time-history

4. EFFECT OF ELASTIC LINKS ON THE STRUCTURAL BEHAVIOR

The effect of elastic links on the structural behavior depends on the elastic stiffness K. Elastic links are active to all loads, so demands of all loads must be taken into account in the determination of elastic stiffness K. In the followings, the effect of elastic stiffness K on static response and seismic response of the Sutong Bridge were analyzed respectively, thereby an appropriate stiffness K was determined.

4.1 Effect of elastic stiffness K on static response

In order to analyze the effect of elastic stiffness on static response, a total of 17 values of K was assumed, namely, K was 0, 5, 10, 15, 20, 30, 40, 60, 80, 100, 120, 140, 160, 200, 300, 400, 500MN/m respectively. K equals 0 represents a floating deck system. Structural Responses caused by temperature change, live load, static wind were calculated respectively, the effects of elastic stiffness K on displacement of deck and bending moment at the bottom of pylon leg were illustrated in Figure 7 and figure 8 respectively.

The two figures indicate that the displacement of deck and bending moment at the bottom of pylon leg are very sensitive to the elastic stiffness when K varies from 0 to 20MN/m, but when K is larger than 50MN/m, the structural responses can not be reduced obviously by increasing elastic stiffness.

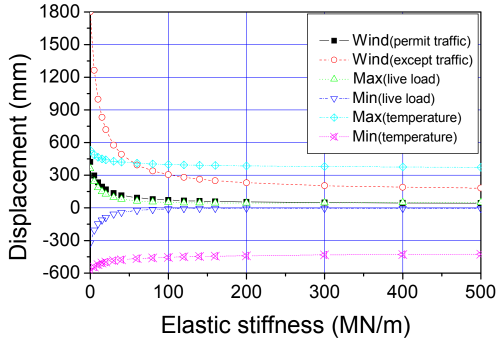

Figure7 Displacement of deck

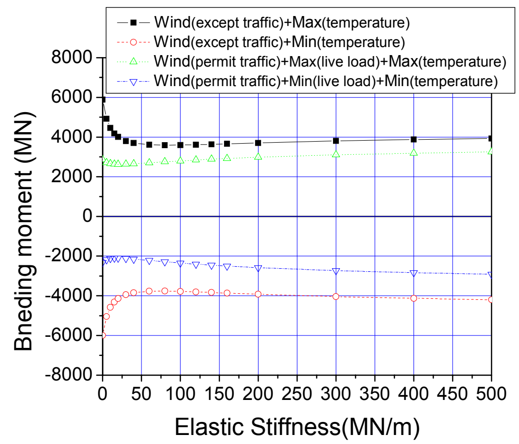

Figure 8 Bending moment at the bottom of pylon leg

4.2 Effect of elastic stiffness K on seismic response

In order to analyze the effect of elastic stiffness on seismic response, a total of 14 values of K was assumed, namely, K equaled 0, 2.5, 5, 10, 12.5, 15, 25, 50, 75, 100, 500, 1000, 1×10^{7}MN/m respectively, and time-history analysis was carried out.

Figure 9 illustrates the change of relative displacement between girder and pylon with the variation of elastic stiffness K, Figure 10 is for the force of elastic link, Figure 11 and 12 are for the deck displacement and bending moment at the bottom of pylon leg. These curves indicate that with the increase of elastic stiffness, the force of link increases monotonously, displacement of deck and between girder and pylon decrease obviously as a whole, while bending moment at the bottom of pylon leg is not sensitive to elastic stiffness. Therefore, the movement of deck can be reduced without increase the bending moment at the bottom of pylon leg using elastic links with appropriate stiffness.

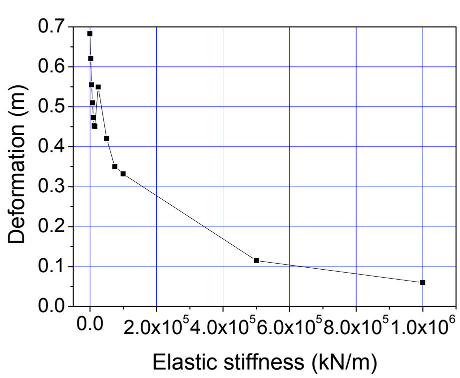

Figure 9 Deformation of the elastic link

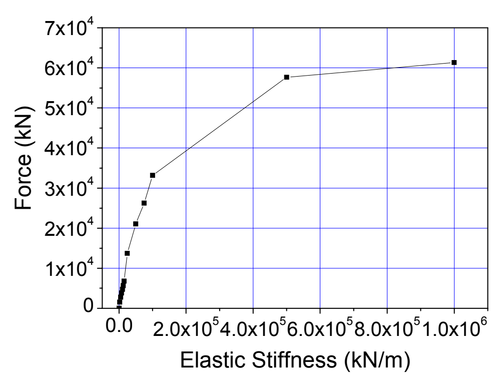

Figure 10 Force of the elastic link

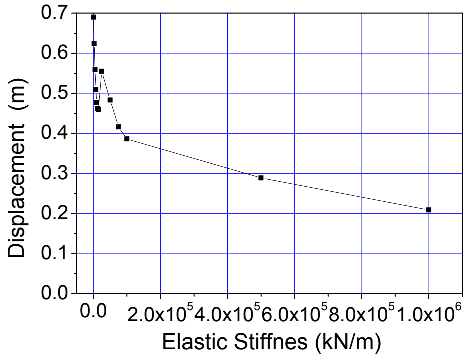

Figure 11 Displacement of deck

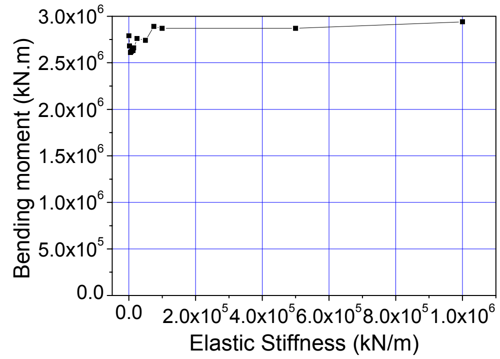

Figure 12 Bending moment at the base of tower

4.3 Determination of the elastic stiffness K

Based on the above analysis, a 50MN/m elastic stiffness of elastic links between girder and one pylon was finally determined after balancing displacements and forces of the bridge.

5. EFFECT OF DAMPERS WITH ULTIMATE STOPS ON THE STRUCTURAL BEHAVIOR

The other alternative for controlling the longitudinal movements of the free floating deck is the combination of dampers and ultimate stops. The dampers will especially be active during a seismic event, but have no effect on the static load cases, namely, the girder will be acting as if it was unrestrained at the pylon. The ultimate stops will be activated by static wind and thereby reduce the movements of girder and forces of pylon. For dynamic wind, the dampers will in principle be active. However, the 10 min mean static wind load acting in the longitudinal direction of the bridge will activate the ultimate stop on minimum one pylon, so the girder will act as if it was rigidly connected to the pylon for dynamic wind load.

It should be ensured that the dampers have adequate movement capacity such that they do not bottom out before the ultimate stop is active, so the movement capacity must meet the movement demands introduced by live load, temperature variation and earthquake. On the other hand, in order to limit the structural response caused by longitudinal static wind, the movement demands caused by earthquake shall be reduced as much as possible.

Therefore, the damper parameters shall be determined based on seismic response analysis, the aim is to limit the longitudinal movements to a given value, and reduce the forces of tower by the way.

5.1 Effect of damper parameters on seismic response

The force (F)-velocity (V) relation for nonlinear fluid viscous dampers can be analytically expressed as a fractional velocity power law:

$$F = C \cdot \operatorname{sgn}(V) \cdot |V|^{\alpha}$$

Where C is the experimentally determined damping coefficient with units of force per velocity raised to the α power, α is a real positive exponent with typical values in the range of 0.35-1 for seismic application, and $\mathrm{sgn}(\cdot)$ is the signum function. The exponent α characterizes the non-linearity of FVDs, for $\alpha = 1$, the above equation becomes $F = C \cdot V$, which represents a linear FVD.

It is obvious that the seismic behavior of a fluid viscous damper depends on two parameters, namely, damping coefficient C and exponent α.

In order to determine appropriate damping coefficient C and exponent α for dampers which will be implemented on the Sutong Bridge, time-history analysis was carried out for the free floating deck system model with longitudinal nonlinear damper erected. The value of α is assumed as 0.3, 0.4, 0.5, 0.7, 1.0 respectively, and value of C ranges from 0 to 25000. A total of ten time-history analyses per C and α were executed using the above mentioned ground motions, and the average responses were adopted.

Among the voluminous results, the displacement and force of damper, the displacement of girder, the bending moment at the bottom of pylon leg are especially monitored. The effects of damper parameters on response of the above components are illustrated in figure 13 to figure 16.

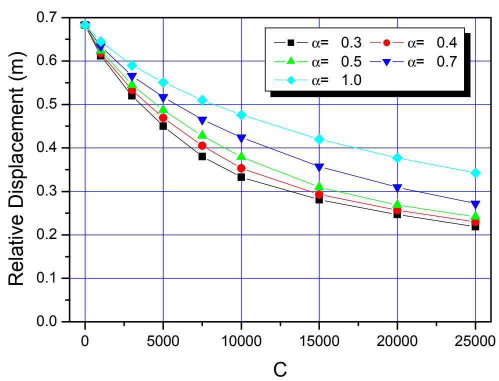

Figure 13 Displacement of the damper

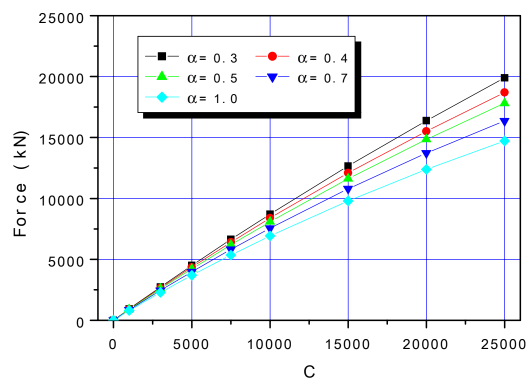

Figure 14 Force of the damper

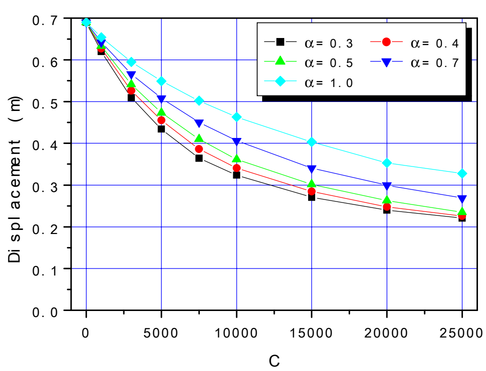

Figure 15 Displacement of deck

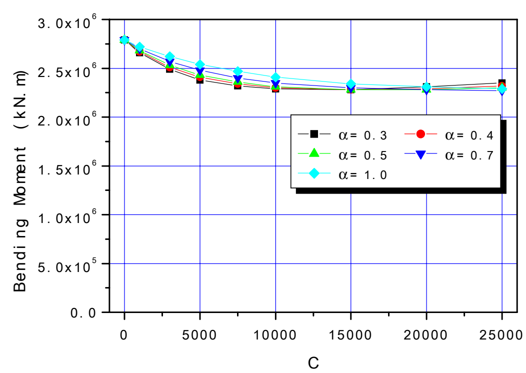

Figure 16 Bending moment at the bottom of tower

Figure 13 to figure 16 indicate that: For a certain exponent α, with the increase of damping coefficient C, the movement of damper and deck decrease, the force of damper increases monotonously, but the bending moment at the bottom of pylon primarily decreases to a minimum value, then increases, and the bending moments are smaller than that of pylon with free floating deck. On the other hand, for a certain damping coefficient C, with the increase of exponent α, the movement of damper and deck increase, but the force of damper decreases. The change of bending moment at the bottom of pylon depends on damping coefficient C, when C is smaller, the bending moment increases with the increase of α, but the trend is contrary for larger C.

It is obvious that viscous dampers can reduce the earthquake response especially displacements notably. In order to limit the movements of deck and damper within 30cm, a velocity exponent α of 0.4, and a damping coefficient C of 15000 were proposed, upon which the maximum velocity of dampers caused by earthquake is 0.58m/s, the maximum displacement of damper is 290mm, and the maximum damper force is 12.1MN.

5.2 Determination of the movement capacity for dampers

The movement capacity must incorporate the demands introduced by live load, temperature variation and earthquake, as shown in Table 1. Therefore, the ultimate stop allows 750mm free relative movement between pylon and girder before it is activated.

Table 1 Determination of movement capacity for dampers

No.	Demands(mm)	Determined capacity (mm)
1	±334(live load)+±348(temperature)=±682	±750
2	±348(temperature)+±290(earthquake)=±638	
3	±185(4-lane live load)+ ±180(temperature variation in a body)+ ±90(greatest wind per day)+±290(earthquake)=±745	

6. FINAL STRUCTURAL SYSTEM

6.1 Selection of final structural system

In table 2, the static and seismic responses of the Sutong Bridge with three systems are compared: 1) the girder is connected by dampers with ultimate stops to pylon, 2) the girder is connected by elastic links to pylon, and 3) the girder is free move to pylon.

Table 2 indicates that:

1) For seismic load, dampers will reduce the deck displacement to 41% compared to a system where the girder is free move to pylon, and the bending moment at the bottom of pylon leg will be reduced to 76%.

2) The ultimate stop is essential for static loads. Compared to a system where the girder is free move to pylon, the ultimate stops allowing 750mm relative movement between girder and pylon will significantly reduce the displacements and forces of the bridge. The displacement of deck will be reduced 46%, and the bending moment at the bottom of pylon leg will be reduced 27%.

3) The effectiveness of elastic links on reducing static response is better than dampers with ultimate stops except for the device force, but for the effectiveness on reducing seismic

response, the latter is much better, because elastic links can't provide energy dissipation during an earthquake event.

Finally, the nonlinear dampers with ultimate stops were proposed by the design group after the advantages of two devices were carefully balanced against their disadvantages.

Table 2 Effect of two restraining devices

Responses		Dampers + stops	Elastic links	Floating deck
		C=15000， α =0.4 ±750mm	K=50MN/m	/
Static Response	Longitudinal displacement of deck (m)	+1.160/-1.189	+0.857/-0.914	+2.151/-2.209
	Longitudinal displacement at pylon top (m)	+1.044/-1.066	+0.848/-0.898	+2.211/-2.263
	Bending moment at pylon bottom (MN.m)	+3940.4/-4011.3	+3653.0/-3810.2	+5400.4/-5516.5
	Device deformation (m)	+0.769/-0.767	+0.468/-0.489	+1.763/-1.789
	Device force (MN)	20.621	22.809/-23.844	/
Seismic response	Longitudinal displacement of deck (m)	0.285/0.272	0.483/0.470	0.690/0.673
	Longitudinal displacement at pylon top (m)	0.371/0.368	0.637/0.625	0.820/0.818
	Bending moment at pylon bottom (MN.m)	2280/1740	2740/2500	2790/2490
	Device deformation (m)	0.293/0.271	0.421/0.439	0.683/0.673
	Device force (MN)	12.1/11.6	21.0/22.0	/

In which, the static critical load combination is wind load except traffic+ temperature, "+" represents toward main span, and "-" represents opposite main span; the seismic response values are: north side/south side.

6.2 Parameters of dampers with ultimate stops

A total of 4 dampers with ultimate stops are placed at each pylon, as shown in Figure 17. The key parameters of each device are listed in Table 3.

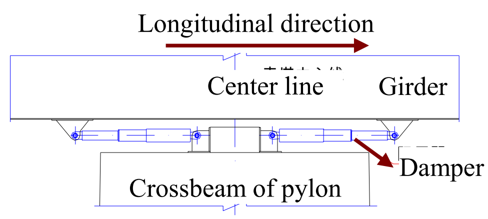

Figure 17 Arrangement of dampers with ultimate stops

Table 3 Key parameters of a damper with ultimate stop

item	parameter	value
Damper	α	0.4
	C $(kN/(m/s)^{0.4})$	3750
	V_{max} (m/s)	0.58
	F_{max} (MN)	3.025
	Movement capacity	±750
	V_{max} caused by temperature	232mm per 10 hours
	F_{max} caused by temperature	<3025×5%=151(kN)
Ultimate stop	F_{max} (MN)	6.58

7. CONCLUSIONS

For a super long-pan cable-stayed bridge, both floating system and fixed system have serious disadvantages, and the combination of floating system and supplementary longitudinal restraining devices may be a good solution. The investigation of structural system for the Sutong Bridge has provided a case study that can supply references to other super long-span cable-stayed bridges.

To limit longitudinal displacements of the bridge from traffic, wind and earthquake, two supplementary restraining devices under investigation, namely, elastic links and dampers with ultimate stops are all effective solutions. The reduction of longitudinal deck movements will reduce the wear of bearings and expansion joints, thereby increase their lifetime. With appropriate parameters which are determined based on the parameter sensitivity analysis, the effectiveness of elastic links on reducing static response is better than dampers with ultimate stops except for the device force, but for the effectiveness on reducing seismic response, the latter is much better. The dampers will notably reduce the seismic responses especially the deck movements of the bridge, but have no effect on the static response, so the ultimate stop is essential for static loads. The ultimate stops allowing 750mm relative movement between girder and pylon will significantly reduce the static displacements and forces of the bridge.

Overall, the combination of dampers and ultimate stops is a good structural solution that ensures the safety of the Sutong Bridge in the critical load cases.

Acknowledgments

Investigations of the structural system for the Sutong Bridge were finished by the Sutong Bridge Design Group and the Bridge Seismic Research Section of the State Key Laboratory for Disaster Reduction in China, so the authors wish to acknowledge all our colleagues.

REFERENCES

Wen-Hsiung Lin and Anil K. Chopra, *Earthquake response of elastic SDF systems with non-linear fluid viscous dampers*, E.E.S.D., 2002, Vol.31

Charles Seim, *The seismic retrofit of the Golden Gate Bridge,* Proceedings of the first PRC-US workshop on seismic analysis and design of special bridges, Technical Report MCEER-03-0004, 2003

Liping Xu, *Analysis of structural systems for super long-span cable-stayed bridges (in Chinese), J*ournal of Tongji University, 2004.4

Liping Xu, Xigang Zhang etc., *Investigation of structural system for the Sutong Bridge (in Chinese),* Proceedings of the Sutong Bridge, Vol.1, Jiangsu Province Sutong Bridge Construction Commanding Department, P.R.C., Chinese Science and Technology Publishing House, 2004.9

Phase-difference-based Simulation of Correlated and Non-stationary Accelerograms

Qingshan YANG and Yuji TIAN

School of Civil Engineering & Architecture, Beijing Jiaotong University, Beijing 100044, China

ABSTRACT: A new approach of spatially correlated and non-stationary earthquake ground motions based on phase difference spectrum is presented. The independent non-stationary accelerograms of the reference points, specified for each different type soil, are simulated by the inverse FFT, in which the Fourier amplitude spectrums are compatible with the specified power spectrum density functions and the Fourier phase spectrums are simulated on the basis of the empirical model of the phase difference spectrum. The spatial correlated and non-stationary earthquake ground motions are simulated by the Kriging technique, on the conditions of incoherency function and reference ground motions.

School of Civil Engineering and Architecture, Beijing Jiaotong University, Beijing 100044, PRC

INTRODUCTION

In the seismic analysis of extended structures and space structures, such as long-span bridge, dams, pipelines, sports stadium, etc., the earthquake excitations of different supports are different, spatial correlated and non-stationary in temporal and frequency domains. Hence a sets of correlated and non-stationary earthquake ground motions is demanded when a multi-support structure is analyzed dynamically. Nevertheless, the recorded earthquake ground motions in arrays of accelerometers, such as SMART-1, LSST, etc., are not consistent with all the different sites; the correlated and non-stationary earthquake ground motions, which satisfied the special conditions of a site, should be simulated.

Based on Vanmarcke et al (1991; 1993; 1999), this new approach to simulate non-stationary fields of earthquake ground motions is presented, in which reference points are added to each different type soil. The ground motions of reference points are generated independently based on their power spectral density functions (Clough and Penzien 1993) and phase difference spectrum (Thráinsson and Kremidjian 2002); then spatially correlated and non-stationary earthquake ground motions are simulated by the Kriging technique.

CONDITIONAL SIMULATION OF CORRELATED GROUND MOTIONS

Let $x_i(t_m)$ denote a zero-mean, stationary and discrete random process at point i,

$$x_i(t_m) = \sum_{k=0}^{K-1}\left[A_{ik}\cos(\omega_k t_m) + B_{ik}\sin(\omega_k t_m)\right] \tag{1}$$

where A_{ik} and B_{ik} are independent, zero-mean, Gaussian random variables; $t_m = m\Delta t$; $\Delta t = \dfrac{t_f}{K-1}$ (t_f is the duration); $\omega_k = k\Delta\omega$; $\Delta\omega = \dfrac{2\pi}{K\Delta t}$; $k = 0,1,\cdots\cdots,K-1$. Eq.(1) can be rewritten as

$$x_i(t_m) = \sum_{k=0}^{K-1}\left[A_{ik}\cos\left(\frac{2\pi km}{K}\right) + B_{ik}\sin\left(\frac{2\pi km}{K}\right)\right] = \sum_{k=0}^{K-1}\left(A_{ik}\,\mathrm{c}_{km} + B_{ik}\,\mathrm{s}_{km}\right) \tag{2}$$

where $c_{km} = \cos\left(\dfrac{2\pi km}{K}\right)$; $s_{km} = \sin\left(\dfrac{2\pi km}{K}\right)$. Coefficients A_{ik} and B_{ik} are related to $x_i(t_m)$ through the discrete Fourier transform

$$A_{ik} = \frac{1}{K}\sum_{m=0}^{K-1}x_i(t_m)c_{km} \quad , \quad B_{ik} = \frac{1}{K}\sum_{m=0}^{K-1}x_i(t_m)\mathrm{s}_{km} \tag{3}$$

and are symmetric and asymmetric, respectively

$$A_{i,K-k} = A_{ik}\ , \quad B_{i,K-k} = -B_{ik}\ , \quad k = 1,2,\cdots\cdots,K/2 \tag{4}$$

The zero-mean Gaussian variables A_{ik} and B_{ik} are generated if their variances are expressed by the power spectrum functions and the spatial coherency functions; then the simulated time histories are generated. The cross-correlation function of a pair of time histories can be expressed in time domain and can also be expressed by cross-spectrum in terms of power spectrum density function and the coherency function; thus the relationships between the variance or covariance of the coefficients and the cross-spectrum are established. The following is the details.

The covariance of A_{ik} and A_{jk} is

$$\begin{aligned} E\left[A_{ik}A_{jk}\right] &= E\left[\frac{1}{K}\sum_{m=0}^{K-1}x_i(t_m)c_{km}\cdot\frac{1}{K}\sum_{n=0}^{K-1}x_j(t_n)c_{kn}\right] \\ &= \frac{1}{K^2}\sum_{m=0}^{K-1}\sum_{n=0}^{K-1}E\left[x_i(t_m)x_j(t_n)\right]c_{km}c_{kn} \\ &= \frac{1}{K^2}\sum_{m=0}^{K-1}\sum_{n=0}^{K-1}R_{ij}(\tau)c_{km}c_{kn} \end{aligned} \tag{5}$$

where $R_{ij}(\tau)=E\left[x_i(t_m)x_j(t_n)\right]$ is the cross-correlation function of points i and j; and $\tau=t_m-t_n$.

The covariance of B_{ik} and B_{jk} is

$$\begin{aligned} E\left[B_{ik}B_{jk}\right] &= E\left[\frac{1}{K}\sum_{m=0}^{K-1}x_i(t_m)s_{km}\cdot\frac{1}{K}\sum_{n=0}^{K-1}x_j(t_n)s_{kn}\right] \\ &= \frac{1}{K^2}\sum_{m=0}^{K-1}\sum_{n=0}^{K-1}E\left[x_i(t_m)x_j(t_n)\right]s_{km}s_{kn} \\ &= \frac{1}{K^2}\sum_{m=0}^{K-1}\sum_{n=0}^{K-1}R_{ij}(\tau)s_{km}s_{kn} \end{aligned} \tag{6}$$

The covariance of A_{ik} and B_{jk} is

$$\begin{aligned} E\left[A_{ik}B_{jk}\right] &= E\left[\frac{1}{K}\sum_{m=0}^{K-1}x_i(t_m)c_{km}\cdot\frac{1}{K}\sum_{n=0}^{K-1}x_j(t_n)s_{kn}\right] \\ &= \frac{1}{K^2}\sum_{m=0}^{K-1}\sum_{n=0}^{K-1}E\left[x_i(t_m)x_j(t_n)\right]c_{km}s_{kn} \\ &= \frac{1}{K^2}\sum_{m=0}^{K-1}\sum_{n=0}^{K-1}R_{ij}(\tau)c_{km}s_{kn} \end{aligned} \tag{7}$$

The cross-correlation function can be written discretely in terms of cross-spectrum, $S_{ij}(\omega_k)$,

$$R_{ij}(\tau)=\sum_{r=0}^{K-1}2\,\mathrm{Re}\left[S_{ij}(\omega_k)\right]\cos\left(\omega_r\tau\right)\Delta\omega-\sum_{r=0}^{K-1}2\,\mathrm{Im}\left[S_{ij}(\omega_k)\right]\sin\left(\omega_r\tau\right)\Delta\omega \tag{8}$$

where $\mathrm{Re}[\bullet]$, $\mathrm{Im}[\bullet]$ stand for real part and image part respectively; and there are

$$\begin{cases}\cos\left(\omega_r\tau\right)=\cos\left(\omega_r t_m-\omega_r t_n\right)=c_{rm}c_{rn}+s_{rm}s_{rn}\\ \sin\left(\omega_r\tau\right)=\sin\left(\omega_r t_m-\omega_r t_n\right)=s_{rm}c_{rn}-c_{rm}s_{rn}\end{cases} \tag{9}$$

Substituting Eq.(9) into Eq.(8), there is

$$R_{ij}(\tau)=2\Delta\omega\cdot\left\{\sum_{r=0}^{K-1}\mathrm{Re}\left[S_{ij}(\omega_k)\right]\left(c_{rm}c_{rn}+s_{rm}s_{rn}\right)-\sum_{r=0}^{K-1}\mathrm{Im}\left[S_{ij}(\omega_k)\right]\left(s_{rm}c_{rn}-c_{rm}s_{rn}\right)\right\} \tag{10}$$

$S_{ij}(\omega_k)$ can be written as

$$S_{ij}(\omega_k)=\gamma_{ij}(\omega_k)\cdot\sqrt{S_i(\omega_k)\cdot S_j(\omega_k)}=\frac{1}{2}\gamma_{ij}(\omega_k)\cdot\sqrt{G_i(\omega_k)\cdot G_j(\omega_k)} \tag{11}$$

where $S_i(\omega_k)$, $S_j(\omega_k)$ are the two-side power spectrum density functions of points i and j, respectively; $G_i(\omega_k)$, $G_j(\omega_k)$ are the one-side power spectrum density functions respectively, which can be specified according to the empirical models (Clough and Penzien 1993; Kanai 1957; Tajimi 1960). $\gamma_{ij}(\omega_k)$ is the spatial coherency function of points i and j, which can be predefined (Harichandran and Vanmarke 1986; Hao, Oliveira and Penzien 1989; Abrahamson 1991; Yang and Chen 2000).

Substituting Eq.(11) into Eq.(10) yields

$$R_{ij}(\tau)=\Delta\omega\sqrt{G_i(\omega_k)\cdot G_j(\omega_k)}\cdot\left\{\sum_{r=0}^{K-1}\mathrm{Re}\left[\gamma_{ij}(\omega_k)\right]\left(c_{rm}c_{rn}+s_{rm}s_{rn}\right)-\sum_{r=0}^{K-1}\mathrm{Im}\left[\gamma_{ij}(\omega_k)\right]\left(s_{rm}c_{rn}-c_{rm}s_{rn}\right)\right\} \tag{12}$$

Substituting Eq.(12) into Eq.(5), Eq.(6), Eq.(7) respectively, there are

$$\begin{aligned}E\left[A_{ik}A_{jk}\right]=\frac{\Delta\omega\sqrt{G_i(\omega_k)\cdot G_j(\omega_k)}}{K^2}&\left\{\sum_{r=0}^{K-1}\mathrm{Re}\left[\gamma_{ij}(\omega_k)\right]\cdot\left(\sum_{m=0}^{K-1}c_{km}c_{rm}\sum_{n=0}^{K-1}c_{kn}c_{rn}+\sum_{m=0}^{K-1}c_{km}s_{rm}\sum_{n=0}^{K-1}c_{kn}s_{rn}\right)\right.\\&\left.-\sum_{r=0}^{K-1}\mathrm{Im}\left[\gamma_{ij}(\omega_k)\right]\cdot\left(\sum_{m=0}^{K-1}c_{km}s_{rm}\sum_{n=0}^{K-1}c_{kn}c_{rn}-\sum_{m=0}^{K-1}c_{km}c_{rm}\sum_{n=0}^{K-1}c_{kn}s_{rn}\right)\right\}\end{aligned} \tag{13}$$

$$\begin{aligned}E\left[B_{ik}B_{jk}\right]=\frac{\Delta\omega\sqrt{G_i(\omega_k)\cdot G_j(\omega_k)}}{K^2}&\left\{\sum_{r=0}^{K-1}\mathrm{Re}\left[\gamma_{ij}(\omega_k)\right]\cdot\left(\sum_{m=0}^{K-1}s_{km}c_{rm}\sum_{n=0}^{K-1}s_{kn}c_{rn}+\sum_{m=0}^{K-1}s_{km}s_{rm}\sum_{n=0}^{K-1}s_{kn}s_{rn}\right)\right.\\&\left.-\sum_{r=0}^{K-1}\mathrm{Im}\left[\gamma_{ij}(\omega_k)\right]\cdot\left(\sum_{m=0}^{K-1}s_{km}s_{rm}\sum_{n=0}^{K-1}s_{kn}c_{rn}-\sum_{m=0}^{K-1}s_{km}c_{rm}\sum_{n=0}^{K-1}s_{kn}s_{rn}\right)\right\}\end{aligned} \tag{14}$$

$$\begin{aligned}E\left[A_{ik}B_{jk}\right]=\frac{\Delta\omega\sqrt{G_i(\omega_k)\cdot G_j(\omega_k)}}{K^2}&\left\{\sum_{r=0}^{K-1}\mathrm{Re}\left[\gamma_{ij}(\omega_k)\right]\cdot\left(\sum_{m=0}^{K-1}c_{km}c_{rm}\sum_{n=0}^{K-1}s_{kn}c_{rn}+\sum_{m=0}^{K-1}c_{km}s_{rm}\sum_{n=0}^{K-1}s_{kn}s_{rn}\right)\right.\\&\left.-\sum_{r=0}^{K-1}\mathrm{Im}\left[\gamma_{ij}(\omega_k)\right]\cdot\left(\sum_{m=0}^{K-1}c_{km}s_{rm}\sum_{n=0}^{K-1}s_{kn}c_{rn}-\sum_{m=0}^{K-1}c_{km}c_{rm}\sum_{n=0}^{K-1}s_{kn}s_{rn}\right)\right\}\end{aligned} \tag{15}$$

Considering the trigonometric identities, there are

$$\sum_{n=0}^{K-1}c_{kn}s_{rn}=0\quad\sum_{m=0}^{K-1}c_{km}s_{rm}=0\quad\sum_{n=0}^{K-1}s_{kn}c_{rn}=0\quad\sum_{m=0}^{K-1}s_{km}c_{rm}=0 \tag{16}$$

$$\sum_{n=0}^{K-1}c_{kn}c_{rn}=\begin{cases}K & ,\quad k=r=0\ or\ K/2\\ K/2 & ,\quad k=r=1,2,\cdots,K/2-1\quad or\quad k=1,2,\cdots,K/2-1\ and\ r=K-k\\ 0 & ,\quad others\end{cases} \tag{17}$$

$$\sum_{n=0}^{K-1}s_{kn}s_{rn}=\begin{cases}K/2 & ,\quad k=r=1,2,\cdots,K/2-1\\ -K/2 & ,\quad k=1,2,\cdots,K/2-1\ and\ \ r=K-k\\ 0 & ,\quad others\end{cases} \tag{18}$$

Substituting Eqs.(16), (17) into Eq.(13), one can obtain

$$E\left[A_{ik}A_{jk}\right]=\begin{cases}\dfrac{\Delta\omega}{2}\mathrm{Re}\left[\gamma_{ij}(\omega_k)\right]\cdot\sqrt{G_i(\omega_k)\cdot G_j(\omega_k)} & ,\quad k=0\\ \dfrac{\Delta\omega}{4}\left\{\mathrm{Re}\left[\gamma_{ij}(\omega_k)\right]\cdot\sqrt{G_i(\omega_k)\cdot G_j(\omega_k)}\right.\\ \quad\left.+\mathrm{Re}\left[\gamma_{ij}(\omega_{K-k})\right]\cdot\sqrt{G_i(\omega_{K-k})\cdot G_j(\omega_{K-k})}\right\} & ,\quad k=1,2,\cdots\cdots K/2-1\\ \Delta\omega\cdot\mathrm{Re}\left[\gamma_{ij}(\omega_k)\right]\cdot\sqrt{G_i(\omega_k)\cdot G_j(\omega_k)} & ,\quad k=K/2\end{cases} \tag{19}$$

Substituting Eqs.(16), (18) into Eq.(14), one can obtain

$$E\left[B_{ik}B_{jk}\right]=\begin{cases}0 & , \quad k=0\\ \dfrac{\Delta\omega}{4}\left\{\mathrm{Re}\left[\gamma_{ij}(\omega_k)\right]\cdot\sqrt{G_i(\omega_k)\cdot G_j(\omega_k)}\right. & \\ \quad \left.+\mathrm{Re}\left[\gamma_{ij}(\omega_{K-k})\right]\cdot\sqrt{G_i(\omega_{K-k})\cdot G_j(\omega_{K-k})}\right\} & , \quad k=1,2,\cdots\cdots K/2\end{cases} \tag{20}$$

Substituting Eqs.(16), (17), (18) into Eq.(15), one can obtain

$$E\left[A_{ik}B_{jk}\right]=\begin{cases}0 & , \quad k=0,K/2\\ \dfrac{\Delta\omega}{4}\left\{\mathrm{Im}\left[\gamma_{ij}(\omega_k)\right]\cdot\sqrt{G_i(\omega_k)\cdot G_j(\omega_k)}\right. & \\ \quad \left.+\mathrm{Im}\left[\gamma_{ij}(\omega_{K-k})\right]\cdot\sqrt{G_i(\omega_{K-k})\cdot G_j(\omega_{K-k})}\right\} & , \quad k=1,2,\cdots\cdots K/2-1\end{cases} \tag{21}$$

Let the vector of simulated Fourier coefficients at frequency ω_k $(k=1,2,\cdots,N)$ be defined as

$$F_k=\left\{A_{s\alpha k}\ B_{s\alpha k} \vdots A_{s\beta k}\ B_{s\beta k}\right\}^T \tag{22}$$

where $\left\{A_{s\alpha k}\right\}=\left\{A_{s1k}\quad A_{s2k}\quad \cdots\cdots \quad A_{snk}\right\}^T$, $\left\{B_{s\alpha k}\right\}=\left\{B_{s1k}\quad B_{s2k}\quad \cdots\cdots\quad B_{snk}\right\}^T$ are the coefficients at the known points where the acceleration time histories are recorded or simulated; and $\left\{A_{s\beta k}\right\}=\left\{A_{s(n+1)k}\quad A_{s(n+2)k}\quad \cdots\cdots \quad A_{sNk}\right\}^T$, $\left\{B_{s\beta k}\right\}=\left\{B_{s(n+1)k}\quad B_{s(n+2)k}\quad \cdots\cdots\quad B_{sNk}\right\}^T$ are the coefficients at the unknown points where the acceleration time histories will be simulated.

The covariance matrix of Fourier coefficients at frequency ω_k is

$$C_k=E\left[F_kF_k^T\right]=\begin{bmatrix}C_{\alpha\alpha k} & C_{\alpha\beta k}\\ C_{\alpha\beta k}^T & C_{\beta\beta k}\end{bmatrix}_{2N\times 2N} \tag{23}$$

where the matrices $C_{\alpha\alpha k}$, $C_{\alpha\beta k}$ $C_{\beta\beta k}$ are, respectively,

$$C_{\alpha\alpha k}=\begin{bmatrix}E\left[A_{s\alpha k}A_{s\alpha k}^T\right] & E\left[A_{s\alpha k}B_{s\alpha k}^T\right]\\ E\left[B_{s\alpha k}A_{s\alpha k}^T\right] & E\left[B_{s\alpha k}B_{s\alpha k}^T\right]\end{bmatrix}, C_{\alpha\beta k}=\begin{bmatrix}E\left[A_{s\alpha k}A_{s\beta k}^T\right] & E\left[A_{s\alpha k}B_{s\beta k}^T\right]\\ E\left[B_{s\alpha k}A_{s\beta k}^T\right] & E\left[B_{s\alpha k}B_{s\beta k}^T\right]\end{bmatrix}, C_{\beta\beta k}=\begin{bmatrix}E\left[A_{s\beta k}A_{s\beta k}^T\right] & E\left[A_{s\beta k}B_{s\beta k}^T\right]\\ E\left[B_{s\beta k}A_{s\beta k}^T\right] & E\left[B_{s\beta k}B_{s\beta k}^T\right]\end{bmatrix} \tag{24}$$

and the elements of $C_{\alpha\alpha k}$ 、 $C_{\alpha\beta k}$ 、 $C_{\beta\beta k}$ are expressed in Eqs.(19)～(21).

C_k is positive definite and can be expressed by means of Cholesky decomposition as the product of a non-singular lower triangular matrix, L_k , and its transpose

$$C_k=L_kL_k^T \tag{25}$$

The simulated coefficients can be defined as

$$\left\{A_{s\alpha k}\ B_{s\alpha k}\vdots A_{s\beta k}\ B_{s\beta k}\right\}^T=L_kU_k \tag{26}$$

where $U_k=\left\{U_{1k}\ \ U_{2k}\ \ \cdots\cdots U_{2Nk}\right\}^T$, $U_{1k},U_{2k},\cdots\cdots,U_{2Nk}$ are independent standard normal random variables.

The best linear unbiased estimators of $A_{s\beta k}$, $B_{s\beta k}$ can be expressed as

$$A_{s\beta k}^*=C_{\alpha\beta k}^TC_{\alpha\alpha k}^{-1}A_{s\alpha k} \quad , \qquad B_{s\beta k}^*=C_{\alpha\beta k}^TC_{\alpha\alpha k}^{-1}B_{s\alpha k} \tag{27}$$

The estimation errors of $A^*_{s\beta k}$, $B^*_{s\beta k}$ are defined, respectively,

$$R_{(A_{s\beta k})} = A_{s\beta k} - A^*_{s\beta k} \quad , \qquad R_{(B_{s\beta k})} = B_{s\beta k} - B^*_{s\beta k} \tag{28}$$

Let $x_\alpha = \{x_1, x_2, \cdots\cdots, x_n\}^T$ be the recorded or simulated acceleration time histories of points $1, 2, \cdots, n$ and $x_\beta = \{x_{n+1}, x_{n+2}, \cdots\cdots, x_N\}^T$ be the unknown acceleration time histories of points $n+1, n+2, \cdots, N$ and thus the field of earthquake ground motions are $x = \{x_\alpha \quad x_\beta\}^T$. Let $A_{\alpha k}$, $B_{\alpha k}$ denote the Fourier coefficients of the recorded accelerograms and $A_{\beta k}$, $B_{\beta k}$ denote the Fourier coefficients of the accelerations at the unknown points. The best linear unbiased estimators of $A_{\beta k}$, $B_{\beta k}$ can be expressed as

$$A^*_{\beta k} = C^T_{\alpha\beta} C^{-1}_{\alpha\alpha} A_{\alpha k} \quad , \qquad B^*_{\beta k} = C^T_{\alpha\beta} C^{-1}_{\alpha\alpha} B_{\alpha k} \tag{29}$$

The estimation errors of $A^*_{\beta k}$, $B^*_{\beta k}$ are defined, respectively,

$$R_{(A_{\beta k})} = A_{\beta k} - A^*_{\beta k} \quad , \qquad R_{(B_{\beta k})} = B_{\beta k} - B^*_{\beta k} \tag{30}$$

Suppose that the errors in Eq.(30) are equal to the errors in Eq.(28), the simulated coefficients of unknown points are

$$A_{\beta k} = A^*_{\beta k} + \left(A_{s\beta k} - A^*_{s\beta k}\right) \quad , \qquad B_{\beta k} = B^*_{\beta k} + \left(B_{s\beta k} - B^*_{s\beta k}\right) \tag{31}$$

then the accelerations of unknown points are generated by inverse FFT technique. In Eq.(31), the first items $A^*_{\beta k}$, $B^*_{\beta k}$ are the linear combination of $A_{\alpha k}$, $B_{\alpha k}$, and $A^*_{\beta k}$, $A_{\alpha k}$ or $B^*_{\beta k}$, $B_{\alpha k}$ have the same means and variances; consequently the non-stationary characteristics of the simulated acceleration histories are similar to those of the acceleration records. The second items $(A_{s\beta k} - A^*_{s\beta k})$, $(B_{s\beta k} - B^*_{s\beta k})$ are the estimation errors and are the differences of two random variables, respectively. Hence the second items are the random perturbations of the first items, respectively.

PHASE-DIFFERENCE-BASED SIMULATION OF CORRELATED ACCELEROGRAMS

It has been shown by Ohsaki (1979), Nigma (1982) and Boore (2003) that the non-stationary characteristics of earthquake ground motions are contained in their phase difference spectrums. Thus, it follows that the non-stationary accelerations of one point or more than one points, which are called reference points, are simulated and the correlated accelerations are simulated by Kriging technique. The independent non-stationary accelerograms of the reference points are simulated by the inverse FFT, in which the Fourier amplitude spectrums are compatible with the specified power spectrum density functions and the Fourier phase spectrums are simulated on the basis of the empirical model of the phase difference spectrum

(Thráinsson and Kremidjian 2002). Suppose that the soil conditions of all target points are identical, one target point may be specified as the reference point (shown in Fig.1). Otherwise more than one reference points are defined (shown in Fig.2); one reference point may be a target point whereas the other reference points are added and each added reference point corresponds to a type of soil conditions.

(a) Positions of target points

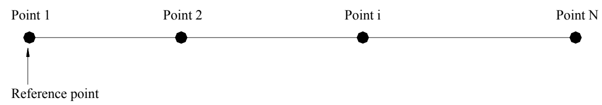

(b) Specifying one target point as the reference point

Fig.1 Choosing one reference point for identical soil conditions

(a) Positions of target points

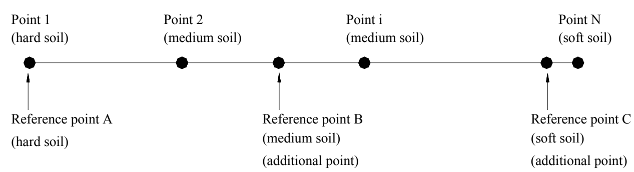

(b) Specifying more than one reference points

Fig.2 Choosing more than one reference points for different soil conditions

The simulated time histories of reference points are independent of each other in that their phase difference spectrums are generated independently. Considering the spatial coherency functions among the target points and the reference points, the correlated and non-stationary accelerograms are simulated as mentioned above. The simulated histories between a pair of target points are correlated, non-stationary in temporal and frequency domains.

NUMERICAL EXAMPLES

In the following two examples, the ground motions of three points are simulated respectively. The configuration of the three points is shown in Fig.3.

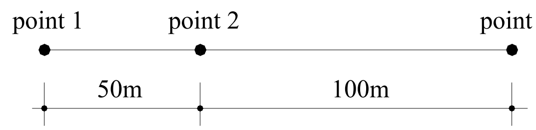

Fig.3 Configuration of three points

The Clough-Penzien acceleration spectrum (Clough and Penzien 1993) is selected for the power spectrum density function, i.e.,

$$S(\omega)=S_0\cdot\left[\frac{1+4\zeta_g^2\left(\omega/\omega_g\right)^2}{\left(1-\left(\omega/\omega_g\right)^2\right)^2+4\zeta_g^2\left(\omega/\omega_g\right)^2}\right]\cdot\left[\frac{\left(\omega/\omega_f\right)^4}{\left(1-\left(\omega/\omega_f\right)^2\right)^2+4\zeta_f^2\left(\omega/\omega_f\right)^2}\right] \tag{32}$$

where S_0 is a constant to determine the intensity of the simulated acceleration time histories; ω_g, ζ_g are frequency and damping ratio of the soil; ω_f, ζ_f are the filtering parameters. The parameters are listed in Table 1 and the power spectrum density functions for rock, hard soil and soft soil are shown in Fig.4.

Table 1 Parameters of Clough-Penzien model

	Rock	Hard soil	Soft soil
ω_g (rad/s)	8π	5π	2.4π
ζ_g	0.60	0.60	0.85
ω_f (rad/s)	0.8π	0.5π	0.24π
ζ_f	0.60	0.60	0.85
S_0 (m^2/s^3)	0.006	0.01	0.018

The Harichandran-Vanmarcke model (1986) is selected to express the coherency function. There is

$$\gamma_{ij}(\omega)=A\exp\left(-\frac{2d_{ij}}{\alpha\theta(\omega)}(1-A+\alpha A)\right)+(1-A)\exp\left(-\frac{2d_{ij}}{\theta(\omega)}(1-A+\alpha A)\right) \tag{33}$$

where $\theta(\omega)=k\left(1+\left(\frac{\omega}{\omega_0}\right)^b\right)^{-\frac{1}{2}}$; d_{ij} is distance between point i and point j ; A,α,k,ω_0,b are regressive parameters. Harichandran and Wang (1990) gives $A=0.626$, $\alpha=0.022$, $k=19700\text{m}$, $\omega_0=12.692\text{rad/s}$, $b=3.47$. The coherency functions among points 1, 2 and 3 are shown in Fig.5.

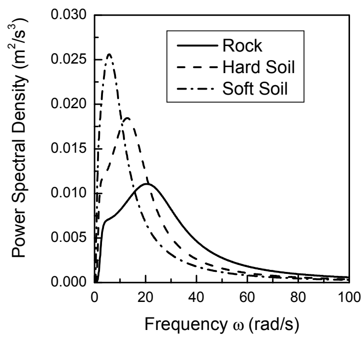

Fig.4 Clough-Penzien spectrum

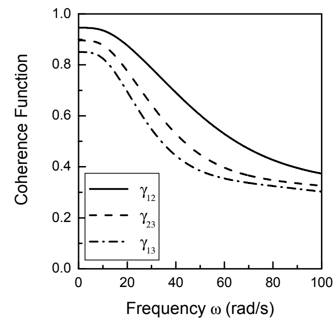

Fig.5 Coherency functions

Example 1

In this example, the local soil of points 1, 2 and 3 are the same as soft soil; and the epicenter distance is 20km; and the magnitude is M_w=7. The procedure of simulating accelerograms of points 1, 2 and 3 is as follows.

Step 1: Simulating non-stationary accelerogram of point 2

Point 2 corresponds to soft soil and its power spectrum is defined by Eq.(32). The Fourier coefficients of point 2 are simulated and the amplitude is computed. The phase difference spectrum of point 2 is simulated on the basis of empirical model presented by Thräinsson and Kremidjian (2002). The non-stationary accelerogram is generated by inverse FFT, shown in Fig.6.

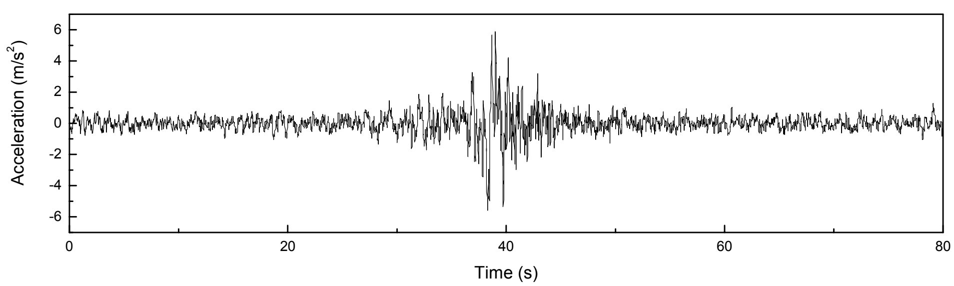

Fig.6 Simulated accelerogram of point 2

Fig.7 gives the evolutionary power spectrum of the simulated accelerogram of point2. It can be seen that the accelerogram is non-stationary in both time and frequency domains.

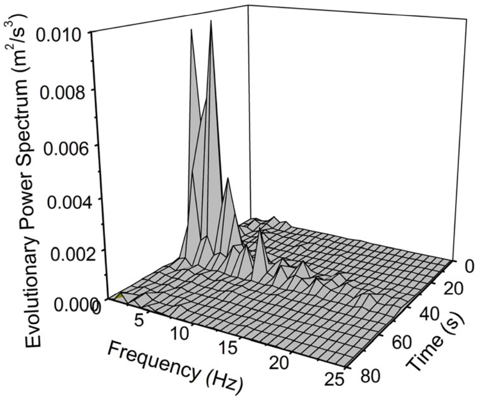

Fig.7 Evolutionary power spectrum of point 2

Step 2: Simulating coherent and non-stationary accelerograms of points 1 and 3

Considering the coherency functions defined in Eq.(33) and the known accelerogram of point 2, the non-stationary accelerograms of point 1 and 3, shown in Fig.8 and Fig.9, respectively, are simulated

.

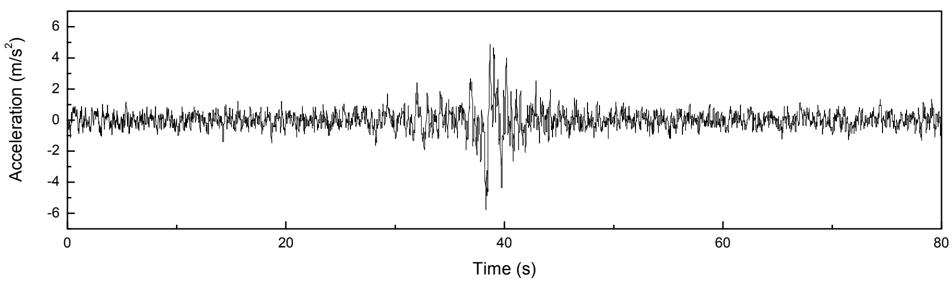

Fig.8 Simulated accelerogram of point 1

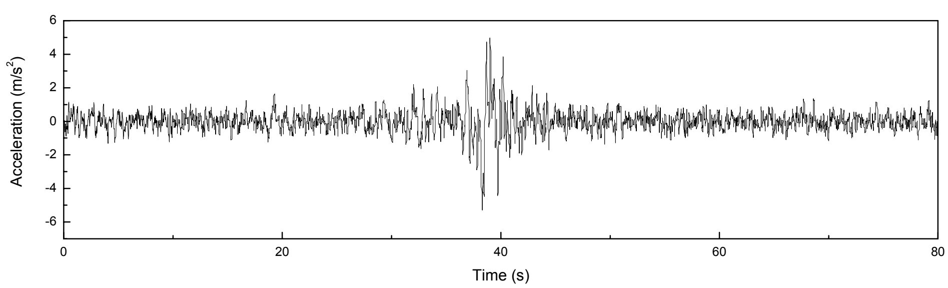

Fig.9 Simulated accelerogram of point 3

Fig.10 and Fig.11 give the evolutionary power spectrums of point 1 and 3 respectively. It can be seen that the simulated accelerograms are fully non-stationary in time and frequency domains.

Fig.12~Fig.14 give the comparisons between the theoretical coherency function and the simulated. It can be seen that the simulated accelerograms of points 1, 2 and 3 reflect correctly the lagged coherency functions.

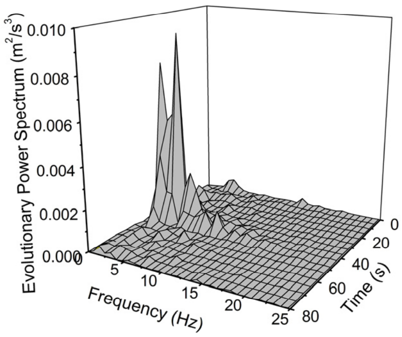

Fig.10　Evolutionary power spectrum of point 1

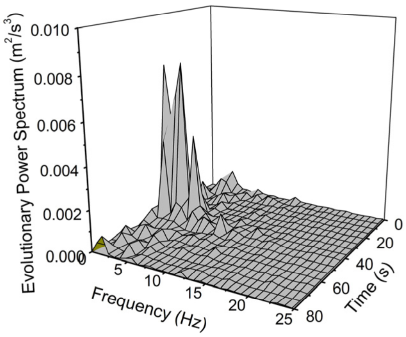

Fig.11　Evolutionary power spectrum of point 3

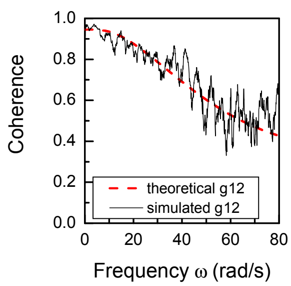

Fig.12　Coherency function　γ_{12}

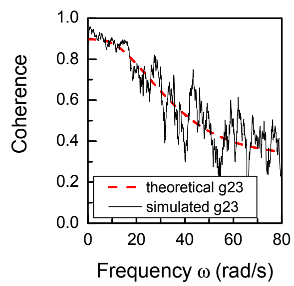

Fig.13　Coherency function　γ_{23}

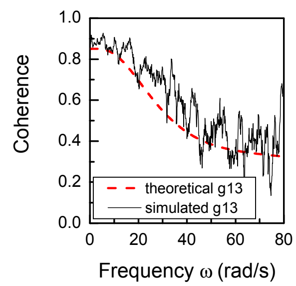

Fig.14　Coherency function　γ_{13}

Example 2

In this example, point 1 corresponds to soft soil and points 2 and 3 correspond to hard soil. The epicenter distance is 20km and the magnitude is M_w=7.0. The following steps will simulate the correlated and non-stationary ground motions.

Step 1: Simulating the non-stationary accelerograms of reference points independently

Unlike example 1, there are two types of soil conditions and two reference points to reflect the different soil conditions. Point 1 is a reference point and another, point 4, is added at the middle of point 2 and 3. The modified configuration of three target points and reference point 4 is shown in Fig.15. The non-stationary accelerograms of point 1 and 4 are shown in Fig.16 and Fig.17.

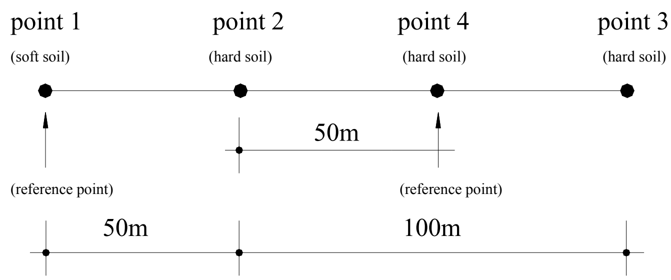

Fig.15　Modified configuration of target points and reference points

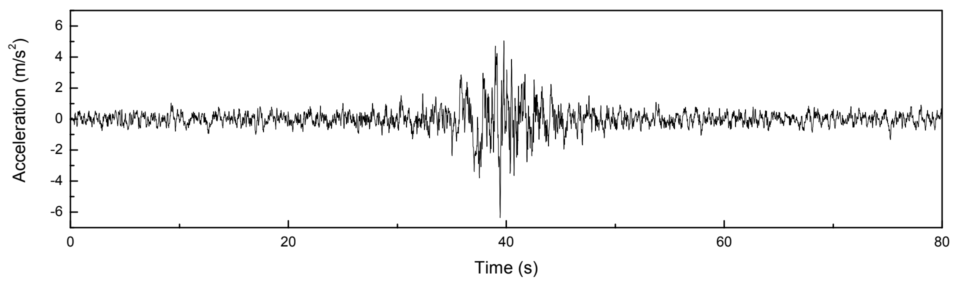

Fig.16　Simulated accelerogram of point 1

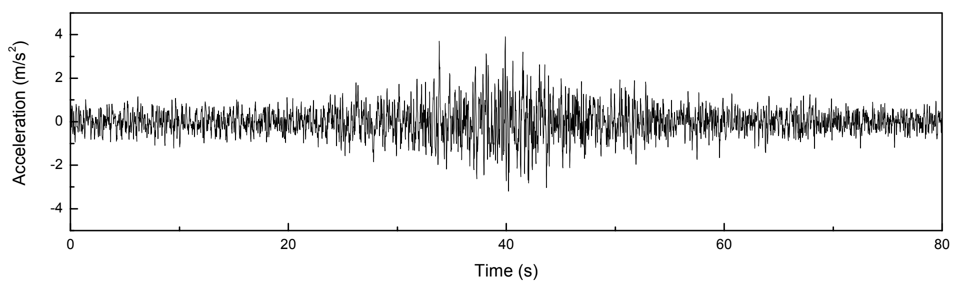

Fig.17　Simulated accelerogram of point 4

Step 2: Simulating coherent and non-stationary accelerograms of points 2 and 3

Considering the coherency functions defined in Eq.(33) and the known accelerogram of points 1 and 4, the non-stationary accelerograms of point 2 and 3, shown in Fig.18 and Fig.19 respectively, are simulated.

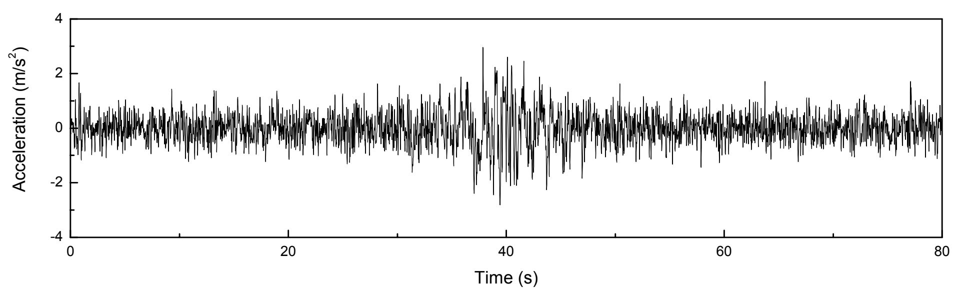

Fig.18　Simulated accelerogram of point 2

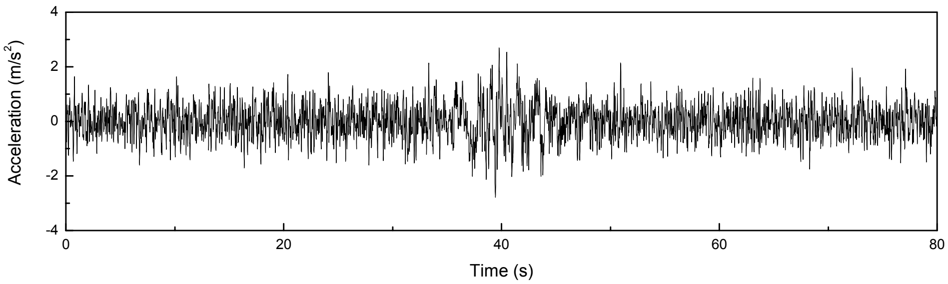

Fig.19 Simulated accelerogram of point 3

The coherency functions are shown in Fig.20~Fig.22. It can be seen that the simulated accelerograms of points 1, 2 and 3 reflect correctly the lagged coherency functions.

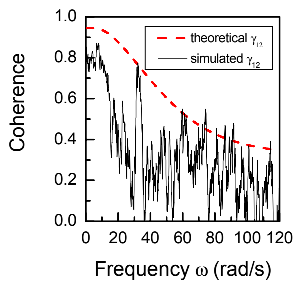

Fig.20 Coherency function γ_{12}

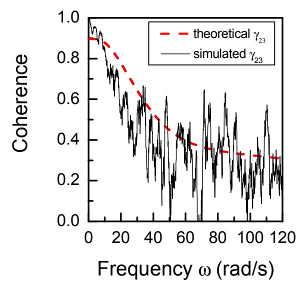

Fig.21 Coherency function γ_{23}

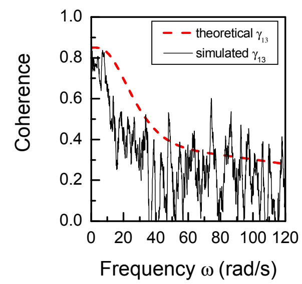

Fig.22 Coherency function γ_{13}

CONCLUSIONS AND COMMENTS

The phase-difference-based non-stationary and spatial correlated field of earthquake accelerograms is simulated. As known, the non-stationary characteristics of an acceleration record in time domain are related to the phase difference spectrum. Based on the power spectrum representative algorithm and the empirical equation of phase difference spectrum, the independent non-stationary accelerograms are simulated at the reference points. Considering the spatial coherency functions and the known accelerograms at the reference points, the correlated accelerograms at the target points are generated by Kriging technique.

ACKNOWLEDGEMENT

The author is grateful for the support from National Natural Science Foundation of China at granted No. 50278001.

REFERENCES

Abrahamson, N.A.(1991), Empirical spatial coherency functions for application to soil-structure interaction analyses, *Earthquake Spectra*, 7: 1-28

Boore, D.M.(2003), Phase Derivatives and Simulation of Strong Ground Motions. *Bulletin of the Seismological Society of America*, 93(3): 1132–1143

Clough R. and Penzien J.(1993), Dynamics of structures, second edition(M). McGraw-Hill, Inc.

Hao, H., Oliveira, C.S. and Penzien, J.(1989), Multiple-station ground motion processing and simulation based on SMART-1 array data, *Nuclear Engng and Design*, 111: 293-310

Harichandran, R.S. and Vanmarke, E.H.(1986), Stochastic Variation of Earthquake Ground Motion in Space and Time, *J. of Engineering Mechanics*, ASCE, 112(2).

Kanai K.(1957), Semi-empirical formula for the seismic characteristics of the ground motion. Bull Earthq Res Inst Univ Tokyo, 35: 309–25.

Nigam N.C.(1982), Phase Properties of a Class of Random Processes, *Earthquake Engineering and Structural Dynamics*, 10: 711–717.

Ohsaki, Y.(1979), On the Significance of Phase Content in Earthquake Ground Motions, *Earthquake Engineering and Structural Dynamics*, 7: 427–439.

Tajimi H.(1960), A statistical method of determining the maximum response of a building structure during an earthquake, *Proc. 2nd WCEE*, vol. II. Tokyo: Science Council of Japan, 1960:781–98.

Thráinsson, H. and Kiremidjian, A.S.(2002), Simulation of digital earthquake accelerograms using the inverse discrete Fourier transform. *Earthquake Engng Struct. Dyn*., 31: 2023–2048

Vanmarcke, E.H. and Fenton, G.A.(1991), Conditioned simulation of local fields of earthquake ground motion. *Structural Safety*, 10: 247-264

Vanmarcke, E.H., Heredia-Zavoni, E. and Fenton, G.A.(1993), Conditional simulation of spatially correlated earthquake ground motion. *J. Engng Mech.*, ASCE, 119(11): 2333-2352

Vanmarcke, E.H., Fenton, G.A. and Heredia-Zavoni, E.(1999), SIMQKE-Ⅱ:Conditioned earthquake ground motion simulator, User’s manual, version 2.1. Princeton University

Yang Q.S. and Chen Y.J.(2000), A practical coherency model for spatial varying ground motions, *Structural Engineering and Mechanics*, 9(2): 141-152

Current and Recommended Bridge Seismic Design Specifications and Implementation in the USA

W. Phillip Yen and Benjamin Tang

ABSTRACT

Our highways are built to transport goods and people, and connect nations, states and cities. As such, they are our lifelines to deliver daily needs such as food, water, and communication with other locations. Among highway systems, bridge is the most vulnerable component to the earthquake hazard. This paper introduced the current design specifications and recommended new design guidelines to the highway bridges in the USA.

Wen-huei Phillip Yen, PE, Ph.D., Office of Infrastructure, R&D, Federal Highway Administration, 6300 Georgetown Pike, T-111, McLean, VA 22101, USA

Benjamin Tang, PE, Office of Bridge Technology, Federal Highway Administration, 400 7th Street NW, Washington, DC 20590, USA

INTRODUCTION: BRIDGE SEISMIC DESIGN IN THE US

The seismic performance of bridges depends greatly on how the bridges were design and constructed. Although in some cases, bridge collapses may not be preventable if fault ruptures created large displacements directly across or near bridge sites, e.g., the Chi-Chi earthquake in Taiwan. Designing with good details has saved many bridges from collapsing due to unseating or shear failure. After the 1971 San Fernando earthquake, the US highway agencies, including The Federal Highway Administration (FHWA) and California Department of Transportation (CALTRANS) started to accelerate the improvement of earthquake resistance of highway bridges. Prior to 1971, the American national bridge seismic design specifications, the American Association of State Highway and Transportation Officials (AASHTO) Specifications, were based in part on the lateral force requirements for building developed by the Structural Engineers Association of California (SEAC). In 1975, the AASHTO adopted part of 1973 CALTRANS design provisions as an interim specification for seismic design. FHWA hired the Applied Technology Council (ATC) in 1979 to evaluate current seismic design criteria and develop new and improved seismic design standards for highway bridges. The findings from this FHWA study formed the basis for the current AASHTO seismic bridge design specifications. This design specification was adopted as the current standard in 1992 by AASHTO.

CURRENT DESIGN SPECIFICATIONS

The design philosophies of the current seismic specifications (AASHTO) are intended to prevent collapse in large earthquakes. In small to moderate earthquakes, the intent of the code is to resist these loads in the elastic range without significant damage to structural components. In large earthquakes, no span or part of a span shall collapse under either code. However, AASHTO considers some damage acceptable in these circumstances, provided it is limited to flexural hinging in pier columns and that it occurs above ground in regions that are visible and accessible for inspection and repair. The design earthquake is based on an event with a 475-year return period. Design forces are calculated from an elastic analysis of the bridge using response spectra approximating the design quake. Then, component forces, such as pier moments, are reduced by dividing them by a specified Response Modification Factor, R. Thus, the loads on these components will exceed their elastic strength, forcing them to go beyond the elastic range. So, if the R-factor is high, such as 3 or 5, then significant plastic hinging will occur. This damage may be irreparable.

Under the AASHTO code, bridges are classified into one of four seismic performance categories (SPC). The seismic performance category is defined on the basis of the acceleration coefficient expected for the specific site (A), and the importance classification of the structure (IC). SPCs are shown in Table 1. Based on the assignment of these SPCs, minimum analysis and design requirements are then specified by AASHTO. Flow charts demonstrating the AASHTO design procedure are shown in Figures 1 and 2. Note that bridges in SPC A are not required by AASHTO to undergo a dynamic analysis. In addition, a dynamic analysis is not required for single-span bridges. However, minimum bearing seat widths must be provided and minimum horizontal connection forces must be satisfied for SPC A and for single span bridges.

Table 1. AASHTO Seismic Performance Categories (SPCs)

Acceleration Coefficient, A	Seismic Performance Category (SPC)	
	Importance Classification (IC)	
	I	II
$A \le 0.09$	A	A
$0.09 < A \le 0.19$	B	B
$0.19 < A \le 0.29$	C	C
$0.29 < A$	D	C

Note: IC = I is for essential bridges; IC = II is for all other bridges.

Basic Concepts

The fundamental concepts under the development of this standard are the following:

- Hazard to life be minimized
- Bridges may suffer damage, but must have a low probability of collapse due to earthquake motions
- Functions of essential bridges be maintained
- Design ground motions have low probability of being exceeded during normal lifetime of bridge
- Provisions be applicable to all of the United States
- Ingenuity of design not to be restricted

Although the detail of design has been frequently updated to improve the seismic resistance of bridges, the current design code has the same design principles such as (1) Resisting small to moderate earthquakes should be resisted within the elastic range of the structural component. This is to protect structural components from any significant damage under small to moderate ground motion. (2) Using realistic seismic ground intensities and forces in the design procedures. Although in some cases, site specific response spectra are not available, closed site response spectra are recommended. (3) Avoiding collapse of all or part of the bridge when exposed to large ground motions (large earthquakes). Where possible, damage that does occur should be readily detectable and accessible for inspection and repair. These principles produce bridges that will stand in the small-to-moderate earthquakes without significant damage in structural components. However, under large earthquakes, which have a very low probability of occurrence in a bridge's service life, the structure will suffer damage but should not collapse. If possible, those damages should be easy to find and repair. Under current design codes, bridge columns are designed as weak components that will yield prior to adjacent components such as superstructures (including bearings) and foundations. This takes advantage of the "easy to find and repair" concept, and gives this component more ductility to absorb the most energy from earthquake shakings.

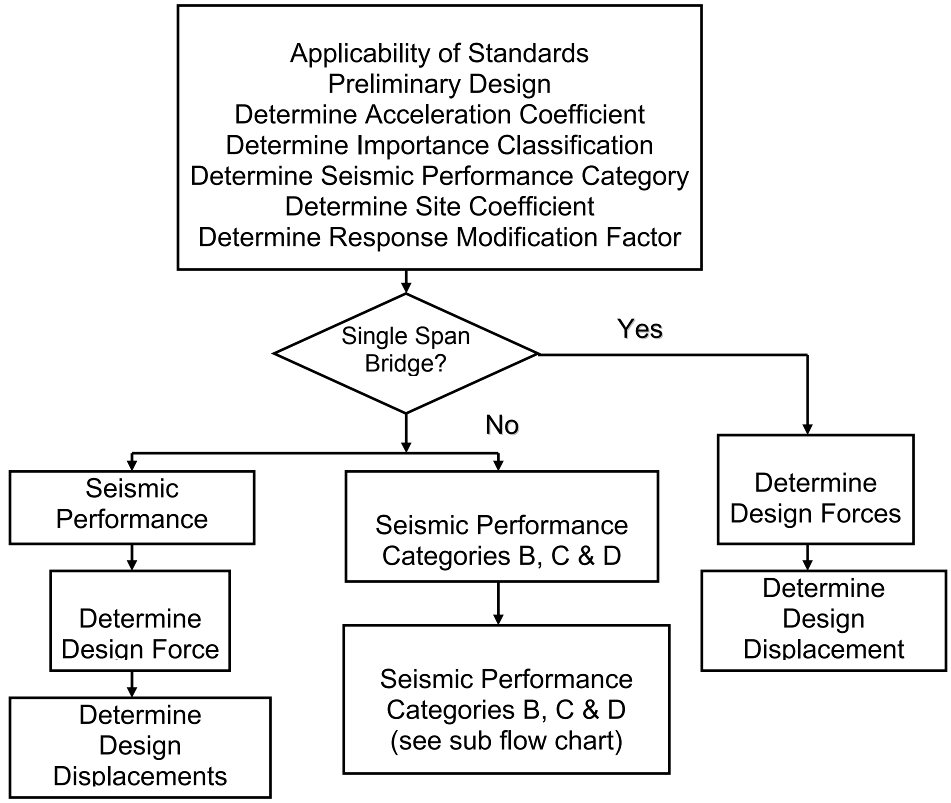

Figure 1. Seismic Design Procedure

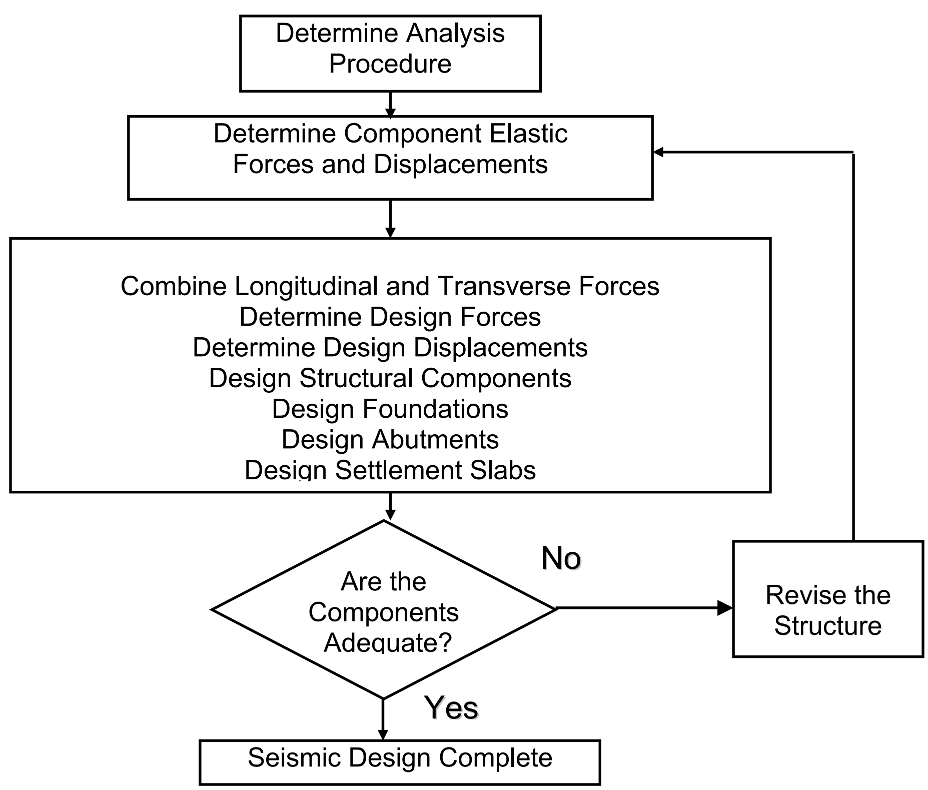

Figure 2. Sub-flow Chart of Seismic Performance Categories B, C & D

Design Procedures

Design procedure is rather simple for a regular bridge, while complex or irregular bridges are required to have more analytical steps in their design. Design requirements in the codes are based on the SPC as discussed earlier. This SPC, basically, is determined from its peak ground accelerations. For bridges located in the SPC A, where the peak ground acceleration is less than 0.09, seismic analysis is not required; however, bearing design forces should be increased 25%.

Inertia Seismic Design Forces

The AASHTO code provides bridge designers he option of using an equivalent elastic analysis method to define the horizontal earthquake load, or a 5-percent damped elastic site-specific response spectrum, which includes the effects of local seismology and site soil conditions.

Based on the elastic seismic response method, the AASHTO code specifies a response coefficient that is to be used with a single mode analysis. This dimensionless coefficient is given in the following equation:

$$Cs = \frac{1.2\,AS}{T^{2/3}} \tag{1}$$

where A is the acceleration coefficient, S is a dimensionless coefficient representing the soil profile characteristics at a site, and T is the natural period of the structure. Note that Cs should not exceed a value of 2.5A and in certain soil profile cases where $A \geq 0.3$, Cs need not exceed 2.0A.

Ductility Factors / Response Modification Factors

Yielding of the structure is permitted by AASHTO provided the structure does not degrade during cyclic loading. The AASHTO code therefore specifies design details to ensure that minimum confinement, anchorage, and splice requirements are satisfied such that plastic hinging may occur without loss of strength or stability. Such a design strategy permits the elastic forces (obtained from the analysis) to be reduced by substantial factors to obtain design forces in those members permitted to yield. These members are usually the bridge columns and, thus, response modification factors (R-factors) for the columns are specified which range from 3 to 5, depending on the number of columns in each bent. Elements not permitted to yield, such as foundations and connections, have R-factors ranging from 0.8 to 1.0.

RECOMMENDED NEW DESIGN SPECIFICATIONS

The loss of life and extensive property damage suffered from recent large earthquakes, including the 1989 Loma Prieta, 1994 Northridge and 1995 Kobe earthquakes, have demonstrated the earthquake vulnerability of highway bridges that were designed to existing seismic codes, and the need to provide new procedures and specifications for constructing earthquake-resistant bridges and highways. In recognition of this need, the FHWA and State Departments of Transportation (DOT) including CALTRANS, are working together to develop new seismic design provisions for highway bridges under the National Cooperative Highway Research Project 12-49. The objective of this research is to enhance safety and economy through the development of a new LRFD specification and commentary for the seismic design of bridges. The recommended provision were completed in April 2001, and will be considered for adoption by the AASHTO Highway Subcommittee on Bridges and Structures in 2002 as guide specifications. This NCHRP 12-49 specification has significant changes in the design approach and criteria to reflect lessons learned from recent earthquakes and research studies. The following is an introduction to the major changes from the recommended design specification:

Seismic Performance Objectives –Two Level Design

Bridge design objectives have been categorized into two levels of seismic performance. They are "Life Safety" and "Operational". Table 2 shows the new design earthquakes and seismic performance objectives. The design forces are based on the probabilities of exceedance stated in the Table 2 (either 3% or 50%) for a normal bridge service life of 75 years. The upper level (3%) design ground motion (or Maximum Considered Earthquake, MCE) defined probabilistically can reach values that exceed deterministic ground motions for the maximum magnitude earthquake considered. The lower level ground motion (50%), equivalent to a 108 year return period, is chosen to be consistent with other natural hazards such as floods. This change extends bridge performance beyond the life safety concern used in most design codes, and ensures different levels of functionality to protect against economic and other indirect losses.

This dual level design allows the designer to have a range of performance objectives. Significant damage is expected in the rare earthquakes (MCE) designed under the "Life Safety" performance level. Thus, to prevent bridge collapse, all bridges and their foundations are required to have a definite earthquake resisting system (ERS). *Conventional Ductile Design* (current design codes), *Seismic Isolation Design* and *Energy Dissipation* Methods are good means of achieving adequate performance.

Table 2 Design Earthquakes and Seismic Performance Objectives

		Performance Level	
Probability of Exceedance for Design Earthquake Ground Motions		Life Safety	Operational
Rare Earthquake (MCE) 3% PE in 75 years/ 1.5 Mean Deterministic	Service	Significant Disruption	Immediate
	Damage	Significant	Minimal
Expected Earthquake 50% PE in 75 years	Service	Immediate	Immediate
	Damage	Minimal	Minimal to None

Design Ground Motion

Either a general procedure or a site-specific procedure is allowed to generate design spectra for the design forces. However, for those important bridges designed for the high-level performance objective, or bridge sites within 10km of a known active fault where a response is expected to be significant, a site-specific design procedure should be used.

Design spectra based on general procedures are constructed differently from procedures in the current design codes. Figure 3 illustrates the so-called "Two Points Method" for constructing design spectra.

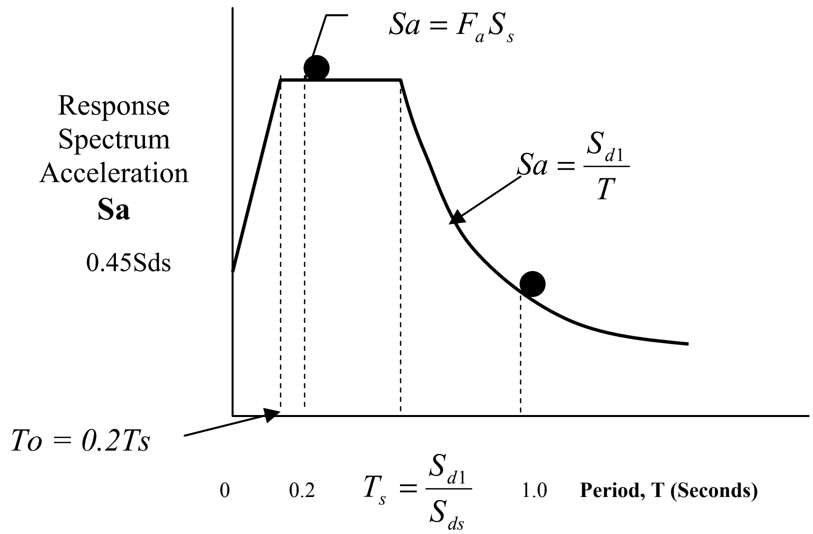

Figure 3. Seismic Design Spectra (Recommended Spec.)

The design response spectrum curve for short periods, which less than or equal to *To*, the design response spectral acceleration, *Sa,* shall be defined by the following equation:

$$Sa = 0.60\frac{Sds}{To}T + 0.40Sds \tag{2}$$

For periods between *To* and *Ts,* including *To* and *Ts*, the design response spectral acceleration, Sa is defined as $Sa = Sds$, and

for periods are greater than Ts, then $Sa = \frac{S_{d1}}{T}$

Where: S_{d1} is defined as $S_{d1} = F_v S_1$ (S_1 can be obtained from the USGS ground motion maps, and F_v is the site coefficient)

Vertical Acceleration Effects

The effects of vertical ground motions are required to be considered if the bridge is within 50km of an active fault, and has a potential maximum magnitude equal to or greater than 7.0. For those structures within 10km of an active fault, a site-specific study is required if it is determined that the response of the bridge could be significantly adversely affected by vertical ground motion. A table, which provides amplification factors from 1.4 to 0.1, based on a bridge's distance from an active fault, is contained in the new specification. This table is based on the ground motion data from many earthquakes in the past 20 years, which have experienced near-fault effects with very high, short-period vertical accelerations being possible. For near-source, moderate-to-large magnitude earthquakes, the customary rule-of-thumb ratio of 2/3 between vertical and horizontal spectra is a poor descriptor of vertical ground motions. At short periods, the vertical-to-horizontal spectral ratios can substantially exceed unity, whereas at long periods, a ratio of two-thirds may be conservative. An FHWA study has demonstrated that current understanding and ability to characterize near-source vertical ground motions is good, especially in the western U.S. where near-source regions are better defined (i.e., near mapped active faults). It was also shown that the high vertical accelerations experienced in near-source regions can significantly affect bridge response and design requirements in some cases.

Design and Analysis Procedure

Based on the bridge locality (Sa, spectral acceleration) and soil profile (Fv, site class), bridges are categorized into four different seismic hazard levels. Bridge designs, then have different requirements for achieving their performance levels. Four different design and analytical methods are provided to designers for use at the different hazard levels:

- Capacity Spectrum Analysis
- Elastic Response Spectrum Analysis
- Nonlinear Static Displacement Capacity Verification, (the so-called "Pushover" Analysis).
- Nonlinear Dynamic Analysis (Time-History Analysis)

Pushover analysis, introduced for the first time in the design specifications, is a displacement-based approach for analyzing dynamic response. The objective is to determine the displacement at which the earthquake-resisting elements (ERE) achieve their inelastic deformation capacity. Damage states are defined by local deformation limits, such as plastic hinge rotation, footing settlement or lift, or abutment displacement. Displacement may be limited by loss of capacity such as degradation of strength under large inelastic deformation or $p-\Delta$ effects. This displacement capacity check method is required in the design of each pier and bent.

CONCLUDING REMARKS

Design methods evolve over time and contain details that directly affect bridge performance under earthquake, and other natural hazard loading. Design is the first step for equipping bridges to resist earthquakes. Design methods are continuously improved based on lessons learned from destructive earthquakes and advanced seismic research. Each earthquake has unique characteristics and often comes with surprises. A dual level design method has been introduced in the recommended design specification. This approach was first considered in the early 1970s for buildings. It entered highway practice when it was included in a bridge design code by the Transportation Corridor Agencies in Southern California in the early 1990s. The recent "ATC-32" research report, titled "*CALTRANS Recommended Bridge Design Codes,"* included the two-level design approach for important bridges. The greatest advantage of the dual-level approach is that it directly addresses safety and functional performance separately, to better assure that performance goals are met. The inclusion of both force and displacement requirements (Pushover Analysis) is a proper way to design bridges in two different levels, i.e., using a force-design approach at the lower level, with other performance issues such as ductility and abutment movement being better resolved by the higher level, which uses the displacement approach. However, the increased cost from the extra design efforts and higher construction costs caused by greater design ground motion are justified by the higher performance goals. Specific requirements to quantify specific designs need to be refined to accomplish the performance level approach.

Lessons learned from three recent earthquakes in Turkey and Taiwan has raised another challenge to bridge seismic design. These three earthquakes resulted in severe damage to highway bridges because of the large ground motion and fault ruptures directly beneath or adjacent to bridge sites. Even with use of modern design codes, bridges cannot be expected to resist such large displacements or offsets in either the superstructure or by the substructure. In most cases, bridge replacement is inevitable if we use the same location to rebuild. One of the great remaining challenges to earthquake engineers is to develop a strategy to deal with a bridge constructed across or near a known fault.

REFERENCES

ATC/MCEER, 2001, *Recommended LRFD Guidelines for the Seismic Design of Highway Bridges*, Part I and II based on NCHRP 12-49, " Comprehensive Specification for the Seismic Design of Bridges", April

2001, *Proceedings of the Forum on Risk Management and Assessments of Natural Hazards*, Office of Federal Coordinator for Meteorological Services and Supporting Research, February

FEMA, 1997, *Multi-Hazard Identification and Risk Assessment* – A Corner Stone of the National Mitigation Strategy, Federal Emergency Management Agency, July

Responses of Long-span Structures Subjected to Multiple Random Ground Excitations

G. W. Tang, J. H. Lin, Y. Zhao

ABSTRACT

Long span bridges are usually important public facilities and so much attention has been given to evaluating their safety during earthquakes. The wave-passage effect caused by the different times at which seismic waves arrive at different supports must be taken into account during their design. The random vibration approach is based on a statistical characterization of the set of motions at the supports. For a long time it has been widely regarded as a good alternative for dealing with the above spatially varying input motions, but finding suitable computational methods has proved to be a difficult problem. This problem is largely overcome by the recently developed Pseudo Excitation Method (PEM), which is a highly efficient and accurate algorithm series. It is accurate because the correlation terms between all participating modes and between all excitations have both been included. It is also easy to use because the stationary random vibration analysis is transformed into a harmonic vibration analysis. Such deterministic computations are very convenient and numerical comparisons given in this paper also show the good applicability of this PEM random vibration method in dealing with the spatial effects.

G. W. Tang, Chongqing Communications Research & Design Institute, Chongqing, 400067, PRC
J. H. Lin , State key laboratory of structural analysis for industrial equipment, Dalian University of Technology, Dalian 116024, PRC
Y. Zhao, Chongqing Communications Research & Design Institute, Chongqing, 400067, PRC

1. INTRODUCTION

Seismic computations of long-span structures have long been an issue of great concern. Such computations are usually executed in terms of the step-by-step (i.e. time history) scheme in the time domain. For short-span bridges, all supports can be assumed to move uniformly and the response spectrum method (RSM) is the most important computation tool. For long-span bridges, however, various spatial effects such as the wave passage effect may be important. Such spatial effects cannot be dealt with directly by the conventional response spectrum method. Instead, the time history method (THM) is the most widely used method. This time history scheme requires resolving the dynamic equations for a number of seismic acceleration samples, and the results are then processed statistically to produce the quantities required by designs. This process is rather complicated and needs tremendous computational effort, and so more efficient and reasonable methods have been under constant investigation. In fact, seismic motion is random in nature (Housner 1947). Such spatial effects can be analyzed using the random vibration approach. In the last two decades, many scholars and experts (Lee and Penzien 1983, Dumanoglu and Severn 1990, Lin, Zhang and Yong 1990, Berrah and Kausel 1992, Kiureghian and Neuenhofer 1992, Ernesto and Vanmarcke 1994) have made great progress in pushing forward the seismic random analysis of long-span structures and its engineering applications. Although available computational methods still need further improvements both in precision and efficiency, the random vibration approach, as a theoretically advanced tool, has been gradually accepted by the earthquake engineering community, e.g. it has been adopted by the European Bridge Code (European Committee for Standardization 1995).

The Pseudo Excitation Method (PEM), developed in recent years (Lin 1992, Lin et al. 1994, 1995, 1997, 2003), is an accurate and highly efficient approach to the random seismic analysis of long-span structures. For typical 3D finite element models of long-span bridges with thousands of degrees of freedom and dozens of supports, when using 100-300 modes for mode-superposition analysis, the seismic responses can be implemented quickly and accurately on a standard personal computer. Numerical results show that the wave passage effect is of particular importance for the seismic analysis of long-span bridges. The details will be given in this paper. PEM has been successfully applied to some practical engineering analyses, and has been proved to be quite effective.

2. MULTI-EXCITED EQUATIONS OF MOTION AND THE PEM-BASED ANALYSIS

Consider a structure with N supports subjected to differential ground motion. In the absolute coordinate system, which is assumed to be static relative to the center of the earth, the equation of motion of this structure can be expressed in the partitioned form(Clough and Penzien 1993)

$$\begin{bmatrix} M_{ss} & M_{sm} \\ M_{ms} & M_{mm} \end{bmatrix} \begin{Bmatrix} \ddot{x}_s \\ \ddot{x}_m \end{Bmatrix} + \begin{bmatrix} C_{ss} & C_{sm} \\ C_{ms} & C_{mm} \end{bmatrix} \begin{Bmatrix} \dot{x}_s \\ \dot{x}_m \end{Bmatrix} + \begin{bmatrix} K_{ss} & K_{sm} \\ K_{ms} & K_{mm} \end{bmatrix} \begin{Bmatrix} x_s \\ x_m \end{Bmatrix} = \begin{Bmatrix} 0 \\ f_m \end{Bmatrix} \tag{1}$$

in which, $\{x_m\}$ represents the enforced displacements of all supports, $\{x_s\}$ represents the displacements of other nodes, $\{f_m\}$ represents the forces of the ground applying on all supports, $[M]$, $[C]$ and $[K]$ are the mass, damping and stiffness matrices of the structure, respectively. If the lumped mass assumption is used, $[M_{sm}]$ and $[M_{ms}]$ are both null matrices.

Now, decompose the absolute displacements into two parts

$$\{x\} = \{x_1\} + \{x_2\} \tag{2}$$

in which, $\{x\} = \{x_s, x_m\}^T$, $\{x_1\} = \{y_s, x_m\}^T$, $\{x_2\} = \{y_r, 0\}^T$. The vector $\{y_s\}$ is known as the quasi-static displacements, and $\{y_r\}$ the relative dynamic displacement. By letting all dynamic terms in eq (1) equal to zero, $\{y_s\}$ can be computed by

$$\{y_s\} = -[K_{ss}]^{-1}[K_{sm}]\{x_m\} \tag{3}$$

Substituting eq (2) into eq (1), expanding its first line, and using eq (3) gives

$$[M_{ss}]\{\ddot{y}_r\} + [C_{ss}]\{\dot{y}_r\} + [K_{ss}]\{y_r\} = -[M_{ss}]\{\ddot{y}_s\} - [C_{sm}]\{\dot{x}_m\} - [C_{ss}]\{\dot{y}_s\} \tag{4}$$

Under the condition of uniform ground motion, eq (4) can not be reduced to the conventional equation of motion

$$[M_{ss}]\{\ddot{y}_r\} + [C_{ss}]\{\dot{y}_r\} + [K_{ss}]\{y_r\} = -[M_{ss}]\{E\}\ddot{x}_m \tag{5}$$

in which $\{E\}$ is a vector denoting the availability of inertia forces.This is because that eq (1) assumes that the damping forces are proportional to the absolute velocity. To avoid such inconsistency, the damping forces are instead assumed to be proportional to the relative velocity vector, i.e. $\{\dot{x}\}$ in eq (1) must be replaced by $\{\dot{x}_2\}$. By doing so, eq (4) will be replaced by

$$[M_{ss}]\{\ddot{y}_r\} + [C_{ss}]\{\dot{y}_r\} + [K_{ss}]\{y_r\} = -[M_{ss}]\{\ddot{y}_s\} \tag{6}$$

The relative dynamic acceleration can be obtained in terms of eq (3) as

$$\{\ddot{y}_s\} = -[K_{ss}]^{-1}[K_{sm}]\{\ddot{x}_m\} \tag{7}$$

Substituting eq (7) into eq (6) gives

$$[M_{ss}]\{\ddot{y}_r\} + [C_{ss}]\{\dot{y}_r\} + [K_{ss}]\{y_r\} = -[M_{ss}][A]\{\ddot{x}_m\} \tag{8}$$

in which $[A] = -[K_{ss}]^{-1}[K_{sm}]$. Equation (8) is the equation of motion when the spatial effects of the ground motion are taken into account. It will be reduced into the form of eq (5) when all supports are assumed to move uniformly.

Provided that a long-span structure is subjected to multiple stationary seismic zero-mean Gaussian excitations, the PSD matrix of the ground accelerations will have the following form

$$\left[S_{\ddot{x}_m\ddot{x}_m}(\omega)\right]=\begin{bmatrix} S_{\ddot{x}_1\ddot{x}_1}(\omega) & S_{\ddot{x}_1\ddot{x}_2}(\omega) & S_{\ddot{x}_1\ddot{x}_3}(\omega) & \cdots & S_{\ddot{x}_1\ddot{x}_N}(\omega) \\ S_{\ddot{x}_2\ddot{x}_1}(\omega) & S_{\ddot{x}_2\ddot{x}_2}(\omega) & S_{\ddot{x}_2\ddot{x}_3}(\omega) & \cdots & S_{\ddot{x}_2\ddot{x}_N}(\omega) \\ \cdots & \cdots & \cdots & \cdots & \cdots \\ S_{\ddot{x}_N\ddot{x}_1}(\omega) & S_{\ddot{x}_N\ddot{x}_2}(\omega) & S_{\ddot{x}_N\ddot{x}_3}(\omega) & \cdots & S_{\ddot{x}_N\ddot{x}_N}(\omega) \end{bmatrix} \tag{9}$$

in which $S_{\ddot{x}_K\ddot{x}_L}(\omega)$ is the cross-PSD between ground nodes K and L. Thus, the above equation can be decomposed into

$$\left[S_{\ddot{x}_m\ddot{x}_m}(\omega)\right]=\left[e^{-i\omega T}\right]^*[S][R][S]\left[e^{-i\omega T}\right] \tag{10}$$

With

$$[S]=diag\ \left[\sqrt{S_{\ddot{x}_1}(\omega)},\sqrt{S_{\ddot{x}_2}(\omega)},\cdots,\sqrt{S_{\ddot{x}_N}(\omega)}\right] \tag{11}$$

$$\left[e^{-i\omega T}\right]\ =diag\left[\exp(-i\omega T_1),\exp(-i\omega T_2),\cdots,\exp(-i\omega T_N)\right] \tag{12}$$

$$[R]=\begin{bmatrix} 1 & \rho_{12} & \rho_{13} & \cdots & \rho_{1N} \\ \rho_{21} & 1 & \rho_{23} & \cdots & \rho_{2N} \\ \cdots & \cdots & \cdots & \cdots & \cdots \\ \rho_{N1} & \rho_{N2} & \rho_{N3} & \cdots & 1 \end{bmatrix} \tag{13}$$

herein, $S_{\ddot{x}_K}(\omega)$ is the PSD of the ground acceleration at node K. It is assumed that the wave-front of an arbitrary seismic wave reaches the reference ground node (usually, it can be assumed to be the origin of the coordinate system) when $t=0$, and then denote T_K as the time when the front reaches node K, and ρ_{KL} as the coherence coefficient between nodes K and L.

The PSD matrix $\left[S_{\ddot{x}_m\ddot{x}_m}(\omega)\right]$ is usually a non-negative Hermitian matrix, and the coherence matrix $[R]$ is a non-negative real symmetric matrix. If the rank of $[R]$ is $r(r \le N)$, then it can be decomposed into

$$[R]=[Q][Q]^T \tag{14}$$

in which $[Q]$ is an $N\times r$ real symmetric matrix. Substituting eq (14) into eq (10) gives

$$\left[S_{x_m x_m}(\omega)\right]=[B]^*[B]^T \tag{15}$$

and

$$[B]=\left[e^{-i\omega T}\right][S][Q] \tag{16}$$

Each column vector $\{b_j\}$ $(j=1,2,3,\cdots,r)$ in matrix $[B]$ can be used to constitute a pseudo acceleration vector and a pseudo displacement vector

$$\{\ddot{\tilde{x}}_{m_j}\}=\{b_j\}\exp(i\omega t) \tag{17}$$

$$\{\tilde{x}_{m_j}\}=-\frac{1}{\omega^2}\{\ddot{\tilde{x}}_{m_j}\} \tag{18}$$

By substituting $\{\ddot{\tilde{x}}_{m_j}\}$ in eq (17) into eq (8), the relative dynamic displacement $\{\tilde{y}_{r_j}\}$ corresponding to the j th pseudo excitation $\{\ddot{\tilde{x}}_{m_j}\}$ can be computed. Then the quasi-static displacement $\{\tilde{y}_{s_j}\}$ can be obtained by substituting eq (18) into eq (3), and the j th absolute displacement $\{\tilde{x}_{s_j}\}$ can be obtained using eq (2), of which the PSD-matrix can be computed by

$$[S_{x_s x_s}(\omega)]=\sum_{j=1}^{r}\{\tilde{x}_{s_j}\}^*\{\tilde{x}_{s_j}\}^T \tag{19}$$

Provided that all elements in matrix $[R]$ equal to unity， eq (19) will reduce to the case for wave passage effect. Furthermore, if the time-lags between all ground nodes are zero, i.e. $T_K=0$ $(k=1,2,3,\cdots,N)$, the equation of motion for uniform ground motion will be derived.

3. PEAKS ANALYSIS OF STATIONARY RANDOM PROCESSES

Davenport approach With seismic excitations assumed to be zero-mean stationary Gaussian processes, an arbitrary linear response of the structure subjected to such excitations, denoted as $y(t)$, will also possess such a probabilistic characteristic. It is also assumed that if a given barrier (threshold) a is sufficiently high, the peaks of $y(t)$ above this barrier will appear independently. Let $N(t)$ be the number up-crossing a within the time interval $(0,t]$, then $N(t)$ will be a Poisson process with a stationary increment(Davenport 1961). Denote the extreme value of $y(t)$ (i.e. the maximum value of all peaks by their absolute values) within the earthquake duration $[0,T_s]$ as y_e, and the standard deviation of $y(t)$ as σ_y. Define η as the dimensionless parameter of y_e, and ν as the mean zero-crossing rate, which can be expressed as

$$\eta=y_e/\sigma_y\ ,\ \nu=\sqrt{\lambda_2/\lambda_0}/\pi \tag{20}$$

Based on the above assumptions, the probabilistic distribution of η can be derived as

$$P(\eta)=\exp\left[-\nu T_s\exp\left(-\eta^2/2\right)\right],\ \eta>0 \tag{21}$$

The expected value of η, known as the peak factor, is approximately

$$E(\eta)\approx\left(2\ln\nu T_s\right)^{1/2}+\gamma/\left(2\ln\nu T_s\right)^{1/2} \tag{22}$$

and its standard deviation is

$$\sigma_\eta \approx \pi/(12\ln \nu T_s)^{1/2} \tag{23}$$

in which $\gamma = 0.5772$ is the Euler constant, while the expected value of y_e is approximately

$$E[y_e] = E[\eta]\sigma_y \tag{24}$$

This quantity is the dynamic response (demand) usually required by engineers.

Vanmarcke approach In the preceding paragraph, the barrier a is assumed to be sufficiently high. Therefore, the peaks of $y(t)$ above this barrier will appear independently; then $N(t)$ can be regarded as a Poisson process. Vanmarcke(1972) considered that the barrier a should not be very high. Therefore, the Poisson process assumption should be replaced by the two-state Markov process assumption, and the probabilistic distribution of η becomes

$$P(\eta) = \left[1 - \exp\left(-\frac{\eta^2}{2}\right)\right] \cdot \exp\left[-\nu T_s \frac{1-\exp\left(-\sqrt{\pi/2}q^{1.2}\eta\right)}{\exp(\eta^2/2) - 1}\right] \tag{25}$$

in which ν and T_s have the same meanings as the above, while the shape factor for the response PSD is

$$\delta_0 = \left(1 - \lambda_1^2/(\lambda_0\lambda_2)\right)^{\frac{1}{2}} \tag{26}$$

Here δ_0 is a band-width parameter with values ranging from 0 to 1. For a narrow band process, δ_0 is close to 0. Based on the probabilistic distribution function eqn (28), Kiureghian proposes the following approximate expressions for the peak factor $E(\eta)$ and standard deviation σ_η when $10 \le \nu\tau \le 1000$ and $0.11 \le q \le 1$, which are of interest in earthquake engineering

$$E(\eta) = (2\ln \nu_e T_s)^{1/2} + \frac{\gamma}{(2\ln \nu_e T_s)^{1/2}} \tag{27}$$

$$\begin{cases} \sigma_\eta = \dfrac{1.2}{(2\ln \nu_e T_s)^{1/2}} - \dfrac{5.4}{13 + (2\ln \nu_e T_s)^{3.2}} & \nu_e T_s > 2.1 \\ \sigma_\eta = 0.65 & \nu_e T_s \le 2.1 \end{cases} \tag{28}$$

in which

$$\begin{cases} \nu_e = (1.63q^{0.45} - 0.38)\nu & \delta_0 < 0.69 \\ \nu_e = \nu_0 & \delta_0 \ge 0.69 \end{cases} \tag{29}$$

4. CASE STUDY

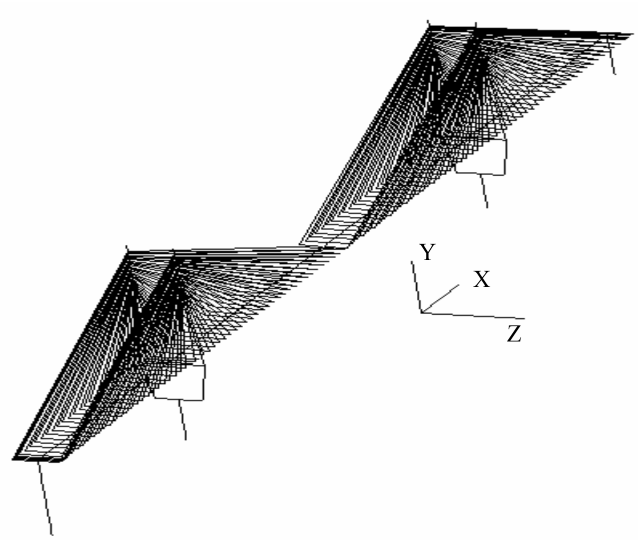

Fig. 1 FEM of Chong-qing DAFOSI Yangtze Rive bridge

The DAFOSI Yangtze Rive bridge, see Fig.1, is located in ChongQing City of China. Its overall length is 1176 m, with a main span of 450 m and a width of 30.6 m. The finite element model had 3960 degrees of freedom, 664 nodes (including 4 supports) and 883 elements. The static equilibrium position of the bridge included the effects of the initial tensions of the cables. The earthquake action was determined by directly gives the ground acceleration response spectrum (ARS) curve for the bridge. The PSD curve was obtained in terms of the Iteration Scheme method(Sun and Jiang 1990), based on which the samples of the ground acceleration time history can be produced. For the analyses 150 modes were used.

All supports move uniformly

Table 1 gives the internal force of this south tower-base due to the seismic P waves, which travel along the longitudinal direction of the deck. All supports of the bridges are assumed to move uniformly. The following four computational models were used:

(1) Response spectrum method (RSM);

(2) Pseudo excitation method (PEM);

(3) Time history method (THM).

Table 1 show that when ground motion is assumed uniform, i.e. the earthquake spatial effects are not taken into account, the RSM, PEM and THM (using ten samples) give very close results if the excitations are properly produced. The RSM is the most popular method, but the newly developed PEM may be the most efficient one. The THM needs be executed for a number of ground acceleration samples, and so was inefficient.

Wave passage **effect is taken into account**

Table 2 gives the internal force of this south tower base due to the seismic P waves, which travel along the longitudinal direction of the deck. All supports of the bridges are assumed to move with certain time-lags, i.e. the wave passage effect is taken into account. The apparent P wave speed is 2 km/s. The following four computational models were used:

(1) PEM (wave passage effect is considered with apparent wave speed v=2 km/s);

(2) THM (wave passage effect is considered with apparent wave speed v=2 km/s).

Table 2 show that when the seismic wave passage effect is taken into account, i.e. the earthquake spatial effects are partly taken into account, the PEM and THM (using ten samples) give very close results. The RSM, which does not consider the wave passage effect, may give quite different results, which may be evidently larger or smaller than, or very close to, the results by the more reasonable PEM or THM analyses. Therefore, such computations are very necessary for evaluating the seismic spatial effects of long-span structures. The PEM gives the most reasonable results with the least computational efforts and therefore this method is strongly recommended.

All computations were executed on a PIII-667 personal computer. The computation times for different methods are listed in Table 3.

Table 1 Internal forces of south tower base (uniform ground motion)

Internal forces	Axial force (N)	Shear force (N)	Moment (N.m)
THM(using one sample)	0.727793E+06	0.877473E+07	0.199498E+09
THM(using one sample)	0.682552E+06	0.107601E+08	0.229815E+09
THM(using one sample)	0.505199E+06	0.985314E+07	0.205560E+09
THM(using one sample)	0.557870E+06	0.956339E+07	0.251122E+09
THM(using one sample)	0.666380E+06	0.103099E+08	0.247555E+09
THM(using one sample)	0.673971E+06	0.274040E+08	0.553565E+09
THM(using one sample)	0.620421E+06	0.113705E+08	0.245074E+09
THM(using one sample)	0.620231E+06	0.919513E+07	0.225970E+09
THM(using one sample)	0.593965E+06	0.979416E+07	0.199169E+09
THM(using one sample)	0.595960E+06	0.985071E+07	0.224334E+09
THM(using three samples)	0.638515E+06	0.979599 E+08	0.211624 E+09
THM(using ten samples)	0.624434E+06	0.116876E+08	0.258166E+09
PEM	0.579084E+06	0.110200E+08	0.243446E+09
RSM	0.581097E+06	0.119185E+08	0.269538E+09

Table 2 Internal forces of south tower base（wave passage effect, v=2000m/s）

Internal forces	Axial force (N)	Shear force (N)	Moment (N.m)
THM(using one samples)	0.439991E+06	0.849114E+07	0.189454E+09
THM(using one samples)	0.508168E+06	0.106000E+08	0.243597E+09
THM(using one samples)	0.318154E+06	0.969146E+07	0.201272E+09
THM(using one samples)	0.357280E+06	0.915151E+07	0.230673E+09
THM(using one samples)	0.409620E+06	0.989041E+07	0.228028E+09
THM(using one samples)	0.477238E+06	0.271743E+08	0.568573E+09
THM(using one samples)	0.465987E+06	0.110937E+08	0.241514E+09
THM(using one samples)	0.413253E+06	0.915743E+07	0.206169E+09
THM(using one samples)	0.336291E+06	0.101088E+08	0.200898E+09
THM(using one samples)	0.412548E+06	0.955524E+07	0.210678E+09
THM(using three samples)	0.422104E+06	0.959420E+07	0.211441E+09
THM(using ten samples)	0.413853E+06	0.114914E+08	0.252086E+09
PEM	0.391992E+06	0.110011E+08	0.238304E+09

Table3 Computing time for three methods

Method used	RSM	PEM	THM(for 1 sample)
Uniform ground motion	9’51”	2’05”	7’31”
Wave passage effect		2’17”	8’26”

Note: the CPU time for mode extraction is not included, extracting 150 modes needs13’17”.

5. CONCLUSIONS

For short-span structures, the ground spatial effects are negligible, and the seismic analyses using RSM, PEM or THM (with a sufficient number of samples) are quite close to one another provided that the ground accelerations have been produced properly, and so are almost equivalent. While they have almost the same accuracy level, their efficiencies are quite different. Amongst the three methods, if the structural models are rather complex, e.g. the FEM models have thousands or more degrees of freedom and need dozens or hundreds of modes for mode superposition, the PEM will have the highest computational efficiency. For long-span structures, the wave passage effect is an important factor for structural seismic responses. The influence may cause more conservative or more dangerous designs. It is difficult to predict which by intuitive experiences, and so computer-based analysis is the only possible choice. The PEM is quite efficient and accurate, and is recommended. When the apparent seismic wave speed is not available, a few possible speeds can be taken for computation, with the most unfavorable results used in the practical design.

REFERENCES

Housner, G. W., “Characteristic of Strong Motion Earthquakes”. Bull. Seism. Soc, Am., 37: 17-31, 1947.

Lee, M. and Penzien, J., “Stochastic Analysis of Structures and Piping Systems Subjected to Stationary Multiple Support Excitations”. Earthquake Engrg. and Struct. Dynamics, 11: 91~110, 1983.

Dumanoglu, A. and Severn, R. T., “Stochastic Response of Suspension Bridges to Earthquake Forces”. Earthquake Engrg. and Struct. Dynamics, 19: 133-152, 1990.

Lin, Y. K., Zhang, R., and Yong, Y., “Multiply Supported Pipeline under Seismic Wave Excitations”. J. Engrg. Mech., 116: 1094-1108, 1990.

Berrah, M. and Kausel, E., “Response Spectrum Analysis of Structures Subjected to Spatially Varying Motions”. Earthquake Engrg. and Struct. Dynamics, 21: 461-470, 1992.

Kiureghian, A. D. and Neuenhofer, A., “Response Spectrum Method for Multi-Support Seismic Excitations”. Earthquake Engrg. and Struct. Dynamics, 21: 713-740, 1992.

Ernesto, H. Z. and Vanmarcke, E. H., “Seismic Random Vibration Analysis of Multi-Support Structural Systems”. J. Engrg. Mech., ASCE, 120: 1107-1128, 1994.

European Committee for Standardization. Eurocode 8, “Structures in seismic regions - design part 2: Bridge”, Brussels, 1995

Lin, J. H. “A Fast CQC Algorithm of PSD Matrices for Random Seismic Responses”. Computers & Structures, 44(3): 683-687, 1992.

Lin, J. H., Zhang, W. S., and Li, J. J., “Structural Responses to Arbitrarily Coherent Stationary Random Excitations”. Computers & Structures, 50: 629-633, 1994.

Lin, J. H., Zhang, W. S., and Williams, F. W., “Pseudo-Excitation Algorithm for Non-Stationary Random Seismic Responses”. Engineering Structures, 16: 270-276, 1994.

Lin ,J. H., Shen, W. P., and Williams, F. W., “A High Precision Direct Integration Scheme for Non-Stationary Random Seismic Responses of Non-Classically Damped Structures”. Structural Engineering and Mechanics, 3(3): 215-228, 1995.

Lin, J. H., Shen, W. P., and Williams, F. W., “A High Precision Direct Integration Scheme for Structures Subjected to Transient Dynamic Loading”. Computers & Structures, 56(1): 113-120, 1995.
Lin, J. H., Li, J. J., Zhang, W. S., and Williams, F. W., “Non-Stationary Random Seismic Responses of Multi-Support Structures in Evolutionary Inhomogeneous Random Fields”. Earthquake Engrg. and Struct. Dynamics, 26: 135-145, 1997.
Lin, J. H., Sun, D. K., Sun, Y., and Williams, F. W., “Structural Responses to Non-Uniformly Modulated Evolutionary Random Seismic Excitations”. Communications in Numerical Methods in Engineering, 13: 605-616, 1997.
Lin, J. H. and Zhang, Y. H., “Pseudo Excitation Method of Random Vibration”. Beijing, Press of Science, 2003 (in Chinese).
Clough, R. W., Penzien, J., Dynamics of structures, McGraw-Hill Inc, 1993.
Davenport, A. G., “Note on the Distribution of the Largest Value of a Random Function with Application to Gust Loading”. Proc. Inst. Civil Eng., 28: 187-196, 1961.
Vanmarcke, E. H., “Properties of Spectral Moments with Applications to Random Vibration”. J. Engrg. Mech., Div. Proc. ASCE, 98 (EM2), 1972.

FHWA Guidance Document for Seismic Performance Testing of Bridge Piers

J. Jerry Shen, W. Phillip Yen, and John O'Fallon

ABSTRACT

In order to provide assistance to seismic performance investigators in efficiently producing or obtaining consistent and reliable experimental testing results, Federal Highway Administration developed the "Recommendations for Seismic Performance Testing of Bridge Piers," which contains information on preparation, execution, and documentation of pier seismic performance testing. This document is purported for use in both academic research and engineering validations. It provides elaborate description on an assembly of available testing procedures while alternatives are offered. In addition to conventional piers made of reinforced concrete, steel, and wood, piers made of advanced material can be tested using the listed methods. Basic requirements on testing record are given, so to allow researchers or engineers to access and verify the testing results in a later time.

Assistance from experienced experimental experts and bridge engineers were requested during the development of the document. An expert panel including members from academia, state highway agencies, and federal government, was assembled to advise the progress and review the product. At the time of completion of this paper, the FHWA guidance document is at its final stage of technical revision and will be published in a short time.

Senior Research Engineer, LENDIS/FHWA, McLean, Virginia, USA. E-mail: Jerry.Shen@fhwa.dot.gov
Research Structural Engineer, Office of Infrastructure, R&D Federal Highway Administration, McLean, Virginia, USA. E-mail: Wen-huei.Yen@fhwa.dot.gov
Bridge Research Engineer, Office of Infrastructure, R&D Federal Highway Administration, McLean, Virginia, USA. E-mail: John.O'Fallon@fhwa.dot.gov

INTRODUCTION

Most of the pre-1980's seismic performance testing of structural members targeted at building elements. These results have been extrapolated for use in bridge design. In recognition of the shortage in seismic performance testing designated for bridge components, organized experimental projects and performance data accumulation for bridge components have been carried out since the early 1980s (Stone and Cheok; 1989). Diverse approaches were used for these testing projects. Without a common guidance on testing apparatus, loading programs, and documentation, these tests produced results that could not be easily compared to each other. Difficulties in interpretation of testing results led to less reliable analytical or empirical models for structural component behavior, and consequently less confidence in design.

Bridge piers differ from other structural components by their large dimensions, complexity of load combination, low redundancy, and importance to public welfare. Due to a variety of functionality, safety, and aesthetic requirements, the design of bridge piers is greatly diversified. A large amount of experimental testing is required to provide a confident estimation of many parameters. In contrary with this demand, seismic testing of bridge piers is often carried out with a limited number of specimens due to high cost and time constraint for constructing and testing each specimen.

The seismic performance testing of new and existing bridge components has a significant impact on the design, construction, and retrofitting of highway brides nationwide. A large amount of effort and funding from state and federal highway agencies have been spent on such testing on a case-by-case basis. As a result of a lack of common baseline on minimum requirements in testing procedure, the testing results cannot be compared or validated at a later time. Pieces of information gathered from these experiments do not merge to provide adequate aids to bridge engineers in implementing performance-based seismic design. A guidance document that provides the minimum requirements and a collection of well-practiced protocols for bridge pier seismic testing can greatly accelerate the knowledge accumulation. A guidance document can also reduce the risk of misinterpretation of testing results by clarifying principles and terms used in testing procedures.

Obstacles and shortcomings prevailing in current experimental research in seismic analysis and design of bridge structures include:

(1) Test results from different organizations or researchers cannot be compared and synthesized due to a lack of generally agreed test conditions and loading protocols.

(2) The use of data by other researchers or engineers may be handicapped by a lack of consistent documentation methods for minimum required information on test conditions and measurements.

(3) Consensus-based testing protocols for seismic performance evaluation of bridge piers do not exist.

(4) Loading protocols or guidelines that address a variety of cyclic testing and other types of testing do not exist.

In response to the growing need for a guidance document, the Federal Highway Administration (FHWA) initiated a task to collect, organize, and revise the practice of seismic performance testing of bridge piers and consequently produced the "Recommendations for Seismic Performance Testing of Bridge Piers."

EXISTING GUIDELINES

There are a few guidance documents available for seismic performance testing of specific purposes. The Applied Technology Council (ATC) published a protocol for cyclic seismic testing of components of steel structures in 1992(ATC, 1992). In 1997, the SAC program (a joint venture of SEAOC, ATC, and CUREe) published a testing protocol specifically developed for steel moment-frame building testing (SAC Joint Venture, 1997). The ATC protocol and SAC protocol were developed for research purpose. The adoption of these protocols as acceptance criteria for steel building design by the "Seismic Provisions for Structural Steel Buildings" of the American Institute of Steel Construction (AISC) invested these protocols with proof-test protocol status. The American Concrete Institute (ACI) also adopted a similar acceptance testing protocol for concrete moment frames since 1999 (ACI, 2001). The Consortium of Universities for Research in Earthquake Engineering (CUREE) woodframe program developed a series of loading protocols for cyclic testing of non-ductile elements under regular and near-fault earthquakes in 2001 (Krawinkler et al, 2001).

OBJECTIVES

Conducting seismic performance testing is expensive and time consuming. The primary thrust for the FHWA guidance document is to make use of all seismic performance testing data for bridges to their maximum extend. This can be accomplished by increasing the consistency of testing conditions and longevity of data life period.

(1) Consistency: Experimental results used for a research subject must have consistent testing conditions in order to compare and identify the effect of the interested parameters.
(2) Longevity: A testing program that is designed to exploit the performance information of one specimen can expand the user base of the testing results. The testing data and document must contain sufficient information regarding assumptions, procedure, testing conditions, and data format, to allow other researchers or engineers to utilize the results.

The increasing capability of conducting remote testing and producing integrated database introduces more rigorous requirements on testing control, measurement methodology, and data format. The scope of FHWA guidance document portrays a subset (highway structures) of current experimental seismic engineering research. The requirements set forth in this document can assist the design or construction of any integrated testing facility or database by specifying the requirements in this subset. The persons or institutes who are involved in the establishment of integrated systems are urged to take these requirements into consideration.

SCOPE AND ORGANIZATION

The FHWA guidance document focuses on one single type of structural component: bridge pier column. However, due to the diversity of pier construction and available testing methodology, the document must be organized to cover a wide range of options in the testing procedure. Bridge pier can be made of conventional construction material (e.g. steel, reinforced concrete, or wood) or innovative material (e.g. fiber-reinforced polymer). These materials or combinations of materials can be roughly divided into two groups: the group with clear yielding behavior and the group without clear yielding behavior.

The Guide Specifications for Seismic Isolation Design classified the functions of isolation bearing testing as system characterization testing, prototype testing, and quality control testing. The prototype testing is not common in pier testing because of the large dimension. The quality control testing is not suitable for pier testing because seismic performance of most bridge pier design involves significant damages. Quality of piers can only be verified by nondestructive evaluations. Such functional classification is clearly inadequate for bridge pier testing. The functions of pier performance testing can be classified as either for academic research (scientific experiment) or engineering application (proof-of-concept testing). Although this functional classification is different from that used in seismic isolation bear testing, it is appropriate for many large-size highway structural components.

Diverse approaches are used for pier testing in order to accommodate various research requirements and capacity limitations of testing facilities. Most of seismic performance testing methods are named by the loading mechanism. Table 1 shows the testing methods, (A) to (E), listed in the FHWA guidance document. The types of the dynamic load can be distinguished by the mechanisms that determine the intensity of the force and the physical loading speed. Each testing methods has advantages and disadvantages that make it suitable for testing with certain purpose and facility limitation. Table 2 provides a concise comparison of these testing methods.

Table 1. Common testing methods by loading mechanism and loading speed

Loading / Speed	Prescribed displacement loading	Inertia loading	
		Distributed load	Point load
Slow	**(A)** Quasi-static Monotonic loading (A1), Quasi-static cyclic loading (A2)	N/A	**(D)** Pseudodynamic tests
Fast	**(B)** Fast monotonic loading (B1), fast cyclic loading (B2). (Not recommended)	**(C)** Distributed mass shaking table tests	**(E)** Lumped-mass shaking table tests (E1), effective force tests (E2), hybrid tests (E3)

Table 2. Advantages and disadvantages of different testing

Testing type	Advantage	Common Purpose
(A)	• Less expensive • Allow large scale • Nonspecific to earthquake • Easy comparison • Easy to make visual record	- Determining load-deformation relationship - Determining load capacity under statistically-established deformation history - Reveal fundamental mechanical properties (stiffness, strength, damage modes, ductility, etc.) - Compare design criteria
(C)	• Realistic response • Accurate for massive and/or slender pier • Reveal unpredicted behavior	- Determining deformation history caused by a deterministic earthquake load - Verification of prediction - Demonstration - Site-specific structural behavior
(D)	• Less expensive than (C) but nearly as realistic • Allow large scale • Allow complicated superstructure • Easy to make visual record	- Large scale test for purposes of (C) - Test for complex structure
(E)	• Nearly as realistic as (C) • Rate-dependent property activated • Allow large scale • Allow complicated superstructure • Can be combined with (C)	- Large scale, real-time test for purposes of (C) - Test for complex structure - Extend equipment capability by combining

To include these common testing methodologies in an organized manner, the procedure of a seismic performance testing of bridge pier is broken down into three stages (Figure 1): specimen preparation, loading, and documentation. In every stage, special requirements and one or a few adequate procedures are given for each testing methods. This arrangement allows possible amendment at any time to include additional testing methods without restructuring the entire document.

Although the guidance document is set to provide assistance in the testing period shown in Figure 1, some information on rationale and limitation on each testing method are included to help justifying the choice of testing methods in the planning stage.

Bridge piers have a variety of dimensions, functionalities, and performance requirements. Furthermore, bridge pier testing often needs to carry multiple purposes due to the high cost and time consumption of each test. A protocol style document does not provide adequate aids to such testing. The FHWA guidance document uses a unique format that imposes less restriction while provides guidance. Options and alternatives are provided to each part of the testing along with explanations of advantages and limitations.

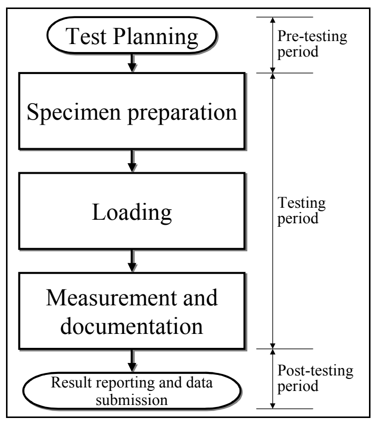

Figure 1. Organization

TESTING PROCEDURES

Test specimens need to be designed and constructed with consideration of the following attributes to produce the optimal results for a specific testing project:

(1) Resemblance to the subject
(2) Generality over a group of subjects
(3) Practical for available resources
(4) Providing access to demanded information

To design a specimen, a prototype must be first determined based on the subject of interest in the study. A prototype can be the structure or structural component of an actual bridge, a virtual bridge (that represents a designated group of bridges), or a generic bridge. A proper scale is then selected based on the facility, equipment, funding, and time restraint. The dimension and material of the specimen is determined by the selected scale and adequate similitude rules.

It is very common in engineering experiments that specimen parameters strictly in compliance with similitude rules cannot be obtained. In such situation, the most significant parameters must be determined and carefully controlled. Specimens with some parameters inconsistent with similitude rules have “distorted” scale. When distortions exist only for parameters known to be insignificant in seismic performance of scale model, the specimen can be considered adequately scaled.

Table 3 shows the commonly accepted scale factors used in bridge component dynamic testing. This set of scaling factors maintains the stress- and strain-related parameters, e.g. elastic modulus, unscaled. Acceleration is also maintained full-scale to be consistent with gravitational acceleration. Viscous stress (not listed in Table 3) is distorted but the effect is considered not very significant. These scale factors can also be used for quasi-static testing by ignoring all time-dependent terms. Figure 2 shows possible configurations of testing apparatus using this scaling system. Many variations can be derived from this basic scaling for different testing apparatus.

Table 3. Common scale factors in seismic performance testing of bridge piers

Variable	Scale factor
Length ℓ	S_L
Time t	$S_L^{0.5}$
Stress σ	1
Strain ε	1
Elastic modulus E	1
Force P	S_L^2
Displacement U	S_L
Bending moment M	S_L^3
Curvature ϕ	S_L^{-1}
Acceleration	1
Superstructure mass (weight)	S_L^2
Frequency	$S_L^{-0.5}$

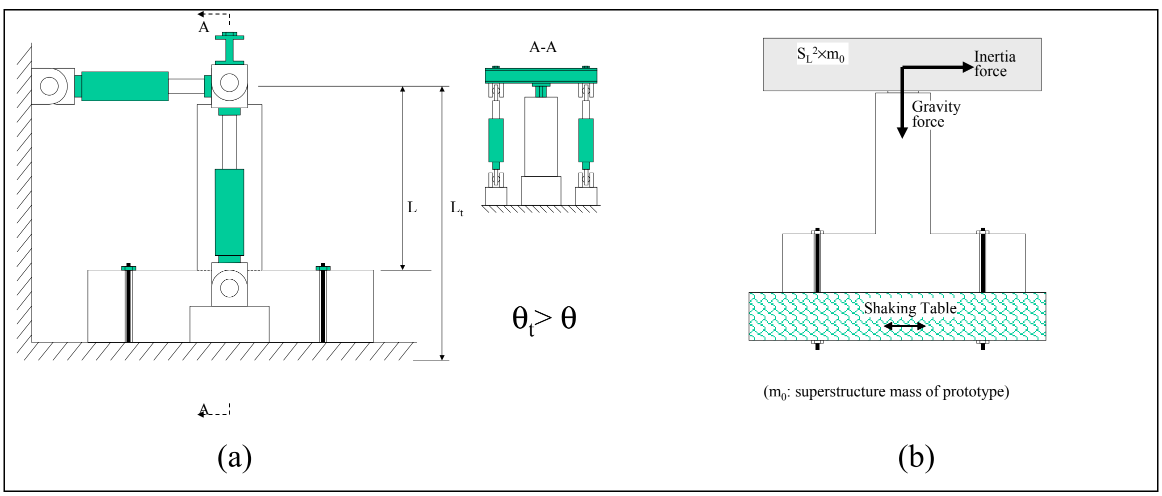

Figure 2. Quasi-static (a) and dynamic (b) testing using the scaling in Table 3

The displacement-prescribed loading program is cost-efficient and easier for large-scale testing. The consistent loading history provides a benchmark measure of performance level under various event sizes in one test. Due to a lack of consensus-based loading programs, unnecessary variations are present in current practice and inflict great difficulties in comparison and interpretation of testing data. The FHWA guidance document provides a collection of displacement programs for various purposes (types of earthquake and specimen). An example is shown in Figure 3.

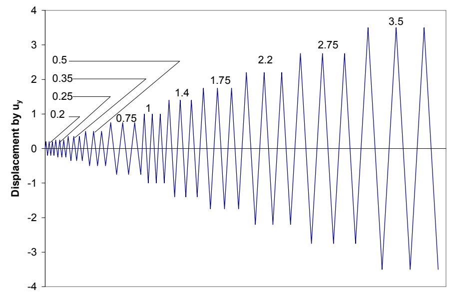

Figure 3. A typical displacement-prescribed loading program

The inertia loading programs can faithfully reproduce an earthquake to provide demonstration of realistic seismic performance of the testing subject. Credible source of the loading history and adequate scaling are important issues in using the inertia loading programs.

Documentation is of paramount importance to the credibility of the test results. An incomplete or inaccurate documentation may render a perfect experiment useless. Many details of the test design and execution can be critical to users of test results. Many of these critical data are emphasized in the corresponding sections in the FHWA guidance document. It is both beneficial and ethical for the investigator to ensure comprehensive record of the details regardless if all information is needed in his or her study.

SIGNIFICANT ISSUES

Limit States

Some limit states are used to describe loading programs or test results. Documentation of these limit states provides critical information to users of the test result. In general, obtaining these limit states is essential but not the sole purpose of a test. The observed limit states should be recorded along with the essential measurements of the specimen (load, deformation, etc.).

Each of the bridge design limit states involves a combination of local behavior. Therefore, the global limit states or performance levels in design are not strictly associated with the local limit states observed in experiments. Table 4 shows an approximate relationship between the limit states and performance levels or damage levels defined in several documents.

The yielding resistance/deformation, ultimate strength, and failure are important parameters directly used in bridge seismic design. They are, therefore, important phenomena to be observed in seismic performance testing. Yielding displacement is not only used in design but also used for designating amplitude of displacement-prescribed loading programs. Although it is only an artificially defined point that indicates the elastic limit of the bilinear idealization of load-deformation curve, it conveys significant influence on severity of loading programs and interpretation of testing results. The Caltrans definition for yielding shown in Figure 4a represents a reasonable approach for design based on simplest test data (from monotonic loading testing) or push-over analysis. It is not consistent with definitions used in most bridge pier testing procedures. The FHWA guidance document provides a favorable method in defining yielding for testing purpose (Figure 4b) and clarification of discrepancies among different definitions. The preferred loading program in the guidance document is less dependent on a clear definition of yielding than loading programs used in other protocols.

Table 4. Limit states and performance levels or damage levels

Experimental Limit State	NCHRP 12-49* Sevice Level	NCHRP 12-49* Damage Level	FEMA 369 (2000) Performance Level	Hose et al (2000) Performance/damage
Onset Cracking	Immediate	None	Operational	I
First Yield		Minimal	Immediate Occupancy	II
Element Yielding (Plastic Hinging) Ultimate Strength Spalling	Significant Disruption	Significant	Life Safe	III
			Near Collapse	IV
Failure	Not permissible	Not permissible	Not permissible	V

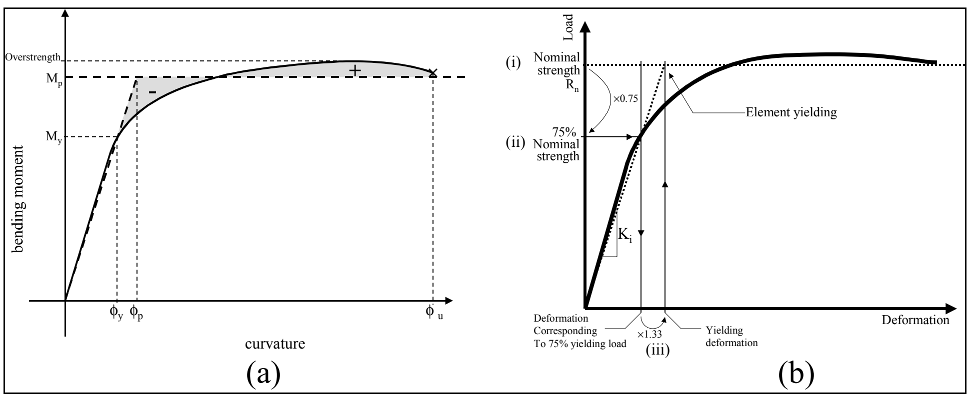

(a) (b)

Figure 4 Yielding definitions used in design and in experiments

The definition of failure used in design does not have much effect on the testing procedure. Although the FHWA guidance document provide a checklist for identifying failure, it does not make implication that the subject bridge pier is useless after the identified failure. The planned loading capacity should be well above the estimated failure resistance/deformation.

Boundary Conditions and Secondary Effect

A complete bridge model is seldom constructed and tested. The selected part of the structure or component needs to be affixed to testing apparatus that properly represent the omitted part of the structure. Adequate measurement should be implemented to monitor the slippage or local deformation that deviate the boundary conditions from that demanded.

The most significant secondary effect in seismic performance testing of bridge piers is the force effect from axial loading mechanism. Most available testing data have been adjusted for the axial load effect (often regarded as P-Δ effect). Figure 5 shows the breakdown of the bending moment diagram from the axial loading mechanism. The swaying effect comes from the change of force direction due to large displacement and produces a triangular bending moment profile that is consistent with the effect from lateral loading mechanism. The P-Δ effect is a result of the offset of axial loading and produces a non-triangular bending moment profile. Each testing apparatus produces unique combination of swaying and P-Δ effects. These effects are converted to the base moment and combined with lateral force effect in some testing reports. It is, in some cases, more adequate to report these effects separately.

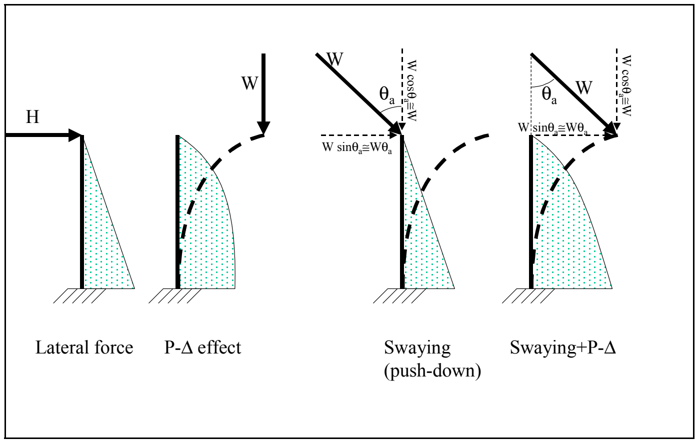

Figure 5. Axial load effect

SUMMARY

- Performance-based seismic design approach inflicts an increasing demand on seismic performance testing data.
- There is a lack of guidance document on seismic performance testing of bridge structural components.
- Without a guidance document, the comparison and interpretation of results from different testing project are difficult. Testing conditions of previous testing cannot be verified and results cannot be reused. Such deficiency in current practice leads to a waste of experimental resource and reduction of confidence in research conclusions.
- The FHWA recommendations on bridge pier testing procedures provide aids on selection of testing methodology, specimen preparation, loading, and instrumentation/documentation. Advantages and limitations of each testing methodology are provided. Critical issues and frequently encountered problems are discussed. Dynamic loading methods suitable for various purposes are collected and refined. Basic documentation requirements and format are given to allow reexamining and reusing of the testing results.
- The FHWA guidance document is not a protocol. It intends to define consistent testing condition without imposing excessive restraints that impedes scientific studies.
- The seismic testing technology is far from mature at this moment. Any guidance document is subject to revising periodically to maintain up-to-date.

REFERENCES

American Concrete Institute (ACI) Innovation Task Group I and Collaborators, (2001). *Acceptance Criteria for Moment Frames Based on Structural Testing*, ACI ITG1/T1.1-01 American Concrete Institute, Farmington Hills, MI.

Applied Technology Council (ATC); (1992). *Guidelines for Cyclic Seismic Testing of Components of Steel Structures*, ATC-24, Applied Technology Council, Redwood City, CA, 1992.

ATC/MCEER (2003). *Recommended LRFD Guidelines for the Seismic Design of Highway Bridges*, Multidisciplinary Center for Earthquake Engineering Research Report No. MCEER-03-SP03, ATC-49, 2003.

Federal Emergency Management Agency (FEMA); (2000). *Prestandard and Commentary for the Seismic Rehabilitation of Buildings*, Prepared by American Society of Civil Engineers, Reston, Virginia, November 2000.

Hose, Y.; Silva, P.; Seible, F. (2000b). "Development of a Performance Evaluation Database for Concrete Bridge Components and Systems under Simulated Seismic Load," *Earthquake Spectra*, V. 16, No. 2, Earthquake Engineering Research Institute.

Krawinkler, H.; Parisi, F.; Ibarra, L.; Ayoub, A.; Medina, R. (2001). *Development of a Testing Protocol for Woodframe Structures*, CUREE Publication No. W-02, Department of Civil and Environmental Engineering, Stanford University.

Stone, W.; Cheok, G.; (1989). Inelastic *Behavior of Full-Scale Bridge Columns Subjected to Cyclic Loading*, NIST Building Science Series 166, Jan. 1989.

A Seismic Measure for Three-span Cable-stayed Bridge in Longitudinal Direction

Long'an LI

ABSTRACT

In this paper, the seismic responses of a cable-stayed bridge with different longitudinal restraint at the tower-girder connections are investigated. The results show that supplement of an elastic restraintt or a fluid damper is useful measure to reduce structural response. Besides, a method which is used to estimate design parameters of longitudinal elastic restraintt or fluid damper is presented, and the corresponding ranges of these parameters are suggested.

Long-an li, Zhongtie Major Bridge Reconnaissance and Design Institute CO., LTD. Wuhan 430050, PRC

1 INTRODUCTION

The appropriate span of steel cable-stayed bridge is 500-800m. In fact, Tataro Bridge has a longest center span of 890m, and Sutong Bridge with a center span of 1088m in china is under construction. However, the appropriate span of concrete cable-stayed bridge is 200-500m, and the Skarnsundet Bridge has the longest center span of 530m.

As for cable-stayed bridge, the vulnerable components are towers, side (or auxiliary) piers and their foundation under earthquake.

Usually, a cable-stayed bridge is classified according to tower-girder connection. The longitudinal restraint has a great effect on seismic response. Different restraint condition will lead to different transfer route of inertia force, thus induces different seismic response. Therefore, an appropriate structure system is very important for its safety in the design of long-span cable-stayed bridge.

2 ELASTIC RESTRAINT SYSTEM OF THREE-SPAN CABLE-STAYED BRIDGE

The elastic stiffness of longitudinal elastic restraints at tower- girder connection has a great effect on seismic performance of the whole structure, thus further investigation is as follow:

The transfer route of inertia force of deck system is shown in Fig. 1.

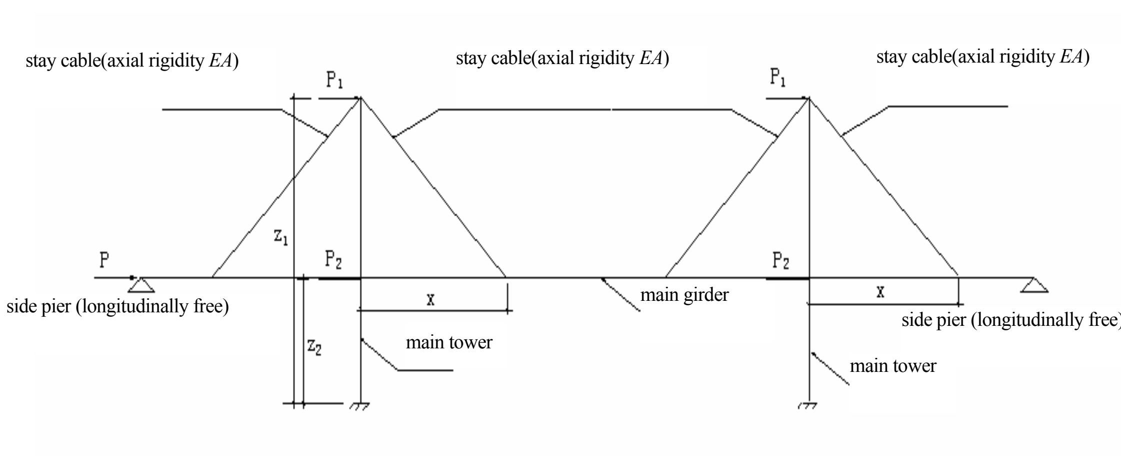

Fig. 1 Transfer route of inertia force of deck system

Where

x is the average distance from tower to deck anchor;

z_1 is the average distance from tower foot to tower anchor;

z_2 is the distance from tower foot to the bearing at tower-girder connection;

EA is the average axial stiffness of stayed cable;

k is the longitudinal restraint stiffness in one side at tower-girder connection;

Δ_x is the displacement of the restraint device at tower-girder connection;

The horizontal inertia force p is transferred to tower along stayed cables and the longitudinal restraint devices at tower-girder connection.

$$p_1 = EAx\frac{\sqrt{(x+\Delta_X)^2+(z_1-z_2)^2}-\sqrt{x^2+(z_1-z_2)^2}}{x^2+(z_1-z_2)^2} \qquad (1)$$

$$p_2 = -k\cdot\Delta_X \qquad (2)$$

Where

p_1 and p_2 are the inertia forces transferred by two different routes;

Thus, the longitudinal moment of tower foot is

$$M = p_1z_1 + p_2z_2 = EAxz_1\frac{\sqrt{(x+\Delta_X)^2+(z_1-z_2)^2}-\sqrt{x^2+(z_1-z_2)^2}}{x^2+(z_1-z_2)^2} - k\cdot\Delta_X\cdot z_2 \qquad (3)$$

In equation (3), the increasing of k will result in the increasing the inertia force p_2 transferred along the longitudinal restraint device. However Δ_x will decrease with the increasing of k. Therefore, M is not a monotonic function and a minimum will be gained.

To get the minimum, differentiate equation (3) with respect of Δ_x and take $\frac{dM}{d\Delta_x}$ equal 0, thus:

$$k = \frac{EAxz_1(x+\Delta_x)}{z_2\left[x^2+(z_1-z_2)^2\right]\sqrt{(x+\Delta_x)^2+(z_1-z_2)^2}} \qquad (4)$$

Usually, the ranges of the above variables are as follows:

$E = 1.95\times10^8\,kpa$; $A = 3.0\times10^{-3} \sim 2.0\times10^{-2}\,m^2$; $x = 80 \sim 280m$;

$z_1 = 80 \sim 300m$; $z_2 = 20 \sim 80m$; $\Delta_x = 0.2 \sim 2m$ (according to seismic response):

Substituting them into Eq.(4) gives: $k = 1.5\times10^4 \sim 1.5\times10^5\ KN/m$

Tab.2 Comparison of the longitudinal restraint stiffness

bridge	specification	Longitudinal restraint rigidity in one side
Shantou Dangshi Bridge	A 54m long tendon comprised of 55 strands 7 ϕ 5 high strength steel wires in each side	$k = 2.73\times10^4 kN/m$
Wuhu Yangtze River Bridge	Two 48m long strands respectively comprised of 85 ϕ 7 high strength steel wires and 187 ϕ 7 high strength steel wires in each side	$\begin{cases} k = 2.658\times10^4 kN/m \\ k = 5.316\times10^4 kN/m \end{cases}$
Haikou Centry Bridge	Two 31m long strands comprised of 73 ϕ 7 high strength steel wires in each side	$k = 3.534\times10^4 kN/m$

Chongqing Fengjie Yangtze River Bridge	Two 30m long strands comprised of 151 ϕ 7 high strength steel wires in each side	$k = 7.555 \times 10^4 kN/m$
Wuhan Baishazhou Yangtze River Bridge	A 103m long strands comprised of 55 ϕ 15 high strength steel wires in each side	$k = 1.458 \times 10^4 kN/m$
Tataro Bridge	Elastic restraint system comprised of shear rubber devices	$k = 4.000 \times 10^4 kN/m$

The longitudinal restraint stiffness of Tataro Bridge and another five bridges in china is listed in Tab.2. And convincingly, none of them is beyond the range of 1.5×10^4-1.5×10^5 KN/m presented above.

3 DAMPING SYSTEM OF THREE-SPAN CABLE-STAYED BRIDGE

3.1 Characteristics of viscous damper

For long-span bridges subjected to dynamic loads such as earthquake etc., the structural vibration will attenuate gradually till stop if the dynamic loads are suppressed. Such phenomenon as the amplitude attenuates with time passing is called damping phenomenon, which reflects the damping property of the bridge structures.

There are a lot of types for dampers, but in this paper only the viscous damper is considered, which has a damping proportional to velocity.

In some developed countries, viscous damper is of priority to be adopted for vibration control of long-span bridges, because it has the advantages as follows:

- Dissipate a lot of energy but no additional stiffness is added to the bridge structure under high velocity;
- No restraint on small displacement under low velocity;
- Have the advantages of wide damping coefficient range, extensive engineering application, perfect product stability, and convenience to construction and maintenance etc.

3.2 Working principle of viscous damper

The possible excitations of the bridge structure under operation include the variable loads (such as wind, vehicle brake force and flow pressure etc.) and accidental loads (earthquake and ship collision). When the excitation frequency is far away from the structural natural frequency, the damping has a little effect on the structural response. But if the excitation frequency is near or equal to the structural natural frequency, the damping will have a great effect on the structural response and must be considered. Among all the excitations earthquake is the strongest one, so the action of earthquake on bridge structures is emphasized in this paper.

3.2.1 Working principle

For a cable-stayed bridge under forced vibration with damping, the system motion equation is

$$M\ddot{X} + C_n \dot{X}^n + KX = -M\ddot{X}_0 \qquad (5)$$

Where

$M\ddot{X}$ is the inertia fore;

KX is the elastic force;

$-M\ddot{X}_0$ is the earthquake excitation force;

$C_n \dot{X}^n$ is the damping force supplied by viscous damper; C_n is the damping coefficient and n is the damping exponent, which all correlate with the damper configuration and are the two most important parameters of viscous damper. According to different values of n, the damper can be divided into three types as follows:

- $n = 1$, linear damper;
- $n < 1$, nonlinear damper;
- $n > 1$, super-linear damper;

(i) For linear damper, the damping force is $C_1 \dot{X}$ where C_1 is called linear viscous damping coefficient. Herein the damping force is lineally proportional to the velocity, which can be simply dealt with in mathematics. Accordingly the motion equation is

$$M\ddot{X} + C_1 \dot{X} + KX = -M\ddot{X}_0 \qquad (6)$$

The characteristics of linear damper are as follows:

When the maximum relative displacement at tower-girder connection is reached, the damping force is equal to zero while the elastic force reaches the maximum;

When the minimum relative displacement at tower-girder connection is reached, the damping force reaches the maximum while the elastic force reaches the minimum;

It is shown that there is a phase difference of 90 degrees between the damping force F_d and the elastic force F_e, so the damping force will not increase the maximum pier force.

(ii) For nonlinear or super-linear damper ($n \neq 1$), the damping force is $C_n \dot{X}^n$. It is more complicated to deal with in mathematics and usually the equivalent viscous damping C_{eq} is used:

$$C_{eq} = C_n \omega^{n-1} A^{n-1} \phi_n \qquad (7)$$

Where A is the amplitude and ϕ_n is equal to $\frac{2}{\pi}\int_{-\pi/2}^{\pi/2} \cos^{n+1} u du$.

3.2.2 Range of damping coefficient

Under the rule of equal maximum damping force and equal maximum displacement, the energy dissipation ratio $\Delta E_n/\Delta E_1$ is shown in Tab.3 for different n, where $\Delta E_1 = \pi c_1 A^2 \omega$ represents the mechanical energy dissipated by linear damper in a period cycle; $\Delta E_n = \pi c_n A^{n+1} \omega^n \phi_n$ represents the mechanical energy dissipated by nonlinear damper or super-linear damper in a period cycle.

Tab.3 $\Delta E_n/\Delta E_1$ for different n

n	0.1	0.2	0.3	0.4	0.5	0.6	0.7	0.8	0.9
$\Delta E_n/\Delta E_1$	1.236	1.201	1.169	1.140	1.113	1.087	1.063	1.041	1.020
n	1.0	2.0	3.0	4.0	5.0	6.0	7.0	8.0	9.0
$\Delta E_n/\Delta E_1$	1.000	0.849	0.750	0.679	0.625	0.582	0.547	0.517	0.492

Tab.3 shows that $\Delta E_n/\Delta E_1$ is more than 1 for n less than 1, which indicates the energy dissipation capacity of nonlinear damper is larger than that of linear viscous damper; $\Delta E_n/\Delta E_1$ is less than 1 for n more than 1, which indicates the energy dissipation capacity of super-linear damper is less than that of linear viscous damper; and $\Delta E_n/\Delta E_1$ is much less than 1 for n more than 2, which indicates the energy dissipation capacity of super-linear damper is much less than that of linear viscous damper;

It is also shown in Tab.3 that the hysteretic curves are different as to different damping exponent n. The comparison of hysteretic curves between $n = 0.3$ and $n = 1$ is shown in Fig.2.

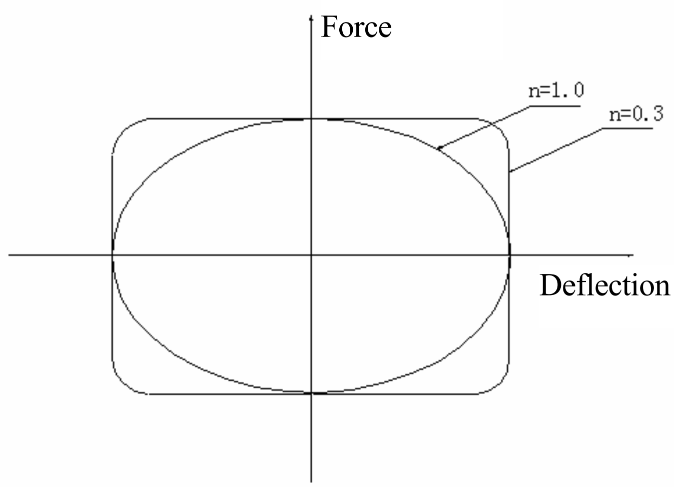

Fig.2 Comparison of hysteretic curves between $n = 0.3$ and $n = 1$

It is shown in Fig.2 that the energy dissipation capacity of nonlinear damper is distinctly larger than that of linear viscous damper under the same maximum damping force and displacement. From Tab.3 it can be known that the energy dissipation ratio of these two damper types is 1.169.

It is indicated in Tab.3 and Fig.2 that the nonlinear damper with a rich hysteretic curve should be adopted to suppress the structural vibration of bridge structures, so the value of 0.1~2.0 for n is usually used in engineering application. For seismic design of highway bridges the value of 0.2~1.0 for n is suggested, while the super-linear damper is rarely used.

Fig.3. shows the relation curve of damping force F_d against velocity $\dot{X}$ for different damping exponent n.

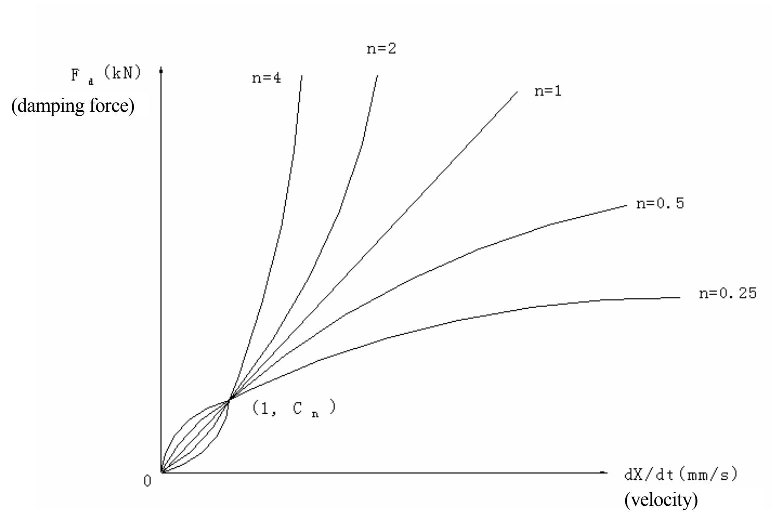

Fig. 3 $F_d - \dot{X}$ curves for different damping exponents

The characteristics of $F_d - \dot{X}$ curves in Fig.3 is as follows:

- All curves are through the point $(1, C_n)$. For the velocity less than 1mm/s, the damping force reduces with the increasing damping exponent, while increases with the increasing damping exponent for the velocity more than 1mm/s.
- The damping force of nonlinear damper is larger than that of linear damper under low velocity, while the damping force of super-linear damper is less than that of linear damper.
- The damping force of nonlinear damper is less than that of linear damper under high velocity, while the damping force of super-linear damper is much larger than that of linear damper.
- The less of damping exponent, the slower of the damping force increases with the velocity under high velocity.

For linear damper, the structural velocity is comparatively low and the damping force is very small under frequent earthquakes, so it can not work effectively. Under rare earthquakes, the structural velocity is comparatively high, and the damping force is so large that the connection elements of the damper will fail due to insufficient strength. However, the case is just opposite for nonlinear damper. Under frequent earthquakes, the nonlinear damper can produce enough damping force to ensure it in effective operation, while under rare earthquakes the damping force increases slightly and the connection elements of the damper are protected.

Fig.3 illuminates the necessity of adopting nonlinear damper in cable-stayed bridges again.

3.2.3 Range of damping coefficient

To obtain the range of damping coefficient C_n, the ranges of the damping force F_d and the velocity $\dot{X}$ should be determined first.

(i) According to equation (2)

$$F_d = k \cdot \Delta_X \qquad (8)$$

Where the maximum seismic response of Δ_X is equals to 2m; and k is between 1.5×10^4 and 1.5×10^5 KN/m.

Substitute the above values, and the damping force can be gained between $3.0\times10^4 KN$ and $3.0\times10^5 KN$

(ii) The horizontal ground velocity is 130mm/s, 250mm/s and 500mm/s respectively corresponding to the peak ground acceleration of 0.1g (□-intensity region), 0.2g (□-intensity region) and 0.4g (□-intensity region), and then the corresponding maximum velocity at tower-girder connection is from 600mm/s to 1000mm/s.

(iii) Substitute the above values into the equation $F_d = C_n \dot{X}_n$, and then the range of 30～500 $KN\Big/\left(\frac{mm}{s}\right)^n$ for C_n is obtained. Considering the rare occurrence of the two extreme cases, the range of 50～300 $KN\Big/\left(\frac{mm}{s}\right)^n$ for C_n is suggested.

3.3 Damping parameters of cable-stayed bridge

The viscous damping force is related to velocity. Generally velocity is the premise of generating damping force. However, the damping force, in turn, reduces both the longitudinal shift velocity and displacement at the end of girder.

The longitudinal shift velocity of girder is very slow under temperature load, low steady wind load or daily vehicle load, and the damper doesn't work at all in this instance.

However, when pulsating wind (or flurry) or vehicle brake force acts on, or even under earthquake, the longitudinal shift velocity of girder will get very high. Consequently, strong damping force, but not exceeding the strength of structure and connectors, is produced.

The behaviors of damper against dynamic load characteristic such as velocity, damping characteristic, displacement feature and forced vibration form is shown in Tab.4.

Tab.4 Table of the effect of damper on different dynamic loads

Dynamic load	Velocity	Damping	Displacement	Forced -vibration form
Annual and daily temperature change	Very low	No damping or low damping	Large displacement	Steady vibration

Normal vehicle load		Low	Low damping	Medium displacement	Transient vibration
Vehicle brake force		High	Medium damping	Medium displacement	Transient vibration
Wind force	Low steady wind	Low	Low damping	Medium displacement	Steady vibration
	Pulsating or flurry wind	High	Medium damping	Medium displacement	Transient vibration
Seismic load		Very high	High damping	Small displacement	Transient vibration

The longitudinal damping restraint stiffness at the tower-girder connection has two main parameters: damping coefficient C_n and damping exponent n. The damping force is: $F_d = C_n \dot{X}^n$.

In fact, there are many parameters of the dampers for structure, the main of which for single damper are listed in Tab.5.

Table 5 Main parameters of single damper

Parameter	Symbol	Parameter	Symbol
Function of damping force against velocity	$F_d = C_n \dot{X}^n$	Max spacing force (kN)	$F_{\max}$
Damping exponent	n	Max. seismic displacement (mm)	P
Damping coefficient $\left(KN/\left(\frac{mm}{s}\right)^n\right)$	C_n	Max spacing displacement (mm)	$P_{\max}$
Max. response speed $\left(mm/s\right)$	$\dot{X}_{\max}$	Horizontal rotary angle(radian)	θ
Max. damping force (kN)	F_d		

In general, the main steps to determine damping coefficient and damping exponent are as follows:

(i) Place longitudinal damper at the tower-girder connection according to Tab.4, and then calculate displacement and damping force of girder respectively under frequent, occasional and rare earthquakes. The damping force against longitudinal shift velocity is listed in Tab.6 (no less than 3 earthquake spectra or waves for frequent, occasional and rare earthquakes respectively).

Tal.6 Damping value for single damper

Longitudinal shift velocity（mm/s）	V_1	V_2	V_3	V_4	……	V_n
Damping force （KN）	F_1	F_2	F_3	F_4	……	F_n

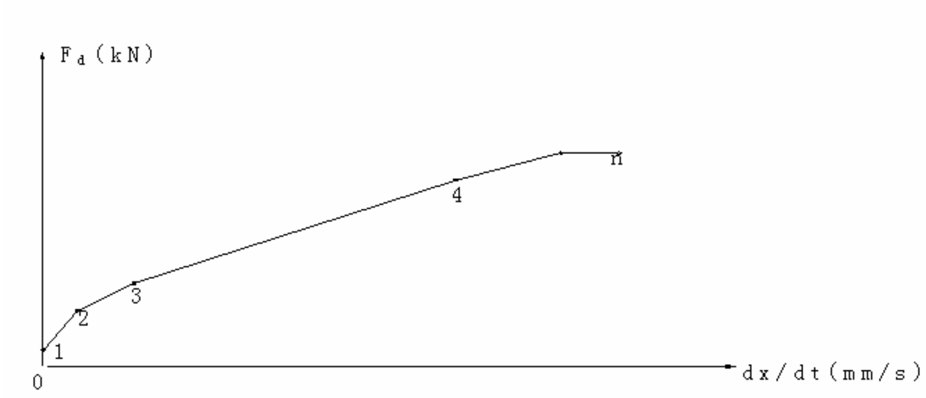

Fig.4 Coordinate of n discrete points in $F_d - \dot{X}$ coordinate system

Fig.4 only shows the coordinate of n discrete points in damping force-velocity coordinate system. If the viscous damping is considered, the relation among damping force F_d, damping coefficient C_n and velocity $\dot{X}$ is $F_d = C_n \dot{X}^n$, where the value for damping coefficient and exponent is determined according to the material and internal damper configuration.

(ii) A series of $F_d - \dot{X}$ curves can be gained according to different values of damping coefficient C_n and damping exponent n. With step-by-step approach method, a curve matching the best with that in Fig.4 is picked as shown in Fig.5.

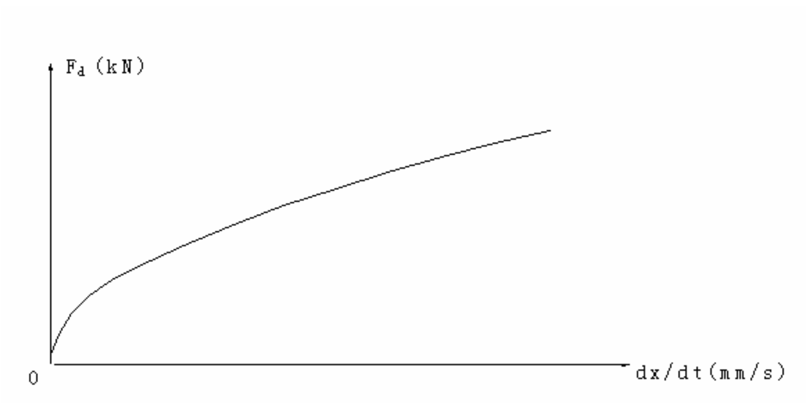

Fig.5 $F_d - \dot{X}$ fitting curve

Fig.4 and Fig.5 show that certain preliminary damping force is set at zero velocity in order to make the damper work in time. Besides, to avoid damper stalemate under high velocity, dropping valve is adopted to keep the loop pressure above certain level and therefore suppress the maximum pressure.

Only earthquake action is considered above and in fact, the other factors listed in Tab.4 should be considered for the damper parameter determination when in application.

4 CONCLUSION

Based on the above analysis, following conclusions can be given:

1. For large-span cable-stayed bridge, using longitudinal elastic restraint, damper or the both at the tower-girder connection can harmonize the structure bearing capacity and deformation ability effectively. They are ideal seismic measures for structure.
2. For large-span cable-stayed bridge, the longitudinal elastic stiffness should be $k = 1.5\times10^4 \sim 1.5\times10^5\ KN/m$
3. For large-span cable-stayed bridge, the damping parameters at the tower-girder connection should be determined as follows: the range of damping exponent n is 0.1～2.0, and 0.2～1.0 for earthquake resistance; the range of damping coefficient C_n is 50～300 $KN\Big/\left(\frac{mm}{s}\right)^n$.

REFERENCES

S. Timoshenko. The vibration problem in civil engineering. Translated by Renli Hu. Fourth edition, Beiing, Published by Universal Railway Press, 1978.

Zhenhua Ni. Vibration dynamics. Xi An. Publishing company of Xi'an jiaotong University.1994

Li Long'an, Zhang Jinwu. Effect of damping ratio on design spectra in seismic design specifications,Research of earthquake and civil engineering earthquake-resistance. Beijing, Publishing company of A-energy.2003, 195～202.

SY/T0450—97,Seismic Resistance of Steel Underground Pipes for Gases

Seismic Risk Assessment Procedures and Mitigation Measures for Highway Bridges in Moderate Earthquake Zones of the Eastern U.S.

Jerome S. O'Connor

ABSTRACT

Because of the infrequent occurrence of earthquakes, the Eastern half of the United States is generally not thought of as being particularly prone to earthquake damage. There have only been a few earthquakes of significant magnitude in recent history and the ones that occur with any kind of regularity are considered mild to moderate. Despite the lack of warning from Mother Nature, the potential for damage to highway bridges in these regions does exist. The vulnerability of the existing bridge population is accentuated by the fact that most were designed and detailed without any consideration of this potential.

All states have a rigorous bridge inspection program to assess the physical condition of their bridges. In addition, some states have a vulnerability assessment program to measure the risk of damage from earthquakes as well as from other unusual occurrences like scour, overweight vehicles, fatigue cracking, and collision. This paper will present the screening and evaluation methodologies used by one such Department of Transportation (DOT) to lessen the potential for damage due to earthquakes, as infrequent or mild as they might be. It will also describe what precautionary design and detailing practices are typically used by DOT's in these regions even when high seismic forces are not anticipated.

Jerome S. O'Connor, Multidisciplinary Center for Earthquake Engineering Research, 102 Red Jacket Quad, University at Buffalo, Buffalo NY, 14261, USA

INTRODUCTION

This paper describes procedures for assessing a large population of existing bridges for mitigating the risk of damage from earthquakes. It is based on a Bridge Safety Assurance (BSA) policy [Shirole', 1992] adopted by New York State (NYS) Department of Transportation (DOT). New York is a state typical of many others that are not overly concerned with the risk of earthquakes but need to take some pre-emptive measures to be sure the traveling public is protected in the rare event that an earthquake does occur. The lightly shaded geographic areas shown in Figure 1 are those that have low to moderate seismicity and are the focus of this discussion. Peak ground accelerations are assumed to be 0.2 g or less.

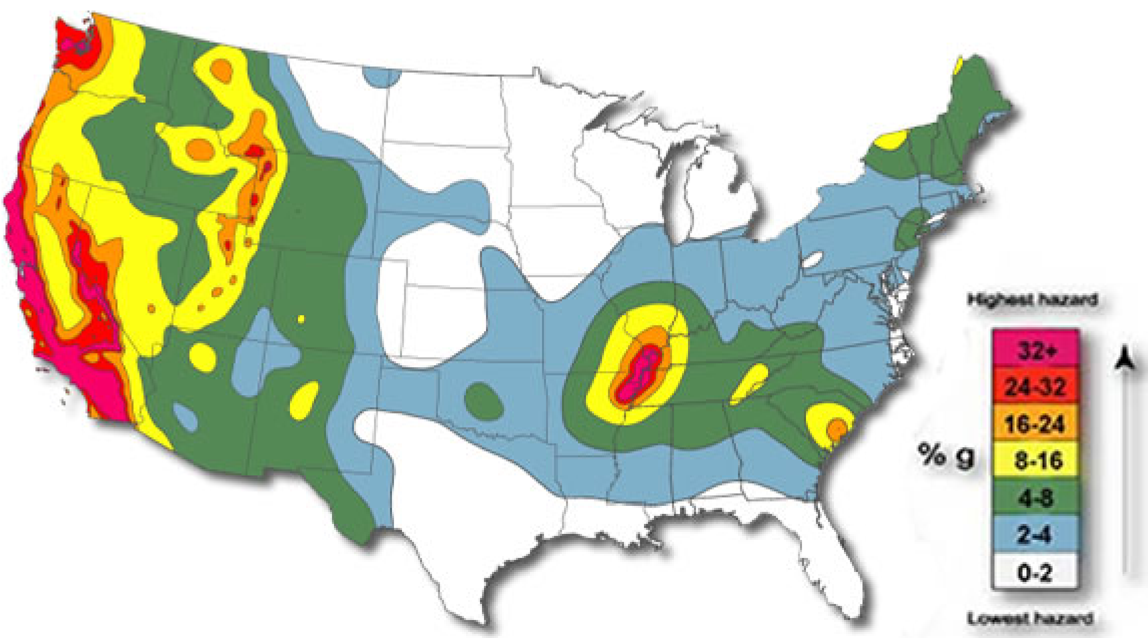

Figure 1. U.S. A. Areas of Seismic Intensity

Recorded history for North America only dates back a few hundred years so knowledge of seismic activity prior to settlement by Europeans in the 18^{th} century is non existent. While the natural landscape prior to this was undoubtedly shaped by earthquakes and glaciers, until recently, our only means of learning the extent of historic seismic forces has been damage to the built environment. The West coast of the United States has intermittently suffered major damage from earthquakes since the territory was settled. The East, which is the oldest part of the country, has had less of a record of damage to structures. This information provides the best indicator of seismic activity that has occurred.

Though uncommon, earthquakes are not unheard of in the Eastern part of the USA. A significant earthquake (estimated to be M6.0) toppled over 1000 brick chimneys in Boston, Massachusetts in 1755. The most widely felt earthquake to hit the continent (M8.0) occurred as part of a series of events between December 16, 1811 and February 7, 1812 in Central USA. It is said that the mighty Mississippi River temporarily flowed backwards as a result of the activity at the New Madrid fault. This is greater than any earthquake ever recorded in California or other

Western states and was felt in one third of what is now the USA. In 1886, a major earthquake (M7.3) shook Southeastern USA and devastated the city of Charlestown, SC which is built on coastal silty soils. The frequency of this type of earthquake is thought to be about 500 years. Both ground shaking and soil liquefaction have been experienced.

As stated, the focus of this paper is the part of the U.S. that does not see these extreme events. One such state is New York. The greatest earthquake to hit New York State was M6.0 in 1944. [NYSGS, 2004] Events (up to M5.0) have occurred at approximately 20 year intervals and lesser events (under M2.5) at least annually though generally unnoticed. While the general population on the West coast is well aware of the dangers presented by earthquakes, most of the people in the East (including policy makers) have only experienced an infrequent, mild earthquake, if one at all.

SEISMIC SPECIFICATIONS

Bridge Design

The design of essentially all public bridges in the United States is done according to standards adopted by the American Association of State Highway and Transportation Officials (AASHTO). Prior to the San Fernando, California earthquake of 1971, seismic specifications for the design of new bridges provided only rudimentary instruction to a bridge designer. Since that time, national guidelines have become more refined, with increasing complexity resulting from the knowledge gained from each subsequent earthquake. These specifications are currently undergoing a major revision so that they will reflect the most recent research and new analysis techniques including additional information on the subject of soil liquefaction. Until the new specifications are adopted by the AASHTO, the chairman of its Technical Committee for Seismic Design (T-3) Rick Land offers the following choices to an agency:

- Site specific design criteria (typically developed for special, long span bridges)
- State specific design criteria (e.g. California and South Carolina)
- AASHTO Standard Specification for Highway Bridges, Division 1A, using the 1998 acceleration maps produced by United States Geological Survey (USGS)
- Criteria stemming from a National Cooperative Highway Research Project called NCHRP 12-49 and published as *Recommended LRFD Guidelines for the Seismic Design of Highway Bridges*. (note: LRFD is Load and Resistance Factor Design methodology). This four volume document is available as MCEER/ATC 49 at http://mceer.buffalo.edu.
- A version of the above that was proposed as agenda item #3 at the 2002 AASHTO Subcommittee Meeting for Bridges and Structures. This is available to states from the Chairman of the T-3 Committee.

AASHTO expects to have new seismic provisions formally adopted by the year 2007, which is its self imposed deadline for the use of Load and Resistance Factor Design (LRFD) on all bridges.

Bridge Retrofit

Retrofitting existing bridges to meet modern day standards always presents unique problems. An older structure may have been designed with no consideration of seismic forces; it may have been modified since it was originally built to accommodate new uses; it may have suffered deterioration that has changed its behavior from when it was originally built; and it may be reaching the end of it remaining fatigue life due to repeated truck loadings. These factors and others prevent the specifications for new bridges from being used when designing retrofitting measures for older bridges. Furthermore, continuously improving an entire population of bridges to meet constantly evolving standards is not economically feasible or justifiable. It is an ongoing challenge to implement new seismic structural standards on a large population of bridges that were not originally designed for earthquake loadings. [Hodel, 2004]

Though the design of new bridges can follow a somewhat regimented methodology, seismically modifying an existing structure always requires more engineering judgment and compromise. As such, guidelines which allow interpretation and judgment are the norm rather than the specifications for new bridges promulgated by AASHTO. The most comprehensive guide for retrofitting highway bridges and the one most widely used is published by the United States Department of Transportation's Federal Highway Administration (FHWA). [FHWA, 1995] In this document, bridges are classified according to location and assigned a Seismic Performance Category (SPC) with A being low risk and needing no detailed evaluation, and C indicating a need for evaluation of bearings and substructure units as well as investigation of the potential for liquefaction. This document is also currently undergoing a major revision. By the end of 2004, it will be superseded by a two part document entitled: *Seismic Retrofitting Manual for Highway Structures: Part 1: Bridges,* and *Part 2: Retaining Structures, Slopes, Tunnels, Culverts, and Pavements. [FHWA, 2004]*

This paper deals with the assessment of seismic risk associated with the numerous existing bridges that carry traffic on public roads. There are 594,000 bridges in the United States and approximately 79% of these are located in states that are considered to have a low to moderate risk of earthquakes. Figure 2 shows "year of construction" for all highway bridges in the USA. With an understanding that modern seismic criteria were not imposed before the 1970's, it becomes apparent that that about half of the bridges in service today may be considered seismically deficient. This is not necessarily cause for alarm because many of these bridges are in low risk areas and most important, long span bridges in high risk areas have been investigated and retrofitted. In order to reduce the level of uncertainty, however, states either informally identify suspect bridges and investigate the need for seismic countermeasures, or on a larger scale, conduct a risk assessment program to see where improvements are most warranted.

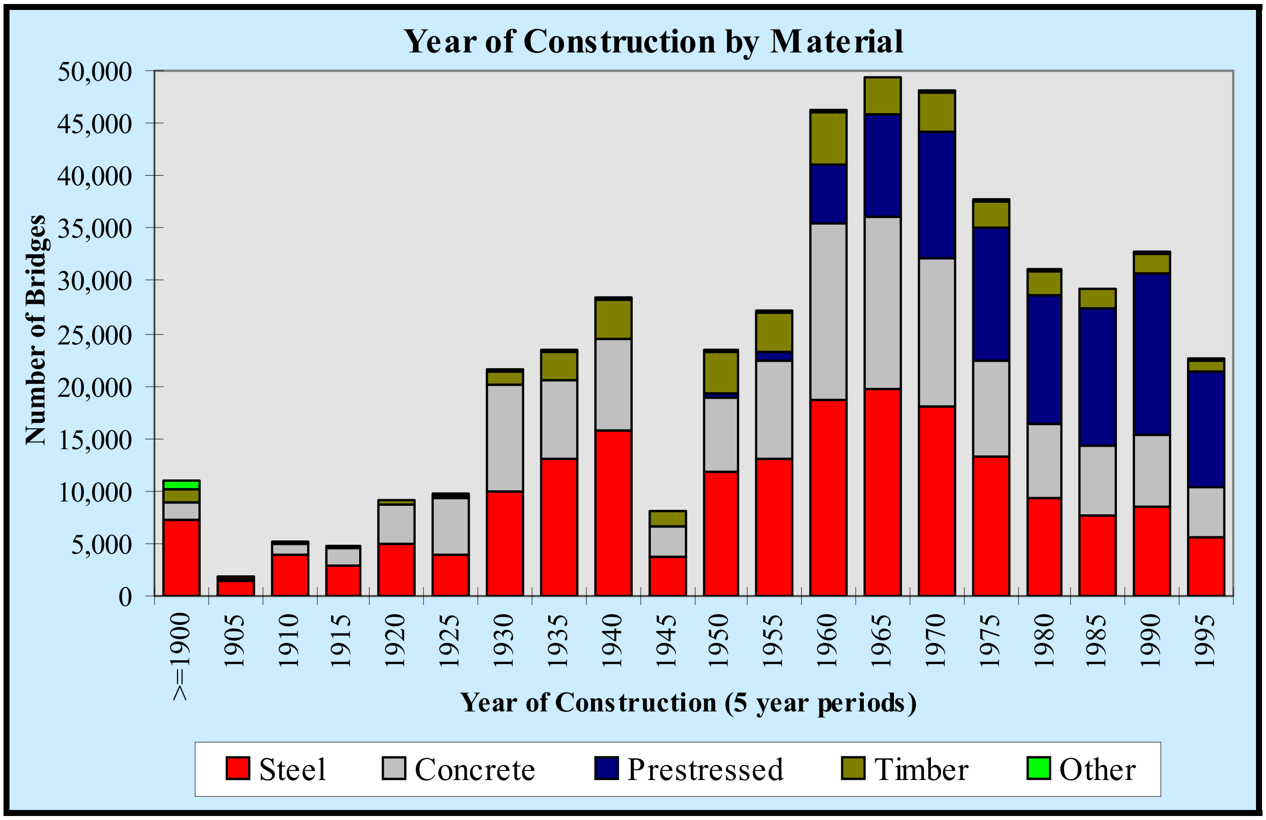

Figure 2. Number of Bridges Built each Decade

Over $6 Billion U. S. dollars are spent each year on bridges. Funds used for “new bridges” or “bridge replacements” employ the AASHTO specification or a state specific code. For bridge rehabilitations that involve seismic retrofit, the FHWA Seismic Retrofitting Manual is commonly used.

VULNERABILITY ASSESSMENT

General Practice

Long span bridges, moveable bridges, or other special bridges are almost always investigated individually to give proper consideration to structural response, soil conditions, proximity to a potential fault lines, and unique structural characteristics. The following discussion relates to the other 95^{+}% of bridges that make up an agencies inventory.

While some states such as California have undertaken programs to seismically retrofit bridges, most states in the Eastern U.S. have not. This is because state DOT’s are more often preoccupied with problems relating to deterioration of condition or capacity. Many older bridges are made of steel, and deicing salts used in severe winter weather accelerate the inevitable corrosion. Environmental problems from lead based paint make painting of bridge more difficult and expensive year by year. Concrete decks and substructures suffer from cracking that stems from rusting reinforcing steel. These issues present a looming infrastructure maintenance problem that overshadows any concern for a potential earthquake.

Rarely, is a bridge programmed for seismic retrofit work alone. Funds for bridges are usually dispensed based on a calculated *sufficiency rating* which is largely based on condition and functionality of a bridge. *Structural deficiency* and *functional obsolescence* are tracked quite closely. Seismic deficiency is not captured in the definition of any of these measures. Although recent federal legislation mandated that $25 Million per year be spent on seismic rehabilitation, much more is spent fixing or replacing *deteriorated* bridges. As funds are allocated, progress is being measured. Though deficiency is the most common means of measuring success in the battle against the deterioration of aging bridges, an improvement in seismic performance does not help a state reduce the number of deficient bridges. In a competitive environment where each bridge is demanding of resources, funds most often flow toward those where improvements are quantifiable and reported upon.

It is therefore typical for states located in moderate earthquake zones to defer major seismic improvements until a bridge is due for replacement or major rehabilitation for some other reason (usually age, condition, or insufficient capacity). Because earthquakes are not seen as an impending threat, there is usually no systematic means for prioritizing seismic retrofit work. If and when a bridge is replaced, all AASHTO criteria for new bridges are incorporated into the design.

For rehabilitations, there are normally state-specific guidelines for addressing seismic improvements. In lieu of these, a careful review of a bridge's as-built plans, a review of any in-depth inspection reports on file, geotechnical logs, a field inspection of the site, along with a solid understanding of bridge engineering principles, will help a designer make good decisions about what seismic improvements to incorporate into a general rehabilitation project. One will often find that the answer is a balance of economic considerations.

In the state of New Jersey, when a rehabilitation project is undertaken, a flowchart is provided to guide designers in determining the extent that a bridge should be retrofitted for seismic concerns. See Figure 3. [NJDOT, 2002] The purpose of the chart is to give due consideration to the cost effectiveness of the proposed work.

New York State Practice

An informal survey of DOT's in the Eastern U.S. shows that DOT bridge programs are driven more by condition assessment than vulnerability assessment. This is discussed above. New York State is no exception. It does, however, have a documented Bridge Safety Assurance (BSA) program in place to rank bridges by risk. Although the program is hampered by competing demands and pressures driven by an aging infrastructure, it serves as a model for integrating of the risk concept into a bridge management system for better understanding and handling of a large population of bridges.

New York's BSA program capitalizes on computer technology to facilitate the management of its 17,356 highway bridges. The ability to rapidly screen and identify suspect bridges provides the foundation for a more thorough and orderly assessment of bridges. This disciplined, pro-active approach is intrinsically more effective than responses that are reactive in nature.

New York State spends over $45 million a year inspecting its bridges. Though the inspection program does an excellent job of determining the physical *condition* of a bridge,

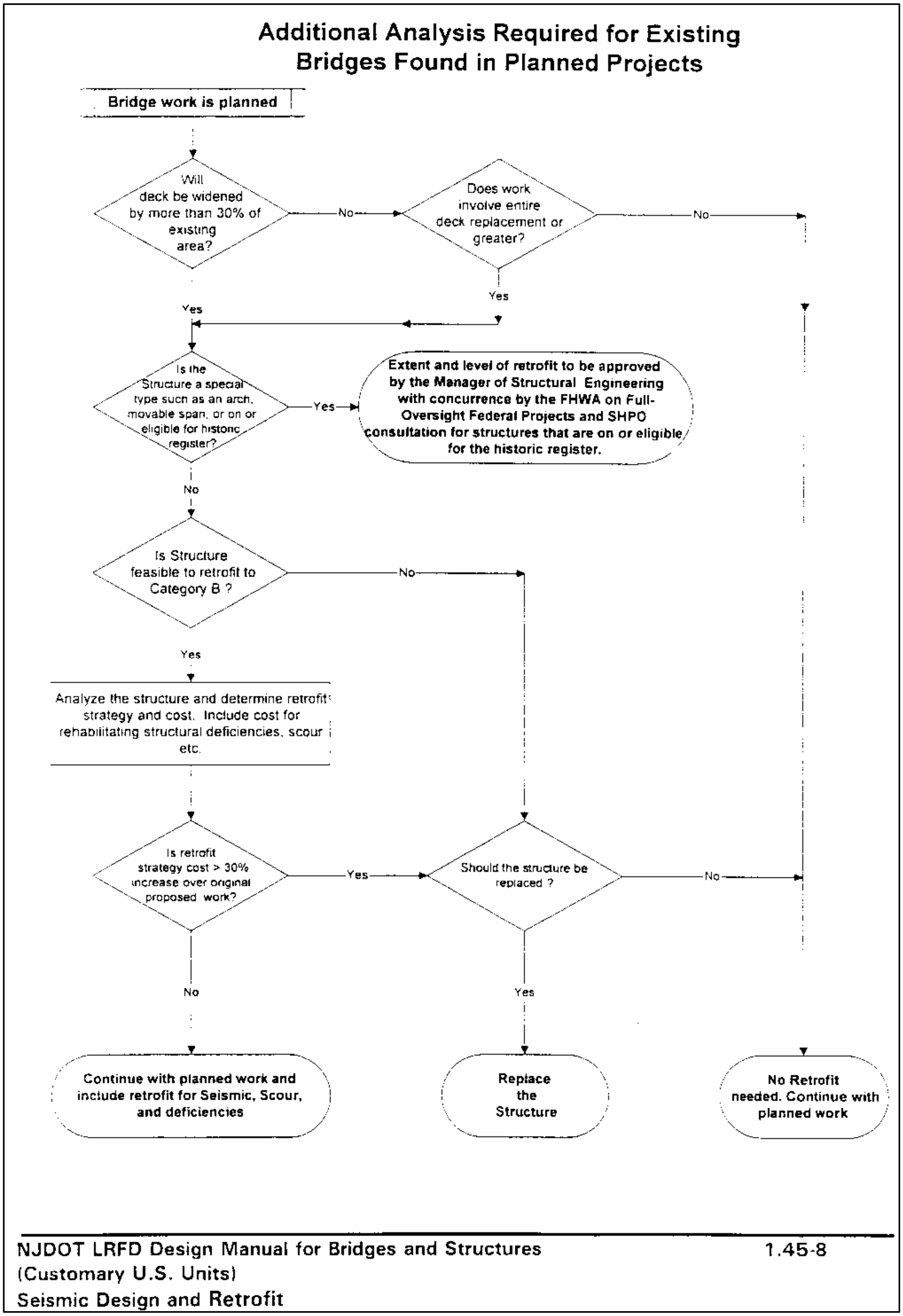

Figure 3. NJ DOT Flowchart for Deciding on Cost Effectiveness of a Seismic Retrofit

[O'Connell, 1997], it does not measure the *risk* of bridge failure. This is the reason that the state's BSA program was established. [O'Connor, 2000]

In the USA, for example, over half of all bridges that have collapsed have failed as a result of hydraulic scour. [O'Connell, 1999] Bridge inspection provides data on condition, which is a measure of a bridge element's integrity over time and its ability to function as originally designed. However, predicting the risk of failure due to scour has little to do with the condition of a bridge. If a bridge was not designed with piles to protect against scour, this vulnerability will not be reflected in the bridge's condition rating. A BSA program like the one in NYS will identify this risk and prioritize it against other potential failure modes and other bridges. For example, it allows one to perform a rudimentary comparison of the risk of losing a bridge due to scour vs. an earthquake.

NYS's Bridge Safety Assurance (BSA) Program

New York's BSA program was adopted to provide a systematic means of identifying situations that pose a threat to the structural integrity of bridges. A traditional bridge inspection program ascertains the *condition* of various bridge elements. This information is typically used to drive an agency's capital and maintenance bridge programs. New York's BSA program supplements this condition based evaluation by taking a slightly different perspective. It assesses and rates the *degree of risk* associated with certain design details and circumstances. The BSA program is used to evaluate a bridge using current design practice as a reference whereas the inspection procedures are used to rate each element of a bridge only according to its condition and ability to function as intended in the original design. Rating all bridges according to their ability to remain safe under current conditions using today's design philosophy provides an ability to evaluate structures using a common reference regardless of when it was built. This is especially important in the field of earthquake engineering because it is such a young science and "best practice" is still evolving.

NYS DOT has implemented vulnerability rating procedures as part of a BSA Program. The program establishes formal procedures for assessing risk and producing numerical ratings as an indicator of vulnerability. These vulnerability ratings put a value on the relative urgency of the need for retrofit or countermeasure. The state's entire population of bridges is being assessed for vulnerability to failure by one of several failure modes. These are *hydraulic scour, overload, steel fatigue, concrete details, collision, and earthquakes*. Since the inception of the program, *security* has been added as a consideration due to the threat of intentional damage from extremist, societal outliers. As with each other potential failure mode, the process used for earthquake assessments is published in a manual. [O'Connell, 2002]

The main purpose of the BSA program is to provide better information to decision makers so they can allocate scarce resources in such a way that the "worst" bridges are replaced, retrofitted or repaired first. Traditionally, "worst" was taken to mean the ones in the poorest condition, as indicated in bridge inspector's reports and ratings. The BSA programs extends that definition to include those which are in good "condition" but may still be at risk due to particular vulnerabilities.

A bridge management system which utilizes both a condition and vulnerability perspectives is innately better because it provides project selection information that insures that the most needing structures are programmed for work.

Program Phases

Dealing with bridges from a bridge safety assurance viewpoint is broken into the following phases. See Figure 4.

1. Identification

2. Vulnerability Assessment
   - Screen
   - Classify
   - Rate

3. Evaluation

4. Corrective Action

Figure 4. Bridge Safety Assurance Program Phases

The first two phases involve an assessment of the entire bridge population. When these phases indicate a relatively high risk of failure for a particular bridge, the other two phases provide for a more in depth response. These steps insure that all of the agency's bridges are evaluated using today's design practice as the standard to preserve the structural integrity of all bridges regardless of when they were built.

Screening

In commencing an overall retrofit program, one failure mode is investigated at a time. The agency's bridge database is used extensively to select bridges that have some potential for damage due to the failure mode under investigation. For instance, when looking at seismic issues, one would screen on the year of construction, to identify those built when standards were sketchy or non existent. With good data, a database query can become even more refined. It can quickly produce results identifying multi-span bridges that are not continuous, or ones that have older style, high bearings. This screening can be done with minimal effort through the use of computers.

Classifying

Since accurate bridge inventory data is necessary to produce meaningful results from a computer assisted assessment process, bridge inspectors need to regularly review and verify all bridge data. They need special instruction on how to identify situations that represent poor seismic details. NYSDOT's assessment procedures provide specific steps for classifying a bridge. These steps use the corporate database and bridge history records to successively refine the information on bridges until there is enough to determine a vulnerability rating for each. After initial screening, bridges are classified into low, medium, or high risk categories by performing an office review of record plans, inspection reports, and other information available in the bridge history folder. A field review is used if necessary to supplement the information on file. Since subsequent steps in the BSA procedure require a more in-depth analysis, the categories listed in Table 1 are needed to insure that the most important bridges are addressed first.

Table 1. Definitions of Classifications

Low	Conditions exist which reveal little or no potential for failure.
Medium	Conditions exist which create a recognizable potential for failure.
High	Conditions exist which create a significant potential for failure. It is quite likely that during the structure's remaining life it may experience such a failure.

Bridges that are unique in nature or have unusual characteristics associated with them may not neatly fit into the standard assessment procedures. These are classified on an individual basis using the intent of the process and sound engineering judgment.

Rating

The final step of the assessment procedure is the assignment of a vulnerability rating (VR) for each one of the six identified failure modes. This gives each bridge a relative measure of the likelihood and also the consequence of failure. The numerical ratings are defined in Table 2.

Table 2. Definitions of BSA Vulnerability Ratings

VR = 1	Safety Priority Action - This rating designates a vulnerability to failure resulting from loads or events that are likely to occur. Remedial work to reduce the vulnerability must be given immediate priority.
VR = 2	Safety Program Action - This rating designates a vulnerability to failure resulting from loads or events that may occur. Remedial work to reduce the vulnerability does not need immediate priority but waiting for Capital Program action would be too long.
VR = 3	Capital Program Action - This rating designates a vulnerability to failure resulting from loads or events that are possible but not likely. The risk can be tolerated until a normal capital construction project can be implemented.
VR = 4	Inspection Program Action - This rating designates a vulnerability to failure presenting minimal risk providing that anticipated conditions or loads on the structure do not change. Unexpected failure can be avoided during the remaining life of the structure by performing the normal scheduled bridge inspections with attention to factors influencing the vulnerability of the structure.
VR = 5	No Action - This rating designates a vulnerability to failure which is less than or equal to the vulnerability of a structure built to the current design standards. Likelihood of failure is remote.
VR = 6	Not Applicable - This rating designates there is no exposure to a specific type of vulnerability.

Vulnerability Rating Code

As ratings are obtained for each of the six identified failure modes, a bridge rating code is compiled for each bridge. This reflects the overall vulnerability and is useful for tracking and programming. Each bridge has a six digit code comprised of the individual ratings. As new ratings are produced for additional failure modes (e.g. security), additional digits can be added.

Bridges with a low vulnerability rating (e.g. VR = 1 or 2) for any of the failure modes merit immediate a more in-depth evaluation or corrective action. After closer scrutiny, the sample countermeasure actions presented later might be appropriate. These actions may serve as an interim repair until a capital project is possible or may be implemented as a long term solution. Bridges with higher ratings (VR = 3 or 4) are monitored and maintained until such time that improvements to the bridge can be planned and funded.

An appropriate response to a low rating may be a more in-depth investigation which could give a more thorough understanding of the situation through better input data, methodology or computational techniques. Field testing may also be undertaken to obtain measurements of a bridge's reaction to loads. When a more thorough understanding does not resolve the concern with a bridge, countermeasures such as those presented may implemented to reduce the risk of failure. In cases where no countermeasure is feasible or it can not be undertaken because of fiscal or other constraints, the responsible agency can increase the frequency or intensity of inspection to insure the public's safety. Though this does not remove the source of the risk completely, it provides a measure of protection above the status quo.

In addition to using the VR's to plan retrofit work, they can be very useful as a useful tool in an emergency. In the flurry of activity common after an extreme event, having bridges ranked can save vital time so that resources can be deployed to the locations where they are needed. When an agency is responsible for hundreds or thousands of bridge in a region, having any means to prioritize them is welcome. In rural locations, an emergency response team can avoid many hours of wasted travel time by having this information at hand.

Evaluation

After the vulnerability assessment phase is completed, (refer to Figure 4.) a more in-depth evaluation is performed on bridges that are ranked lowest. A *Structural Integrity Evaluation (SIE)* report is produced. [NYSCRR, 1989] This is custom prepared by a registered professional engineer providing an in-depth look at all aspects of the bridge. As part of this report, an intensive analysis (e.g. pushover analysis, finite element model, etc) is performed. The intent is to insure that the bridges identified as vulnerable are thoroughly understood and a strategy for future action is laid out.

Once improvements are made or there is less risk because of a more thorough understanding of the bridge, the VR may be updated. Afterwards, on future general bridge inspections, bridge inspectors are asked to recommend when the VR might need to be changed again. This might be due to changed environmental conditions or modifications to the bridge. These ratings and other available information are used with a Bridge Management System for the selection of projects for the capital program.

Mitigation Measures

Acceptable actions to improve performance and reduce the risk of failure are a function of site conditions such as soil type, structure type, original design detailing, as-is condition, and importance. Though relatively inexpensive retrofit measures such as bearing replacements can be easily justified when the original bridge component needs replacing anyway, other, more extensive measures, need to be weighed in against the cost and the expected damage. Whereas, a determination of a structure's capacity to resist seismic forces was the norm not long ago, consideration of performance has shown to be a better approach. Functionality will be determined by the extent of damage and displacement. To assess performance, failure scenarios need to be scrutinized and consideration given to the ease of post event inspection, repair, and restoration to service.

Though a detailed description of vulnerabilities and possible retrofit measures is not possible as part of this paper, Table 3 serves as a summary that might be useful as a checklist when considering a bridge rehabilitation. As mentioned earlier, the states in question would pick and choose from this list to determine which measures are considered cost effective, given the condition and anticipated remaining service life for a given structure.

Some of these measures might be taken by a DOT as a precautionary design and detailing practices even when high seismic forces are not anticipated.

Table 3. Typical Retrofit Measures

Vulnerability	Typical Retrofit Measure
Lack of confinement in reinforced concrete column	Steel jackets, tensioned steel strands, or composite fiber wraps
Loss of superstructure support at pier	Longitudinal restraint cables
Excessive lateral movement of superstructure	Install lateral restraint device; cables or shear blocks
Uplift	Secure bearings
Toppling of bearings and dropping of superstructure	Replace bearings with elastomeric or other low bearing
Lack of superstructure continuity on a multi-span bridge	Join the spans to provide live load continuity
Excessive load transfer to substructure	Install isolation bearings
Loss of support at abutment	Widen bridge seat
Insufficient lap splices between column and footing or piles and pile cap; lack of top mat tension reinforcement in footing	Footing-column modification; additional piles and extended pile caps; micropiles
Unequal bent stiffness	Detailed analysis and retrofit
Masonry substructure construction	Exterior reinforcement and confinement
Liquefaction	Silty soil remediation by compaction grouting, stone columns, or micropiles
Excessive longitudinal forces	Install load transfer devices
Single column bridge piers	Provide redundancy by adding columns or outriggers
Poor reinforcement detailing	Reconstruct joint

CONCLUSION

Although the frequency of major earthquakes is less in the Eastern part of the United States, than in other parts of the world, there is still a real risk of damage or even failure. Risk is a function of the likelihood of the occurrence and the consequence or the penalty to be paid, so careful consideration needs to be given to the relative importance of a structure. While the likelihood is low, the consequences could be devastating if the event occurred.

An informal survey of states in moderate earthquake zones finds that most do *not* use a formal method to prioritize seismic retrofit work. Certain bridges receive special attention because of their importance but for the vast majority of bridges, remedial work is deferred until the end of a bridge's useful life (in which case, the most up-to-date seismic design specification would be applied). If a bridge is programmed for rehabilitation for other reasons, such as condition or capacity, seismic improvements are usually considered. Whether these improvements are incorporated depends on their cost relative to the overall project and the replacement value of the structure. Since it is difficult and costly to retrofit a bridge to the same standards of a new bridge, major upgrades are sometimes forgone for the sake of keeping the rehabilitation a feasible project alternative. Rarely is a rehabilitation project initiated for seismic concerns alone.

In NYS, the vulnerability assessment program enables the DOT to prioritize the need for in-depth analysis and retrofit work. It gives consideration to risk of failure to complement the condition information provided by the state's extensive inspection program. The vulnerability ratings produced are also useful in a post event response situation because they help identify the most vulnerable bridges quickly so inspection teams and resources can be sent to the places where they can do the most good.

The general BSA strategy can be applied to other potential modes of bridge damage or failure (e.g. security issues). It provides a means to weigh the relative risk of various failure modes.

The BSA assessment methods provide for a more uniform and thorough assessment of structures. Agencies like NYSDOT should find this preferable to assessing risk informally or without any clearly defined approach. It also serves to document the evaluation process which may assist in demonstrating that the agency is fulfilling its inherent obligation to the public and meeting the objective of insuring that its bridges are functional and safe.

DISCLAIMER

Statements and opinions expressed are the responsibility of the author and do not presented as official policy of MCEER, FHWA, any state DOT, or other agency.

REFERENCES

FHWA, *Seismic Retrofitting Manual for Highway Bridges*, FHWA report RD-94-052, McLean, VA, 1995.

FHWA, *Seismic Retrofitting Manual for Highway Structures: Part 1: Bridges,* and *Part 2: Retaining Structures, Slopes, Tunnels, Culverts, and Pavements,* McLean, VA, 2004

Hodel, C., Trello, M., Tobias, D., "Seismic Retrofitting in Illinois: Bridge Population Implementation", *Proceedings of 4th National Seismic Conference and Workshop on Bridges and Highways*, Memphis TN, 2004

NJDOT, H., *New Jersey Department of Transportation Bridges and Structures Design Manual*, Fourth Edition, 2002

NYSCRR, "Structural Integrity Evaluation", Uniform Code of Bridge Inspection, *New York State Compilation of Rules and Regulations, Part 165.11*, 1989

NYSGS, New York State Geological Survey, http://www.nysm.nysed.gov/geosige.html, 2004

O'Connell, J. M., NYSDOT, *Bridge Safety Assurance Seismic Vulnerability Manual*, New York State Department of Transportation, Albany, NY, 2002

O'Connell, J. M.., "New York State Bridge Inspection Manual", NYSDOT, Albany, NY, 1997

O'Connell, J. M.., "Bridge Failure Database", NYSDOT, Albany, NY 1999

O'Connor, J. S., "Bridge Safety Assurance Measures Taken in New York State", Transportation Research Record, 5th International Bridge Conference, Tampa, Transportation Research Board, Washington, DC, 2000

Shirole', A. M., "New York State Policy on Bridge Safety Assurance", NYSDOT, Albany, NY, 1992

Yanev, B., "Addressing the Seismic Vulnerability of Bridges in New York City", *Proceedings of 3rd International Workshop on Performance-Based Seismic Design and Retrofit of Transportation Facilities*, Tokyo, Japan, 2002

Buckling Restrained Braces for Ductile End Cross Frames in Steel Girder Bridges

Lyle P. Carden, Ahmad M. Itani and Ian G. Buckle

ABSTRACT

Buckling restrained braces (BRBs) have been shown to be a cost-effective way of improving the seismic performance of moment-frame buildings. In this paper the application of these devices to bridge structures is explored and in particular BRBs are investigated as ductile members of the end cross frames in steel plate girder bridges. Component experiments on a series of braces are first described and it is shown that they exhibit good cyclic behavior, although loading history and strain rate affect their performance and ultimate limit state. System experiments on a 0.4 scale model of a two-girder bridge using a pair of shake tables at the University of Nevada Reno are next described. BRBs are used in the ductile end cross-frames of this model and the results show a significant reduction in the shear demand in the bridge. Furthermore, the cross-sectional drift in the superstructure is less than when angle X-braces are used in the end frames. Ductile end cross frames are thus shown to be an effective means of improving the seismic performance of steel girder bridges and believed to be most effective when both the superstructure and substructure are relatively rigid.

Lyle P. Carden, Center for Civil Engineering Earthquake Research, University of Nevada Reno, Reno, NV 89557-0152, USA.
Ahmad M. Itani, Center for Civil Engineering Earthquake Research, University of Nevada Reno, Reno, NV 89557-0152, USA.
Ian G. Buckle, Center for Civil Engineering Earthquake Research, University of Nevada Reno, Reno, NV 89557-0152, USA.

INTRODUCTION

The end cross frames or diaphragms in steel plate girder bridges have been determined to be critical in the transverse load path for seismic loading. Past earthquakes have resulted in damage to these end cross frames as described by Astaneh-Asl et al. (1994), Bruneau et al. (1996) and Shinozuka et al.(1995). It has become apparent that the end cross frames need to be designed for the transverse earthquake loading (Carden et al. 2003). There are essentially two approaches which can be considered in their design. The first is to design them to perform elastically, protected by the capacity design of the substructure as described by Itani and Reno (1995). The second is to design the cross frames to be ductile and use these ductile elements to protect other parts of the superstructure and substructure. Studies have been performed by Astaneh-Asl (1996) and Zahrai and Bruneau (1999a, 1999b) investigating the potential for use of cross frames as ductile elements. These studies investigated different systems, including special cross braces, shear panel systems (SPS), eccentric braced frames (EBF) and a triangular-plate added damping and stiffness (TADAS) device. The studies demonstrated the feasibility of ductile end cross frames as long as the substructure is not too flexible.

Buckling restrained braces (BRBs) have emerged as an attractive form of bracing in buildings during earthquakes. They have been shown to have good hysteretic behavior without stiffness and strength degradation as observed in concentric braced framing systems. In this project buckling restrained braces were investigated as a potential form of ductile end cross frame in steel plate girder bridges. For this application the braces were shorter in length compared to those typically used in buildings, making the connection details particularly important. They also had a relatively small core dimensions.

In order to perform experiments on ductile end cross frames with buckling restrained braces, a $^{2}/_{5}{}^{th}$ scale model of a two steel plate girder bridge superstructure was used, as shown in Figure 1. "Unbonded" braces, a type of BRB constructed by Nippon Steel Corporation using low yield point (LYP-225) steel, were placed diagonally at the ends of the bridge model as shown. The end cross frames also consisted of a top chord to provide a direct load path for transverse earthquake loads between the deck and the end cross frames, with implications as described by Carden et al. (2002). A bottom chord was also provided to evenly distribute loads between the bearings. The top and bottom chords were constructed with pinned connections to minimize their lateral stiffness and therefore minimize post-yield stiffness in the ductile end cross frames. Several shear studs connecting the deck and the girders were removed at the ends of the girders in order to allow the girders to rotate about their longitudinal axis to further minimize post-yield stiffness in the ductile end cross frames. Transverse earthquake loading was simulated using shake tables at either end of the bridge model. Experiments were also performed on the bridge model with special angle X-braces and with seismic isolation bearings although the results from these experiments are referred to only briefly in this paper.

COUPON TESTS

Two coupon tests were performed by Nippon Steel (2002) on the LYP-225 steel used in the unbonded braces. The resulting material properties for the two tests are given in Table 1. The yield strength of the steel coupons was shown to be close to the expected yield strength of 225 MPa. Unlike most US steels where the nominal strength is generally defined at a minimum specified strength, the nominal strength for the LYP-225 steel is defined in the middle of a relatively tight range of acceptable yield strengths. Therefore, the nominal strength of 225 ksi was taken as the expected strength for this material. The ultimate strength of the LYP-225 steel was around 30% higher than the yield strength, compared to 50% for comparable A36 steel coupons tested for this project, indicating less strain hardening in LYP-225 steel. The ultimate strain was much higher at around 65% for the LYP-225 steel compared to 30-35% for the A36 steel.

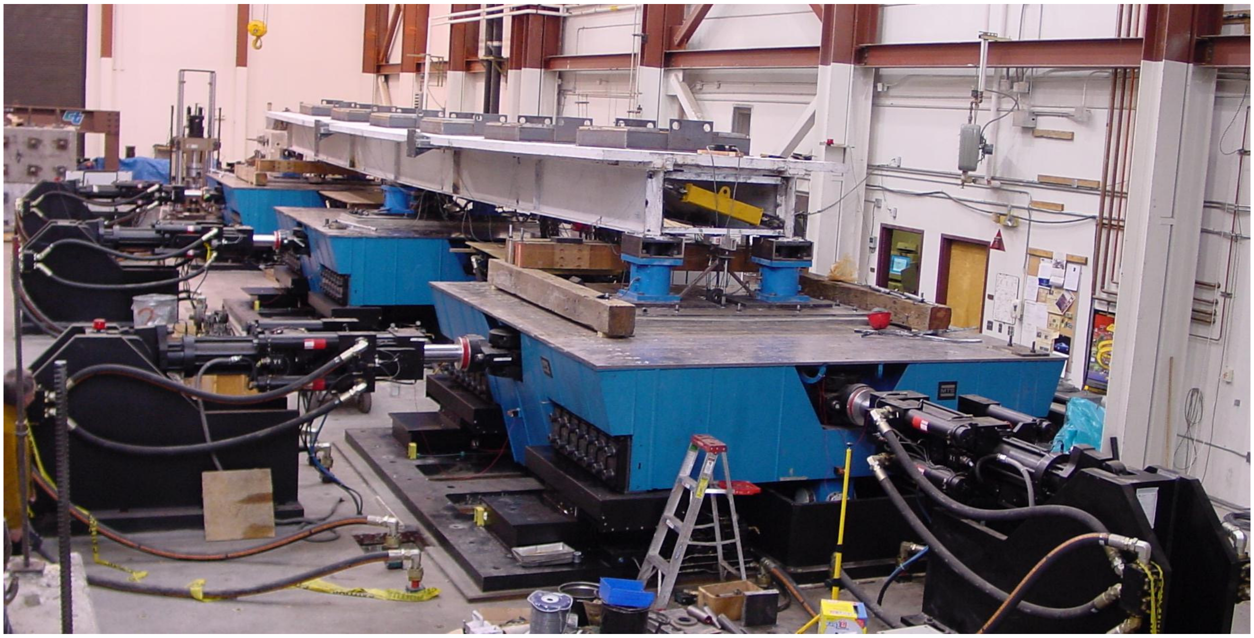

Figure 1. Shake Table Experiment on Bridge Model with Unbonded Braces

Table 1: Properties of LYP-225 Steel from Coupon Tests

Coupon Test #		**#1**	**#2**
Yield Stress	(MPa)	223	235
Ultimate Stress	(MPa)	302	302
Ultimate Elongation	(%)	64	65

AXIAL COMPONENT EXPERIMENTS

Overview

Component experiments were performed on unbonded braces identical to those used in the bridge model in order to characterize the properties of the braces and compare these to the design properties. Of seven braces provided, four were used solely for component experiments, and the remaining three were used in bridge experiments before being tested to failure in the component experiment assembly. Axial component experiments were performed to evaluate overall brace behavior, cumulative displacement capacity of the braces, the effect of different loading histories, and the effect of dynamic loading.

Experimental Setup and Loading

Axial loads were applied to the unbonded braces using an MTS load frame as shown in Figure 2. The overall length of the brace was equal to 968 mm (38 $^{1}/_{8}$ in). The deformable length was calculated to be 518 mm (20 $^{3}/_{8}$ in) between the centres of the transitions from the maximum cruciform to the minimum core sections. The core plate was equal to 25 x 16 mm (1 x $^{5}/_{8}$ in). The first brace was connected to grip plates in the load frame with pin ended connections. This connection was designed to be an ideal pin for rotation in the plane of the cross frame. Out of plane partial fixity was provided using gusset plates on either side of the bearing stiffener as illustrated in Figure 2a. The remaining braces were tested with fixed connections which were designed to be slip-critical based on the serviceability criteria in the AISC LRFD provisions (AISC 1997).

Three of the unbonded braces were instrumented with four strain gauges to measure strains on each side of the plate at each end of the deformable length. The braces were also instrumented with two displacement transducers on either side of the brace to measure displacements across the deformable length, as shown in Figure 2. The displacement was also measured at the head of the actuator to give the total displacement including deformations in the connection regions. The axial force was measured by the actuator load cell.

The loading history for each of the braces differed. Unbonded Brace A was subjected to a modified ATC-24 (ATC 1992) loading history. This history subjected the brace to two cycles at each excursion and was based on the expected force up until yielding then continued based on the displacement at yield. As slippage in the pinned connection was considerable, the history was modified to achieve reasonable displacements in the deformable region. The loading rate for this history was slow.

The loading history for the second brace (Brace B) was based on the loading history in the draft Recommended Provisions for Buckling-Restrained Brace Frames (BRBF) by SEAONC (2003). The loading history is defined by a number of cycles at different levels of displacement ductility. After applying the prescribed cycles of increasing amplitudes each specimen was cycled at a constant amplitude until failure at the maximum displacement amplitude. The displacements were controlled using the total displacements measured in the actuator. The yield displacement used to define the loading history was based on the estimated displacement calculated at a 0.2% offset strain which was equal to 1.63 mm (0.064 in). No slippage was observed before yielding therefore it did not affect the yield displacement. It is important to note that the displacement at 0.2% offset strain was considerably higher than the yield displacement if estimated using the ATC-24 procedure based on the slope at 75% of the yield force. As the BRBF guidelines do not define the way in which the yield displacement is to be estimated, the 0.2% strain method which

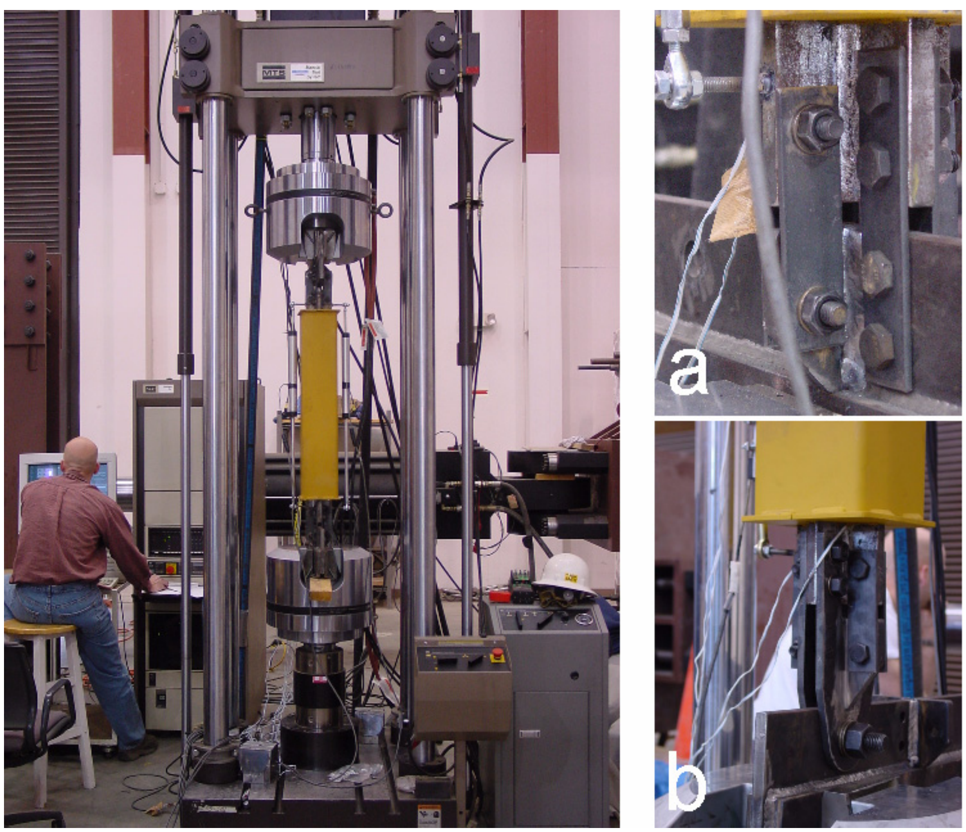

Figure 2. Experimental Setup for Axial Component Experiments on Unbonded Braces with Details a) upper right: Fixed Slip Critical Connection, and b) lower right: Pinned Connection

resulted in the more severe displacements was used. The loading history for Unbonded Brace C was the reverse of the BRBF loading history, and therefore had the maximum amplitude cycles at the beginning of the history, followed by smaller cycles. At the end of the history the brace was subjected to the maximum amplitude cycles to failure. The loading history for Unbonded Brace C was applied at a slow rate. For Unbonded Brace D the same loading history as for Brace C was used, but this time applied dynamically to the brace at a frequency of 2 Hz, to simulate a bridge with a 0.5s effective period.

The remaining braces were used in experiments on the bridge model and had already been subjected to some inelastic deformation but in each case had not fractured. They were subjected to further inelastic deformation in the component experiment assembly. Unbonded Brace E was used in the north end of the bridge model. First one cycle of loading was slowly applied this brace to simulate the maximum loading in the brace during bridge experiments, then the same loading history as that applied to Brace D was applied at a dynamic rate of 2 Hz. Unbonded Brace F was the brace used in the south end of the bridge model. It was subjected to a cycle of loading equal to the maximum cycle measured during the bridge experiments then cycled to failure at a constant relatively low amplitude. The remaining brace, Unbonded Brace G, was the brace in the midspan of the bridge model. It was subjected to one cycle as seen in the bridge model followed by a few large amplitude reversals until failure.

Hysteretic Properties

The force-displacement curves for the first four unbonded braces are shown in Figures 3-6. The hysteresis loops exhibit good energy dissipation characteristics and repeatable behavior. Figure 3 shows that there was a large difference between the displacements measured across the deformable length and the total displacement in Brace A. This was due to slippage, which was expected in the pinned ended connection. The remaining braces were designed to have slip critical connections, with slippage expected to occur, based on the AISC (1997) serviceability criteria for slip critical connections, at a force of 40.1 kip. Figure 4 shows that for Brace B there was little difference between the overall displacement and displacement measured across the deformable length of the brace at low amplitude cycles. The small difference can be attributed to elastic deformations in the connection region. At the large amplitude cycles however the difference between the displacements increased, indicating some slippage, at a maximum force level of -30.6 kips. This was lower than the calculated slippage force. For Brace C no slippage was observed with a maximum force of -31.0 kips. More slippage was observed in the dynamic experiments with Braces D and E and the with the large amplitude displacements of Brace G. Therefore, although the bolts were consistently tightened with a torque wrench, the force at which slippage was expected was unconservative in these experiments, particularly when loads were applied dynamically.

A series of properties used to characterize BRBs were calculated for each brace. The yield force for each unbonded brace was estimated using the force at a 0.2% offset strain. The overstrength factor, ω, describes the maximum measured tensile force measured in the brace divided by the expected yield strength. The compression strength adjustment factor, β, is defined as the maximum compression force divided by the maximum tension force. These values are tabulated in Table 2 for each of the unbonded braces.

Table 2 shows that the measured yield forces were slightly larger than the expected yield forces but within 12% in all cases. The ω factors for forces in tension were generally around 1.35 but were larger in some instances. Unbonded Brace D had the largest overstrength factor and was attributed to strain rate effects which increased the force in the brace, particularly during the first cycle of the loading. This can be observed comparing Figures 5 and 6 which compare the response to the same loading history applied slowly for Unbonded Brace C and dynamically for Brace D. In Brace D the forces in the first cycle were 30% larger than for the comparable cycle in Brace C. This 30% difference due to a higher strain rate is much larger than might be expected. As it was based on just one experiment, further study is needed. After the first cycle the difference between the braces loaded statically and dynamically reduced and stabilized to around 10 - 15%. Although not shown, Brace E had been previously loading in the bridge model and as a result the first cycle of dynamically applied loading was around 10 - 15% larger than the comparable cycle in Brace C. The braces subjected to larger maximum strains, Unbonded Braces A and G, also exhibited larger ω factors.

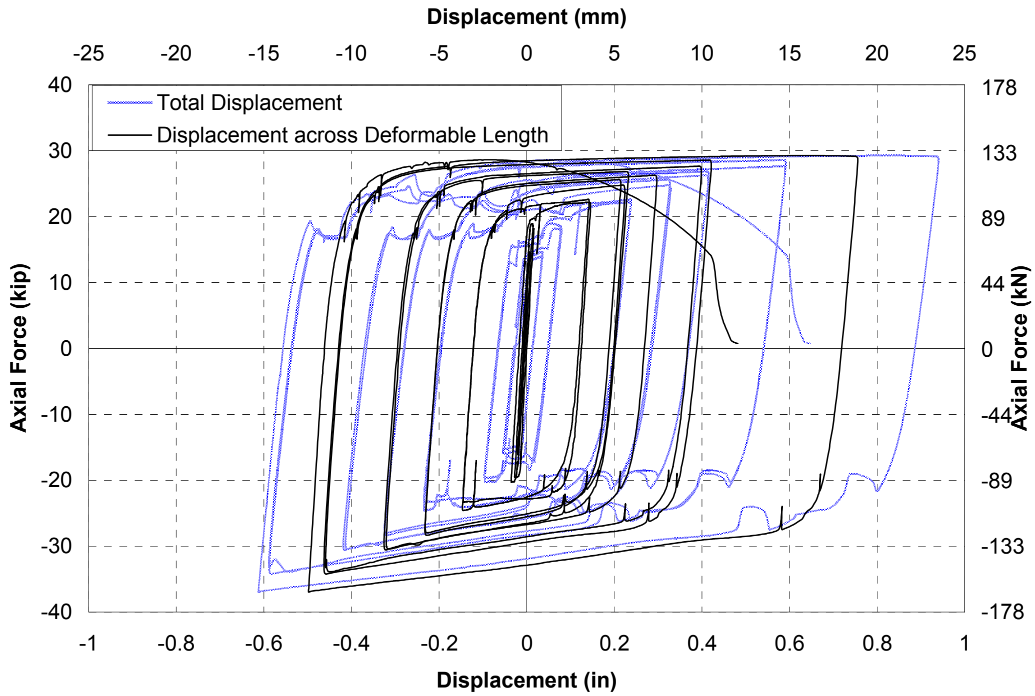

Figure 3. Hysteresis loop for Component Experiment of Unbonded Brace A – Pseudo-static Modified ATC-24 History

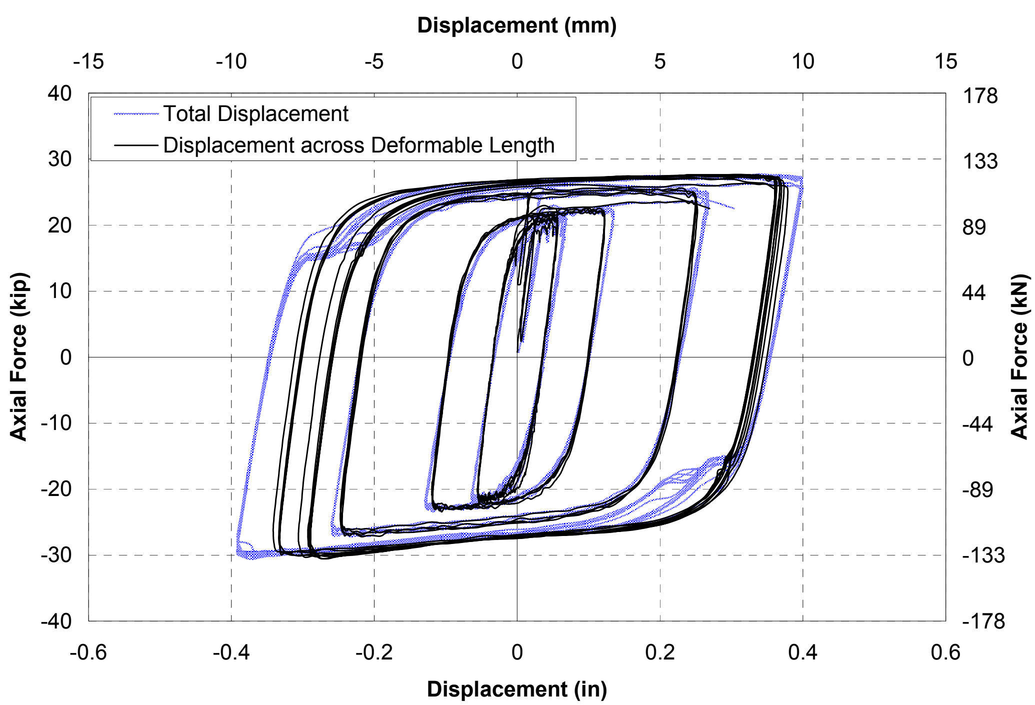

Figure 4. Hysteresis loop for Component Experiment of Unbonded Brace B– Pseudo-static BRBF History

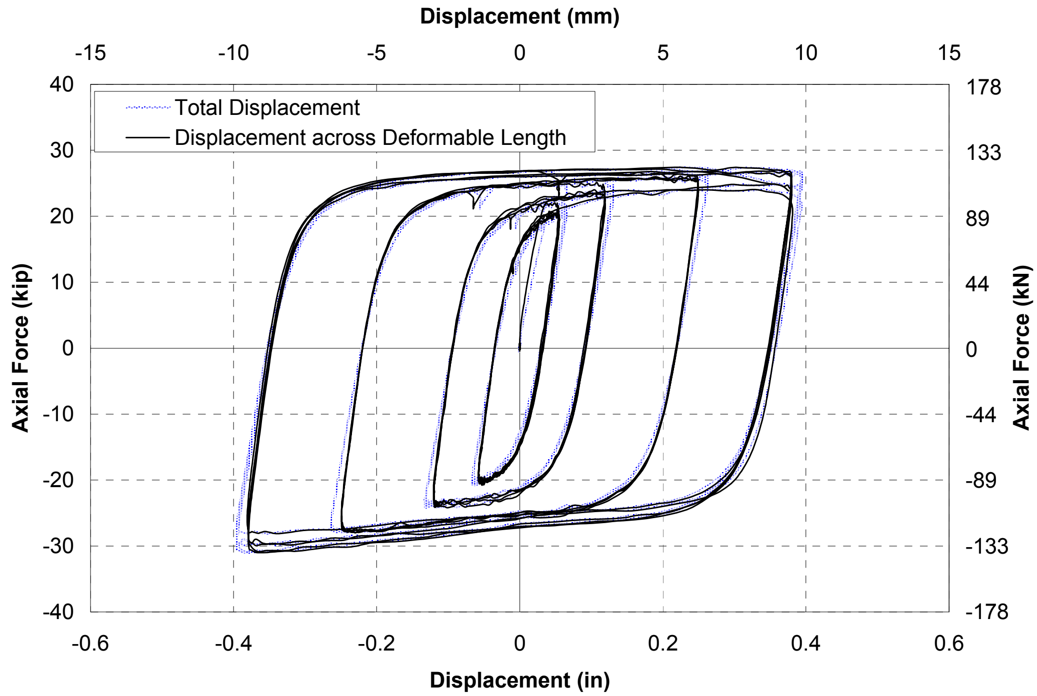

Figure 5. Hysteresis loop for Component Experiment of Unbonded Brace C – Pseudo-static Reverse BRBF History

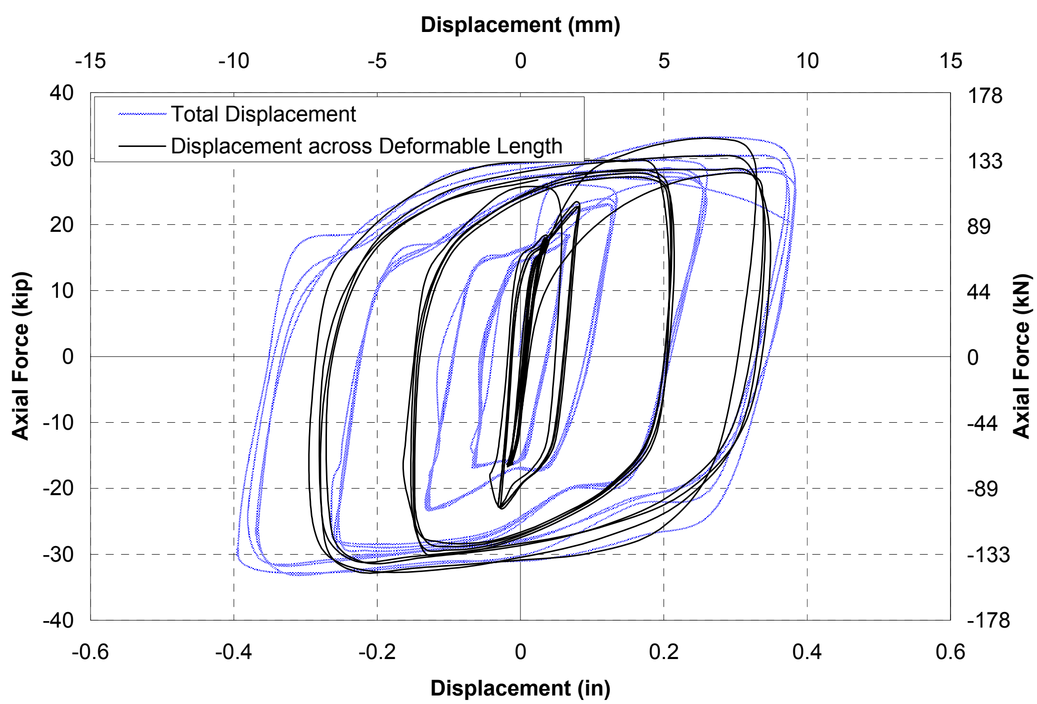

Figure 6. Hysteresis loop for Component Experiment of Unbonded Brace D – Dynamic Reverse BRBF History

Table 2. Summary of Properties for Unbonded Braces

Brace	Loading History	Expected Yield Force (kN)	Measured Yield Force (kN)	Maximum Tension Force (kN)	Maximum Compress. Force (kN)	α	β
A	Modified ATC-24	91	96	130	-164	1.44	1.26
B	Normal Static	91	94	123	-136	1.36	1.11
C	Reversed Static	91	101	122	-138	1.35	1.13
D	Reversed Dynamic	91	102	147	-145	1.62	0.99
E	Bridge and Reversed Dynamic	91	96	140	-167	1.55	1.19
F	Bridge and Constant Static	91	96	124	-135	1.37	1.08
G	Bridge and Constant Static	91	98	134	-154	1.47	1.15

α = maximum measured tension force divided by the expected yield force

β = ratio of maximum compression force to maximum tension force

The compression strength adjustment factor, β, was typically around 1.10 to 1.15. β was largest for the braces with the largest maximum strains in the brace, as shown for Braces A and G, while the reverse is true for smaller strains as in Brace F. This is attributed to increased friction between the core plate and the surrounding material as the axial compression deformations increased, in part due to high mode buckling effects. For Brace D the maximum compression force was actually less than the maximum tension force due to the large observed tension force in the first reversal of the dynamically loaded specimen.

Ultimate and Cumulative Displacement Capacity

The maximum displacements, converted to equivalent strains across the deformable length of the unbonded braces during each of the component experiments, are given in Table 3. For the standard BRBF history the maximum strain was approximately 1.9% although slightly less in cases where slippage occurred. The maximum strain in Brace A was 3.7 %. These strains are consistent with levels from past experiments on unbonded braces (Black et al. 2002).

The cumulative displacement capacity was evaluated for each brace using cumulative plastic ductility. This was calculated using an algorithm which added the displacements in excess of the calculated yield displacement after each reversal of loading. The yield displacement was assumed to be equal to the theoretical yield displacement over the deformable length using the expected yield stress for the LYP-225 material. This resulted in a yield displacement of 0.58 mm (0.0229 in). Note that this estimate of the yield displacement was around 29% less than the average yield displacement measured in the braces using the ATC-24 (ATC 1992) procedure. Furthermore the calculated yield displacement was only approximately 36% of the displacement calculated at a 0.2% offset strain. The difference highlights the importance of clearly defining the method in which the yield displacement is calculated. The theoretical yield displacement was used as it was consistent between braces and with previous experiments, and also computable. The resulting calculated cumulative plastic ductilities for each specimen are given in Table 3.

Comparing the cumulative plastic ductilities and maximum strains in Braces A and B, both with increasing amplitude statically applied loading, showed that a larger maximum strain reduced the cumulative displacement capacity of the braces, as one might expect. Comparing Braces B and C, with the normal and reversed, slowly applied BRBF loading histories, showed that having the large amplitude cycles at the

Table 3. Cumulative Plastic Ductilities for Unbonded Braces

Brace	Loading History	Maximum Applied Strain (%)		Cumulative Plastic Ductility	
		Bridge	Component	Bridge	Component
1	Modified ATC-24	-	3.71	-	479
2	Normal Static	-	1.86	-	875
3	Reversed Static	-	1.87	-	588
4	Reversed Dynamic	-	1.71	-	337
5	Bridge and Reversed Dynamic	1.76	1.77	366	352
6	Bridge and Constant Static	2.22	0.92	205	1109
7	Bridge and Constant Static	2.29	2.51	674	192

beginning of the history reduced the overall cumulative plastic ductility capacity of the brace. The reduction when these two braces were compared was 33%. Furthermore, applying the loading history dynamically as in Brace D further reduced the cumulative plastic capacity. Although Brace E, which was subjected to deformations in the bridge model as well as in the load frame had a similar total cumulative plastic ductility as Brace C. It was difficult to draw definitive conclusions from those braces used in the bridge model as their loading histories were highly variable. Again the range of cumulative plastic ductilities was similar to the range measured in previous experiments (Black et al. 2002).

TRANSVERSE SEISMIC PERFORMANCE OF BRIDGE MODEL WITH UNBONDED BRACES

Braces with Pin Ended Connections

The bridge model, with unbonded braces in the ends (Figure 1), was excited with increasing amplitude motion in the transverse direction. Because the braces were relatively short compared to those typically used in building applications, flexural action in the braces was expected to be potentially significant. While the axial properties of these braces are relatively well understood, the flexural properties are not. Therefore in order to eliminate bending moments in the braces, they were designed with pinned connections to the bearing stiffeners.

The force-displacement curve for the north end of the bridge, due to the north-south component of the 1940 El Centro earthquake scaled by a factor 2.0 is shown in Figure 7. The south end, although not given, shows a similar response. The displacement was measured as the relative transverse displacement between the top and bottom flanges of the girders. The end shear was measured using load cells underneath each bearing. There was a large amount of slippage in the connections between the unbonded brace and the bearing stiffeners. At this level of excitation, and with the slippage in the connections, the inelastic deformation measured across the deformable length of the brace accounts for only a relatively small proportion of the overall deformation in the end region. Nevertheless, the overall hysteretic behavior is stable with reasonable energy dissipation despite the hysteresis loop showing a fair amount of pinching due to slippage.

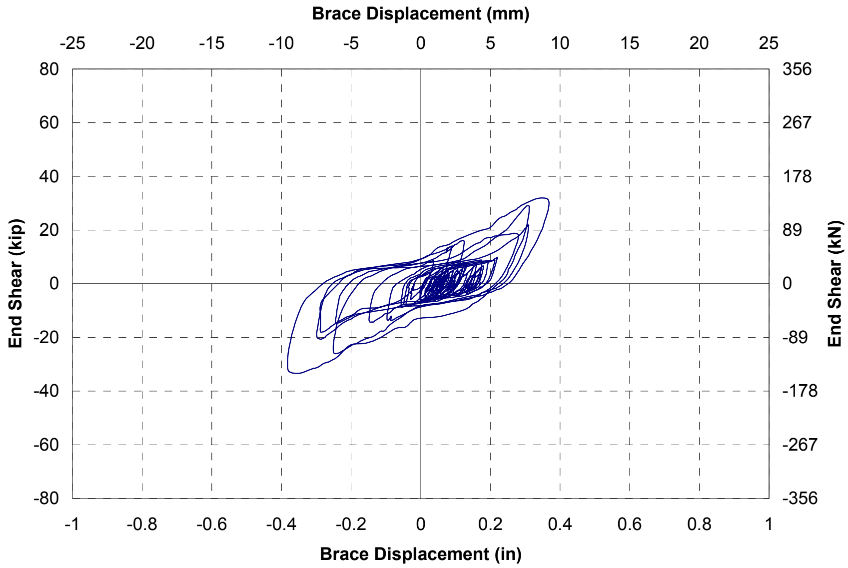

Figure 7. Hysteretic loop for Unbonded Brace with Pinned Connections at North End in Response to 2.0 x 1940 El Centro Earthquake

Braces with Fixed Ended Connections

Due to the large amount of slippage with the pinned connections, the connections were welded to simulate a slip critical fully fixed connection. The resulting hysteresis loop at the north end of the bridge in response to 2.0 x El Centro applied in the transverse direction is shown in Figure 8. This figure shows that the apparent stiffness had increased in the prevention of slippage and the resulting displacements had decreased. The maximum force in the system at this level of excitation increased a small amount. The displacements across the deformable length of the braces also increased, and can account for 85% of the total displacement in the end region. The remaining 15% can be accounted for by the connection regions.

Small hysteresis loops can be observed inside the large hysteresis loops. These can be seen at amplitudes where the unbonded braces remained elastic. The hysteresis loops can be attributed to the top and bottom chords, bearings and other components in the transverse load path which have some hysteretic behavior associated with them.

The disadvantage of the fully fixed connections is shown when the braces were subjected to larger amplitude ground motion. The response to a JMA ground motion in the north-south direction from the 1995 Kobe earthquake is shown in Figure 9. This figure shows that the maximum force is around 2 times the maximum force measured during component experiments. Some of this increase in force is associated with the hysteretic behavior of components in the transverse load path such as bearings, stiffeners, shear studs and top and bottom chords. However, experiments to characterize the effects of these components indicate that the force in the braces was still 50% greater in the bridge model at comparable brace strains. This additional force can be attributed to flexural action in the braces. With the pin connected braces it was expected that the force would be considerably less and the effect of slippage would become less significant in response to the large amplitude Kobe excitation. No experiment was performed with the pin connections at this level of excitation.

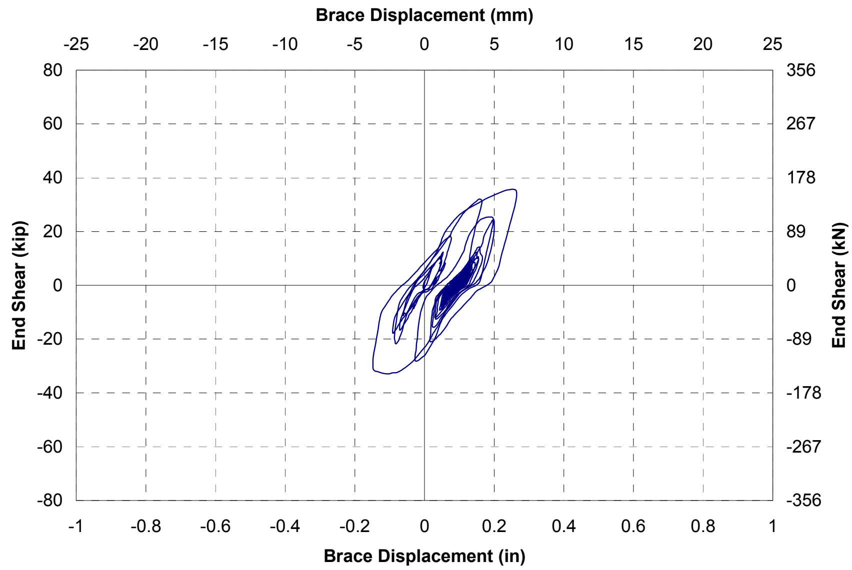

Figure 8. Hysteretic loop for Unbonded Brace with Fixed Connections at North End in Response to 2.0 x 1940 El Centro

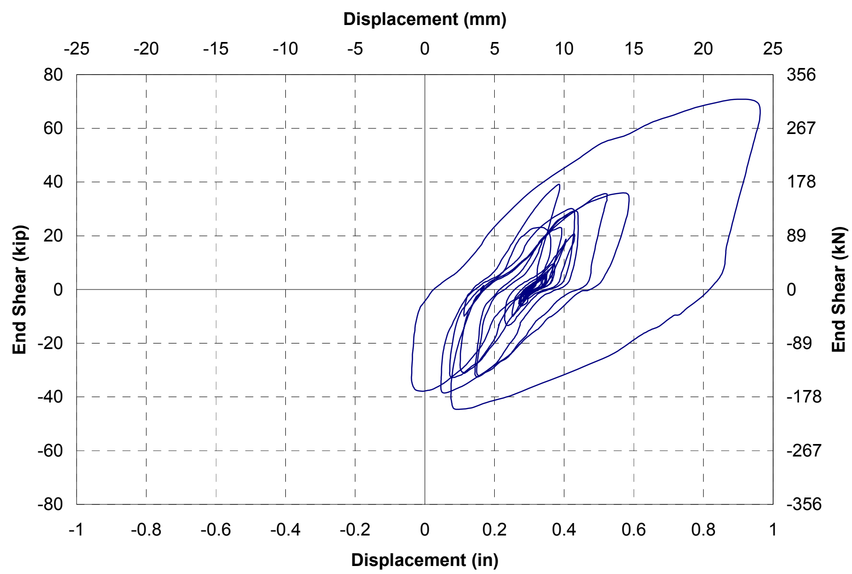

Figure 9. Hysteretic loop for Unbonded Brace with Fixed Connections at North End in Response to the north-south component recorded at the JMA station from the 1995 Kobe earthquake

It is recommended that pinned connections be used with relatively short braces required for use as ductile end cross frames to avoid uncertainty relating to flexure in the braces. In the bridge model and in component experiments no loss in performance was observed due to an increased potential for buckling in the braces using the pin ended connections compared to fixed connections. Although simple single bolt pinned connections were used in the bridge model, two bolt connections should be used as standard practice in bridge design for better high cycle fatigue performance.

Comparisons and Limitations

The unbonded braces exhibited similar hysteretic behavior as previous systems used in experiments on ductile end cross frames. The maximum drift in the cross frames in response to Kobe was equal to 4%, which was larger than the ultimate drifts in the previously used ductile diaphragms which were estimated at 3.0%, 3.0% and 3.5% for SPS, EBF and TADAS systems respectively (Zahrai and Bruneau 1999b). At 4% drift the braces had not failed. Based on geometry of the system, and an ultimate strain of 3.7% as measured during the component experiment on Brace A, the expected drift at failure of the brace was expected to be around 5.6%. In a full scale bridge it should be possible to increase maximum drift further with more efficient connections and a larger deformable brace length. Therefore the unbonded braces have an advantage over the other systems with a larger displacement capacity.

As well as the unbonded braces, the response of the bridge model was calculated with ductile end X-braces and elastic cross frames, up to an amplitude of 2.0 x El Centro applied in the transverse direction. The resulting maximum forces and displacements in the ends of the bridge model for the different configurations, averaged between the two ends of the bridge, in response to 2.0 x El Centro, are given in Table 3. The unbonded brace response is given for the pin ended braces. Results are normalized to the maximum force and end displacement in the bridge model with elastically responding cross frames.

Table 3. Comparisons of Bridge Model Response to 2.0 x El Centro with Different End Cross Frame Configurations

Cross Frame Configuration	**Max. Shear / Elastic Shear**	**Max. Drift / Elastic Drift**
"Heavy" X-Braces	1.00	1.00
"Light" X-Braces	0.61	7.32
Unbonded Braces	0.70	4.06

This table shows that the unbonded braces had significantly smaller displacements than the X-braces even though the forces levels were similar. Thus the unbonded braces proved to more effective than concentric X-braces even though slippage was observed in the connections.

The table also demonstrates the effect of the relatively flexible two girder bridge superstructure. The bridge model had only two girders and a relatively low transverse stiffness compared to a typical bridge with more girder lines. This meant that in order to obtain a relatively small decrease in the base shear of the structure, a relatively large increase in the end displacements was necessary. This is because the natural period of the structure was dominated not only by the effective stiffness of the cross frames but also overall stiffness of the superstructure. The same would be true if a bridge had a flexible substructure. Therefore a steel girder bridge with a superstructure that is flexurally almost rigid about its vertical axis and also has a relatively rigid substructure is likely to be the best candidate for use of ductile end cross frames. For this type of bridge the elastic period will be relatively short and the seismic demand will be at its maximum for a typical earthquake excitation. Ductile end cross frames should lengthen the period and increase damping in the structure sufficiently to allow a notable reduction in base shear. In this respect the bridge model was not the ideal bridge for the application of ductile end cross frames.

Studies were also performed on the bridge model with isolation bearings although the results are not presented here. It was possible to achieve larger displacements and therefore a larger period shift and reduction in seismic demand using seismic isolation. Therefore in general seismic isolation should also be considered as an alternative to using ductile end cross frames. However if modification of the response is only desired in the transverse direction, or there is some other reason for not using seismic isolation, then buckling restrained braces in the end cross frame are an effective system for reducing seismic demand in a steel plate girder bridge.

CONCLUSIONS AND RECOMMENDATIONS

Component experiments on a series of buckling restrained unbonded braces for use as ductile end cross frames showed that these braces had stable and repeatable ductile behavior, although reversed loading history and strain rate reduced the cumulative plastic capacity of the braces. Dynamically applied loads resulted in larger forces than measured pseudo-statically with the difference particularly noticeable in the first reversal.

Unbonded braces used as ductile end cross frames in a straight steel girder bridge model were able to reduce the shear demand in the bridge. While fixed ended connections had smaller displacements in the end cross frames than the pin ended connections, they resulted in considerable overstrength attributed to flexure in the braces. Pinned connections resulted in increased displacements due to slippage particularly noticeable at lower amplitude excitations, however they are recommended to prevent flexural actions in the braces. The unbonded braces resulted in much smaller displacements than corresponding X-braces. They had similar hysteretic behavior but a larger displacement capacity than the SPS, EBF and TADAS systems. The effect of a relatively flexible superstructure in the bridge model was illustrated with larger displacements than the corresponding reduction in base shear. Ductile end cross frames are believed to be most effective when both the superstructure and substructure are relatively rigid. Seismic isolation should still be considered as an alternative to using ductile end cross frames.

ACKNOWLEDGEMENTS

The authors would like to acknowledge and thank Isao Kimura and Nippon Steel Corporation for the donation of the unbonded braces towards this study. Funding for the project from CALTRANS and FHWA is gratefully appreciated.

REFERENCES

American Association of State Highway and Transportation Officials (AASHTO), 2000. *Guide Specifications for Seismic Isolation Design, (Second Edition including Interim Revisions)*. Washington, DC: AASHTO.

American Institute of Steel Construction (AISC), 1997. *Manual of Steel Construction - Load Factor and Resistance Design, 2nd Edition*. Chicago, IL: AISC.

Applied Technology Council (ATC), 1992. *ATC 24 - Guidelines for Cyclic Seismic Testing of Components of Steel Structures.* Redwood City, CA: ATC.

Astaneh-Asl A., 1996. *Notes on the Cyclic Behavior and Design of Steel Bridges - Volume I - Response Modification Factor Based Design.* Washington DC: American Iron and Steel Institute.

Astaneh-Asl A., Bolt B., McMullin K.M., Donikian R.R., Modjtahedi D., Cho S., 1994. “Seismic Performance of Steel Bridges during the 1994 Northridge Earthquake.” Technical Report, UCB/CE-STEEL-94/01, Department of Civil Engineering, University of California at Berkeley, CA.

Black C., Makris N., Aiken I., 2002. “Component Testing, Stability Analysis and Characterization of Buckling Restrained Unbonded Braces™.” Technical Report, PEER Report 2002/08, Berkeley, CA.

Bruneau M, Wilson J.W., Tremblay R., 1996. “Performance of Steel Bridges during the 1995 Hyogoken-Nambu (Kobe, Japan) Earthquake.” *Canadian J. of Civil Engrg.,* 23(3): 678-713.

Carden, L.P., Itani A.M., Buckle I.G., 2002. “Composite Action in Steel Girder Bridge Superstructures subjected to Transverse Earthquake Loading.” *Transportation Research Record*, 1814: 245-252.

Carden L.P., Itani A.M., Buckle I.G., 2003. “An Experimental Study into the Distribution of Earthquake Forces in Steel Plate Girder Bridges.” Proceedings of the *Pacific Conference on Earthquake Engineering,* (CD Rom). Christchurch, New Zealand. February 14-16.

Itani A.M., Reno M.L., 1995. “Seismic Design of Modern Steel Highway Connectors.” Proceedings of the *ASCE Structure Congress XIII*, Boston, MA. v2 1528-1531. April 2-5.

Nippon Steel Corporation, 2002. “Seismic Behavior of Typical Steel (Unbonded Brace) - Tensil Test Report for Steel Material of LYP-225.” Report, Nippon Steel Corporation, Japan.

Shinozuka M.(ed), Ballantyne D., Borcherdt R., Buckle I., O’Rourke T., Schiff A., 1995. “The Hanshin-Awaji Earthquake of January 17, 1995 Performance of Lifelines.” Technical Report NCEER-95-0015, National Centre for Earthquake Engineering Research, Buffalo, NY.

Structural Engineering Association of Northern California (SEAoNC) BRBF ad-hoc Committee, 2003. “Recommended Provisions for Buckling-Restrained Brace Frames.” Sacramento, CA: SEAOC.

Zahrai S.M., Bruneau M., 1999a. “Ductile End-Diaphragms for Seismic Retrofit of Slab-on-Girder Steel Bridges.” *J. of Struct. Engrg.*, 125(1): 71-80.

Zahrai S.M., Bruneau M., 1999b. “Cyclic Testing of Ductile End-Diaphragms for Slab-on-Girder Steel Bridges.” *J. of Struct. Engrg.*, 125(9): 987-996.

Structural Seismic Analysis of Nanning Bridge

Zhi-qiang Wang[1]

ABSTRACT

Nanning Bridge has its own particularity in seismic analysis. In order to improve the seismic performance of the vulnerable parts of this Bridge, initial research of the Bridge's seismic response was carried out for this project, and for three design methods of expansion joints, different seismic response of the bridge's main span were discussed in this article. It's the conclusion that two additional expansion joints should be set up between the main bridge and the approach bridge so as to separate the seismic response of main bridge from that of the approach bridge in longitudinal direction, and finally reduce the longitudinal seismic response of the main bridge. This conclusion can be referred in the following design of the Bridge.

[1]DEPARTMENT OF BRIDGE ENGINEERING , TONGJI UNIVERSITY, SHANGHAI 200092, PRC

INTRODUCTION

Nanning Bridge locates at the west side of QingxiuShan scene area, southeast of Naning City, crosses the Yong River and connects the QingxiuShan scene area and Panlong new town. The Bridge, intersecting the coastwise road, is one of the door to enter Naning city and urban circular expressway,whose construction plays a great role in connecting two banks of Yong River and promoting the development of the new Town. Fig 1 shows its geographic location.

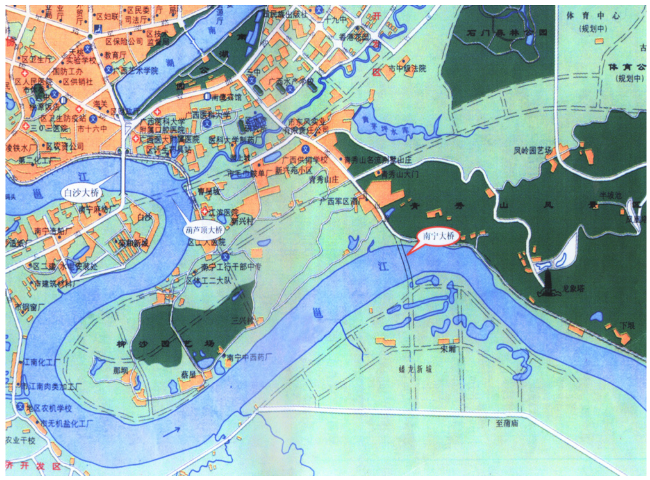

Figure 1 The geographic situation of Naning Bridge

SEISMIC SAFETY EVALUATION FOR THE CONSTRUCTION SITE

According to the <report on determination of seismic design parameters of Construction Site of Nanning Bridge >, piers of Nanning Bridge are located at the Site Category II, medium sand layer of which will not be liquefied excited by earthquake leveled 7 degree. Because of the different site conditions of south bank and north bank, their site response spectrum are also different, the horizontal acceleration response spectrum at free surface are shown in Figure 2.

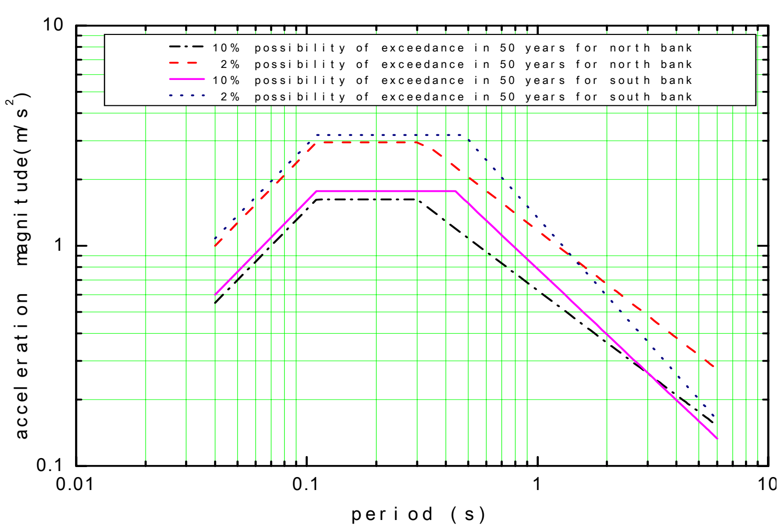

Figure 2 Acceleration response spectrum of different exceeding possibility

THE GENERAL LAYOUT OF NANNIG BRIDGE

Spans of Nannning Bridge are arranged as 3 × 46+50+300.502+50+4 × 46m, totally 732.502m, of which the main span is 308.502m. The main bridge and approach bridge are all in the horizontal curve with 1500m in diameter, no super-elevation is designed, but 2% bilateral transverse slope is placed. Single fold line is use for the consideration of fabrication of steel box girder. The elevation of main line is in the concave vertical curve with 8130.205m in diameter, convex curve with 9000m in diameter and strait grade line successively, the maximum longitudinal slope if which is 2%. The main bridge is in the convex curve with 9000m in diameter.

The main bridge is an unsymmetrical rib arch with the span of 300m, consists of two inclined steel-boxed arch ribs, curved steel boxed girder, inclined suspenders, tied bar and the platform between two ribs.

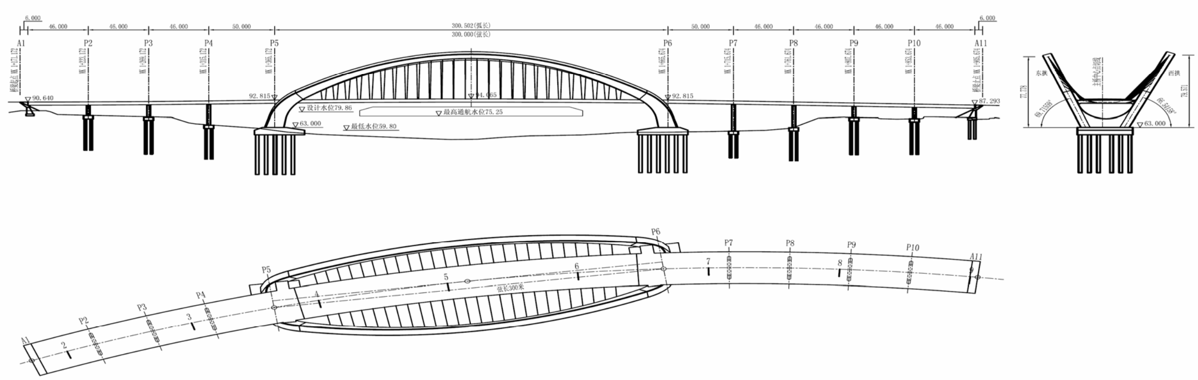

Figure 3 General Layout of Nanning Bridge

The box girder of main span is separated form the platform between two ribs, which is supported by the corbel extended form the platform. There are totally 4 expansion joints located on the abutments and corbels.

The Fortification Criteria and Performance Objective

The research on bridge seismic performance must have a clear performance objective so as to make a rational seismic checking computation of the structure.

Table 1 Fortification Criteria and Performance Objective of Nanning Bridge

Fortification criteria		Performance objective of main bridge	Performance objective of the approach
Criteria I	10% exceeding possibility in 50 years(i.e. 475 years' Return period)	Arch ribs, main girder and the platform between ribs and the pile foundation are elastic, $\sigma_a \le [\sigma_a]$, bearings are serviceable	Concrete of piers are allowed to go into plastic stage, bearing are serviceable, pile foundation is elastic.
Criteria II	2% exceeding possibility in 50 years(i.e. 2450 years' Return period)	Arch ribs and the platform are should meet the strength requirement of limit status, shear failure is allowed for bearings	Sufficient ductility should required for piers to prevent from collapse, shear failure is allowed for bearings

Modeling of Structural dynamic analysis FE model

According to the above characteristics of Nanning Bridge, the three-dimensional structure model for seismic analysis should include both the main bridge and the approach bridge so as to obtain the correct seismic response.

The main girder of main main bridge,arch ribs, the main girder of approach bridge and piers are simulated with beam elements. The bridge deck is made up of a single steel box girder with totally 35m in width, 3.5m in height and with 2% bilateral slope on the surface, as shown in Figure 4.

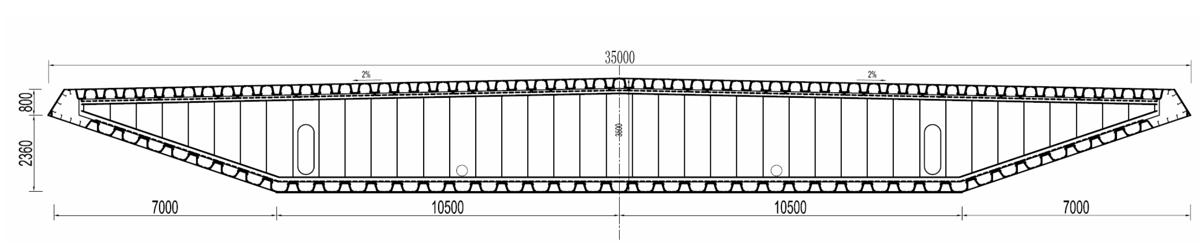

Figure 4. Steel box section of girder for main bridge

The arch ribs east side and west side consist of steel box segments and concrete ones, they all incline outside the vertical plane. The single box single cell section with constant width of 7.4m but variable height from 5.6 in the middle up to 10m at the arch spring is used for steel box segments as shown in Figure 5.

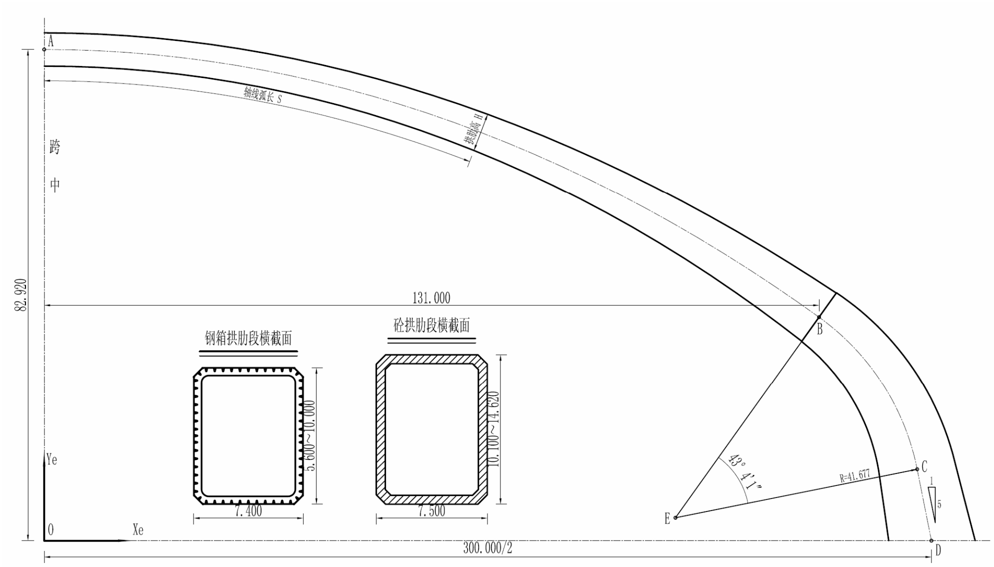

Figure 5. Elevation of arch rib

The approach spans are continuous pre-stressed concrete box beam, consisting of 3×46+50m for north approach and 50+4×46m for south approach. The approach spans are connected with the main span at the platform of between two ribs. Figure 6 shows its section.

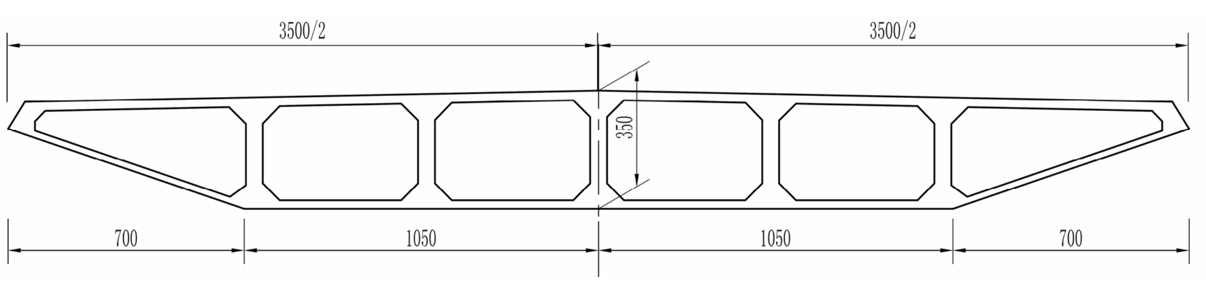

Figure 6. Steel box section of girder for approach bridge

The pier of approach bridge is Y shape solid pier, and modified with arc in the middle to correspond with the arch abutment of main bridge. The pier is 2.5m thick,15.0m wide for the lower parts and 25.77m wide at the top. Among all the piers, P7 is the highest with 29.5m, and P2 is the lowest with 11.5m.

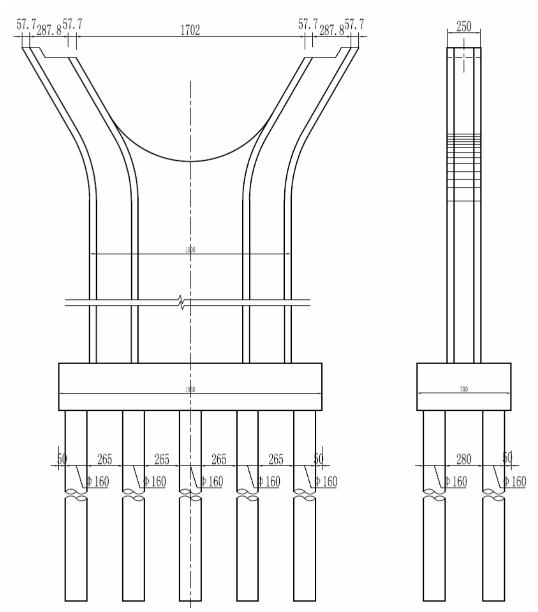

Figure 7 Section of piers for approach bridge

The horizontal tied bar and suspenders are simulated with truss elements but including the effect of geometric stiffness of dead load. There are 16 straight tied bars, 16 curved tied bars and 52 groups suspenders in the whole bridge. Layout of horizontal tied bars and suspenders are shown in Figure 8 and 9.

The pile foundation is simulated with soil spring, the cross wall between two ribs are simulated with shell element and the corbels extend from the platform and the expansion joints are simulated through master-slave relationship. The platform and cross wall are shown in figure 10 and figure 11, respectively.

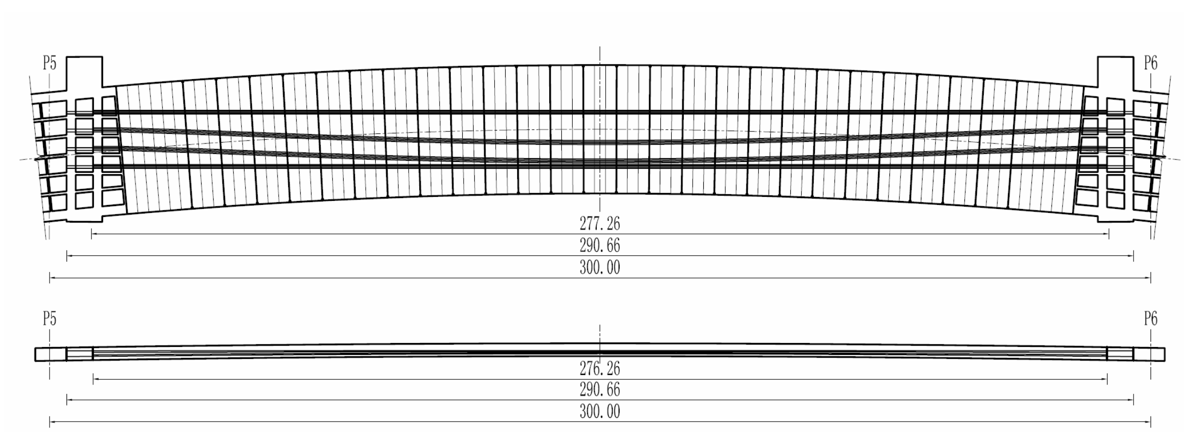

Figure 8 Lay out of horizontal tied bars

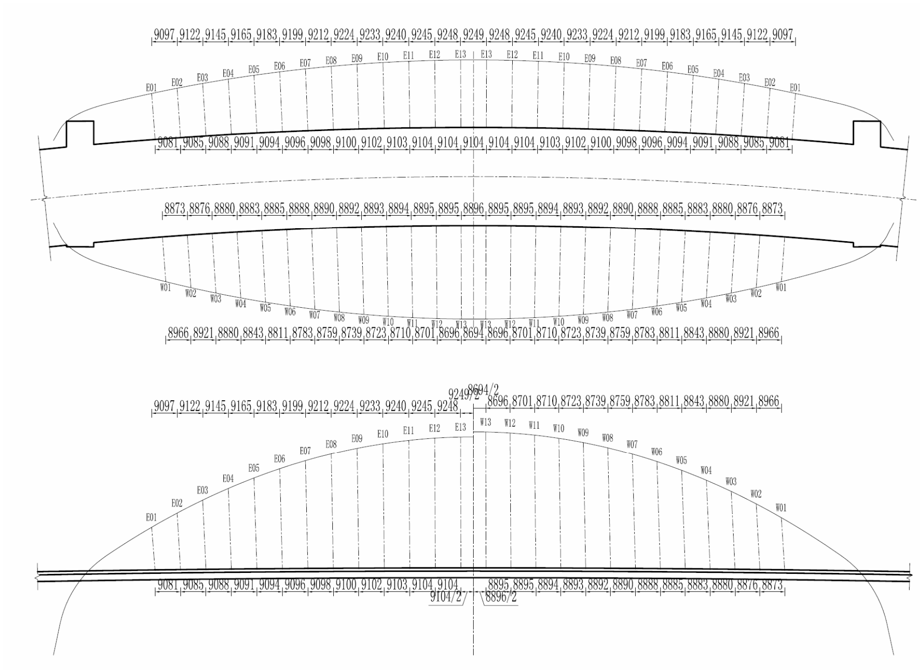

Figure 9 Lay out of suspenders

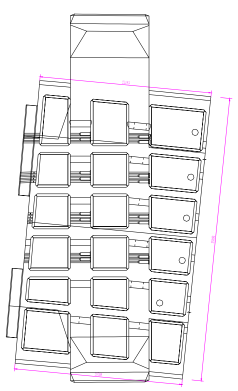

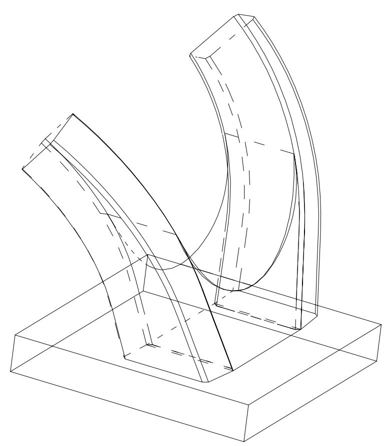

Figure 10 Sketch map for platform   Figure 11 Sketch map for cross wall

According to the above key parameters of structural components, the FE model for dynamic analysis is shown in Figure 12.

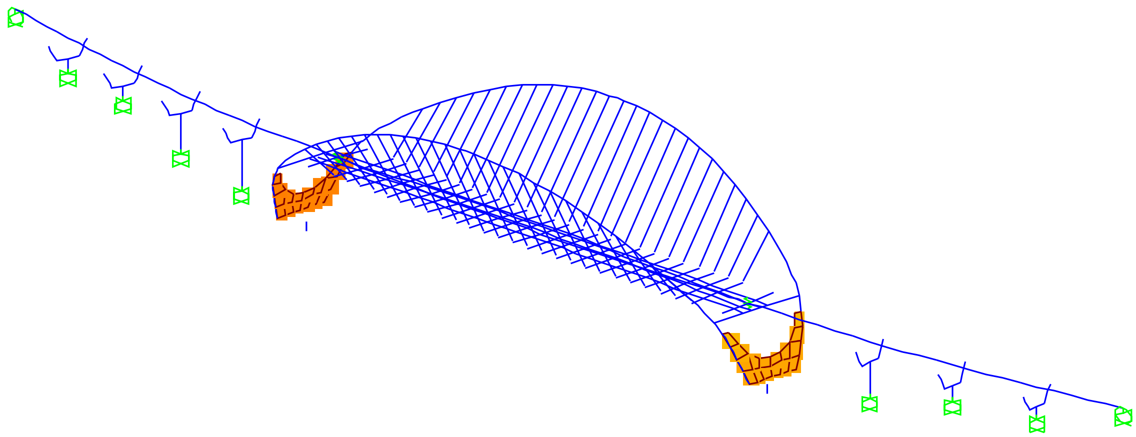

Figure 12 FE model for dynamic analysis

Dynamic characteristics of Stucture

Dynamic analysis of Nanning Bridge is performed to get the structural dynamic response using the FE model. Subspace iteration method is used to solve the Eigen equation in the dynamic characteristics analysis.

Table 2 Dynamic Characteristics of Structure

Mode	Period	Frequency	Mode shape
1	11.160393	0.089603	Longitudinal floating
2	2.113911	0.47306	Arch ribs lateral vibrating in the same direction
3	1.955561	0.51136	Arch ribs lateral vibrating in opposite direction
4	1.193861	0.83762	Arch, beam 1st unsymmetrical vertical vibrating
5	1.072111	0.93274	Arch, beam 1st symmetrical vertical vibrating
6	1.010742	0.98937	Main beam tensional vibrating
7	0.925963	1.0800	Main beam, arch rib vertical vibrating, coupled lateral vibrating for arch rib
8	0.867035	1.1534	Arch rib lateral vibrating, coupled slightly vertical vibrating
9	0.727428	1.3747	main girder torsional vibrating, arch rib vertical vibrating
10	0.709269	1.4099	Main girder torsional vibrating, arch rib vertical vibrating
11	0.692837	1.4433	Arch, girder 2nd systematical vertical vibrating
12	0.667236	1.4987	—

13	0.663603	1.5069	the tallest pier of South approach bridge longitudinal vibrating
14	0.618065	1.6180	—
15	0.609391	1.6410	—
16	0.547535	1.8264	—
17	0.530869	1.8837	—
18	0.521445	1.9177	—
19	0.514364	1.9441	—
20	0.474281	2.1085	—

Structural response spectrum Analysis

Based on the dynamic characteristics of Nanning Bridge obtained, response spectrum method is used to analyze the structural seismic response with 2% possibility of exceedance in 50 years. The input excitation includes longitudinal plus vertical, transverse plus vertical. RITZ method is used to compute the modes of structure, and orders up to 300th are taken into consideration. The results are shown in Table 3 and Figure 13-18.

Table 3 Key points Displacements (units: mm)

Location	2% possibility of exceedance in 50 years						2% possibility of exceedance in 50 years					
	X+Z			Y+Z			X+Z			Y+Z		
	Ux	Uy	Uz	Ux	Uy	Uz	Ux	Uy	Uz	Ux	Uy	Uz
vault of east arch	20	4	7	0.0	66	45	34	7	13	1	102	77
vault of west arch	22	4	8	0.0	82	48	38	7	15	1	123	77

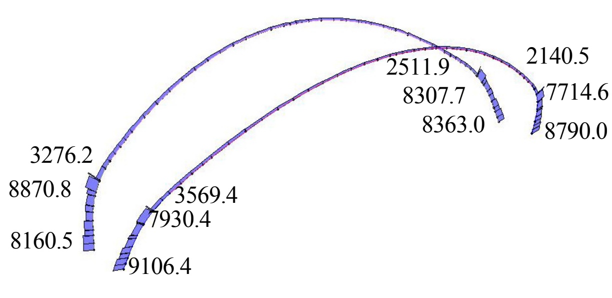

Figure 13 Dynamic axial force of arch rib under longitudinal excitation

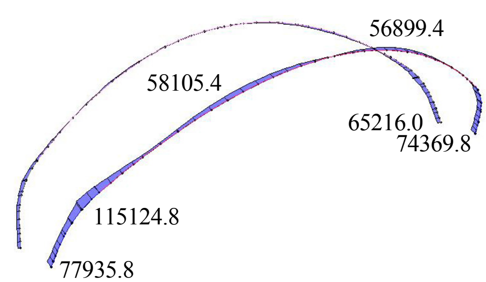

Figure 14 Dynamic bending moment of arch rib under longitudinal excitationM22

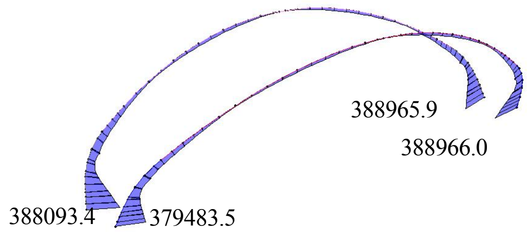

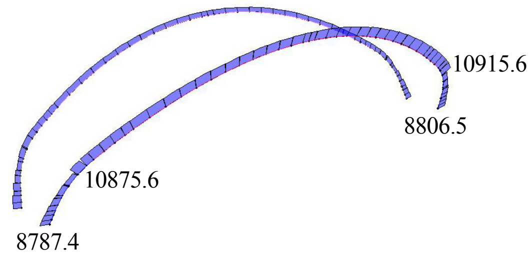

Figure 15 Dynamic bending moment of arch rib under longitudinal excitationM33

Figure 16 Dynamic axial force of arch rib under transverse excitation

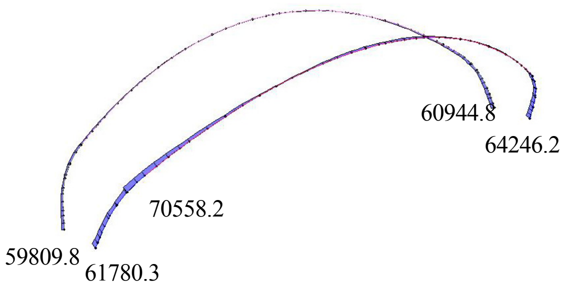

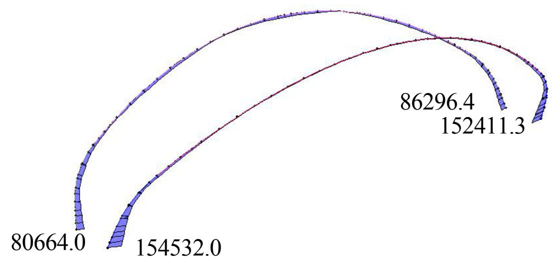

Figure 17 Dynamic bending moment of arch rib under transverse excitationM22

Figure 18 Dynamic bending moment of arch rib under transverse excitationM33

Seen from the results of response spectrum analysis, the vulnerable parts of this Bridge are shown in Figure 19.

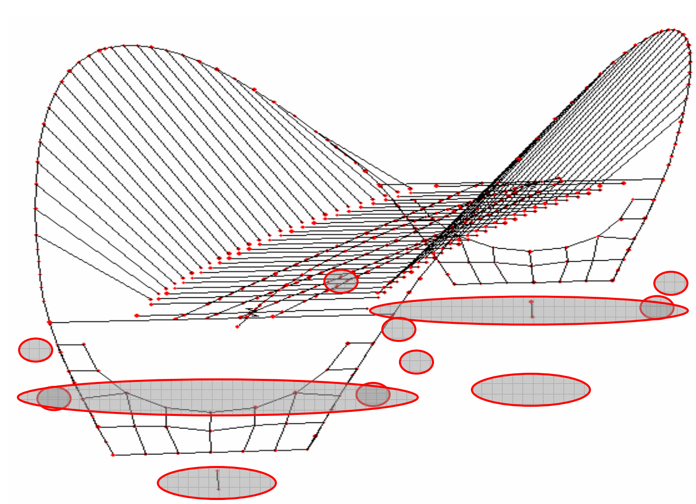

Figure 19 Vulnerable parts of Naning Bridge under earthquake excitaion

In order to improve the seismic performance of the vulnerable parts of the bridge, several methods are promoted from the viewpoint of reducing the structural earthquake requirement. One of them is to change the expansion joint locations and numbers. The original design includes 4 expansion joints. 3 schemes of expansion joints are compared to investigate the seismic response of the main bridge. As a result, 2 additional expansion joints are set up between the main bridge and the approach bridge so as to separate the seismic response of main bridge from that of the approach bridge in longitudinal direction, and finally reduce the longitudinal seismic response of the main bridge. The results are shown in Figure 21-26. (The numbers in the X axis form 1 up to 20 represent the steel spring of east arch, the concrete spring of east arch, the arch rib over platform, the arch rib under platform, arch rib at cross wall, the steel spring of west arch, the concrete spring of west arch, the arch rib over platform, the arch rib under platform, arch rib at cross wall, respectively.)

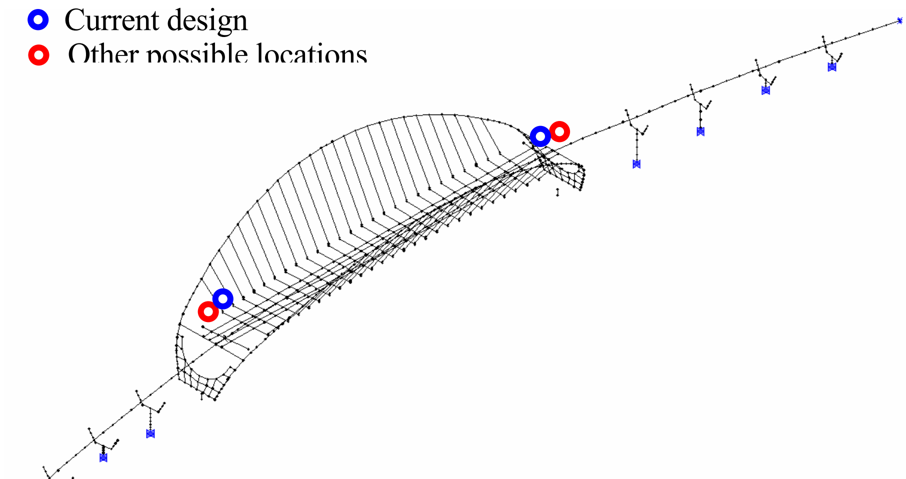

Figure 20 Locations of expansion

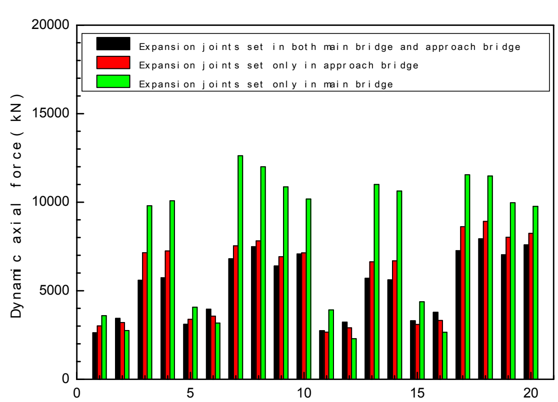

Figure 21 Comparation of dynamic axial force

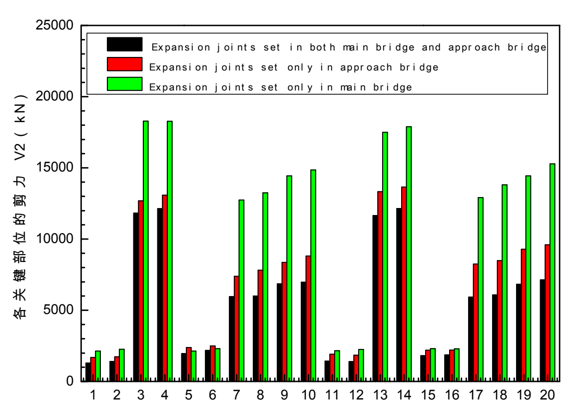

Figure 22 Comparation of dynamic shear

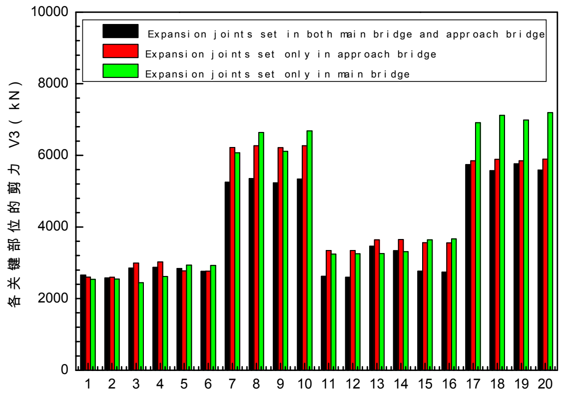

Figure 23 Comparation of dynamic shear

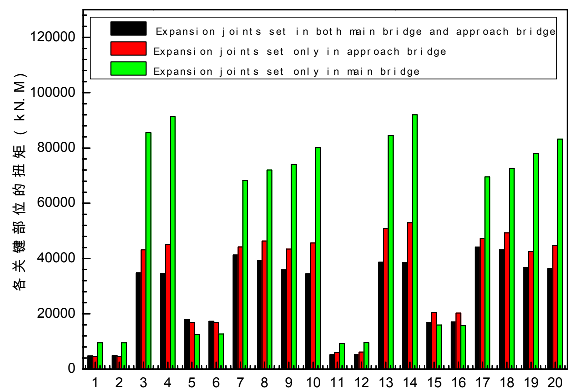

Figure 24 Comparation of dynamic torsion

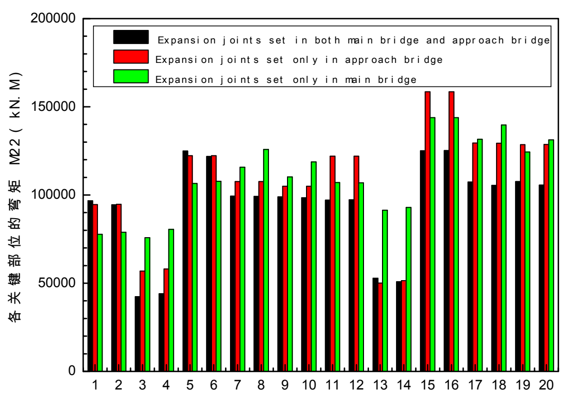

Figure 25 Comparation of dynamic moment(M22)

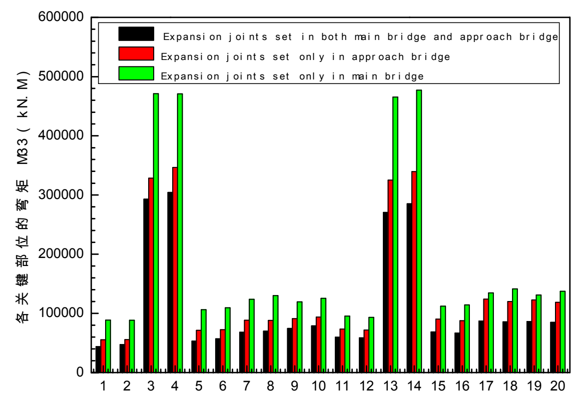

Figure 26 Comparation of dynamic moment(M33)

Seen from the above figures, one can see that among the 3 schemes of expansion joint, the one that uses expansion joint only in the main bridge gives the maximum response at key components, and the one that uses expansion joints both in the main bridge and the approach bridge gives the minimum response at key components.

In addition, due to the expansion joints set up at the two ends of the main girder, the 1st period of the main bridge is the main girder longitudinal floating, with quite long period, which induces the considerable large displacements of expansion joints, therefore, damping devices are suggested to use herein to control the large displacements.

Since Nanning bridge is still in the preliminary design stage, its seismic performance has just started, the further research includes pile-soil interaction, incompatible excitation and the further investigation for the key components such as the platform between two ribs, etc.

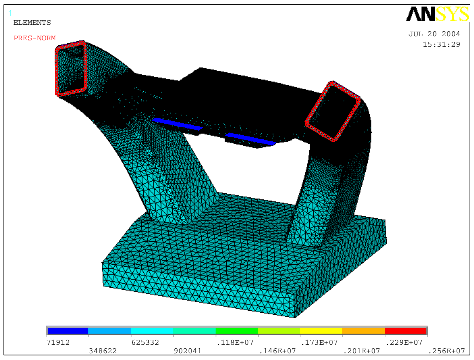
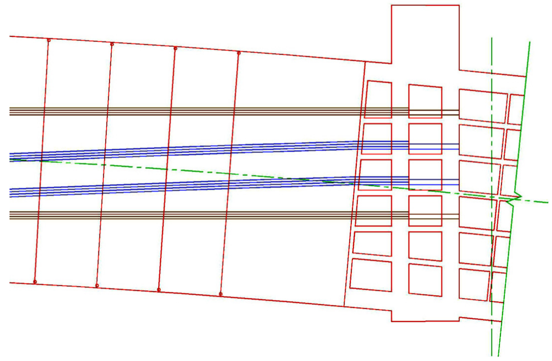

Summary and Suggestion

The preliminary seismic research only fouses on the 2 possibilites(10% exceeding possibilities and 2% exceeding possibilities in 50years).

The results of response spectrum analysis based on the dynamic characteristics show that the approach bridge has heavy effect on the longitudinal responses of the main bridge, However, the longitudinal seismic performance of the main bridge could be improved by changing the locations of expansion joints and using the dampers to reduce its relative displacements.

REFERENCE

Li-chu Fan,Shi-di Hu and Ai-jun Ye. 2001. "Seismic Design For Long Span Bridge," People's Communication Publishing House (in Chinese)

Li-chu Fan.1997. "Seismic Design Of Highway Bridge",Huajie International Publishing Co. limited

On Modeling of Nonlinear Responses of Seismic Isolation Bridge Bearings

George C. Lee[1] and Zach Liang[2]
Multidisciplinary Center for Earthquake Engineering Research
University at Buffalo, Buffalo, NY 14260 USA

ABSTRACT

Seismic isolation for highway bridges employs various bearings, most of which possess nonlinear lateral stiffness. The nonlinear behavior may be approximated by using a model of a bi-linear parallelogram. For design purposes the slope of the diagonal of the parallelogram has been used as the effective lateral stiffness of the bearings (AASHTO "Guide Specification for Seismic Isolation Design," 2000). The linearization enables the designer to obtain the "effective period" for isolation design.

In this paper, a statistical study on the model of the bi-linear parallelogram is carried out to determine the effect of the shape of the parallelogram on the accuracy of isolation by using the AASHTO approach. Theoretical formulation is made and numerical results are obtained. For bearing with "fat" hysteretic loops (lateral force vs. lateral displacement relationships) the error in isolation design can be very large.

Analyses were carried out on the lateral force and the bearing displacement by using a general bi-linear hysteretic model. Numerical results show quantitatively the underestimation of the peak values of acceleration and displacement by using the linearized approach.

Following closely the approach used in the current AASHTO guidelines for isolation bearing design (i.e. to obtain an "effective period" for a nonlinear bearing) a set of expressions for estimating the "effective stiffness" and other properties of the bearings are formulated. They may be used to improve the AASHTO design for bearings with large characteristic strength and with large damping.

While results presented herewith may be used to check the bridge bearing design by using the current AASHTO guidelines, the fundamental purpose of this FHWA sponsored research program is intend to pursue principles and guidelines for the next generation of bridge isolation systems including new and innovative devices and approaches. This paper addresses one of the issues on modeling of nonlinear bearing responses.

---

[1] George C. Lee, Multidisciplinary Center for Earthquake Engineering Research, University at Buffalo, 429 Bell Hall, Buffalo, NY 14260, USA, 716-645-2039, 716-645-3940 Fax, gclee@mceermail.buffalo.edu
[2] Zach Liang, Multidisciplinary Center for Earthquake Engineering Research, University at Buffalo, Ketter Hall, Buffalo, NYU 14260, USA, 716-645-2114 Ext. 2432, 716-645-3940 Fax, zliang@acsu.buffalo.edu

THE LINEARIZED APPROACH

Seismic design of structure in general and bridge isolation design in particular is often carried out by using a simplified approach based on design response spectra, or by time-history analysis. Such an approach has served the structural engineering profession well over several decades. It is well accepted that the maximum value of structural responses under a seismic excitation cannot be predicted exactly, although the input is considered to have a bound. However, such maximum values are needed for aseismic design. Historically, based on statistical surveys, the design response spectra are used to provide the needed quantities, and this method has been adopted for the isolation design. The response spectra are based on linear systems but practically speaking, most types of isolation bearings are nonlinear. Thus, a linearization process was introduced and widely used. In this paper, we discuss the nonlinear responses of seismic isolation bearings by using the symbols and figures published in AASHTO "Guide Specifications for Seismic Isolation Design, Interim (2000)," which is called the "Guide" in this paper. (Also see Naeim and Kelly (2000), Komodromos (2000), as other examples). The purpose of keeping the same nomenclature used in the Guide is to avoid unnecessary confusing to the readers who wish to use the findings of this study to supplement and to validate their designs based on the linearized approach defined in the Guide.

Figure 1(a) is the bi-linear model approximating the nonlinear lateral force vs. displacement relationship of an isolation bearing. It is conceptually reproduced from Figures C1-4 of the Guide" (AASHTO, 2000).

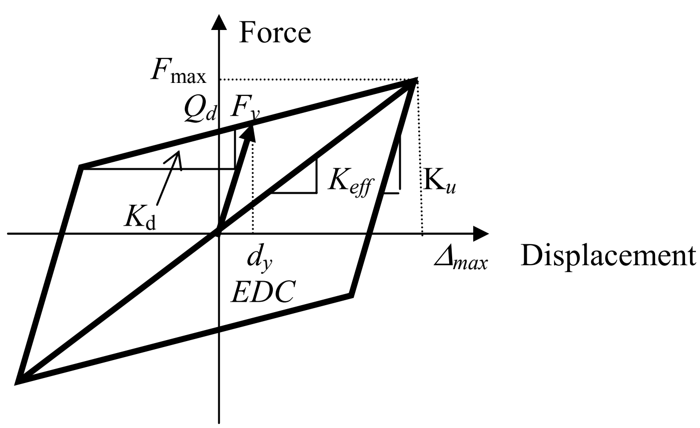

Figure 1(a). Bi-linear relationship of force vs. displacement.

In Figure 1(a), Q_d is the characteristic strength, which is actually the dissipative force corresponding to zero bearing displacement. F_{max} is the maximum force at the maximum bearing displacement, Δ_{max}. K_d and K_u are respectively the post-elastic and elastic (unloading) stiffness. Accordingly,

$$K_{eff} = F_{max}/\Delta_{max}\ , \tag{1}$$

which is defined as the *effective stiffness* in the guide.

In addition, EDC is the area of the hysteresis loop of the parallelogram. It is the energy dissipation per cycle, and can be computed from,

$$EDC = 4\, Q_d\, (\Delta_{max} - d_y) \tag{2}$$

Here d_y is the deformation of the bearing when the yield force F_y is reached.

A second quantity, the critical damping ratio β, is defined in the Guide as follows:

$$\beta = EDC/(2\, \pi\, K_{eff}\, \Delta_{max}^{\ 2}\ ) \tag{3}$$

With the help of the damping ratio, the *damping coefficients B* are given by Table 1 (see Table 7.1-1 in the "Guide")

Table 1. Damping Coefficient *B*

Damper ratio (%)	≤ 2	5	10	20	30	40	50
B	0.8	1.0	1.2	1.5	1.7	1.9	2.0

From Table 1, it is seen that, when the damping coefficient changes from 5% to 50%, the damping coefficients is doubled.

Given the effective stiffness and the damping coefficient as the natural parameters of the bearing(s), the Guide further provides two design parameters. The first is the *statically equivalent seismic force*, *F*, given by, (see equation (1) in the Guide)

$$F = C_s\, W \tag{4}$$

Here W is the total weight of the superstructure and C_s is called the elastic seismic response coefficient. (See equation (2) and (2a) in the Guide), given by

$$C_s = \frac{K_{eff} \times \Delta_{max}}{W} = \frac{AS_i}{T_{eff} B} \tag{5}$$

In equation (5), A and S_i are, respectively, the peak ground acceleration with unit g ranging from 0.15 to 0.40 and the site coefficient for seismic isolation ranging from 1 to 2.7. The product of AS_i can be treated as the excitation level ranging from 0.15 up to 1.08. And, the *effective period* T_{eff} is defined by (see equation (4) in the Guide)

$$T_{eff} = 2\pi \sqrt{\frac{W}{K_{eff}\ g}} \tag{6}$$

Equation (4) implies the concept that the seismic force F can be approximated by the product of the factor C_s and the weight of the superstructure. Therefore, C_s is equivalent to the quantity of *absolute acceleration* of the superstructure.

The second most important design parameter of the Guide is the *bearing displacement* d. Practically speaking, $d = \Delta_{max}$, and d is given by

$$d = \Delta_{max} = \frac{250\ A\ S_i\ T_{eff}}{B}\,(mm) = \frac{0.25\ A\ S_i\ T_{eff}}{B}\,(m) \tag{7}$$

The acceleration C_s and the displacement d, defined by equations (5) and (7) are the two major parameters in isolation design. They can be determined with the assumption of the linearized K_{eff} defined by equation (1). As mentioned above, the computation of C_s and d is based on the design response spectra, (see Figure C1-5, response spectrum for isolated bridge in the Guide), which are obtained from linear systems.

ACCURACY OF LINEARIZATION

The accuracy of the current approach is examined by using 28 earthquake records (AASHTO, 2000) and by conducting time history analyses. The values of both the acceleration C_s and displacement d are obtained from equations (8) and (9):

$$C_s = \text{mean}\,(A_i) + \text{std}(A_i) \qquad i = 1..\ 22 \tag{8}$$

And

$$d = \text{mean}\,(\Delta_i) + \text{std}(\Delta_i) \qquad i = 1..22 \tag{9}$$

Here, A_i and Δ_i are, respectively, the i^{th} peak values of acceleration and displacement time histories. Typical results are given in Figure 2, where the symbols used as those defined in Figure 1. Figure 2(a) and 2(b) give the variations of accelerations and displacements calculated through time history analysis, respectively. In order to plot the results between equations (5) and (6) and equations (7) and (8) for purpose of comparison, the period of the horizontal axes is based on the current AASHTO definition.

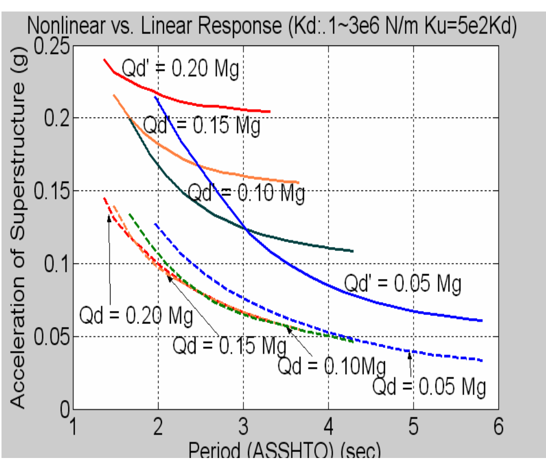

Figure 2(a). Variation of acceleration vs. change of post-elastic stiffness.

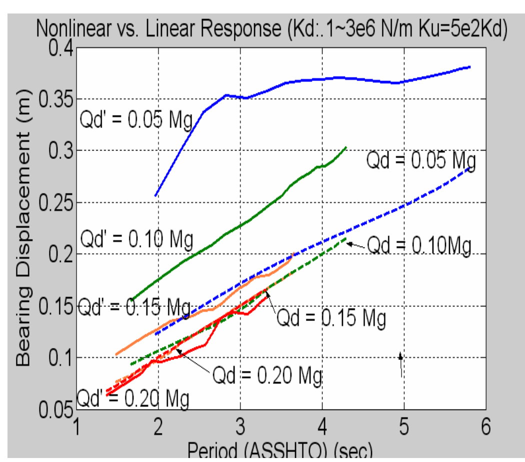

Figure 2(b). Variation of displacement vs. change of post-elastic stiffness

From these figures, we see that

a) The nonlinear approach by using equations (8) and (9) yields considerably higher values in peak acceleration and displacement than the ones calculated by using the AASHTO expressions. Results obtained for most of the ranges of K_d, Q_d and ground excitation, considerable differences exist between the nonlinear peak accelerations using a bi-linear model and those based on the linearized approach.
b) Large differences can also be observed in energy dissipation between the nonlinear (bi-linear) approach and the linearized approach. This reflects the effect of clamping considered by the two different approaches.
c) The effect of period (or the effective stiffness) can also be seen from Figure 2. In the linearized approach, equations (5) and (7) the period has the same amount of influence on the acceleration and displacement, as visualized by the constant slopes of the curves. However, it influences acceleration and displacement calculated from the bi-linear model is clearly nonlinear.

NONLINEAR LATERAL STIFFNESS AND DAMPING

To determine the nonlinear bearing behavior by using the bi-linear relationship can be described by a model shown in Figure 3, with the hysteretic loop defined in Figure 1(b).

In Figure 3, when cart M travels between position A and C, it travels the displacement 2 Δ_{max}. From equation (10), the maximum potential energy restored in spring 1 is ½ $K_d\,\Delta_{max}^2$. Since when $F_2 = F_F$, the friction damper starts to be unlocked, the maximum deformation of spring 2, denoted by D_2 is $D_2 = F_2 / K_2 = Q_d / K_2$. Therefore, the maximum potential energy stored in spring 2, denoted by E_2, is given by

$$E_2 = \tfrac{1}{2} K_2 D_2^2 = \tfrac{1}{2} Q_d^2 / K_2 \qquad (10)$$

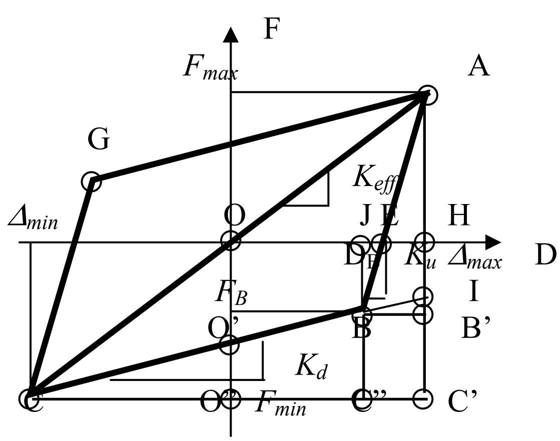

Figure 1(b). Bi-linear relationship of force vs. displacement.

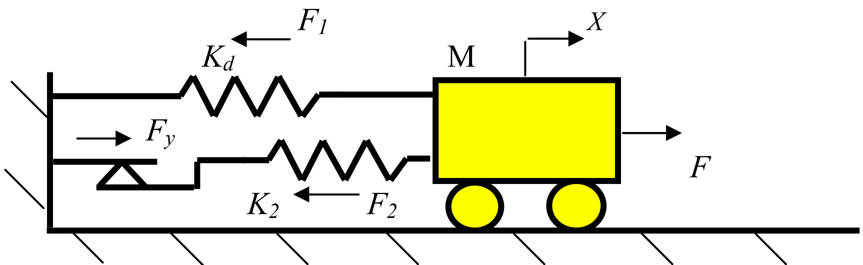

Figure 3. Physical model of bi-linear displacement.

Therefore, the total potential energy E_p is

$$E_p = E_1 + E_2 = ½ (K_d\, \Delta_{max}^2 + Q_d^2 /K_2) \tag{11}$$

We can now define an effective stiffness K_{eff} such that when cart M travels distance $\Delta_{max,}$ the potential energy $E_e = ½\, K_{eff}\, D_2^2 = E_p$. This new effective stiffness is (see Liang and Lee, (2004) for detailed discussion)

$$K_{eff} = K_d + (Q_d^2 /\Delta_{max}^2) /K_2 \tag{12}$$

It can, therefore, be proven that we also have

$$K_{eff} = K_d + (d_y /\Delta_{max})\, K_2 \tag{13}$$

On the other hand, we have

$$K_{eff}= F_{max} / \Delta_{max} = (K_d\Delta_{max} + Q_d)/\Delta_{max} = K_d + Q_d/\Delta_{max} \tag{14}$$

Comparing equations (13) and (14), the second term on the right hand side has a factor to represent the difference. The factor is $Q_d/(\Delta_{max}K_2)$. From Figure 1(b), it is seen this factor is the ratio of OO'/O'O", that is,

$$\gamma = \mathrm{OO'/O'O"} = Q_d/(\Delta_{max}K_2) \tag{15}$$

The above analysis shows that the nonlinear stiffness cannot be simply represented by the AASHTO approach of equation (1) if the nonlinearity is large. Theoretically speaking, corresponding to maximum displacement Δ_{max}, the maximum force F_{max} actually contains two components, a conservative force, $\mathrm{F_C}$, and a dissipative force $\mathrm{F_D}$:

$$\mathrm{F_{max} = F_C + F_D} \tag{16}$$

Note that, the symbols used in the new formulation are regular to distinguish those used in the Guide, which are "italic".

With the newly established expression of the effective stiffness, equation (12), the period of the isolation system becomes

$$T_{eff} = 2\pi\sqrt{\frac{W}{K_{eff}\, g}} \tag{17}$$

And the damping coefficient becomes

$$\beta = EDC/(2\, \pi\, K_{eff}\, \Delta_{max}^{\ 2}\,) \tag{18}$$

With the help of equation (17) and (18), it can be proven that new expressions to estimate the parameter C_s and d can be established. (Details are given in a forthcoming MCEER Technical Report.)

$$C_s = \frac{A}{4\beta}\left(\frac{\sqrt{1+2\beta^2}}{T_{eff}}\right)^{1/2} + Q_A \tag{19}$$

And,

$$d = \frac{A\, g\, \{ T_{eff}\, \sqrt{1+2\beta^2}\, \}^{3/2}}{16\, \pi^2\, \beta} \tag{20}$$

In these equations, A = 0.4, (stands for the input level of 0.4 g). Note that, in equation (19), the site factor S_i is not included. And, for the purpose of comparison, the safety factor is also not included.

These equations are only valid when the input level is 0.4g. Equations (19) and (20) can be further modified by adding appropriate safety factors as a more accurate isolation design equation in the future.

Comparisons have been carried out on results between those obtained from equations (19) and (20) with those obtained from the computer simulation (equations (8) and (9)) where T_{eff} is obtained from the bi-linear model. Typical results are illustrated in figures (4) and (5).

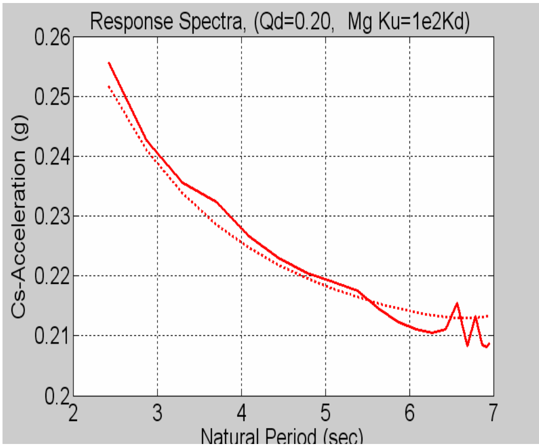

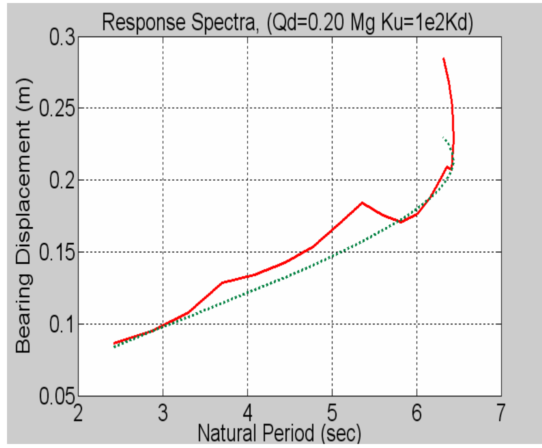

Figure 4. Acceleration, simulated vs. calculated, Q_d = 0.20 Mg, K_u =100 K_d

Figure 5. Displacement, simulated vs. calculated, Q_d = 0.20 Mg, K_u =100 K_d

SUMMARY AND CONCLUSIONS

Many types of seismic isolation bearings have nonlinear lateral stiffness, bi-linear model is widely accepted as the model to describe the nonlinear bearing behavior. For design purpose, ASSHTO further uses this model to obtain the linearized bearing stiffness as well as damping. This approach, although very simple and easy to use, could not estimate the behavior well for nonlinear bearings with large hysteretic loops (large characteristic strength and large damping). For such cases, it is necessary to distinct conservative and dissipative components of the forces and to use only the conservative component to determine the 'effective period" (or "effective stiffness"). This is formulated theoretically in this paper by using the bi-linear model which resulted in different expression for those provided in the Guide that are based on linearized effective stiffness. Although rigorously speaking, a nonlinear system does not have natural period and damping ratio, using the newly defined effective stiffness, an "effective period" is suggested for design purposes. To obtain the effective period, the maximum bearing displacement needs to be specified first, which is often unavailable the time history computation is performed. Method to determine this value has been presented together with many related issues on input ground motions and behavior and design of nonlinear isolation bearings in a separate technical report but not reported herein.

ACKNOWLEDGEMENT

This study is carried our under a FHWA contract (No. DTFH 6198C-00094) awarded to the Multidisciplinary Center for Earthquake Engineering Research, University at Buffalo, State University of New York. The authors would like to acknowledge the advice and valuable comments from Dr. Jianwei Song and Dr. Joseph Penzein.

REFERENCES

American Association of State Highway and Transportation Officials, 2000, *Guide Specifications for Seismic Isolation Design, Interim 2000*, Washington, DC.: American Association of State Highway and Transportation Officials.

Komodromos, P. I., 2000, *Seismic Isolation for Earthquake-resistant Structures*. WIT Press, December 2000.

Liang, Z., J. Song and G. C. Lee, 2004 (in process). *Lateral Stiffness of Bearings and Isolation Design.* MCEER Technical Report.

Naeim, F. and J. M. Kelly, 1999, "Design Seismic Isolated Structures—From Theory to Practice." J. Wiley and Sons, Inc., New York.

Development of Double Spherical Seismic Isolation Bearing

Tian-bo Peng, Jian-zhong Li and Li-chu Fan

ABSTRACT

The actual state of China's seismic design of continuous girder bridges is discussed and seismic isolation design principle is recommended for this kind of bridge. The configuration and working mechanism of the double spherical seismic isolation bearing developed recently is introduced briefly. The test results of the bearing are introduced in detail and it's shown that this kind of bearing is suitable for the seismic design of continuous girder bridges.

Tian-bo Peng, Department of Bridge Engineering, Tongji University. Shanghai 200092, PRC
Jian-zhong Li, Department of Bridge Engineering, Tongji University. Shanghai 200092, PRC
Li-chu Fan, Department of Bridge Engineering, Tongji University. Shanghai 200092, PRC

INTRODUCTION

Continuous girder bridge is a universally adopted bridge type in China, and it's very significant to investigate seismic mitigation techniques for continuous girder bridges. For small and middle-sized bridges, laminated rubber bearings and lead rubber bearings can be used to mitigate seismic response. For large-sized bridges, in the transverse direction of the bridge, fixed bearings are often adopted to share the inertia force of the girder by all the piers under transverse earthquakes. However in the longitudinal direction of the bridge, fixed bearings are arranged only on the middle pier in all the spans, and sliding bearings on the other piers. Seismic force demands of piers with sliding bearing are ignorable under longitudinal earthquakes, and the inertia force of the girder is almost born only by the pier with fixed bearing. Consequently, the seismic design of the pier with fixed bearing is the key point of the whole bridge.

Seismic isolation principle is recommended to mitigate seismic response of the pier with fixed bearings where ordinary fixed bearings are substituted by seismic isolation bearings. The role of seismic isolation bearings is to satisfy the requirement of daily service operation and to ensure the safety of the global structure under earthquakes. Five necessary function requirements for seismic isolation bearings are as follows:

(1) Sufficient stiffness under daily service operation: it's important to provide sufficient lateral and vertical stiffness to resist daily traffic load and lateral wind force.

(2) Flexibility under earthquakes: the fundamental vibration period of a flexible structure is at a range beyond the strong period components of the earthquake ground motion. Therefore, the main function for seismic isolation is to increase the structural vibration period.

(3) Restoring force after sliding: without restoring force, a structure on sliding bearings would likely dislocate after earthquakes and even unseat under aftershocks, so restoring force is necessary to stabilize the structure and prevent structural collapse.

(4) Capacity of seismic energy dissipation under earthquakes: a damping mechanism is often introduced into the seismic isolation bearing to reduce the seismic force and displacement demand simultaneously.

(5) Sufficient maximum design displacement: larger displacement is needed to dissipate seismic energy, and furthermore it can prevent the pounding between superstructure and substructure, which would produce much more force demand in piers than just support the girder with fixed bearings.

In order to correct the misunderstanding of the concept of seismic isolation of bridges and fill the domestic blank of seismic isolation bearing in the real sense, double spherical seismic isolation bearing is developed on the base of spherical sliding bearing whose technology is very mature and reliable. The working mechanism is almost the same as the FPS (friction pendulum sliding) bearing invented by Earthquake Protection System Company, and our considerations about how to dissipate seismic energy and how to operate as a fixed bearing daily are also included to the new product. The bearing can satisfy all the five functions listed above, which will be introduced later.

CONFIGURATION AND WORKING MECHANISM OF THE BEARING

Double spherical seismic isolation bearing is made by substituting the flat sliding surface of spherical sliding bearing with another spherical surface. It is composed of a top bearing plate with sliding concave spherical surface, a slider with double convex spherical surfaces and a bottom bearing plate with rotation concave spherical surface as shown in figure 1. Both sliding surfaces consist of a polished stainless steel spherical plate and a PTFE plate. Round the bottom bearing plate there is a steel ring connected to the top bearing plate with bolts. The steel ring is used to prevent the relative lateral movement between the top and bottom bearing plates under daily service operation. Under earthquakes, when the seismic force resisted by the bearing exceeds the design value, the bolts will be snipped off, the ring drops down and the top bearing plate can move laterally under seismic action like a sliding bearing, so the first function requirement of seismic isolation bearing listed above is satisfied.

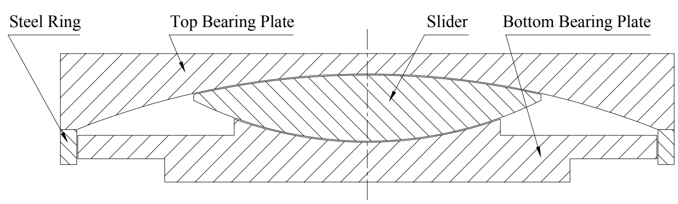

Figure 1. Configuration of the double spherical seismic isolation bearing

The lateral force of the bearing may be written as the sum of a restoring force and a friction force [1, 2, 3, 4]:

$$F = \frac{W}{R} D + \mu W \left(\operatorname{sgn} \dot{D}\right) \tag{1}$$

where, W is the weight supported by the bearings, D is the lateral displacement between the top and bottom bearing plates, R is the curvature radius of the sliding spherical surface, and μ is the friction coefficient of the sliding spherical surface. Restoring force of the bearing is provided by the tangent force along the sliding surface of the structural weight, which can help the girder recenter to the initial position, and the third requirement is satisfied. Lateral stiffness of the bearing is almost invariable after the surfaces begin to slide, and is defined as:

$$K_h = \frac{W}{R} \tag{2}$$

Suppose fixed bearings of a rigid system are substituted by this kind of bearings, the isolation period is given by:

$$T = 2\pi\left(\frac{R}{g}\right)^{1/2} \tag{3}$$

So the fundamental period is increased to the range that exceeds the strong period components of the earthquake ground motion, and the second requirement is satisfied. The effective stiffness is given by:

$$K_{eff} = \frac{W}{R} + \mu\frac{W}{D_D} \tag{4}$$

where, D_D is the maximum design lateral displacement, which is a independent parameter and should be designed carefully to satisfy the fifth requirement. Seismic energy is dissipated by the friction action between the sliding surfaces to satisfy the fourth requirement. The capacity of seismic energy dissipation is evaluated by the factor of effective damping ratio given by:

$$\beta_{eff} = \frac{E_D}{2\pi K_{eff} {D_D}^2} \tag{5}$$

where, E_D is the energy dissipated in a loading cycle. For this kind of bearing, the expression above can be simplified as:

$$\beta_{eff} = \frac{2}{\pi}\cdot\frac{\mu}{D_D/R+\mu} \tag{6}$$

For a lateral displacement of D, the vertical displacement of the bearing is given by:

$$\delta_V = R\left[1-\cos\left(\arcsin\frac{D}{R}\right)\right] \tag{7}$$

As shown, this kind of bearing can satisfy all the function requirements for seismic design of continuous girder bridges and possesses many advantages, such as compact configuration, simple physical model, and reliable performance. And more important, only the maximum design lateral displacement, the curvature radius and friction coefficient of the sliding spherical surface are needed to be determined for a seismic design.

TEST INVESTIGATION OF THE BEARING

Specimen

In order to validate the seismic performance of double spherical seismic isolation bewaring, test investigation is conducted in state key laboratory for disaster reduction in civil engineering of Tongji University. The design requirements of bearing specimen include:

(1) vertical design loading capacity is 6000kN;

(2) lateral maximum design displacement is ±250mm;

(3) friction coefficient of the sliding spherical surface is 0.02 to 0.03;

(4) lateral stiffness after sliding is 2000 kN/m;
(5) restoring force is required after sliding;
(6) the horizontal force when bolts are snipped off is 600kN.

Test Contents and Methods

Lateral hysteresis characteristics of the bearing are investigated because the earthquake effect of superstructure is mainly along the horizontal direction. Test contents include friction coefficient measurement test, lateral hysteresis characteristics test and restoring force test.

Friction coefficient measurement test

The problem of attaching PTFE plate to convex spherical surface is settled by the mosaic technique of PTFE wafers. Two kinds of standard PTFE wafers are selected; the white one with lesser friction coefficient is composite PTFE wafer, and the red one with larger friction coefficient is complete PTFE wafer. Different PTFE wafers have the same thickness and can be mingled in a bearing. Based on these techniques, friction coefficient of a bearing can be adjusted precisely according to the design requirements by the mingling standard PTFE wafers of different friction performance. In order to investigate the influence of different friction coefficients to the seismic isolation effect, 3 different friction coefficients are selected.

In the test, vertical design load of 6000kN is applied first, and then the horizontal load imposed to make the specimen begin to slide is recorded. Friction coefficient is defined as the ratio of the horizontal load recorded to the vertical load.

Lateral hysteresis characteristics test

The relationship of lateral displacement and horizontal load of the bearing is given by the lateral hysteresis curve, which shows the characteristics of lateral stiffness and energy dissipation capacity.

In the test, the vertical load of 6000kN is applied first, and then the lateral displacement history is imposed by the horizontal actuators under the displacement control mode. The lateral displacement history imposed to the specimen includes cycles with maximum displacements of 50, 100, 150,200 and 250mm. The lateral displacement and corresponding horizontal load of the bearing are recorded in the test.

Restoring force test

Restoring force of the bearing is provided by the tangent force along the sliding surface of the structural weight, so the key point in the test is to keep the vertical load constant.

In the test, the vertical load of 6000kN is applied first, and then the lateral maximum design displacement of 250mm is applied by the horizontal actuators under the displacement control mode. Then lateral restraint is released to drive the bearing move freely under the vertical load and the capacity to produce restoring force is examined

Test Device and Installation of the Specimen

The test was conducted on the Electro-Hydraulic Servo Loading System for bearing with the vertical load capacity of 20MN. The device is composed of an indigenous vertical electro- hydraulic servo actuator of 20MN and 2 horizontal electro-hydraulic servo actuator of 2MN imported from USA. The main features of the system includes: imposing vertical load of 20MN and horizontal load of 2MN simultaneously, conducting large displacement test with a stroke of 1000mm, and offering a work space with the dimensions of 2.5×1.7×2.8m (length×width×height). On all accounts, it's the best among all the domestic devices for bearing testing.

The specimen is fixed on the shear platform of the system, and a temposonic transducer to measure the lateral displacement is also mounted along the loading direction.

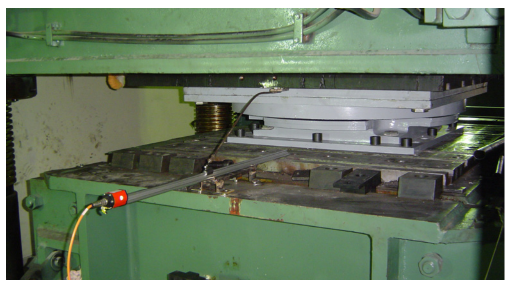

Figure 2. Specimen installation

Test Results

Friction coefficient measurement test

Three test cases are conducted with different friction coefficients and the friction coefficient measurements are listed in table 1. As shown, for each mingle mode, friction coefficient values measured in five sequences are almost the same, which indicates the friction performance is very stable and reliable. Because it's not complicated to alter the mingle mode of PTFE wafers, the friction coefficient value can be controlled easily to satisfy different design requirements.

Tab.1 Friction coefficient measurement results

Sequences	Friction coefficient		
	Case 1	Case 2	Case 3
1	0.008	0.047	0.022
2	0.009	0.046	0.023
3	0.009	0.044	0.025
4	0.010	0.046	0.025
5	0.010	0.044	0.024
Average	0.010	0.045	0.024

The energy dissipation capacity is controlled by the friction performance. Therefore the larger friction coefficient will reduce the displacement demand of the bearing. But it's not best for a too much friction coefficient. For the same stiffness after sliding, the larger friction coefficient will increase the force resisted by the bearing itself and transferred to the substructure. So the appropriate value of friction coefficient should be selected carefully.

Lateral hysteresis characteristics test

Hysteresis loops of each friction coefficient are given in figure 3 and effective damping ratios calculated by equation 5 are listed in table 2. As shown, the width of hysteresis loop is determined by the value of friction coefficient. The Larger friction coefficient will widen the hysteresis loops and increase the effective damping ratio, so larger value of friction coefficient is preferable from a perspective to ensure the energy dissipation capacity.

Tab.2 Effective damping ratio

Sequences	Effective damping ratio		
	Case 1	Case 2	Case 3
1	0.23	0.66	0.29
2	0.12	0.39	0.22
3	0.09	0.31	0.19
4	0.08	0.27	0.16
5	0.07	0.22	0.14
Average	0.12	0.37	0.20

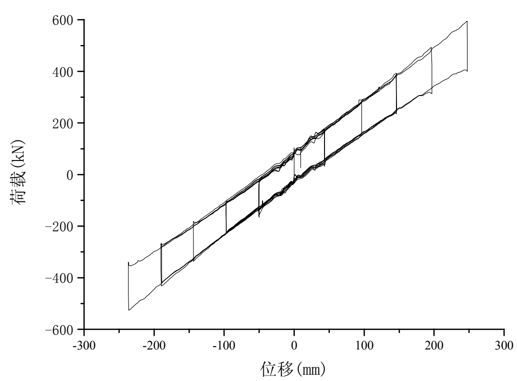

Figure 3a. Lateral hysteresis loops of case 1

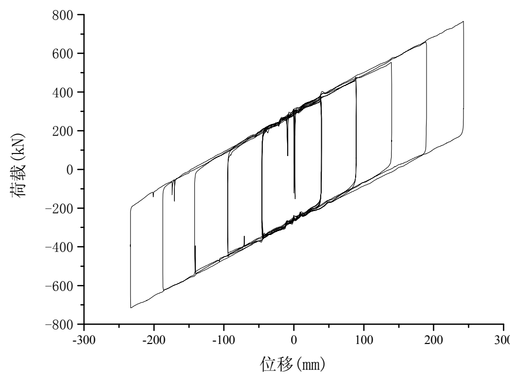

Figure 3b. Lateral hysteresis loops of case 2

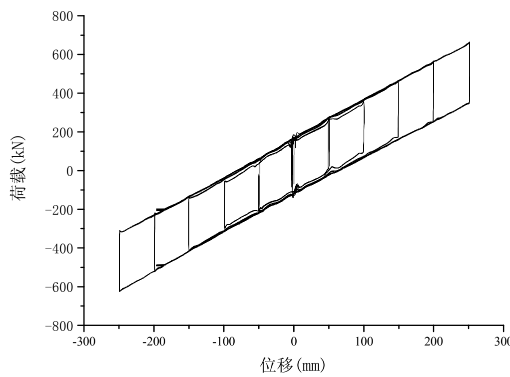

Figure 3c. Lateral hysteresis loops of case 3

Figure 3. Lateral hysteresis loops of the bearing

The lateral stiffnesses after sliding measured in the test are listed in table 3. As shown, all the values are close to the design stiffness of 2000kN/m, which verifies the equation 2. As shown in figure 3, the repeatability of all the hysteresis loops is very perfect, which proves that the seismic isolation performance of the bearing is stable and reliable even after a succession of earthquakes.

Tab.3 Lateral stiffness after sliding

Sequences	Lateral stiffness after sliding (kN/m)		
	Case 1	Case 2	Case 3
1	1623	2153	2111
2	2017	2172	1922
3	2086	1924	2005
4	2070	1981	2000
5	2053	1983	1969
Average	1970	2043	2001

As shown in figure 3, all the shapes of the hysteresis loops are very regular and standard parallelogram, which can be easily simulated in structural analysis software. The response of continuous girder bridges with this kind of bearings can be predicted accurately, which is a preferable feature to the designers.

Restoring force test

In the test, the vertical load is applied, the lateral maximum design displacement is applied, and then lateral restraint is released to drive the bearing move freely. The bearing has the ability to recenter to the initial position in all the cases. However, as shown in equation 1, the lateral force equals the restoring force minus the friction force and residual displacement is unavoidable when the bearing stops moving. Larger friction coefficient will lead to larger residual displacement. However, even for the case of maximum friction coefficient, the lateral residual displacement is not more than 90mm, and the vertical residual displacement is not more than 2mm. All these residual displacements have no much influence to the global performance of the bridge. In addition, because earthquake displacement response is a kind of to-and-fro motion, the lateral residual displacement in actual earthquake should less than in test.

CONCLUSIONS

One kind of seismic isolation bearing, the double spherical seismic isolation bearing, is introduced and recommended for the seismic design of continuous girder bridges. It's verified by test investigation that the bearing can satisfy all the five function requirements for seismic isolation design of continuous girder bridges and possesses many advantages, such as compact configuration, simple physical model and reliable performance. Furthermore, only three parameters are needed to be determined for a seismic design.

References

Kelly, T.E., (2001), "Base Isolation of Structures -Design Guidelines", Holmes Consulting Group Ltd.

Kunde, M.C., Jangid, R.S., "Seismic behavior of isolated bridges: A-state-of-the-art review", Electronic Journal of Structural Engineering, No.3, 140-170.

Priestley, M.J.N., Seible, F. and Calvi, G.M. (1996). "Seismic design and retrofit of bridges", John Wiley and Sons, New York

Tsopelas, P., Constantinou, M. C., Kim, Y. S., Okamoto, S., (1996). "Experimental Study of FPS System in Bridge Seismic Isolation," Earthquake Engineering and Structural Dynamics, vol. 25, 65-78.

Agenda

THURSDAY, OCTOBER 21st

9:00 am-9:10 am	Welcome by Professor Fan and Professor Lee
9:10 am-10:10 am	Two Invited Papers (30 minutes for each)
	M. Lwin, "Construction Materials and Methods for Building Seismic Resistant Bridges and Structures"
	Xi Zhu, "Inelastic Response and Damage Analysis of High-rise Bridge Pier under Pulse-Type Near-Fault Ground Motions"
10:10 am-10:30 am	BREAK
10:30 am-11:30 am	Two Invited Papers (30 minutes for each)
	M. Shinozuka, "Fragility Analysis for Highway Bridges"
	Jian-zhong Li, "Investigation of Ductility Capacity for Tall Piers"
11:30 am-2:30 pm	LUNCH AND SHORT BREAK
2:30 pm-3:50 pm	Four Papers (20 minutes for each)
	M. Bruneau, "Proof-of-Concept Testing of a Laterally Stable Eccentrically Braced Frame for Steel Bridge Piers"
	Gui-ping Yan, Presented by Guan-Yuan Zhao (Ph.D student) "A Comparison of Minimum Confinement in European and American Codes for Circular RC Bridge Columns"
	V. Wagh, "Evolution of Seismic Risk Assessment of the Tappan Zee Bridge"
	Yan-Ping Ni, "Brief Introduction to the New Code for Seismic Design of Railway Engineering and Some Practical Examples about Seismic Design"
3:50 pm-4:10 pm	BREAK

4:10 pm-5:10 pm	Three Papers (20 minutes for each)
	T. Ingham, (presented by B. Prishtina) "Protective Measures in the Seismic Design and Retrofit of Long-Span Bridges"
	Ai -Jun Ye, "A Structural System for Controlling Longitudinal Movements of a Super Long-Span Cable-stayed Bridge"
	Qingshan Yang, "Phase-difference-based Simulation of Correlated and Non-stationary Accelerograms"
10:00 pm	Reception at Oudao West Restaurant, the First Floor of Guangdong Hotel (Shanghai)

FRIDAY, OCTOBER 22nd

9:00 am-10:40 am	Five Papers (20 minutes for each)
	B. Tang, "New Proposed Highway Bridges Seismic Design Provisions and Implementation"
	G. W. Tang, "Responses of Long-span Structures Subjected to Multiple Random Ground Excitations"
	W.P. Yen, "Recommendations for the Seismic Performance Testing in Bridge Piers"
	Long-an Li, "Longitudinal Earthquake Mitigation Method for Cable Stayed Bridge"
	J. O'Connor, "Seismic Risk Assessment Procedures and Mitigation Measures for Highway Bridges in Moderate Earthquake Zones of the Eastern U.S."
10:40 am-11:00 am	BREAK
11:00 am-12:20 pm	Four Papers (20 minutes for each)
	I.G. Buckle, "Buckling-Restrained Braces for Ductile End Cross Frames in Steel Plate Girder Bridges"
	Zhi-Qiang Wang, "Seismic Analysis of GuangXi Nanning Bridge"
	G.C. Lee, "Responses of Nonlinear Seismic Isolation Bearings"

Tian-Bo Peng, "Development of Double Spherical Seismic Isolation Bearing"

12:20-2:40 pm	LUNCH AND SHORT BREAK
2:40-4:40 pm	Summary and Recommendations for Future Research
19:00 pm	Banquet at Shikumen Chinese Restaurant, the Third Floor of Guangdong Hotel (Shanghai)

SATURDAY, OCTOBER 23rd

7:00 am	Depart from Guangdong Hotel (Shanghai) for Technical Tour to Hangzhou, return to Shanghai in the late evening

Participants List

US Participants

Bruneau, Michel
Director and Professor of Civil Engineering
Multidisciplinary Center for Earthquake Engineering Research
University at Buffalo
105 Red Jacket Quadrangle
Buffalo, NY 14261
e-mail: bruneau@buffalo.edu
(unable to attend)

Buckle, Ian
Professor
University of Nevada, Reno
Department of Civil Engineering
MS 248
Reno, NV 89557
e-mail: igbuckle@unr.edu

Lee, George C.
S.P. Capen Professor of Engineering and Special Tasks Director
Multidisciplinary Center for Earthquake Engineering Research
University at Buffalo
122 Red Jacket Quad
Buffalo, NY 14261
e-mail: gclee@mceermail.buffalo.edu

Lwin, Myint
Director, Office of Bridge Technology
Federal Highway Administration
US DOT
HIBT Room 3202
400 Seventh Street, NW
Washington, D.C. 20590
e-mail: myint.lwin@fhwa.dot.gov

O'Connor, Jerry
Sr. Program Officer, Transportation Research
Multidisciplinary Center for Earthquake Engineering Research
107 Red Jacket Quadrangle
Buffalo, NY 14261
e-mail: jso7@buffalo.edu

Prishtina, Bashkim, Ph.D. P.E.
Operations Manager
T Y Lin International
3 Harrison Street
San Francisco, CA 94105
e-mail: kprishtina@tylin.com

Shinozuka, M.
Distinguished Professor and Chair
University of California, Irvine
Department of Civil & Environmental Engineering
E/4150 Engineering Gateway
Irvine, CA 92697-2175
e-mail: shino@uci.edu

Tang, Benjamin
Senior Structural Engineer
Federal Highway Administration
400 7th Street SW
HIBT-10
Room 3203
Washington, D.C. 20590
e-mail: benjamin.tang@fhwa.dot.gov

Participants List (Cont'd)

Wagh, Vikas
President
Wagh Engineers, P.C.
224 West 35th Street
17th Floor
New York, NY 10001-2812
e-mail: waghny@waghengineers.com

Yen, W. Phillip
Federal Highway Administration (COTR)
Seismic Hazard Mitigation (HRDI-07)
Office of Infrastructure R & D
Bridge Design & Hazard Mitigation T-111
6300 Georgetown Pike
McLean, VA 22101
email: wen-huei.yen@fhwa.dot.gov

PRC Participants

Hu, Shidi
Professor
Tongji University, SLDRCE
Department of Bridge Engineering
1239 Siping Road
Shanghai, 200092, China
e-mail: Hushidec@online.sh.cn

Li, Jian-Zhong
Director of Bridge Seismic Group
Tongji University, SLDRCE
Department of Bridge Engineering
1239 Siping Road
Shanghai 200092, China
e-mail: lijianzh@mail.tongji.edu.cn

Ni, Yan-Ping
The First Survey & Design Institute of
China Railway
Lanzhou, 730000, China
E-mail: niyanp@sohu.com

Peng, Tian-bo
Lecturer
Tongji University, SLDRCE
Department of Bridge Engineering
1239 Siping Road
Shanghai 200092, China
e-mail: ptb@mail.tongji.edu.cn

Tang, G.W.
Senior Engineer, Director of the Structural
Dynamics Group
Chongqing Communications Research &
Design Institute
Chongqing, 400067, China
E-mail: tangguangwu@ccrdi.com

Wang, Junjie
Professor
Tongji University, SLDRCE
Department of Bridge Engineering
1239 Siping Road
Shanghai 200092, China
e-mail: jjwang@mail.tongji.edu.cn

Wang, Zhi-qiang
Lecturer
Tongji University, SLDRCE
Department of Bridge Engineering
1239 Siping Road
Shanghai 200092, China
e-mail: wangshiq@mail.tongji.edu.cn

Participants List (Cont'd)

Wei, Hongyi
Associate Professor
Tongji University, SLDRCE
Department of Bridge Engineering
1239 Siping Road
Shanghai, 200092, China

Yang, Qingshan
Professor
College of Engineering and Architecture
Beijing Jiaotong University
Beijing, 100044, China
email: qshyang6620@sina.com

Ye, Ai-jun
Associate Professor
Tongji University, SLDRCE
Department of Bridge Engineering
1239 Siping Road
Shanghai 200092, China
E-mail: yeaijun@mail.tongji.edu.cn

Yuan, Wancheng
Professor
Tongji University, SLDRCE
Department of Bridge Engineering
1239 Siping Road
Shanghai 200092, China

Zhao, Guan-yuan
Ph.D Student
Beijing Jiaotong University
Beijing 100044, China

Zhu, Xi
Professor
Beijing Jiaotong University
School of Civil Engineering and Architecture
Beijing 100044, China
Phone: (086) 010-51683590
E-mail: xzhu@center.njtu.edu.cn

Secretary of 3rd PRC-US Workshop

Yan Xu (Helen)
Lecturer
Tongji University, SLDRCE
Department of Bridge Engineering
1239 Siping Road
Shanghai 200092, China
email: Helen_xyz@163.com

Transportation

Jianjun Jang (Master student)
Yu Wang
Zhongguo Guan
Lei Guo (Ph.D student)

Hospitality

Juhui Zhang (Master student)

Photographers

Peijun Zhang (Master student)
Haiquan Yan (Ph.D student)

Multidisciplinary Center for Earthquake Engineering Research
List of Technical Reports

The Multidisciplinary Center for Earthquake Engineering Research (MCEER) publishes technical reports on a variety of subjects related to earthquake engineering written by authors funded through MCEER. These reports are available from both MCEER Publications and the National Technical Information Service (NTIS). Requests for reports should be directed to MCEER Publications, Multidisciplinary Center for Earthquake Engineering Research, State University of New York at Buffalo, Red Jacket Quadrangle, Buffalo, New York 14261. Reports can also be requested through NTIS, 5285 Port Royal Road, Springfield, Virginia 22161. NTIS accession numbers are shown in parenthesis, if available.

NCEER-87-0001 "First-Year Program in Research, Education and Technology Transfer," 3/5/87, (PB88-134275, A04, MF-A01).

NCEER-87-0002 "Experimental Evaluation of Instantaneous Optimal Algorithms for Structural Control," by R.C. Lin, T.T. Soong and A.M. Reinhorn, 4/20/87, (PB88-134341, A04, MF-A01).

NCEER-87-0003 "Experimentation Using the Earthquake Simulation Facilities at University at Buffalo," by A.M. Reinhorn and R.L. Ketter, to be published.

NCEER-87-0004 "The System Characteristics and Performance of a Shaking Table," by J.S. Hwang, K.C. Chang and G.C. Lee, 6/1/87, (PB88-134259, A03, MF-A01). This report is available only through NTIS (see address given above).

NCEER-87-0005 "A Finite Element Formulation for Nonlinear Viscoplastic Material Using a Q Model," by O. Gyebi and G. Dasgupta, 11/2/87, (PB88-213764, A08, MF-A01).

NCEER-87-0006 "Symbolic Manipulation Program (SMP) - Algebraic Codes for Two and Three Dimensional Finite Element Formulations," by X. Lee and G. Dasgupta, 11/9/87, (PB88-218522, A05, MF-A01).

NCEER-87-0007 "Instantaneous Optimal Control Laws for Tall Buildings Under Seismic Excitations," by J.N. Yang, A. Akbarpour and P. Ghaemmaghami, 6/10/87, (PB88-134333, A06, MF-A01). This report is only available through NTIS (see address given above).

NCEER-87-0008 "IDARC: Inelastic Damage Analysis of Reinforced Concrete Frame - Shear-Wall Structures," by Y.J. Park, A.M. Reinhorn and S.K. Kunnath, 7/20/87, (PB88-134325, A09, MF-A01). This report is only available through NTIS (see address given above).

NCEER-87-0009 "Liquefaction Potential for New York State: A Preliminary Report on Sites in Manhattan and Buffalo," by M. Budhu, V. Vijayakumar, R.F. Giese and L. Baumgras, 8/31/87, (PB88-163704, A03, MF-A01). This report is available only through NTIS (see address given above).

NCEER-87-0010 "Vertical and Torsional Vibration of Foundations in Inhomogeneous Media," by A.S. Veletsos and K.W. Dotson, 6/1/87, (PB88-134291, A03, MF-A01). This report is only available through NTIS (see address given above).

NCEER-87-0011 "Seismic Probabilistic Risk Assessment and Seismic Margins Studies for Nuclear Power Plants," by Howard H.M. Hwang, 6/15/87, (PB88-134267, A03, MF-A01). This report is only available through NTIS (see address given above).

NCEER-87-0012 "Parametric Studies of Frequency Response of Secondary Systems Under Ground-Acceleration Excitations," by Y. Yong and Y.K. Lin, 6/10/87, (PB88-134309, A03, MF-A01). This report is only available through NTIS (see address given above).

NCEER-87-0013 "Frequency Response of Secondary Systems Under Seismic Excitation," by J.A. HoLung, J. Cai and Y.K. Lin, 7/31/87, (PB88-134317, A05, MF-A01). This report is only available through NTIS (see address given above).

NCEER-87-0014 "Modelling Earthquake Ground Motions in Seismically Active Regions Using Parametric Time Series Methods," by G.W. Ellis and A.S. Cakmak, 8/25/87, (PB88-134283, A08, MF-A01). This report is only available through NTIS (see address given above).

NCEER-87-0015 "Detection and Assessment of Seismic Structural Damage," by E. DiPasquale and A.S. Cakmak, 8/25/87, (PB88-163712, A05, MF-A01). This report is only available through NTIS (see address given above).

NCEER-87-0016 "Pipeline Experiment at Parkfield, California," by J. Isenberg and E. Richardson, 9/15/87, (PB88-163720, A03, MF-A01). This report is available only through NTIS (see address given above).

NCEER-87-0017 "Digital Simulation of Seismic Ground Motion," by M. Shinozuka, G. Deodatis and T. Harada, 8/31/87, (PB88-155197, A04, MF-A01). This report is available only through NTIS (see address given above).

NCEER-87-0018 "Practical Considerations for Structural Control: System Uncertainty, System Time Delay and Truncation of Small Control Forces," J.N. Yang and A. Akbarpour, 8/10/87, (PB88-163738, A08, MF-A01). This report is only available through NTIS (see address given above).

NCEER-87-0019 "Modal Analysis of Nonclassically Damped Structural Systems Using Canonical Transformation," by J.N. Yang, S. Sarkani and F.X. Long, 9/27/87, (PB88-187851, A04, MF-A01).

NCEER-87-0020 "A Nonstationary Solution in Random Vibration Theory," by J.R. Red-Horse and P.D. Spanos, 11/3/87, (PB88-163746, A03, MF-A01).

NCEER-87-0021 "Horizontal Impedances for Radially Inhomogeneous Viscoelastic Soil Layers," by A.S. Veletsos and K.W. Dotson, 10/15/87, (PB88-150859, A04, MF-A01).

NCEER-87-0022 "Seismic Damage Assessment of Reinforced Concrete Members," by Y.S. Chung, C. Meyer and M. Shinozuka, 10/9/87, (PB88-150867, A05, MF-A01). This report is available only through NTIS (see address given above).

NCEER-87-0023 "Active Structural Control in Civil Engineering," by T.T. Soong, 11/11/87, (PB88-187778, A03, MF-A01).

NCEER-87-0024 "Vertical and Torsional Impedances for Radially Inhomogeneous Viscoelastic Soil Layers," by K.W. Dotson and A.S. Veletsos, 12/87, (PB88-187786, A03, MF-A01).

NCEER-87-0025 "Proceedings from the Symposium on Seismic Hazards, Ground Motions, Soil-Liquefaction and Engineering Practice in Eastern North America," October 20-22, 1987, edited by K.H. Jacob, 12/87, (PB88-188115, A23, MF-A01). This report is available only through NTIS (see address given above).

NCEER-87-0026 "Report on the Whittier-Narrows, California, Earthquake of October 1, 1987," by J. Pantelic and A. Reinhorn, 11/87, (PB88-187752, A03, MF-A01). This report is available only through NTIS (see address given above).

NCEER-87-0027 "Design of a Modular Program for Transient Nonlinear Analysis of Large 3-D Building Structures," by S. Srivastav and J.F. Abel, 12/30/87, (PB88-187950, A05, MF-A01). This report is only available through NTIS (see address given above).

NCEER-87-0028 "Second-Year Program in Research, Education and Technology Transfer," 3/8/88, (PB88-219480, A04, MF-A01).

NCEER-88-0001 "Workshop on Seismic Computer Analysis and Design of Buildings With Interactive Graphics," by W. McGuire, J.F. Abel and C.H. Conley, 1/18/88, (PB88-187760, A03, MF-A01). This report is only available through NTIS (see address given above).

NCEER-88-0002 "Optimal Control of Nonlinear Flexible Structures," by J.N. Yang, F.X. Long and D. Wong, 1/22/88, (PB88-213772, A06, MF-A01).

NCEER-88-0003 "Substructuring Techniques in the Time Domain for Primary-Secondary Structural Systems," by G.D. Manolis and G. Juhn, 2/10/88, (PB88-213780, A04, MF-A01).

NCEER-88-0004 "Iterative Seismic Analysis of Primary-Secondary Systems," by A. Singhal, L.D. Lutes and P.D. Spanos, 2/23/88, (PB88-213798, A04, MF-A01).

NCEER-88-0005 "Stochastic Finite Element Expansion for Random Media," by P.D. Spanos and R. Ghanem, 3/14/88, (PB88-213806, A03, MF-A01).

NCEER-88-0006 "Combining Structural Optimization and Structural Control," by F.Y. Cheng and C.P. Pantelides, 1/10/88, (PB88-213814, A05, MF-A01).

NCEER-88-0007 "Seismic Performance Assessment of Code-Designed Structures," by H.H-M. Hwang, J-W. Jaw and H-J. Shau, 3/20/88, (PB88-219423, A04, MF-A01). This report is only available through NTIS (see address given above).

NCEER-88-0008 "Reliability Analysis of Code-Designed Structures Under Natural Hazards," by H.H-M. Hwang, H. Ushiba and M. Shinozuka, 2/29/88, (PB88-229471, A07, MF-A01). This report is only available through NTIS (see address given above).

NCEER-88-0009 "Seismic Fragility Analysis of Shear Wall Structures," by J-W Jaw and H.H-M. Hwang, 4/30/88, (PB89-102867, A04, MF-A01).

NCEER-88-0010 "Base Isolation of a Multi-Story Building Under a Harmonic Ground Motion - A Comparison of Performances of Various Systems," by F-G Fan, G. Ahmadi and I.G. Tadjbakhsh, 5/18/88, (PB89-122238, A06, MF-A01). This report is only available through NTIS (see address given above).

NCEER-88-0011 "Seismic Floor Response Spectra for a Combined System by Green's Functions," by F.M. Lavelle, L.A. Bergman and P.D. Spanos, 5/1/88, (PB89-102875, A03, MF-A01).

NCEER-88-0012 "A New Solution Technique for Randomly Excited Hysteretic Structures," by G.Q. Cai and Y.K. Lin, 5/16/88, (PB89-102883, A03, MF-A01).

NCEER-88-0013 "A Study of Radiation Damping and Soil-Structure Interaction Effects in the Centrifuge," by K. Weissman, supervised by J.H. Prevost, 5/24/88, (PB89-144703, A06, MF-A01).

NCEER-88-0014 "Parameter Identification and Implementation of a Kinematic Plasticity Model for Frictional Soils," by J.H. Prevost and D.V. Griffiths, to be published.

NCEER-88-0015 "Two- and Three- Dimensional Dynamic Finite Element Analyses of the Long Valley Dam," by D.V. Griffiths and J.H. Prevost, 6/17/88, (PB89-144711, A04, MF-A01).

NCEER-88-0016 "Damage Assessment of Reinforced Concrete Structures in Eastern United States," by A.M. Reinhorn, M.J. Seidel, S.K. Kunnath and Y.J. Park, 6/15/88, (PB89-122220, A04, MF-A01). This report is only available through NTIS (see address given above).

NCEER-88-0017 "Dynamic Compliance of Vertically Loaded Strip Foundations in Multilayered Viscoelastic Soils," by S. Ahmad and A.S.M. Israil, 6/17/88, (PB89-102891, A04, MF-A01).

NCEER-88-0018 "An Experimental Study of Seismic Structural Response With Added Viscoelastic Dampers," by R.C. Lin, Z. Liang, T.T. Soong and R.H. Zhang, 6/30/88, (PB89-122212, A05, MF-A01). This report is available only through NTIS (see address given above).

NCEER-88-0019 "Experimental Investigation of Primary - Secondary System Interaction," by G.D. Manolis, G. Juhn and A.M. Reinhorn, 5/27/88, (PB89-122204, A04, MF-A01).

NCEER-88-0020 "A Response Spectrum Approach For Analysis of Nonclassically Damped Structures," by J.N. Yang, S. Sarkani and F.X. Long, 4/22/88, (PB89-102909, A04, MF-A01).

NCEER-88-0021 "Seismic Interaction of Structures and Soils: Stochastic Approach," by A.S. Veletsos and A.M. Prasad, 7/21/88, (PB89-122196, A04, MF-A01). This report is only available through NTIS (see address given above).

NCEER-88-0022 "Identification of the Serviceability Limit State and Detection of Seismic Structural Damage," by E. DiPasquale and A.S. Cakmak, 6/15/88, (PB89-122188, A05, MF-A01). This report is available only through NTIS (see address given above).

NCEER-88-0023 "Multi-Hazard Risk Analysis: Case of a Simple Offshore Structure," by B.K. Bhartia and E.H. Vanmarcke, 7/21/88, (PB89-145213, A05, MF-A01).

NCEER-88-0024 "Automated Seismic Design of Reinforced Concrete Buildings," by Y.S. Chung, C. Meyer and M. Shinozuka, 7/5/88, (PB89-122170, A06, MF-A01). This report is available only through NTIS (see address given above).

NCEER-88-0025 "Experimental Study of Active Control of MDOF Structures Under Seismic Excitations," by L.L. Chung, R.C. Lin, T.T. Soong and A.M. Reinhorn, 7/10/88, (PB89-122600, A04, MF-A01).

NCEER-88-0026 "Earthquake Simulation Tests of a Low-Rise Metal Structure," by J.S. Hwang, K.C. Chang, G.C. Lee and R.L. Ketter, 8/1/88, (PB89-102917, A04, MF-A01).

NCEER-88-0027 "Systems Study of Urban Response and Reconstruction Due to Catastrophic Earthquakes," by F. Kozin and H.K. Zhou, 9/22/88, (PB90-162348, A04, MF-A01).

NCEER-88-0028 "Seismic Fragility Analysis of Plane Frame Structures," by H.H-M. Hwang and Y.K. Low, 7/31/88, (PB89-131445, A06, MF-A01).

NCEER-88-0029 "Response Analysis of Stochastic Structures," by A. Kardara, C. Bucher and M. Shinozuka, 9/22/88, (PB89-174429, A04, MF-A01).

NCEER-88-0030 "Nonnormal Accelerations Due to Yielding in a Primary Structure," by D.C.K. Chen and L.D. Lutes, 9/19/88, (PB89-131437, A04, MF-A01).

NCEER-88-0031 "Design Approaches for Soil-Structure Interaction," by A.S. Veletsos, A.M. Prasad and Y. Tang, 12/30/88, (PB89-174437, A03, MF-A01). This report is available only through NTIS (see address given above).

NCEER-88-0032 "A Re-evaluation of Design Spectra for Seismic Damage Control," by C.J. Turkstra and A.G. Tallin, 11/7/88, (PB89-145221, A05, MF-A01).

NCEER-88-0033 "The Behavior and Design of Noncontact Lap Splices Subjected to Repeated Inelastic Tensile Loading," by V.E. Sagan, P. Gergely and R.N. White, 12/8/88, (PB89-163737, A08, MF-A01).

NCEER-88-0034 "Seismic Response of Pile Foundations," by S.M. Mamoon, P.K. Banerjee and S. Ahmad, 11/1/88, (PB89-145239, A04, MF-A01).

NCEER-88-0035 "Modeling of R/C Building Structures With Flexible Floor Diaphragms (IDARC2)," by A.M. Reinhorn, S.K. Kunnath and N. Panahshahi, 9/7/88, (PB89-207153, A07, MF-A01).

NCEER-88-0036 "Solution of the Dam-Reservoir Interaction Problem Using a Combination of FEM, BEM with Particular Integrals, Modal Analysis, and Substructuring," by C-S. Tsai, G.C. Lee and R.L. Ketter, 12/31/88, (PB89-207146, A04, MF-A01).

NCEER-88-0037 "Optimal Placement of Actuators for Structural Control," by F.Y. Cheng and C.P. Pantelides, 8/15/88, (PB89-162846, A05, MF-A01).

NCEER-88-0038 "Teflon Bearings in Aseismic Base Isolation: Experimental Studies and Mathematical Modeling," by A. Mokha, M.C. Constantinou and A.M. Reinhorn, 12/5/88, (PB89-218457, A10, MF-A01). This report is available only through NTIS (see address given above).

NCEER-88-0039 "Seismic Behavior of Flat Slab High-Rise Buildings in the New York City Area," by P. Weidlinger and M. Ettouney, 10/15/88, (PB90-145681, A04, MF-A01).

NCEER-88-0040 "Evaluation of the Earthquake Resistance of Existing Buildings in New York City," by P. Weidlinger and M. Ettouney, 10/15/88, to be published.

NCEER-88-0041 "Small-Scale Modeling Techniques for Reinforced Concrete Structures Subjected to Seismic Loads," by W. Kim, A. El-Attar and R.N. White, 11/22/88, (PB89-189625, A05, MF-A01).

NCEER-88-0042 "Modeling Strong Ground Motion from Multiple Event Earthquakes," by G.W. Ellis and A.S. Cakmak, 10/15/88, (PB89-174445, A03, MF-A01).

NCEER-88-0043 "Nonstationary Models of Seismic Ground Acceleration," by M. Grigoriu, S.E. Ruiz and E. Rosenblueth, 7/15/88, (PB89-189617, A04, MF-A01).

NCEER-88-0044 "SARCF User's Guide: Seismic Analysis of Reinforced Concrete Frames," by Y.S. Chung, C. Meyer and M. Shinozuka, 11/9/88, (PB89-174452, A08, MF-A01).

NCEER-88-0045 "First Expert Panel Meeting on Disaster Research and Planning," edited by J. Pantelic and J. Stoyle, 9/15/88, (PB89-174460, A05, MF-A01).

NCEER-88-0046 "Preliminary Studies of the Effect of Degrading Infill Walls on the Nonlinear Seismic Response of Steel Frames," by C.Z. Chrysostomou, P. Gergely and J.F. Abel, 12/19/88, (PB89-208383, A05, MF-A01).

NCEER-88-0047 "Reinforced Concrete Frame Component Testing Facility - Design, Construction, Instrumentation and Operation," by S.P. Pessiki, C. Conley, T. Bond, P. Gergely and R.N. White, 12/16/88, (PB89-174478, A04, MF-A01).

NCEER-89-0001 "Effects of Protective Cushion and Soil Compliancy on the Response of Equipment Within a Seismically Excited Building," by J.A. HoLung, 2/16/89, (PB89-207179, A04, MF-A01).

NCEER-89-0002 "Statistical Evaluation of Response Modification Factors for Reinforced Concrete Structures," by H.H-M. Hwang and J-W. Jaw, 2/17/89, (PB89-207187, A05, MF-A01).

NCEER-89-0003 "Hysteretic Columns Under Random Excitation," by G-Q. Cai and Y.K. Lin, 1/9/89, (PB89-196513, A03, MF-A01).

NCEER-89-0004 "Experimental Study of `Elephant Foot Bulge' Instability of Thin-Walled Metal Tanks," by Z-H. Jia and R.L. Ketter, 2/22/89, (PB89-207195, A03, MF-A01).

NCEER-89-0005 "Experiment on Performance of Buried Pipelines Across San Andreas Fault," by J. Isenberg, E. Richardson and T.D. O'Rourke, 3/10/89, (PB89-218440, A04, MF-A01). This report is available only through NTIS (see address given above).

NCEER-89-0006 "A Knowledge-Based Approach to Structural Design of Earthquake-Resistant Buildings," by M. Subramani, P. Gergely, C.H. Conley, J.F. Abel and A.H. Zaghw, 1/15/89, (PB89-218465, A06, MF-A01).

NCEER-89-0007 "Liquefaction Hazards and Their Effects on Buried Pipelines," by T.D. O'Rourke and P.A. Lane, 2/1/89, (PB89-218481, A09, MF-A01).

NCEER-89-0008 "Fundamentals of System Identification in Structural Dynamics," by H. Imai, C-B. Yun, O. Maruyama and M. Shinozuka, 1/26/89, (PB89-207211, A04, MF-A01).

NCEER-89-0009 "Effects of the 1985 Michoacan Earthquake on Water Systems and Other Buried Lifelines in Mexico," by A.G. Ayala and M.J. O'Rourke, 3/8/89, (PB89-207229, A06, MF-A01).

NCEER-89-R010 "NCEER Bibliography of Earthquake Education Materials," by K.E.K. Ross, Second Revision, 9/1/89, (PB90-125352, A05, MF-A01). This report is replaced by NCEER-92-0018.

NCEER-89-0011 "Inelastic Three-Dimensional Response Analysis of Reinforced Concrete Building Structures (IDARC-3D), Part I - Modeling," by S.K. Kunnath and A.M. Reinhorn, 4/17/89, (PB90-114612, A07, MF-A01). This report is available only through NTIS (see address given above).

NCEER-89-0012 "Recommended Modifications to ATC-14," by C.D. Poland and J.O. Malley, 4/12/89, (PB90-108648, A15, MF-A01).

NCEER-89-0013 "Repair and Strengthening of Beam-to-Column Connections Subjected to Earthquake Loading," by M. Corazao and A.J. Durrani, 2/28/89, (PB90-109885, A06, MF-A01).

NCEER-89-0014 "Program EXKAL2 for Identification of Structural Dynamic Systems," by O. Maruyama, C-B. Yun, M. Hoshiya and M. Shinozuka, 5/19/89, (PB90-109877, A09, MF-A01).

NCEER-89-0015 "Response of Frames With Bolted Semi-Rigid Connections, Part I - Experimental Study and Analytical Predictions," by P.J. DiCorso, A.M. Reinhorn, J.R. Dickerson, J.B. Radziminski and W.L. Harper, 6/1/89, to be published.

NCEER-89-0016 "ARMA Monte Carlo Simulation in Probabilistic Structural Analysis," by P.D. Spanos and M.P. Mignolet, 7/10/89, (PB90-109893, A03, MF-A01).

NCEER-89-P017 "Preliminary Proceedings from the Conference on Disaster Preparedness - The Place of Earthquake Education in Our Schools," Edited by K.E.K. Ross, 6/23/89, (PB90-108606, A03, MF-A01).

NCEER-89-0017 "Proceedings from the Conference on Disaster Preparedness - The Place of Earthquake Education in Our Schools," Edited by K.E.K. Ross, 12/31/89, (PB90-207895, A012, MF-A02). This report is available only through NTIS (see address given above).

NCEER-89-0018 "Multidimensional Models of Hysteretic Material Behavior for Vibration Analysis of Shape Memory Energy Absorbing Devices, by E.J. Graesser and F.A. Cozzarelli, 6/7/89, (PB90-164146, A04, MF-A01).

NCEER-89-0019 "Nonlinear Dynamic Analysis of Three-Dimensional Base Isolated Structures (3D-BASIS)," by S. Nagarajaiah, A.M. Reinhorn and M.C. Constantinou, 8/3/89, (PB90-161936, A06, MF-A01). This report has been replaced by NCEER-93-0011.

NCEER-89-0020 "Structural Control Considering Time-Rate of Control Forces and Control Rate Constraints," by F.Y. Cheng and C.P. Pantelides, 8/3/89, (PB90-120445, A04, MF-A01).

NCEER-89-0021 "Subsurface Conditions of Memphis and Shelby County," by K.W. Ng, T-S. Chang and H-H.M. Hwang, 7/26/89, (PB90-120437, A03, MF-A01).

NCEER-89-0022 "Seismic Wave Propagation Effects on Straight Jointed Buried Pipelines," by K. Elhmadi and M.J. O'Rourke, 8/24/89, (PB90-162322, A10, MF-A02).

NCEER-89-0023 "Workshop on Serviceability Analysis of Water Delivery Systems," edited by M. Grigoriu, 3/6/89, (PB90-127424, A03, MF-A01).

NCEER-89-0024 "Shaking Table Study of a 1/5 Scale Steel Frame Composed of Tapered Members," by K.C. Chang, J.S. Hwang and G.C. Lee, 9/18/89, (PB90-160169, A04, MF-A01).

NCEER-89-0025 "DYNA1D: A Computer Program for Nonlinear Seismic Site Response Analysis - Technical Documentation," by Jean H. Prevost, 9/14/89, (PB90-161944, A07, MF-A01). This report is available only through NTIS (see address given above).

NCEER-89-0026 "1:4 Scale Model Studies of Active Tendon Systems and Active Mass Dampers for Aseismic Protection," by A.M. Reinhorn, T.T. Soong, R.C. Lin, Y.P. Yang, Y. Fukao, H. Abe and M. Nakai, 9/15/89, (PB90-173246, A10, MF-A02). This report is available only through NTIS (see address given above).

NCEER-89-0027 "Scattering of Waves by Inclusions in a Nonhomogeneous Elastic Half Space Solved by Boundary Element Methods," by P.K. Hadley, A. Askar and A.S. Cakmak, 6/15/89, (PB90-145699, A07, MF-A01).

NCEER-89-0028 "Statistical Evaluation of Deflection Amplification Factors for Reinforced Concrete Structures," by H.H.M. Hwang, J-W. Jaw and A.L. Ch'ng, 8/31/89, (PB90-164633, A05, MF-A01).

NCEER-89-0029 "Bedrock Accelerations in Memphis Area Due to Large New Madrid Earthquakes," by H.H.M. Hwang, C.H.S. Chen and G. Yu, 11/7/89, (PB90-162330, A04, MF-A01).

NCEER-89-0030 "Seismic Behavior and Response Sensitivity of Secondary Structural Systems," by Y.Q. Chen and T.T. Soong, 10/23/89, (PB90-164658, A08, MF-A01).

NCEER-89-0031 "Random Vibration and Reliability Analysis of Primary-Secondary Structural Systems," by Y. Ibrahim, M. Grigoriu and T.T. Soong, 11/10/89, (PB90-161951, A04, MF-A01).

NCEER-89-0032 "Proceedings from the Second U.S. - Japan Workshop on Liquefaction, Large Ground Deformation and Their Effects on Lifelines, September 26-29, 1989," Edited by T.D. O'Rourke and M. Hamada, 12/1/89, (PB90-209388, A22, MF-A03).

NCEER-89-0033 "Deterministic Model for Seismic Damage Evaluation of Reinforced Concrete Structures," by J.M. Bracci, A.M. Reinhorn, J.B. Mander and S.K. Kunnath, 9/27/89, (PB91-108803, A06, MF-A01).

NCEER-89-0034 "On the Relation Between Local and Global Damage Indices," by E. DiPasquale and A.S. Cakmak, 8/15/89, (PB90-173865, A05, MF-A01).

NCEER-89-0035 "Cyclic Undrained Behavior of Nonplastic and Low Plasticity Silts," by A.J. Walker and H.E. Stewart, 7/26/89, (PB90-183518, A10, MF-A01).

NCEER-89-0036 "Liquefaction Potential of Surficial Deposits in the City of Buffalo, New York," by M. Budhu, R. Giese and L. Baumgrass, 1/17/89, (PB90-208455, A04, MF-A01).

NCEER-89-0037 "A Deterministic Assessment of Effects of Ground Motion Incoherence," by A.S. Veletsos and Y. Tang, 7/15/89, (PB90-164294, A03, MF-A01).

NCEER-89-0038 "Workshop on Ground Motion Parameters for Seismic Hazard Mapping," July 17-18, 1989, edited by R.V. Whitman, 12/1/89, (PB90-173923, A04, MF-A01).

NCEER-89-0039 "Seismic Effects on Elevated Transit Lines of the New York City Transit Authority," by C.J. Costantino, C.A. Miller and E. Heymsfield, 12/26/89, (PB90-207887, A06, MF-A01).

NCEER-89-0040 "Centrifugal Modeling of Dynamic Soil-Structure Interaction," by K. Weissman, Supervised by J.H. Prevost, 5/10/89, (PB90-207879, A07, MF-A01).

NCEER-89-0041 "Linearized Identification of Buildings With Cores for Seismic Vulnerability Assessment," by I-K. Ho and A.E. Aktan, 11/1/89, (PB90-251943, A07, MF-A01).

NCEER-90-0001 "Geotechnical and Lifeline Aspects of the October 17, 1989 Loma Prieta Earthquake in San Francisco," by T.D. O'Rourke, H.E. Stewart, F.T. Blackburn and T.S. Dickerman, 1/90, (PB90-208596, A05, MF-A01).

NCEER-90-0002 "Nonnormal Secondary Response Due to Yielding in a Primary Structure," by D.C.K. Chen and L.D. Lutes, 2/28/90, (PB90-251976, A07, MF-A01).

NCEER-90-0003 "Earthquake Education Materials for Grades K-12," by K.E.K. Ross, 4/16/90, (PB91-251984, A05, MF-A05). This report has been replaced by NCEER-92-0018.

NCEER-90-0004 "Catalog of Strong Motion Stations in Eastern North America," by R.W. Busby, 4/3/90, (PB90-251984, A05, MF-A01).

NCEER-90-0005 "NCEER Strong-Motion Data Base: A User Manual for the GeoBase Release (Version 1.0 for the Sun3)," by P. Friberg and K. Jacob, 3/31/90 (PB90-258062, A04, MF-A01).

NCEER-90-0006 "Seismic Hazard Along a Crude Oil Pipeline in the Event of an 1811-1812 Type New Madrid Earthquake," by H.H.M. Hwang and C-H.S. Chen, 4/16/90, (PB90-258054, A04, MF-A01).

NCEER-90-0007 "Site-Specific Response Spectra for Memphis Sheahan Pumping Station," by H.H.M. Hwang and C.S. Lee, 5/15/90, (PB91-108811, A05, MF-A01).

NCEER-90-0008 "Pilot Study on Seismic Vulnerability of Crude Oil Transmission Systems," by T. Ariman, R. Dobry, M. Grigoriu, F. Kozin, M. O'Rourke, T. O'Rourke and M. Shinozuka, 5/25/90, (PB91-108837, A06, MF-A01).

NCEER-90-0009 "A Program to Generate Site Dependent Time Histories: EQGEN," by G.W. Ellis, M. Srinivasan and A.S. Cakmak, 1/30/90, (PB91-108829, A04, MF-A01).

NCEER-90-0010 "Active Isolation for Seismic Protection of Operating Rooms," by M.E. Talbott, Supervised by M. Shinozuka, 6/8/9, (PB91-110205, A05, MF-A01).

NCEER-90-0011 "Program LINEARID for Identification of Linear Structural Dynamic Systems," by C-B. Yun and M. Shinozuka, 6/25/90, (PB91-110312, A08, MF-A01).

NCEER-90-0012 "Two-Dimensional Two-Phase Elasto-Plastic Seismic Response of Earth Dams," by A.N. Yiagos, Supervised by J.H. Prevost, 6/20/90, (PB91-110197, A13, MF-A02).

NCEER-90-0013 "Secondary Systems in Base-Isolated Structures: Experimental Investigation, Stochastic Response and Stochastic Sensitivity," by G.D. Manolis, G. Juhn, M.C. Constantinou and A.M. Reinhorn, 7/1/90, (PB91-110320, A08, MF-A01).

NCEER-90-0014 "Seismic Behavior of Lightly-Reinforced Concrete Column and Beam-Column Joint Details," by S.P. Pessiki, C.H. Conley, P. Gergely and R.N. White, 8/22/90, (PB91-108795, A11, MF-A02).

NCEER-90-0015 "Two Hybrid Control Systems for Building Structures Under Strong Earthquakes," by J.N. Yang and A. Danielians, 6/29/90, (PB91-125393, A04, MF-A01).

NCEER-90-0016 "Instantaneous Optimal Control with Acceleration and Velocity Feedback," by J.N. Yang and Z. Li, 6/29/90, (PB91-125401, A03, MF-A01).

NCEER-90-0017 "Reconnaissance Report on the Northern Iran Earthquake of June 21, 1990," by M. Mehrain, 10/4/90, (PB91-125377, A03, MF-A01).

NCEER-90-0018 "Evaluation of Liquefaction Potential in Memphis and Shelby County," by T.S. Chang, P.S. Tang, C.S. Lee and H. Hwang, 8/10/90, (PB91-125427, A09, MF-A01).

NCEER-90-0019 "Experimental and Analytical Study of a Combined Sliding Disc Bearing and Helical Steel Spring Isolation System," by M.C. Constantinou, A.S. Mokha and A.M. Reinhorn, 10/4/90, (PB91-125385, A06, MF-A01). This report is available only through NTIS (see address given above).

NCEER-90-0020 "Experimental Study and Analytical Prediction of Earthquake Response of a Sliding Isolation System with a Spherical Surface," by A.S. Mokha, M.C. Constantinou and A.M. Reinhorn, 10/11/90, (PB91-125419, A05, MF-A01).

NCEER-90-0021 "Dynamic Interaction Factors for Floating Pile Groups," by G. Gazetas, K. Fan, A. Kaynia and E. Kausel, 9/10/90, (PB91-170381, A05, MF-A01).

NCEER-90-0022 "Evaluation of Seismic Damage Indices for Reinforced Concrete Structures," by S. Rodriguez-Gomez and A.S. Cakmak, 9/30/90, PB91-171322, A06, MF-A01).

NCEER-90-0023 "Study of Site Response at a Selected Memphis Site," by H. Desai, S. Ahmad, E.S. Gazetas and M.R. Oh, 10/11/90, (PB91-196857, A03, MF-A01).

NCEER-90-0024 "A User's Guide to Strongmo: Version 1.0 of NCEER's Strong-Motion Data Access Tool for PCs and Terminals," by P.A. Friberg and C.A.T. Susch, 11/15/90, (PB91-171272, A03, MF-A01).

NCEER-90-0025 "A Three-Dimensional Analytical Study of Spatial Variability of Seismic Ground Motions," by L-L. Hong and A.H.-S. Ang, 10/30/90, (PB91-170399, A09, MF-A01).

NCEER-90-0026 "MUMOID User's Guide - A Program for the Identification of Modal Parameters," by S. Rodriguez-Gomez and E. DiPasquale, 9/30/90, (PB91-171298, A04, MF-A01).

NCEER-90-0027 "SARCF-II User's Guide - Seismic Analysis of Reinforced Concrete Frames," by S. Rodriguez-Gomez, Y.S. Chung and C. Meyer, 9/30/90, (PB91-171280, A05, MF-A01).

NCEER-90-0028 "Viscous Dampers: Testing, Modeling and Application in Vibration and Seismic Isolation," by N. Makris and M.C. Constantinou, 12/20/90 (PB91-190561, A06, MF-A01).

NCEER-90-0029 "Soil Effects on Earthquake Ground Motions in the Memphis Area," by H. Hwang, C.S. Lee, K.W. Ng and T.S. Chang, 8/2/90, (PB91-190751, A05, MF-A01).

NCEER-91-0001 "Proceedings from the Third Japan-U.S. Workshop on Earthquake Resistant Design of Lifeline Facilities and Countermeasures for Soil Liquefaction, December 17-19, 1990," edited by T.D. O'Rourke and M. Hamada, 2/1/91, (PB91-179259, A99, MF-A04).

NCEER-91-0002 "Physical Space Solutions of Non-Proportionally Damped Systems," by M. Tong, Z. Liang and G.C. Lee, 1/15/91, (PB91-179242, A04, MF-A01).

NCEER-91-0003 "Seismic Response of Single Piles and Pile Groups," by K. Fan and G. Gazetas, 1/10/91, (PB92-174994, A04, MF-A01).

NCEER-91-0004 "Damping of Structures: Part 1 - Theory of Complex Damping," by Z. Liang and G. Lee, 10/10/91, (PB92-197235, A12, MF-A03).

NCEER-91-0005 "3D-BASIS - Nonlinear Dynamic Analysis of Three Dimensional Base Isolated Structures: Part II," by S. Nagarajaiah, A.M. Reinhorn and M.C. Constantinou, 2/28/91, (PB91-190553, A07, MF-A01). This report has been replaced by NCEER-93-0011.

NCEER-91-0006 "A Multidimensional Hysteretic Model for Plasticity Deforming Metals in Energy Absorbing Devices," by E.J. Graesser and F.A. Cozzarelli, 4/9/91, (PB92-108364, A04, MF-A01).

NCEER-91-0007 "A Framework for Customizable Knowledge-Based Expert Systems with an Application to a KBES for Evaluating the Seismic Resistance of Existing Buildings," by E.G. Ibarra-Anaya and S.J. Fenves, 4/9/91, (PB91-210930, A08, MF-A01).

NCEER-91-0008 "Nonlinear Analysis of Steel Frames with Semi-Rigid Connections Using the Capacity Spectrum Method," by G.G. Deierlein, S-H. Hsieh, Y-J. Shen and J.F. Abel, 7/2/91, (PB92-113828, A05, MF-A01).

NCEER-91-0009 "Earthquake Education Materials for Grades K-12," by K.E.K. Ross, 4/30/91, (PB91-212142, A06, MF-A01). This report has been replaced by NCEER-92-0018.

NCEER-91-0010 "Phase Wave Velocities and Displacement Phase Differences in a Harmonically Oscillating Pile," by N. Makris and G. Gazetas, 7/8/91, (PB92-108356, A04, MF-A01).

NCEER-91-0011 "Dynamic Characteristics of a Full-Size Five-Story Steel Structure and a 2/5 Scale Model," by K.C. Chang, G.C. Yao, G.C. Lee, D.S. Hao and Y.C. Yeh," 7/2/91, (PB93-116648, A06, MF-A02).

NCEER-91-0012 "Seismic Response of a 2/5 Scale Steel Structure with Added Viscoelastic Dampers," by K.C. Chang, T.T. Soong, S-T. Oh and M.L. Lai, 5/17/91, (PB92-110816, A05, MF-A01).

NCEER-91-0013 "Earthquake Response of Retaining Walls; Full-Scale Testing and Computational Modeling," by S. Alampalli and A-W.M. Elgamal, 6/20/91, to be published.

NCEER-91-0014 "3D-BASIS-M: Nonlinear Dynamic Analysis of Multiple Building Base Isolated Structures," by P.C. Tsopelas, S. Nagarajaiah, M.C. Constantinou and A.M. Reinhorn, 5/28/91, (PB92-113885, A09, MF-A02).

NCEER-91-0015 "Evaluation of SEAOC Design Requirements for Sliding Isolated Structures," by D. Theodossiou and M.C. Constantinou, 6/10/91, (PB92-114602, A11, MF-A03).

NCEER-91-0016 "Closed-Loop Modal Testing of a 27-Story Reinforced Concrete Flat Plate-Core Building," by H.R. Somaprasad, T. Toksoy, H. Yoshiyuki and A.E. Aktan, 7/15/91, (PB92-129980, A07, MF-A02).

NCEER-91-0017 "Shake Table Test of a 1/6 Scale Two-Story Lightly Reinforced Concrete Building," by A.G. El-Attar, R.N. White and P. Gergely, 2/28/91, (PB92-222447, A06, MF-A02).

NCEER-91-0018 "Shake Table Test of a 1/8 Scale Three-Story Lightly Reinforced Concrete Building," by A.G. El-Attar, R.N. White and P. Gergely, 2/28/91, (PB93-116630, A08, MF-A02).

NCEER-91-0019 "Transfer Functions for Rigid Rectangular Foundations," by A.S. Veletsos, A.M. Prasad and W.H. Wu, 7/31/91, to be published.

NCEER-91-0020 "Hybrid Control of Seismic-Excited Nonlinear and Inelastic Structural Systems," by J.N. Yang, Z. Li and A. Danielians, 8/1/91, (PB92-143171, A06, MF-A02).

NCEER-91-0021 "The NCEER-91 Earthquake Catalog: Improved Intensity-Based Magnitudes and Recurrence Relations for U.S. Earthquakes East of New Madrid," by L. Seeber and J.G. Armbruster, 8/28/91, (PB92-176742, A06, MF-A02).

NCEER-91-0022 "Proceedings from the Implementation of Earthquake Planning and Education in Schools: The Need for Change - The Roles of the Changemakers," by K.E.K. Ross and F. Winslow, 7/23/91, (PB92-129998, A12, MF-A03).

NCEER-91-0023 "A Study of Reliability-Based Criteria for Seismic Design of Reinforced Concrete Frame Buildings," by H.H.M. Hwang and H-M. Hsu, 8/10/91, (PB92-140235, A09, MF-A02).

NCEER-91-0024 "Experimental Verification of a Number of Structural System Identification Algorithms," by R.G. Ghanem, H. Gavin and M. Shinozuka, 9/18/91, (PB92-176577, A18, MF-A04).

NCEER-91-0025 "Probabilistic Evaluation of Liquefaction Potential," by H.H.M. Hwang and C.S. Lee," 11/25/91, (PB92-143429, A05, MF-A01).

NCEER-91-0026 "Instantaneous Optimal Control for Linear, Nonlinear and Hysteretic Structures - Stable Controllers," by J.N. Yang and Z. Li, 11/15/91, (PB92-163807, A04, MF-A01).

NCEER-91-0027 "Experimental and Theoretical Study of a Sliding Isolation System for Bridges," by M.C. Constantinou, A. Kartoum, A.M. Reinhorn and P. Bradford, 11/15/91, (PB92-176973, A10, MF-A03).

NCEER-92-0001 "Case Studies of Liquefaction and Lifeline Performance During Past Earthquakes, Volume 1: Japanese Case Studies," Edited by M. Hamada and T. O'Rourke, 2/17/92, (PB92-197243, A18, MF-A04).

NCEER-92-0002 "Case Studies of Liquefaction and Lifeline Performance During Past Earthquakes, Volume 2: United States Case Studies," Edited by T. O'Rourke and M. Hamada, 2/17/92, (PB92-197250, A20, MF-A04).

NCEER-92-0003 "Issues in Earthquake Education," Edited by K. Ross, 2/3/92, (PB92-222389, A07, MF-A02).

NCEER-92-0004 "Proceedings from the First U.S. - Japan Workshop on Earthquake Protective Systems for Bridges," Edited by I.G. Buckle, 2/4/92, (PB94-142239, A99, MF-A06).

NCEER-92-0005 "Seismic Ground Motion from a Haskell-Type Source in a Multiple-Layered Half-Space," A.P. Theoharis, G. Deodatis and M. Shinozuka, 1/2/92, to be published.

NCEER-92-0006 "Proceedings from the Site Effects Workshop," Edited by R. Whitman, 2/29/92, (PB92-197201, A04, MF-A01).

NCEER-92-0007 "Engineering Evaluation of Permanent Ground Deformations Due to Seismically-Induced Liquefaction," by M.H. Baziar, R. Dobry and A-W.M. Elgamal, 3/24/92, (PB92-222421, A13, MF-A03).

NCEER-92-0008 "A Procedure for the Seismic Evaluation of Buildings in the Central and Eastern United States," by C.D. Poland and J.O. Malley, 4/2/92, (PB92-222439, A20, MF-A04).

NCEER-92-0009 "Experimental and Analytical Study of a Hybrid Isolation System Using Friction Controllable Sliding Bearings," by M.Q. Feng, S. Fujii and M. Shinozuka, 5/15/92, (PB93-150282, A06, MF-A02).

NCEER-92-0010 "Seismic Resistance of Slab-Column Connections in Existing Non-Ductile Flat-Plate Buildings," by A.J. Durrani and Y. Du, 5/18/92, (PB93-116812, A06, MF-A02).

NCEER-92-0011 "The Hysteretic and Dynamic Behavior of Brick Masonry Walls Upgraded by Ferrocement Coatings Under Cyclic Loading and Strong Simulated Ground Motion," by H. Lee and S.P. Prawel, 5/11/92, to be published.

NCEER-92-0012 "Study of Wire Rope Systems for Seismic Protection of Equipment in Buildings," by G.F. Demetriades, M.C. Constantinou and A.M. Reinhorn, 5/20/92, (PB93-116655, A08, MF-A02).

NCEER-92-0013 "Shape Memory Structural Dampers: Material Properties, Design and Seismic Testing," by P.R. Witting and F.A. Cozzarelli, 5/26/92, (PB93-116663, A05, MF-A01).

NCEER-92-0014 "Longitudinal Permanent Ground Deformation Effects on Buried Continuous Pipelines," by M.J. O'Rourke, and C. Nordberg, 6/15/92, (PB93-116671, A08, MF-A02).

NCEER-92-0015 "A Simulation Method for Stationary Gaussian Random Functions Based on the Sampling Theorem," by M. Grigoriu and S. Balopoulou, 6/11/92, (PB93-127496, A05, MF-A01).

NCEER-92-0016 "Gravity-Load-Designed Reinforced Concrete Buildings: Seismic Evaluation of Existing Construction and Detailing Strategies for Improved Seismic Resistance," by G.W. Hoffmann, S.K. Kunnath, A.M. Reinhorn and J.B. Mander, 7/15/92, (PB94-142007, A08, MF-A02).

NCEER-92-0017 "Observations on Water System and Pipeline Performance in the Limón Area of Costa Rica Due to the April 22, 1991 Earthquake," by M. O'Rourke and D. Ballantyne, 6/30/92, (PB93-126811, A06, MF-A02).

NCEER-92-0018 "Fourth Edition of Earthquake Education Materials for Grades K-12," Edited by K.E.K. Ross, 8/10/92, (PB93-114023, A07, MF-A02).

NCEER-92-0019 "Proceedings from the Fourth Japan-U.S. Workshop on Earthquake Resistant Design of Lifeline Facilities and Countermeasures for Soil Liquefaction," Edited by M. Hamada and T.D. O'Rourke, 8/12/92, (PB93-163939, A99, MF-E11).

NCEER-92-0020 "Active Bracing System: A Full Scale Implementation of Active Control," by A.M. Reinhorn, T.T. Soong, R.C. Lin, M.A. Riley, Y.P. Wang, S. Aizawa and M. Higashino, 8/14/92, (PB93-127512, A06, MF-A02).

NCEER-92-0021 "Empirical Analysis of Horizontal Ground Displacement Generated by Liquefaction-Induced Lateral Spreads," by S.F. Bartlett and T.L. Youd, 8/17/92, (PB93-188241, A06, MF-A02).

NCEER-92-0022 "IDARC Version 3.0: Inelastic Damage Analysis of Reinforced Concrete Structures," by S.K. Kunnath, A.M. Reinhorn and R.F. Lobo, 8/31/92, (PB93-227502, A07, MF-A02).

NCEER-92-0023 "A Semi-Empirical Analysis of Strong-Motion Peaks in Terms of Seismic Source, Propagation Path and Local Site Conditions, by M. Kamiyama, M.J. O'Rourke and R. Flores-Berrones, 9/9/92, (PB93-150266, A08, MF-A02).

NCEER-92-0024 "Seismic Behavior of Reinforced Concrete Frame Structures with Nonductile Details, Part I: Summary of Experimental Findings of Full Scale Beam-Column Joint Tests," by A. Beres, R.N. White and P. Gergely, 9/30/92, (PB93-227783, A05, MF-A01).

NCEER-92-0025 "Experimental Results of Repaired and Retrofitted Beam-Column Joint Tests in Lightly Reinforced Concrete Frame Buildings," by A. Beres, S. El-Borgi, R.N. White and P. Gergely, 10/29/92, (PB93-227791, A05, MF-A01).

NCEER-92-0026 "A Generalization of Optimal Control Theory: Linear and Nonlinear Structures," by J.N. Yang, Z. Li and S. Vongchavalitkul, 11/2/92, (PB93-188621, A05, MF-A01).

NCEER-92-0027 "Seismic Resistance of Reinforced Concrete Frame Structures Designed Only for Gravity Loads: Part I - Design and Properties of a One-Third Scale Model Structure," by J.M. Bracci, A.M. Reinhorn and J.B. Mander, 12/1/92, (PB94-104502, A08, MF-A02).

NCEER-92-0028 "Seismic Resistance of Reinforced Concrete Frame Structures Designed Only for Gravity Loads: Part II - Experimental Performance of Subassemblages," by L.E. Aycardi, J.B. Mander and A.M. Reinhorn, 12/1/92, (PB94-104510, A08, MF-A02).

NCEER-92-0029 "Seismic Resistance of Reinforced Concrete Frame Structures Designed Only for Gravity Loads: Part III - Experimental Performance and Analytical Study of a Structural Model," by J.M. Bracci, A.M. Reinhorn and J.B. Mander, 12/1/92, (PB93-227528, A09, MF-A01).

NCEER-92-0030 "Evaluation of Seismic Retrofit of Reinforced Concrete Frame Structures: Part I - Experimental Performance of Retrofitted Subassemblages," by D. Choudhuri, J.B. Mander and A.M. Reinhorn, 12/8/92, (PB93-198307, A07, MF-A02).

NCEER-92-0031 "Evaluation of Seismic Retrofit of Reinforced Concrete Frame Structures: Part II - Experimental Performance and Analytical Study of a Retrofitted Structural Model," by J.M. Bracci, A.M. Reinhorn and J.B. Mander, 12/8/92, (PB93-198315, A09, MF-A03).

NCEER-92-0032 "Experimental and Analytical Investigation of Seismic Response of Structures with Supplemental Fluid Viscous Dampers," by M.C. Constantinou and M.D. Symans, 12/21/92, (PB93-191435, A10, MF-A03). This report is available only through NTIS (see address given above).

NCEER-92-0033 "Reconnaissance Report on the Cairo, Egypt Earthquake of October 12, 1992," by M. Khater, 12/23/92, (PB93-188621, A03, MF-A01).

NCEER-92-0034 "Low-Level Dynamic Characteristics of Four Tall Flat-Plate Buildings in New York City," by H. Gavin, S. Yuan, J. Grossman, E. Pekelis and K. Jacob, 12/28/92, (PB93-188217, A07, MF-A02).

NCEER-93-0001 "An Experimental Study on the Seismic Performance of Brick-Infilled Steel Frames With and Without Retrofit," by J.B. Mander, B. Nair, K. Wojtkowski and J. Ma, 1/29/93, (PB93-227510, A07, MF-A02).

NCEER-93-0002 "Social Accounting for Disaster Preparedness and Recovery Planning," by S. Cole, E. Pantoja and V. Razak, 2/22/93, (PB94-142114, A12, MF-A03).

NCEER-93-0003 "Assessment of 1991 NEHRP Provisions for Nonstructural Components and Recommended Revisions," by T.T. Soong, G. Chen, Z. Wu, R-H. Zhang and M. Grigoriu, 3/1/93, (PB93-188639, A06, MF-A02).

NCEER-93-0004 "Evaluation of Static and Response Spectrum Analysis Procedures of SEAOC/UBC for Seismic Isolated Structures," by C.W. Winters and M.C. Constantinou, 3/23/93, (PB93-198299, A10, MF-A03).

NCEER-93-0005 "Earthquakes in the Northeast - Are We Ignoring the Hazard? A Workshop on Earthquake Science and Safety for Educators," edited by K.E.K. Ross, 4/2/93, (PB94-103066, A09, MF-A02).

NCEER-93-0006 "Inelastic Response of Reinforced Concrete Structures with Viscoelastic Braces," by R.F. Lobo, J.M. Bracci, K.L. Shen, A.M. Reinhorn and T.T. Soong, 4/5/93, (PB93-227486, A05, MF-A02).

NCEER-93-0007 "Seismic Testing of Installation Methods for Computers and Data Processing Equipment," by K. Kosar, T.T. Soong, K.L. Shen, J.A. HoLung and Y.K. Lin, 4/12/93, (PB93-198299, A07, MF-A02).

NCEER-93-0008 "Retrofit of Reinforced Concrete Frames Using Added Dampers," by A. Reinhorn, M. Constantinou and C. Li, to be published.

NCEER-93-0009 "Seismic Behavior and Design Guidelines for Steel Frame Structures with Added Viscoelastic Dampers," by K.C. Chang, M.L. Lai, T.T. Soong, D.S. Hao and Y.C. Yeh, 5/1/93, (PB94-141959, A07, MF-A02).

NCEER-93-0010 "Seismic Performance of Shear-Critical Reinforced Concrete Bridge Piers," by J.B. Mander, S.M. Waheed, M.T.A. Chaudhary and S.S. Chen, 5/12/93, (PB93-227494, A08, MF-A02).

NCEER-93-0011 "3D-BASIS-TABS: Computer Program for Nonlinear Dynamic Analysis of Three Dimensional Base Isolated Structures," by S. Nagarajaiah, C. Li, A.M. Reinhorn and M.C. Constantinou, 8/2/93, (PB94-141819, A09, MF-A02).

NCEER-93-0012 "Effects of Hydrocarbon Spills from an Oil Pipeline Break on Ground Water," by O.J. Helweg and H.H.M. Hwang, 8/3/93, (PB94-141942, A06, MF-A02).

NCEER-93-0013 "Simplified Procedures for Seismic Design of Nonstructural Components and Assessment of Current Code Provisions," by M.P. Singh, L.E. Suarez, E.E. Matheu and G.O. Maldonado, 8/4/93, (PB94-141827, A09, MF-A02).

NCEER-93-0014 "An Energy Approach to Seismic Analysis and Design of Secondary Systems," by G. Chen and T.T. Soong, 8/6/93, (PB94-142767, A11, MF-A03).

NCEER-93-0015 "Proceedings from School Sites: Becoming Prepared for Earthquakes - Commemorating the Third Anniversary of the Loma Prieta Earthquake," Edited by F.E. Winslow and K.E.K. Ross, 8/16/93, (PB94-154275, A16, MF-A02).

NCEER-93-0016 "Reconnaissance Report of Damage to Historic Monuments in Cairo, Egypt Following the October 12, 1992 Dahshur Earthquake," by D. Sykora, D. Look, G. Croci, E. Karaesmen and E. Karaesmen, 8/19/93, (PB94-142221, A08, MF-A02).

NCEER-93-0017 "The Island of Guam Earthquake of August 8, 1993," by S.W. Swan and S.K. Harris, 9/30/93, (PB94-141843, A04, MF-A01).

NCEER-93-0018 "Engineering Aspects of the October 12, 1992 Egyptian Earthquake," by A.W. Elgamal, M. Amer, K. Adalier and A. Abul-Fadl, 10/7/93, (PB94-141983, A05, MF-A01).

NCEER-93-0019 "Development of an Earthquake Motion Simulator and its Application in Dynamic Centrifuge Testing," by I. Krstelj, Supervised by J.H. Prevost, 10/23/93, (PB94-181773, A-10, MF-A03).

NCEER-93-0020 "NCEER-Taisei Corporation Research Program on Sliding Seismic Isolation Systems for Bridges: Experimental and Analytical Study of a Friction Pendulum System (FPS)," by M.C. Constantinou, P. Tsopelas, Y-S. Kim and S. Okamoto, 11/1/93, (PB94-142775, A08, MF-A02).

NCEER-93-0021 "Finite Element Modeling of Elastomeric Seismic Isolation Bearings," by L.J. Billings, Supervised by R. Shepherd, 11/8/93, to be published.

NCEER-93-0022 "Seismic Vulnerability of Equipment in Critical Facilities: Life-Safety and Operational Consequences," by K. Porter, G.S. Johnson, M.M. Zadeh, C. Scawthorn and S. Eder, 11/24/93, (PB94-181765, A16, MF-A03).

NCEER-93-0023 "Hokkaido Nansei-oki, Japan Earthquake of July 12, 1993, by P.I. Yanev and C.R. Scawthorn, 12/23/93, (PB94-181500, A07, MF-A01).

NCEER-94-0001 "An Evaluation of Seismic Serviceability of Water Supply Networks with Application to the San Francisco Auxiliary Water Supply System," by I. Markov, Supervised by M. Grigoriu and T. O'Rourke, 1/21/94, (PB94-204013, A07, MF-A02).

NCEER-94-0002 "NCEER-Taisei Corporation Research Program on Sliding Seismic Isolation Systems for Bridges: Experimental and Analytical Study of Systems Consisting of Sliding Bearings, Rubber Restoring Force Devices and Fluid Dampers," Volumes I and II, by P. Tsopelas, S. Okamoto, M.C. Constantinou, D. Ozaki and S. Fujii, 2/4/94, (PB94-181740, A09, MF-A02 and PB94-181757, A12, MF-A03).

NCEER-94-0003 "A Markov Model for Local and Global Damage Indices in Seismic Analysis," by S. Rahman and M. Grigoriu, 2/18/94, (PB94-206000, A12, MF-A03).

NCEER-94-0004 "Proceedings from the NCEER Workshop on Seismic Response of Masonry Infills," edited by D.P. Abrams, 3/1/94, (PB94-180783, A07, MF-A02).

NCEER-94-0005 "The Northridge, California Earthquake of January 17, 1994: General Reconnaissance Report," edited by J.D. Goltz, 3/11/94, (PB94-193943, A10, MF-A03).

NCEER-94-0006 "Seismic Energy Based Fatigue Damage Analysis of Bridge Columns: Part I - Evaluation of Seismic Capacity," by G.A. Chang and J.B. Mander, 3/14/94, (PB94-219185, A11, MF-A03).

NCEER-94-0007 "Seismic Isolation of Multi-Story Frame Structures Using Spherical Sliding Isolation Systems," by T.M. Al-Hussaini, V.A. Zayas and M.C. Constantinou, 3/17/94, (PB94-193745, A09, MF-A02).

NCEER-94-0008 "The Northridge, California Earthquake of January 17, 1994: Performance of Highway Bridges," edited by I.G. Buckle, 3/24/94, (PB94-193851, A06, MF-A02).

NCEER-94-0009 "Proceedings of the Third U.S.-Japan Workshop on Earthquake Protective Systems for Bridges," edited by I.G. Buckle and I. Friedland, 3/31/94, (PB94-195815, A99, MF-A06).

NCEER-94-0010 "3D-BASIS-ME: Computer Program for Nonlinear Dynamic Analysis of Seismically Isolated Single and Multiple Structures and Liquid Storage Tanks," by P.C. Tsopelas, M.C. Constantinou and A.M. Reinhorn, 4/12/94, (PB94-204922, A09, MF-A02).

NCEER-94-0011 "The Northridge, California Earthquake of January 17, 1994: Performance of Gas Transmission Pipelines," by T.D. O'Rourke and M.C. Palmer, 5/16/94, (PB94-204989, A05, MF-A01).

NCEER-94-0012 "Feasibility Study of Replacement Procedures and Earthquake Performance Related to Gas Transmission Pipelines," by T.D. O'Rourke and M.C. Palmer, 5/25/94, (PB94-206638, A09, MF-A02).

NCEER-94-0013 "Seismic Energy Based Fatigue Damage Analysis of Bridge Columns: Part II - Evaluation of Seismic Demand," by G.A. Chang and J.B. Mander, 6/1/94, (PB95-18106, A08, MF-A02).

NCEER-94-0014 "NCEER-Taisei Corporation Research Program on Sliding Seismic Isolation Systems for Bridges: Experimental and Analytical Study of a System Consisting of Sliding Bearings and Fluid Restoring Force/Damping Devices," by P. Tsopelas and M.C. Constantinou, 6/13/94, (PB94-219144, A10, MF-A03).

NCEER-94-0015 "Generation of Hazard-Consistent Fragility Curves for Seismic Loss Estimation Studies," by H. Hwang and J-R. Huo, 6/14/94, (PB95-181996, A09, MF-A02).

NCEER-94-0016 "Seismic Study of Building Frames with Added Energy-Absorbing Devices," by W.S. Pong, C.S. Tsai and G.C. Lee, 6/20/94, (PB94-219136, A10, A03).

NCEER-94-0017 "Sliding Mode Control for Seismic-Excited Linear and Nonlinear Civil Engineering Structures," by J. Yang, J. Wu, A. Agrawal and Z. Li, 6/21/94, (PB95-138483, A06, MF-A02).

NCEER-94-0018 "3D-BASIS-TABS Version 2.0: Computer Program for Nonlinear Dynamic Analysis of Three Dimensional Base Isolated Structures," by A.M. Reinhorn, S. Nagarajaiah, M.C. Constantinou, P. Tsopelas and R. Li, 6/22/94, (PB95-182176, A08, MF-A02).

NCEER-94-0019 "Proceedings of the International Workshop on Civil Infrastructure Systems: Application of Intelligent Systems and Advanced Materials on Bridge Systems," Edited by G.C. Lee and K.C. Chang, 7/18/94, (PB95-252474, A20, MF-A04).

NCEER-94-0020 "Study of Seismic Isolation Systems for Computer Floors," by V. Lambrou and M.C. Constantinou, 7/19/94, (PB95-138533, A10, MF-A03).

NCEER-94-0021 "Proceedings of the U.S.-Italian Workshop on Guidelines for Seismic Evaluation and Rehabilitation of Unreinforced Masonry Buildings," Edited by D.P. Abrams and G.M. Calvi, 7/20/94, (PB95-138749, A13, MF-A03).

NCEER-94-0022 "NCEER-Taisei Corporation Research Program on Sliding Seismic Isolation Systems for Bridges: Experimental and Analytical Study of a System Consisting of Lubricated PTFE Sliding Bearings and Mild Steel Dampers," by P. Tsopelas and M.C. Constantinou, 7/22/94, (PB95-182184, A08, MF-A02).

NCEER-94-0023 “Development of Reliability-Based Design Criteria for Buildings Under Seismic Load,” by Y.K. Wen, H. Hwang and M. Shinozuka, 8/1/94, (PB95-211934, A08, MF-A02).

NCEER-94-0024 “Experimental Verification of Acceleration Feedback Control Strategies for an Active Tendon System,” by S.J. Dyke, B.F. Spencer, Jr., P. Quast, M.K. Sain, D.C. Kaspari, Jr. and T.T. Soong, 8/29/94, (PB95-212320, A05, MF-A01).

NCEER-94-0025 “Seismic Retrofitting Manual for Highway Bridges,” Edited by I.G. Buckle and I.F. Friedland, published by the Federal Highway Administration (PB95-212676, A15, MF-A03).

NCEER-94-0026 “Proceedings from the Fifth U.S.-Japan Workshop on Earthquake Resistant Design of Lifeline Facilities and Countermeasures Against Soil Liquefaction,” Edited by T.D. O’Rourke and M. Hamada, 11/7/94, (PB95-220802, A99, MF-E08).

NCEER-95-0001 "Experimental and Analytical Investigation of Seismic Retrofit of Structures with Supplemental Damping: Part 1 - Fluid Viscous Damping Devices," by A.M. Reinhorn, C. Li and M.C. Constantinou, 1/3/95, (PB95-266599, A09, MF-A02).

NCEER-95-0002 "Experimental and Analytical Study of Low-Cycle Fatigue Behavior of Semi-Rigid Top-And-Seat Angle Connections," by G. Pekcan, J.B. Mander and S.S. Chen, 1/5/95, (PB95-220042, A07, MF-A02).

NCEER-95-0003 "NCEER-ATC Joint Study on Fragility of Buildings," by T. Anagnos, C. Rojahn and A.S. Kiremidjian, 1/20/95, (PB95-220026, A06, MF-A02).

NCEER-95-0004 "Nonlinear Control Algorithms for Peak Response Reduction," by Z. Wu, T.T. Soong, V. Gattulli and R.C. Lin, 2/16/95, (PB95-220349, A05, MF-A01).

NCEER-95-0005 "Pipeline Replacement Feasibility Study: A Methodology for Minimizing Seismic and Corrosion Risks to Underground Natural Gas Pipelines," by R.T. Eguchi, H.A. Seligson and D.G. Honegger, 3/2/95, (PB95-252326, A06, MF-A02).

NCEER-95-0006 "Evaluation of Seismic Performance of an 11-Story Frame Building During the 1994 Northridge Earthquake," by F. Naeim, R. DiSulio, K. Benuska, A. Reinhorn and C. Li, to be published.

NCEER-95-0007 "Prioritization of Bridges for Seismic Retrofitting," by N. Basöz and A.S. Kiremidjian, 4/24/95, (PB95-252300, A08, MF-A02).

NCEER-95-0008 "Method for Developing Motion Damage Relationships for Reinforced Concrete Frames," by A. Singhal and A.S. Kiremidjian, 5/11/95, (PB95-266607, A06, MF-A02).

NCEER-95-0009 "Experimental and Analytical Investigation of Seismic Retrofit of Structures with Supplemental Damping: Part II - Friction Devices," by C. Li and A.M. Reinhorn, 7/6/95, (PB96-128087, A11, MF-A03).

NCEER-95-0010 "Experimental Performance and Analytical Study of a Non-Ductile Reinforced Concrete Frame Structure Retrofitted with Elastomeric Spring Dampers," by G. Pekcan, J.B. Mander and S.S. Chen, 7/14/95, (PB96-137161, A08, MF-A02).

NCEER-95-0011 "Development and Experimental Study of Semi-Active Fluid Damping Devices for Seismic Protection of Structures," by M.D. Symans and M.C. Constantinou, 8/3/95, (PB96-136940, A23, MF-A04).

NCEER-95-0012 "Real-Time Structural Parameter Modification (RSPM): Development of Innervated Structures," by Z. Liang, M. Tong and G.C. Lee, 4/11/95, (PB96-137153, A06, MF-A01).

NCEER-95-0013 "Experimental and Analytical Investigation of Seismic Retrofit of Structures with Supplemental Damping: Part III - Viscous Damping Walls," by A.M. Reinhorn and C. Li, 10/1/95, (PB96-176409, A11, MF-A03).

NCEER-95-0014 "Seismic Fragility Analysis of Equipment and Structures in a Memphis Electric Substation," by J-R. Huo and H.H.M. Hwang, 8/10/95, (PB96-128087, A09, MF-A02).

NCEER-95-0015 "The Hanshin-Awaji Earthquake of January 17, 1995: Performance of Lifelines," Edited by M. Shinozuka, 11/3/95, (PB96-176383, A15, MF-A03).

NCEER-95-0016 "Highway Culvert Performance During Earthquakes," by T.L. Youd and C.J. Beckman, available as NCEER-96-0015.

NCEER-95-0017 "The Hanshin-Awaji Earthquake of January 17, 1995: Performance of Highway Bridges," Edited by I.G. Buckle, 12/1/95, to be published.

NCEER-95-0018 "Modeling of Masonry Infill Panels for Structural Analysis," by A.M. Reinhorn, A. Madan, R.E. Valles, Y. Reichmann and J.B. Mander, 12/8/95, (PB97-110886, MF-A01, A06).

NCEER-95-0019 "Optimal Polynomial Control for Linear and Nonlinear Structures," by A.K. Agrawal and J.N. Yang, 12/11/95, (PB96-168737, A07, MF-A02).

NCEER-95-0020 "Retrofit of Non-Ductile Reinforced Concrete Frames Using Friction Dampers," by R.S. Rao, P. Gergely and R.N. White, 12/22/95, (PB97-133508, A10, MF-A02).

NCEER-95-0021 "Parametric Results for Seismic Response of Pile-Supported Bridge Bents," by G. Mylonakis, A. Nikolaou and G. Gazetas, 12/22/95, (PB97-100242, A12, MF-A03).

NCEER-95-0022 "Kinematic Bending Moments in Seismically Stressed Piles," by A. Nikolaou, G. Mylonakis and G. Gazetas, 12/23/95, (PB97-113914, MF-A03, A13).

NCEER-96-0001 "Dynamic Response of Unreinforced Masonry Buildings with Flexible Diaphragms," by A.C. Costley and D.P. Abrams," 10/10/96, (PB97-133573, MF-A03, A15).

NCEER-96-0002 "State of the Art Review: Foundations and Retaining Structures," by I. Po Lam, to be published.

NCEER-96-0003 "Ductility of Rectangular Reinforced Concrete Bridge Columns with Moderate Confinement," by N. Wehbe, M. Saiidi, D. Sanders and B. Douglas, 11/7/96, (PB97-133557, A06, MF-A02).

NCEER-96-0004 "Proceedings of the Long-Span Bridge Seismic Research Workshop," edited by I.G. Buckle and I.M. Friedland, to be published.

NCEER-96-0005 "Establish Representative Pier Types for Comprehensive Study: Eastern United States," by J. Kulicki and Z. Prucz, 5/28/96, (PB98-119217, A07, MF-A02).

NCEER-96-0006 "Establish Representative Pier Types for Comprehensive Study: Western United States," by R. Imbsen, R.A. Schamber and T.A. Osterkamp, 5/28/96, (PB98-118607, A07, MF-A02).

NCEER-96-0007 "Nonlinear Control Techniques for Dynamical Systems with Uncertain Parameters," by R.G. Ghanem and M.I. Bujakov, 5/27/96, (PB97-100259, A17, MF-A03).

NCEER-96-0008 "Seismic Evaluation of a 30-Year Old Non-Ductile Highway Bridge Pier and Its Retrofit," by J.B. Mander, B. Mahmoodzadegan, S. Bhadra and S.S. Chen, 5/31/96, (PB97-110902, MF-A03, A10).

NCEER-96-0009 "Seismic Performance of a Model Reinforced Concrete Bridge Pier Before and After Retrofit," by J.B. Mander, J.H. Kim and C.A. Ligozio, 5/31/96, (PB97-110910, MF-A02, A10).

NCEER-96-0010 "IDARC2D Version 4.0: A Computer Program for the Inelastic Damage Analysis of Buildings," by R.E. Valles, A.M. Reinhorn, S.K. Kunnath, C. Li and A. Madan, 6/3/96, (PB97-100234, A17, MF-A03).

NCEER-96-0011 "Estimation of the Economic Impact of Multiple Lifeline Disruption: Memphis Light, Gas and Water Division Case Study," by S.E. Chang, H.A. Seligson and R.T. Eguchi, 8/16/96, (PB97-133490, A11, MF-A03).

NCEER-96-0012 "Proceedings from the Sixth Japan-U.S. Workshop on Earthquake Resistant Design of Lifeline Facilities and Countermeasures Against Soil Liquefaction, Edited by M. Hamada and T. O'Rourke, 9/11/96, (PB97-133581, A99, MF-A06).

NCEER-96-0013 "Chemical Hazards, Mitigation and Preparedness in Areas of High Seismic Risk: A Methodology for Estimating the Risk of Post-Earthquake Hazardous Materials Release," by H.A. Seligson, R.T. Eguchi, K.J. Tierney and K. Richmond, 11/7/96, (PB97-133565, MF-A02, A08).

NCEER-96-0014 "Response of Steel Bridge Bearings to Reversed Cyclic Loading," by J.B. Mander, D-K. Kim, S.S. Chen and G.J. Premus, 11/13/96, (PB97-140735, A12, MF-A03).

NCEER-96-0015 "Highway Culvert Performance During Past Earthquakes," by T.L. Youd and C.J. Beckman, 11/25/96, (PB97-133532, A06, MF-A01).

NCEER-97-0001 "Evaluation, Prevention and Mitigation of Pounding Effects in Building Structures," by R.E. Valles and A.M. Reinhorn, 2/20/97, (PB97-159552, A14, MF-A03).

NCEER-97-0002 "Seismic Design Criteria for Bridges and Other Highway Structures," by C. Rojahn, R. Mayes, D.G. Anderson, J. Clark, J.H. Hom, R.V. Nutt and M.J. O'Rourke, 4/30/97, (PB97-194658, A06, MF-A03).

NCEER-97-0003 “Proceedings of the U.S.-Italian Workshop on Seismic Evaluation and Retrofit,” Edited by D.P. Abrams and G.M. Calvi, 3/19/97, (PB97-194666, A13, MF-A03).

NCEER-97-0004 "Investigation of Seismic Response of Buildings with Linear and Nonlinear Fluid Viscous Dampers," by A.A. Seleemah and M.C. Constantinou, 5/21/97, (PB98-109002, A15, MF-A03).

NCEER-97-0005 "Proceedings of the Workshop on Earthquake Engineering Frontiers in Transportation Facilities," edited by G.C. Lee and I.M. Friedland, 8/29/97, (PB98-128911, A25, MR-A04).

NCEER-97-0006 "Cumulative Seismic Damage of Reinforced Concrete Bridge Piers," by S.K. Kunnath, A. El-Bahy, A. Taylor and W. Stone, 9/2/97, (PB98-108814, A11, MF-A03).

NCEER-97-0007 "Structural Details to Accommodate Seismic Movements of Highway Bridges and Retaining Walls," by R.A. Imbsen, R.A. Schamber, E. Thorkildsen, A. Kartoum, B.T. Martin, T.N. Rosser and J.M. Kulicki, 9/3/97, (PB98-108996, A09, MF-A02).

NCEER-97-0008 "A Method for Earthquake Motion-Damage Relationships with Application to Reinforced Concrete Frames," by A. Singhal and A.S. Kiremidjian, 9/10/97, (PB98-108988, A13, MF-A03).

NCEER-97-0009 "Seismic Analysis and Design of Bridge Abutments Considering Sliding and Rotation," by K. Fishman and R. Richards, Jr., 9/15/97, (PB98-108897, A06, MF-A02).

NCEER-97-0010 "Proceedings of the FHWA/NCEER Workshop on the National Representation of Seismic Ground Motion for New and Existing Highway Facilities," edited by I.M. Friedland, M.S. Power and R.L. Mayes, 9/22/97, (PB98-128903, A21, MF-A04).

NCEER-97-0011 "Seismic Analysis for Design or Retrofit of Gravity Bridge Abutments," by K.L. Fishman, R. Richards, Jr. and R.C. Divito, 10/2/97, (PB98-128937, A08, MF-A02).

NCEER-97-0012 "Evaluation of Simplified Methods of Analysis for Yielding Structures," by P. Tsopelas, M.C. Constantinou, C.A. Kircher and A.S. Whittaker, 10/31/97, (PB98-128929, A10, MF-A03).

NCEER-97-0013 "Seismic Design of Bridge Columns Based on Control and Repairability of Damage," by C-T. Cheng and J.B. Mander, 12/8/97, (PB98-144249, A11, MF-A03).

NCEER-97-0014 "Seismic Resistance of Bridge Piers Based on Damage Avoidance Design," by J.B. Mander and C-T. Cheng, 12/10/97, (PB98-144223, A09, MF-A02).

NCEER-97-0015 “Seismic Response of Nominally Symmetric Systems with Strength Uncertainty,” by S. Balopoulou and M. Grigoriu, 12/23/97, (PB98-153422, A11, MF-A03).

NCEER-97-0016 “Evaluation of Seismic Retrofit Methods for Reinforced Concrete Bridge Columns,” by T.J. Wipf, F.W. Klaiber and F.M. Russo, 12/28/97, (PB98-144215, A12, MF-A03).

NCEER-97-0017 “Seismic Fragility of Existing Conventional Reinforced Concrete Highway Bridges,” by C.L. Mullen and A.S. Cakmak, 12/30/97, (PB98-153406, A08, MF-A02).

NCEER-97-0018 “Loss Asssessment of Memphis Buildings,” edited by D.P. Abrams and M. Shinozuka, 12/31/97, (PB98-144231, A13, MF-A03).

NCEER-97-0019 “Seismic Evaluation of Frames with Infill Walls Using Quasi-static Experiments,” by K.M. Mosalam, R.N. White and P. Gergely, 12/31/97, (PB98-153455, A07, MF-A02).

NCEER-97-0020 “Seismic Evaluation of Frames with Infill Walls Using Pseudo-dynamic Experiments,” by K.M. Mosalam, R.N. White and P. Gergely, 12/31/97, (PB98-153430, A07, MF-A02).

NCEER-97-0021 “Computational Strategies for Frames with Infill Walls: Discrete and Smeared Crack Analyses and Seismic Fragility,” by K.M. Mosalam, R.N. White and P. Gergely, 12/31/97, (PB98-153414, A10, MF-A02).

NCEER-97-0022 "Proceedings of the NCEER Workshop on Evaluation of Liquefaction Resistance of Soils," edited by T.L. Youd and I.M. Idriss, 12/31/97, (PB98-155617, A15, MF-A03).

MCEER-98-0001 "Extraction of Nonlinear Hysteretic Properties of Seismically Isolated Bridges from Quick-Release Field Tests," by Q. Chen, B.M. Douglas, E.M. Maragakis and I.G. Buckle, 5/26/98, (PB99-118838, A06, MF-A01).

MCEER-98-0002 "Methodologies for Evaluating the Importance of Highway Bridges," by A. Thomas, S. Eshenaur and J. Kulicki, 5/29/98, (PB99-118846, A10, MF-A02).

MCEER-98-0003 "Capacity Design of Bridge Piers and the Analysis of Overstrength," by J.B. Mander, A. Dutta and P. Goel, 6/1/98, (PB99-118853, A09, MF-A02).

MCEER-98-0004 "Evaluation of Bridge Damage Data from the Loma Prieta and Northridge, California Earthquakes," by N. Basoz and A. Kiremidjian, 6/2/98, (PB99-118861, A15, MF-A03).

MCEER-98-0005 "Screening Guide for Rapid Assessment of Liquefaction Hazard at Highway Bridge Sites," by T. L. Youd, 6/16/98, (PB99-118879, A06, not available on microfiche).

MCEER-98-0006 "Structural Steel and Steel/Concrete Interface Details for Bridges," by P. Ritchie, N. Kauhl and J. Kulicki, 7/13/98, (PB99-118945, A06, MF-A01).

MCEER-98-0007 "Capacity Design and Fatigue Analysis of Confined Concrete Columns," by A. Dutta and J.B. Mander, 7/14/98, (PB99-118960, A14, MF-A03).

MCEER-98-0008 "Proceedings of the Workshop on Performance Criteria for Telecommunication Services Under Earthquake Conditions," edited by A.J. Schiff, 7/15/98, (PB99-118952, A08, MF-A02).

MCEER-98-0009 "Fatigue Analysis of Unconfined Concrete Columns," by J.B. Mander, A. Dutta and J.H. Kim, 9/12/98, (PB99-123655, A10, MF-A02).

MCEER-98-0010 "Centrifuge Modeling of Cyclic Lateral Response of Pile-Cap Systems and Seat-Type Abutments in Dry Sands," by A.D. Gadre and R. Dobry, 10/2/98, (PB99-123606, A13, MF-A03).

MCEER-98-0011 "IDARC-BRIDGE: A Computational Platform for Seismic Damage Assessment of Bridge Structures," by A.M. Reinhorn, V. Simeonov, G. Mylonakis and Y. Reichman, 10/2/98, (PB99-162919, A15, MF-A03).

MCEER-98-0012 "Experimental Investigation of the Dynamic Response of Two Bridges Before and After Retrofitting with Elastomeric Bearings," by D.A. Wendichansky, S.S. Chen and J.B. Mander, 10/2/98, (PB99-162927, A15, MF-A03).

MCEER-98-0013 "Design Procedures for Hinge Restrainers and Hinge Sear Width for Multiple-Frame Bridges," by R. Des Roches and G.L. Fenves, 11/3/98, (PB99-140477, A13, MF-A03).

MCEER-98-0014 "Response Modification Factors for Seismically Isolated Bridges," by M.C. Constantinou and J.K. Quarshie, 11/3/98, (PB99-140485, A14, MF-A03).

MCEER-98-0015 "Proceedings of the U.S.-Italy Workshop on Seismic Protective Systems for Bridges," edited by I.M. Friedland and M.C. Constantinou, 11/3/98, (PB2000-101711, A22, MF-A04).

MCEER-98-0016 "Appropriate Seismic Reliability for Critical Equipment Systems: Recommendations Based on Regional Analysis of Financial and Life Loss," by K. Porter, C. Scawthorn, C. Taylor and N. Blais, 11/10/98, (PB99-157265, A08, MF-A02).

MCEER-98-0017 "Proceedings of the U.S. Japan Joint Seminar on Civil Infrastructure Systems Research," edited by M. Shinozuka and A. Rose, 11/12/98, (PB99-156713, A16, MF-A03).

MCEER-98-0018 "Modeling of Pile Footings and Drilled Shafts for Seismic Design," by I. PoLam, M. Kapuskar and D. Chaudhuri, 12/21/98, (PB99-157257, A09, MF-A02).

MCEER-99-0001 "Seismic Evaluation of a Masonry Infilled Reinforced Concrete Frame by Pseudodynamic Testing," by S.G. Buonopane and R.N. White, 2/16/99, (PB99-162851, A09, MF-A02).

MCEER-99-0002 "Response History Analysis of Structures with Seismic Isolation and Energy Dissipation Systems: Verification Examples for Program SAP2000," by J. Scheller and M.C. Constantinou, 2/22/99, (PB99-162869, A08, MF-A02).

MCEER-99-0003 "Experimental Study on the Seismic Design and Retrofit of Bridge Columns Including Axial Load Effects," by A. Dutta, T. Kokorina and J.B. Mander, 2/22/99, (PB99-162877, A09, MF-A02).

MCEER-99-0004 "Experimental Study of Bridge Elastomeric and Other Isolation and Energy Dissipation Systems with Emphasis on Uplift Prevention and High Velocity Near-source Seismic Excitation," by A. Kasalanati and M. C. Constantinou, 2/26/99, (PB99-162885, A12, MF-A03).

MCEER-99-0005 "Truss Modeling of Reinforced Concrete Shear-flexure Behavior," by J.H. Kim and J.B. Mander, 3/8/99, (PB99-163693, A12, MF-A03).

MCEER-99-0006 "Experimental Investigation and Computational Modeling of Seismic Response of a 1:4 Scale Model Steel Structure with a Load Balancing Supplemental Damping System," by G. Pekcan, J.B. Mander and S.S. Chen, 4/2/99, (PB99-162893, A11, MF-A03).

MCEER-99-0007 "Effect of Vertical Ground Motions on the Structural Response of Highway Bridges," by M.R. Button, C.J. Cronin and R.L. Mayes, 4/10/99, (PB2000-101411, A10, MF-A03).

MCEER-99-0008 "Seismic Reliability Assessment of Critical Facilities: A Handbook, Supporting Documentation, and Model Code Provisions," by G.S. Johnson, R.E. Sheppard, M.D. Quilici, S.J. Eder and C.R. Scawthorn, 4/12/99, (PB2000-101701, A18, MF-A04).

MCEER-99-0009 "Impact Assessment of Selected MCEER Highway Project Research on the Seismic Design of Highway Structures," by C. Rojahn, R. Mayes, D.G. Anderson, J.H. Clark, D'Appolonia Engineering, S. Gloyd and R.V. Nutt, 4/14/99, (PB99-162901, A10, MF-A02).

MCEER-99-0010 "Site Factors and Site Categories in Seismic Codes," by R. Dobry, R. Ramos and M.S. Power, 7/19/99, (PB2000-101705, A08, MF-A02).

MCEER-99-0011 "Restrainer Design Procedures for Multi-Span Simply-Supported Bridges," by M.J. Randall, M. Saiidi, E. Maragakis and T. Isakovic, 7/20/99, (PB2000-101702, A10, MF-A02).

MCEER-99-0012 "Property Modification Factors for Seismic Isolation Bearings," by M.C. Constantinou, P. Tsopelas, A. Kasalanati and E. Wolff, 7/20/99, (PB2000-103387, A11, MF-A03).

MCEER-99-0013 "Critical Seismic Issues for Existing Steel Bridges," by P. Ritchie, N. Kauhl and J. Kulicki, 7/20/99, (PB2000-101697, A09, MF-A02).

MCEER-99-0014 "Nonstructural Damage Database," by A. Kao, T.T. Soong and A. Vender, 7/24/99, (PB2000-101407, A06, MF-A01).

MCEER-99-0015 "Guide to Remedial Measures for Liquefaction Mitigation at Existing Highway Bridge Sites," by H.G. Cooke and J. K. Mitchell, 7/26/99, (PB2000-101703, A11, MF-A03).

MCEER-99-0016 "Proceedings of the MCEER Workshop on Ground Motion Methodologies for the Eastern United States," edited by N. Abrahamson and A. Becker, 8/11/99, (PB2000-103385, A07, MF-A02).

MCEER-99-0017 "Quindío, Colombia Earthquake of January 25, 1999: Reconnaissance Report," by A.P. Asfura and P.J. Flores, 10/4/99, (PB2000-106893, A06, MF-A01).

MCEER-99-0018 "Hysteretic Models for Cyclic Behavior of Deteriorating Inelastic Structures," by M.V. Sivaselvan and A.M. Reinhorn, 11/5/99, (PB2000-103386, A08, MF-A02).

MCEER-99-0019 "Proceedings of the 7th U.S.- Japan Workshop on Earthquake Resistant Design of Lifeline Facilities and Countermeasures Against Soil Liquefaction," edited by T.D. O'Rourke, J.P. Bardet and M. Hamada, 11/19/99, (PB2000-103354, A99, MF-A06).

MCEER-99-0020 "Development of Measurement Capability for Micro-Vibration Evaluations with Application to Chip Fabrication Facilities," by G.C. Lee, Z. Liang, J.W. Song, J.D. Shen and W.C. Liu, 12/1/99, (PB2000-105993, A08, MF-A02).

MCEER-99-0021 "Design and Retrofit Methodology for Building Structures with Supplemental Energy Dissipating Systems," by G. Pekcan, J.B. Mander and S.S. Chen, 12/31/99, (PB2000-105994, A11, MF-A03).

MCEER-00-0001 "The Marmara, Turkey Earthquake of August 17, 1999: Reconnaissance Report," edited by C. Scawthorn; with major contributions by M. Bruneau, R. Eguchi, T. Holzer, G. Johnson, J. Mander, J. Mitchell, W. Mitchell, A. Papageorgiou, C. Scaethorn, and G. Webb, 3/23/00, (PB2000-106200, A11, MF-A03).

MCEER-00-0002 "Proceedings of the MCEER Workshop for Seismic Hazard Mitigation of Health Care Facilities," edited by G.C. Lee, M. Ettouney, M. Grigoriu, J. Hauer and J. Nigg, 3/29/00, (PB2000-106892, A08, MF-A02).

MCEER-00-0003 "The Chi-Chi, Taiwan Earthquake of September 21, 1999: Reconnaissance Report," edited by G.C. Lee and C.H. Loh, with major contributions by G.C. Lee, M. Bruneau, I.G. Buckle, S.E. Chang, P.J. Flores, T.D. O'Rourke, M. Shinozuka, T.T. Soong, C-H. Loh, K-C. Chang, Z-J. Chen, J-S. Hwang, M-L. Lin, G-Y. Liu, K-C. Tsai, G.C. Yao and C-L. Yen, 4/30/00, (PB2001-100980, A10, MF-A02).

MCEER-00-0004 "Seismic Retrofit of End-Sway Frames of Steel Deck-Truss Bridges with a Supplemental Tendon System: Experimental and Analytical Investigation," by G. Pekcan, J.B. Mander and S.S. Chen, 7/1/00, (PB2001-100982, A10, MF-A02).

MCEER-00-0005 "Sliding Fragility of Unrestrained Equipment in Critical Facilities," by W.H. Chong and T.T. Soong, 7/5/00, (PB2001-100983, A08, MF-A02).

MCEER-00-0006 "Seismic Response of Reinforced Concrete Bridge Pier Walls in the Weak Direction," by N. Abo-Shadi, M. Saiidi and D. Sanders, 7/17/00, (PB2001-100981, A17, MF-A03).

MCEER-00-0007 "Low-Cycle Fatigue Behavior of Longitudinal Reinforcement in Reinforced Concrete Bridge Columns," by J. Brown and S.K. Kunnath, 7/23/00, (PB2001-104392, A08, MF-A02).

MCEER-00-0008 "Soil Structure Interaction of Bridges for Seismic Analysis," I. PoLam and H. Law, 9/25/00, (PB2001-105397, A08, MF-A02).

MCEER-00-0009 "Proceedings of the First MCEER Workshop on Mitigation of Earthquake Disaster by Advanced Technologies (MEDAT-1), edited by M. Shinozuka, D.J. Inman and T.D. O'Rourke, 11/10/00, (PB2001-105399, A14, MF-A03).

MCEER-00-0010 "Development and Evaluation of Simplified Procedures for Analysis and Design of Buildings with Passive Energy Dissipation Systems," by O.M. Ramirez, M.C. Constantinou, C.A. Kircher, A.S. Whittaker, M.W. Johnson, J.D. Gomez and C. Chrysostomou, 11/16/01, (PB2001-105523, A23, MF-A04).

MCEER-00-0011 "Dynamic Soil-Foundation-Structure Interaction Analyses of Large Caissons," by C-Y. Chang, C-M. Mok, Z-L. Wang, R. Settgast, F. Waggoner, M.A. Ketchum, H.M. Gonnermann and C-C. Chin, 12/30/00, (PB2001-104373, A07, MF-A02).

MCEER-00-0012 "Experimental Evaluation of Seismic Performance of Bridge Restrainers," by A.G. Vlassis, E.M. Maragakis and M. Saiid Saiidi, 12/30/00, (PB2001-104354, A09, MF-A02).

MCEER-00-0013 "Effect of Spatial Variation of Ground Motion on Highway Structures," by M. Shinozuka, V. Saxena and G. Deodatis, 12/31/00, (PB2001-108755, A13, MF-A03).

MCEER-00-0014 "A Risk-Based Methodology for Assessing the Seismic Performance of Highway Systems," by S.D. Werner, C.E. Taylor, J.E. Moore, II, J.S. Walton and S. Cho, 12/31/00, (PB2001-108756, A14, MF-A03).

MCEER-01-0001 "Experimental Investigation of P-Delta Effects to Collapse During Earthquakes," by D. Vian and M. Bruneau, 6/25/01, (PB2002-100534, A17, MF-A03).

MCEER-01-0002 "Proceedings of the Second MCEER Workshop on Mitigation of Earthquake Disaster by Advanced Technologies (MEDAT-2)," edited by M. Bruneau and D.J. Inman, 7/23/01, (PB2002-100434, A16, MF-A03).

MCEER-01-0003 "Sensitivity Analysis of Dynamic Systems Subjected to Seismic Loads," by C. Roth and M. Grigoriu, 9/18/01, (PB2003-100884, A12, MF-A03).

MCEER-01-0004 "Overcoming Obstacles to Implementing Earthquake Hazard Mitigation Policies: Stage 1 Report," by D.J. Alesch and W.J. Petak, 12/17/01, (PB2002-107949, A07, MF-A02).

MCEER-01-0005 "Updating Real-Time Earthquake Loss Estimates: Methods, Problems and Insights," by C.E. Taylor, S.E. Chang and R.T. Eguchi, 12/17/01, (PB2002-107948, A05, MF-A01).

MCEER-01-0006 "Experimental Investigation and Retrofit of Steel Pile Foundations and Pile Bents Under Cyclic Lateral Loadings," by A. Shama, J. Mander, B. Blabac and S. Chen, 12/31/01, (PB2002-107950, A13, MF-A03).

MCEER-02-0001 "Assessment of Performance of Bolu Viaduct in the 1999 Duzce Earthquake in Turkey" by P.C. Roussis, M.C. Constantinou, M. Erdik, E. Durukal and M. Dicleli, 5/8/02, (PB2003-100883, A08, MF-A02).

MCEER-02-0002 "Seismic Behavior of Rail Counterweight Systems of Elevators in Buildings," by M.P. Singh, Rildova and L.E. Suarez, 5/27/02. (PB2003-100882, A11, MF-A03).

MCEER-02-0003 "Development of Analysis and Design Procedures for Spread Footings," by G. Mylonakis, G. Gazetas, S. Nikolaou and A. Chauncey, 10/02/02, (PB2004-101636, A13, MF-A03, CD-A13).

MCEER-02-0004 "Bare-Earth Algorithms for Use with SAR and LIDAR Digital Elevation Models," by C.K. Huyck, R.T. Eguchi and B. Houshmand, 10/16/02, (PB2004-101637, A07, CD-A07).

MCEER-02-0005 "Review of Energy Dissipation of Compression Members in Concentrically Braced Frames," by K.Lee and M. Bruneau, 10/18/02, (PB2004-101638, A10, CD-A10).

MCEER-03-0001 "Experimental Investigation of Light-Gauge Steel Plate Shear Walls for the Seismic Retrofit of Buildings" by J. Berman and M. Bruneau, 5/2/03, (PB2004-101622, A10, MF-A03, CD-A10).

MCEER-03-0002 "Statistical Analysis of Fragility Curves," by M. Shinozuka, M.Q. Feng, H. Kim, T. Uzawa and T. Ueda, 6/16/03, (PB2004-101849, A09, CD-A09).

MCEER-03-0003 "Proceedings of the Eighth U.S.-Japan Workshop on Earthquake Resistant Design f Lifeline Facilities and Countermeasures Against Liquefaction," edited by M. Hamada, J.P. Bardet and T.D. O'Rourke, 6/30/03, (PB2004-104386, A99, CD-A99).

MCEER-03-0004 "Proceedings of the PRC-US Workshop on Seismic Analysis and Design of Special Bridges," edited by L.C. Fan and G.C. Lee, 7/15/03, (PB2004-104387, A14, CD-A14).

MCEER-03-0005 "Urban Disaster Recovery: A Framework and Simulation Model," by S.B. Miles and S.E. Chang, 7/25/03, (PB2004-104388, A07, CD-A07).

MCEER-03-0006 "Behavior of Underground Piping Joints Due to Static and Dynamic Loading," by R.D. Meis, M. Maragakis and R. Siddharthan, 11/17/03, (PB2005-102194, A13, A03, CD-A00).

MCEER-03-0007 "Seismic Vulnerability of Timber Bridges and Timber Substructures," by A.A. Shama, J.B. Mander, I.M. Friedland and D.R. Allicock, 12/15/03.

MCEER-04-0001 "Experimental Study of Seismic Isolation Systems with Emphasis on Secondary System Response and Verification of Accuracy of Dynamic Response History Analysis Methods," by E. Wolff and M. Constantinou, 1/16/04 (PB2005-102195, A99, E08, CD-A00).

MCEER-04-0002 "Tension, Compression and Cyclic Testing of Engineered Cementitious Composite Materials," by K. Kesner and S.L. Billington, 3/1/04, (PB2005-102196, A08, CD-A08).

MCEER-04-0003 "Cyclic Testing of Braces Laterally Restrained by Steel Studs to Enhance Performance During Earthquakes," by O.C. Celik, J.W. Berman and M. Bruneau, 3/16/04, (PB2005-102197, A13, A03, CD-A00).

MCEER-04-0004 "Methodologies for Post Earthquake Building Damage Detection Using SAR and Optical Remote Sensing: Application to the August 17, 1999 Marmara, Turkey Earthquake," by C.K. Huyck, B.J. Adams, S. Cho, R.T. Eguchi, B. Mansouri and B. Houshmand, 6/15/04.

MCEER-04-0005 "Nonlinear Structural Analysis Towards Collapse Simulation: A Dynamical Systems Approach," by M.V. Sivaselvan and A.M. Reinhorn, 6/16/04.

MCEER-04-0006 "Proceedings of the Second PRC-US Workshop on Seismic Analysis and Design of Special Bridges," edited by G.C. Lee and L.C. Fan, 6/25/04.

MCEER-04-0007 "Seismic Vulnerability Evaluation of Axially Loaded Steel Built-up Laced Members," by K. Lee and M. Bruneau, 6/30/04.

MCEER-04-0008 "Evaluation of Accuracy of Simplified Methods of Analysis and Design of Buildings with Damping Systems for Near-Fault and for Soft-Soil Seismic Motions," by E.A. Pavlou and M.C. Constantinou, 8/16/04.

MCEER-04-0009 "Assessment of Geotechnical Issues in Acute Care Facilities in California," by M. Lew, T.D. O'Rourke, R. Dobry and M. Koch, 9/15/04.

MCEER-04-0010 "Scissor-Jack-Damper Energy Dissipation System," by A.N. Sigaher-Boyle and M.C. Constantinou, 12/1/04.

MCEER-04-0011 "Seismic Retrofit of Bridge Steel Truss Piers Using a Controlled Rocking Approach," by M. Pollino and M. Bruneau, 12/20/04.

MCEER-05-0001 "Experimental and Analytical Studies of Structures Seismically Isolated with an Uplift-Restraint Isolation System," by P.C. Roussis and M.C. Constantinou, 1/10/05.

MCEER-05-0002 "A Versatile Experimentation Model for Study of Structures Near Collapse Applied to Seismic Evaluation of Irregular Structures," by D. Kusumastuti, A.M. Reinhorn and A. Rutenberg, 3/31/05.

MCEER-05-0003 "Proceedings of the Third PRC-US Workshop on Seismic Analysis and Design of Special Bridges," edited by L.C. Fan and G.C. Lee, 4/20/05.

MCEER
MULTIDISCIPLINARY CENTER FOR EARTHQUAKE ENGINEERING RESEARCH
A National Center of Excellence in Advanced Technology Applications
University at Buffalo, State University of New York
Red Jacket Quadrangle ■ Buffalo, New York 14261
Phone: (716) 645-3391 ■ Fax: (716) 645-3399
E-mail: ***mceer@mceermail.buffalo.edu*** **■ WWW Site** ***http://mceer.buffalo.edu***
University at Buffalo *The State University of New York*